UNIVERSITY OF CALIFORNIA

Santa Barbara

New Marine Siderophores: Discovery, Characterization, and Origin of Hydrolysis Products

A dissertation submitted in partial satisfaction of the

requirements for the degree Doctor of Philosophy

in Chemistry

by

Aneta Maria Jelowicki

Committee in charge:

Professor Alison Butler, Chair

Professor Mahdi Abu-Omar

Professor Frederick Dahlquist

Professor Peter Ford

December 2022

The dissertation of Aneta Maria Jelowicki is approved.

_____

Mahdi Abu-Omar

_____

Frederick Dahlquist

_____

Peter Ford

_____

Alison Butler, Committee Chair

October 2022

New Marine Siderophores: Discovery, Characterization, and Origin of Hydrolysis Products

by

Aneta Maria Jelowicki

ACKNOWLEDGEMENTS

I would like to express my deepest gratitude to my advisor, Professor Alison Butler for her mentorship and support throughout my graduate career. Her constant encouragement, enthusiasm, and thoughtful scientific discussions have guided and shaped my experience in graduate school. I would also like to thank my committee members Professor Peter Ford, Professor Mahdi Abu-Omar, and Professor Frederick Dahlquist for their interest and their thought-provoking questions.

I especially wish to thank Dr. Rachel Behrens for her continual dedication to the UPLC-MS instrument and having the patience for teaching me how to properly use the instrument. These skills that she has shared with me are invaluable and will go a long way in my career.

I am thankful for my fellow group members. To Jeffrey Carmichael, Clifford Hardy, Parker Stow, Emil Thomsen, Haley Ogasawara, Robert Augustynski, Christina Makris and Zachary Reitz. Your friendship, insightful scientific discussion, and helpful group dynamic created a fun lab work environment. I hope we are able to keep in touch over the years and manage to meet up every so often at Captain Fatty's!

I am sincerely thankful for my friends who I have met through church. To Asia, Claire, Selena, Bridget, Haley, Sarah, and Christine. Uniting together as Women of Faith and in STEM played an enormous role in my graduate school experience and has strengthened my faith. You have been the best supporters, gym-buddies, and friends, and I cannot wait to see what God has in store for us!

This endeavor would not have been possible without my family. To my parents, Tomasz and Teresa, who have taught me the true meaning of perseverance and resilience

through their hardworking ethic. To my brothers Aleksander and Albert, and my sister-in-law Victoria. Thank you for your unwavering support, and the constant reminder that I can and have to finish this degree. I never would have completed this journey without your encouragement to keep going. Going home on weekends, receiving lots of hugs and kisses (primarily from our dog Czarek) really helped bring a positive light and relaxation when it was needed.

Lastly, I would like to acknowledge that God has been a steady and leading influence throughout my research experience and these years in Santa Barbara. I believe in the saying that "A little science estranges men from God, but much science leads them back to Him"- Unknown. These years here in Santa Barbara have brought me closer and strengthened my relationship with God and I want to thank everyone who has been a part of this journey.

Thank you, I love you all very much.

VITA OF ANETA MARIA JELOWICKI

October 2022

EDUCATION

Doctor of Philosophy in Chemistry, October 2022
University of California, Santa Barbara

Bachelor of Science in Biochemistry, *Cum laude*, May 2016
California State University, Fullerton

PUBLICATIONS

Butler, A.; Jelowicki, A.M.; Ogasawara, H.A.; Reitz, Z.L.; Stow, P.R.; Thomsen, E.; Mining elements of siderophore chirality encoded in microbial genomes. *FEBS Letters*, **2022**; https://doi.org/10.1002/1873-3468.14539

Jelowicki, A. M.; Butler, A. On the origin of amphi-enterobactin fragments produced by Vibrio campbellii species. *J. Biol. Inorg. Chem* **2022**; 27:565-572. https://doi.org/10.1007/s00775-022-01949-0

Naka, H.; Reitz, Z. L.; Jelowicki, A. M.; Butler, A.; Haygood, M. G. Amphi-enterobactin commonly produced among *Vibrio campbellii* and *Vibrio harveyi* strains can be taken up by a novel outer membrane protein FapA that also can transport canonical Fe(III)-enterobactin. *J. Biol. Inorg. Chem.* **2018**; 23(7): 1009-1022 https://doi.org/10.1007/s00775-018-1601-5

O'Rourke, K. F.; Jelowicki, A. M.; Boehr, D. D.; Controlling active site loop dynamics in the $(\beta/\alpha)_8$ barrel enzyme indole-3-glycerol phosphate synthase. *Catalysts*, **2016**; 6(9):129 https://doi.org/10.3390/catal6090129

AWARDS

2020 Mananya Tantiwiwat Award, UCSB College of Letters and Science. **2020**

DeWolfe Distinguished Teaching Fellow Award, UCSB Department of Chemistry. **2019**

Outstanding Service to the Department Award, UCSB Department of Chemistry. **2017, 2018**

Eli Lilly Travel Award for 2018 ACS Meeting, Women Chemists Committee -ACS. **2018**

CONFERENCES AND MEETINGS

"Iron Acquisition in *Vibrio* Species" poster presentation at the 7th International Symposium on Metallomics. Warsaw, Poland. July **2019**

"Mechanistic Investigations of the Thioesterase Domain in Cyclic Siderophore Biosynthesis" at the 255th American Chemical Society National Meeting, New Orleans, LA. March **2018**

TEACHING EXPERIENCE

Teaching Assistant: Physical Organic Mechanisms Lecture
University of California, Santa Barbara, Spring **2022**

Transitioned General Chemistry Labs to Online Teaching: COVID-19
University of California, Santa Barbara, March **2020** – June **2020**

Teaching Assistant: General Chemistry Laboratory
University of California, Santa Barbara, Spring **2021**

Lead Teaching Assistant: General Chemistry Labs
University of California, Santa Barbara, Fall **2017** – Fall **2020**

Teaching Assistant: General Chemistry Laboratory
University of California, Santa Barbara, Fall **2016** – Spring **2017**

LEADERSHIP EXPERIENCE

Executive Committee Member: Chemical Sciences Student Seminar (CSSS)
University of California, Santa Barbara, Spring **2019** – Spring **2020**

Workshop Leader: Campus Wide Teaching Assistant Orientation
University of California, Santa Barbara, Summer **2017, 2018, 2019**

Campus Wide Lead Teaching Assistant Institute
University of California, Santa Barbara, Summer **2017**

ABSTRACT

New Marine Siderophores: Discovery, Characterization, and Origin of Hydrolysis Products

by

Aneta Maria Jelowicki

Iron is an essential nutrient required for many organisms, however, obtaining ferric iron becomes challenging due to its low solubility. One strategy that bacteria have evolved to obtain iron is the production of siderophores, low molecular weight organic compounds that bind Fe(III) with high affinity. These siderophores coordinate Fe(III) and are taken up by the cell through outer membrane receptor proteins. Iron is then released for utilization by the microbe. This work focuses on the structural characterization of siderophores containing the catecholate Fe(III)-binding functional group found in several bacterial strains.

Due to the organization of non-ribosomal peptide synthetases (NRPS) into distinct domains with predictable functions and amino acid substrates, genome mining has enabled the prediction and discovery of many new siderophore structures. The analysis of genome sequences revealed *Marinomonas mediterranea* MMB-1 possessing two putative siderophore biosynthesis gene clusters, one with high similarity to acinetobactin biosynthesis in *Acinetobacter baumannii* ATCC 19606, and one with high similarity to turnerbactin biosynthesis in *Teredinibacter turnerae* T7901. However, analysis of the second biosynthetic gene cluster reveals a two-module NRPS consistent with a triscatechol siderophore (DHB-

^{D}AA-^{L}Ser). The first module contains an epimerization domain, suggesting production of a D-amino acid in this siderophore, however, a specific amino acid was not predicted by the Stachelhaus code. After bacterial culture isolation and characterization, mediterraneabactin, with the same molecular weight as turnerbactin (*m/z* 1030.40 $[M+H]^+$ was found. Through derivatization with Marfey's reagent, the presence of ^{D}Orn was established, making mediterraneabactin a diastereomer to turnerbactin with ^{L}Orn. The identification of this siderophore with ^{D}Orn is novel and completes the combinatoric suite of triscatecholate siderophores. The stereochemical variation has an effect on the chirality around the metal center, which in turn hints at the importance of chirality during the iron uptake process in bacteria.

Amphi-enterobactin is an amphiphilic siderophore initially isolated from *Vibrio campbellii* ATCC BAA-1116 (formerly *V. harveyi* BAA-1116). . Like enterobactin, amphi-enterobactin is a triscatecholate siderophore, however it is framed on an expanded tetralactone core comprised of four L-Ser residues, of which one L-Ser is appended by a fatty acid and the remaining L-Ser residues are appended by 2,3-dihydroxybenzoate (DHB). The biosynthesis and structural characterization of amphi-enterobactin has been studied, as well as the outer membrane recognition of the Fe(III)-amphi-enterobactin complex. While it is established that amphi-enterobactins are produced by several *Vibrio harveyi* and *V. campbellii* strains, fragments of these amphi-enterobactins composed of 2-Ser-1-DHB-FA and 3-Ser-2-DHB-FA are present in the culture supernatant. Fragments may originate from premature release due to an inefficient biosynthetic pathway, or an enzymatic/non-enzymatic hydrolysis after biosynthesis of the siderophore. Tandem mass spectrometry analysis was used to determine if selected fragments originate from hydrolysis of the amphi-enterobactin macrolactone

siderophore. Unique masses in the tandem MS analysis establish that certain fragments isolated from the culture supernatant must originate from hydrolysis of the amphi-enterobactin macrolactone, while others cannot be distinguished from premature release during biosynthesis or hydrolysis of amphi-enterobactin.

Table of Contents

LIST OF FIGURES

LIST OF TABLES

1. Introduction: Siderophore-Mediated Iron Acquisition

1.1. Environmental Need of Iron

Iron is a cofactor required by many enzymes involved in essential cellular processes within an organism to survive. However, at neutral pH in aerobic environments obtaining iron becomes challenging due to its low solubility [K_{sp} of $Fe(OH)_3$ = 10^{-39}]. One strategy that bacteria have evolved to obtain iron is the biosynthesis of siderophores, low molecular weight organic compounds that coordinate Fe(III) with high selectivity and stability.[1 2 3] Siderophore-mediated iron acquisition begins with the biosynthesis of the small molecule that is then secreted into the environment to scavenge for iron(III). Fe(III)-siderophore complexes are recognized by a specific outer membrane receptor on the cell surface and transported into the cell via an active transport mechanism (Figure 1.1). In Gram-negative bacteria, uptake into the cell involves an outer membrane receptor, a periplasmic binding protein, and an inner membrane ATP-binding cassette transporter.

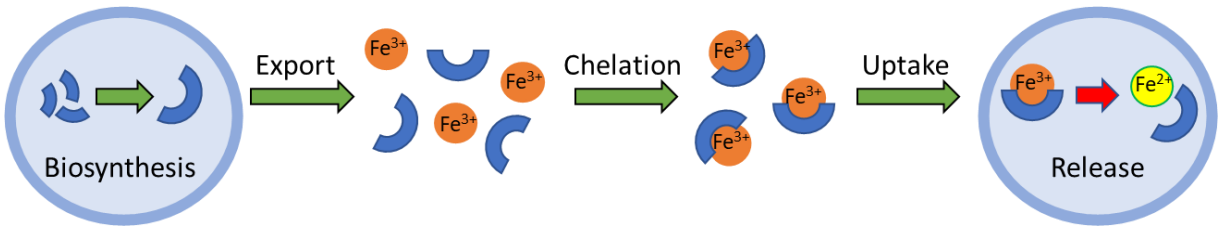

Figure 1.1 Siderophore-mediated iron acquisition in bacteria. Siderophores are biosynthesized then secreted into the environment, where the small molecule chelates Fe(III). The Fe(III)-siderophore complex is taken up by the bacterial cell upon recognition by the outer membrane receptor and iron is released.

1.2. Siderophore Structural Features

Over 500 structurally diverse secondary metabolites have been classified as siderophores.[4] Despite the structural variety, these siderophores most commonly chelate ferric iron in either a bidentate or hexadentate fashion. Siderophores typically use hard donor atoms, most commonly charged oxygens, but on some occasions, nitrogen, or sulfur act as the donor atom as well. [4] The higher the charge on the donor atom, the tighter the interaction between iron(III) and the siderophore. Siderophores are classified by their Fe(III) binding groups. Some of the most common groups include catechols, hydroxamic acids, α-hydroxy carboxylic acids, and β-hydroxyaspartic acids (Figure 1.2).[5] [6] Siderophores can have one or more of the three types of binding groups for iron coordination. These siderophores function in either a hexadentate or a tetradentate fashion with varying affinities for Fe^{3+} chelation.[7]

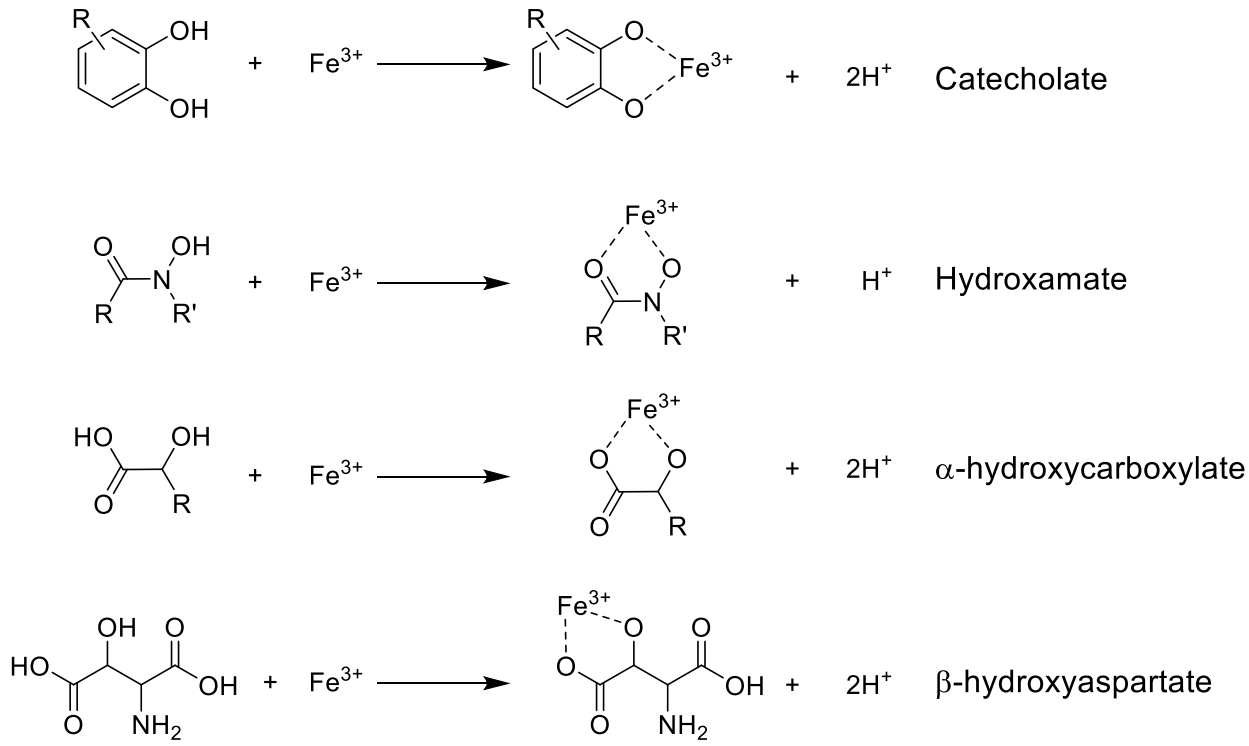

Figure 1.2. Common iron(III) binding functional groups found in siderophores.

1.2.1. Catecholate Siderophores

Catechol as a functional group has high affinity for iron(III) because it contains two phenolate oxygens with a high charge density.[4] Enterobactin, the most well studied catechol siderophore isolated by Pollak and Neilands in 1970,[8] is composed a macrolactone of tris-(*N*-2,3-dihydroxy-benzoyl-L serine) that coordinates iron(III) with three 2,3-dihydroxybenzoate (DHB) catechol groups in a hexadentate fashion. The three catecholate OO' donors bind iron(III) in a Δ configuration at the metal center,[9] and has a proton independent stability constant of 10^{49}, making the complex thermodynamically stable.[10]

Other tris-catecholate siderophores similar in structure to enterobactin have been isolated and characterized from various bacterial species (Figure 1.3). Bacillibactin is a

hexadentate catecholate siderophore produced by *Bacillus subtilis*, and is thought to be the enterobactin equivalent for Gram-positive bacteria.[11] . Bacillibactin is similar to enterobactin in that the two siderophores contain a trilactone macrocycle amide linked to three 2,3-catecholate units that coordinate iron(III) in a hexadentate fashion. The differing structural feature in bacillibactin is the trilactone core made up of threonine residues instead of serines as are found in enterobactin. [9] This siderophore also has a glycine spacer between the trilactone core and the catechol functional group.[9] *Salmonella enterica*, a Gram-negative human pathogen, produces the siderophore salmochelin, a C-glucosylated enterobactin.[12] The salmochelin siderophore is the first glucosylated siderophore found and its structure contains three catechol functional groups with either one, two, or three of the 2,3-dihydroxybenzoly serine groups glucosylated.[12] Unlike enterobactin, salmochelins have the ability to evade siderocalin, a mammalian protein used to prevent iron acquisition in pathogenic bacteria.[13]

Amphi-enterobactin is another siderophore that is structurally similar to enterobactin. It is a triscatecholate siderophore, with two distinct structural features, a fatty acid tail and an expanded tetralactone core.[14] This siderophore was initially isolated from *Vibrio harveyi* BAA-1116, but has also been produced by several *Vibiro harveyi* and *Vibrio campbellii* strains. [14 15] Amphi-enterobactins are produced in a suite of varying fatty acid chains, ranging in length from C_{10} to C_{14}, hydroxylation, and saturation.[14] The biosynthesis of amphi-enterobactin is discussed in a later section.

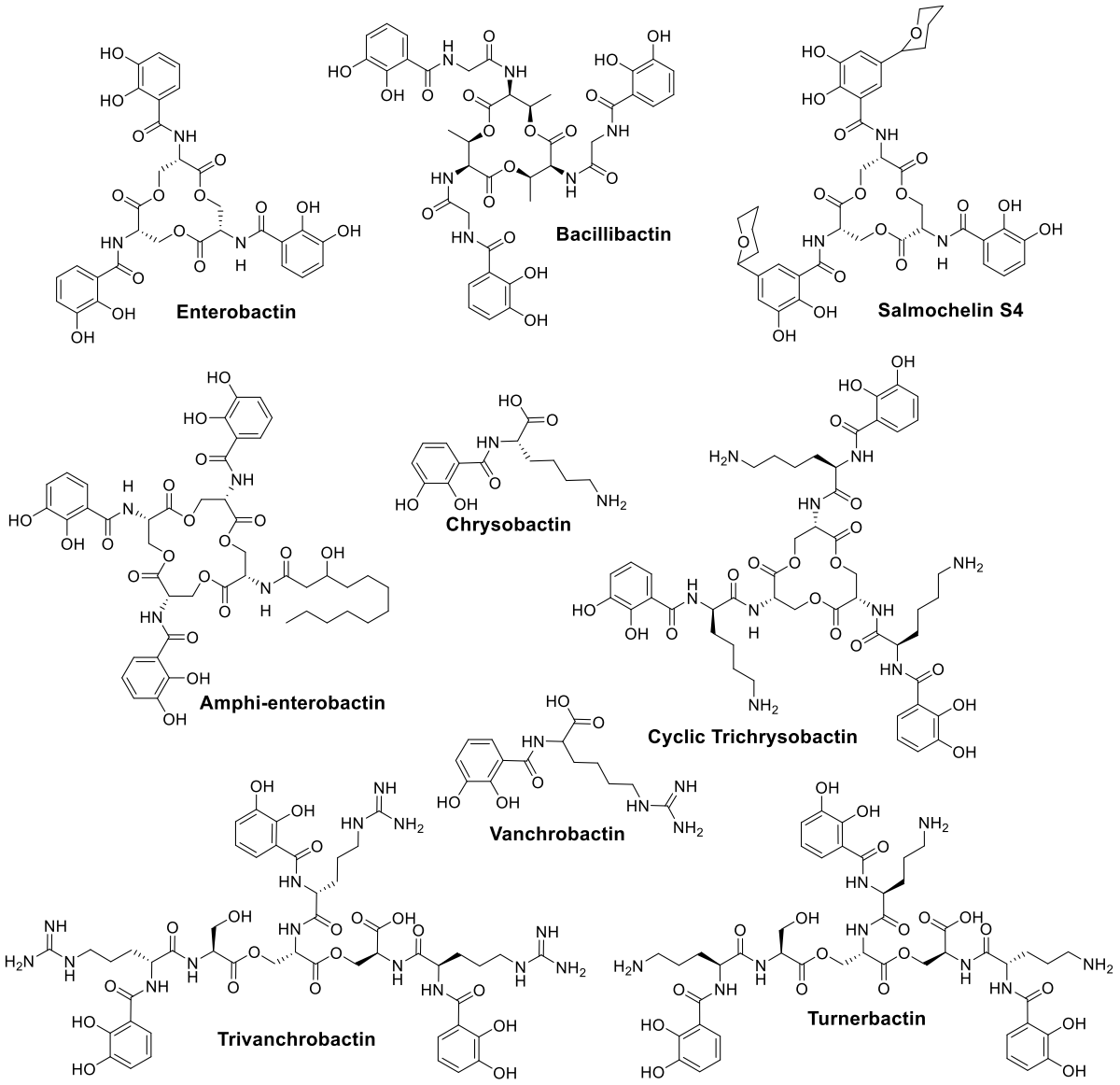

Figure 1.3. Examples of cyclic and linear tris-catechol siderophores.

Other tris-catecholate siderophores incorporate an additional amino acid spacer between the L-Ser and catechol moiety, in turn constructing a 2,3-DHB-XX-L-Ser motif. In the following examples, the spacer residues are the cationic amino acids arginine, lysine, and ornithine. Vanchrobactin from *Vibrio anguillarum*,[16] is a monomeric unit composed of 2,3-DHB-D-Arg-L-Ser, and chrysobactin from *Dickeya dadantii* 3937,[17] is a monomer unit composed of 2,3-DHB-D-Lys-L-Ser. The following siderophores are composed of three units

of the 2,3-DHB-XX-L-Ser motif. Trivanchrobactin, from *Vibrio campbellii* DS40M4,[18] is a trimer composed of 2,3-DHB-D-Arg-L-Ser, cyclic trichrysobactin from *Dickeya chrysanthemi* EC16, [19] is a trimer composed of 2,3-DHB-D-Lys-L-Ser, and turnerbactin from *Teredinibacter turnerae* T7901,[20] is a trimer of 2,3-DHB-L-Orn-L-Ser (Figure 1.3).

Not all catecholate siderophores resemble enterobactin or fall into the serine-catecholate family of siderophores that have been depicted above. The amonabactins isolated from *Aeromonas hydrophila*, is an example of a different linear catecholate siderophore.[21-23] This bis-catecholate siderophore has four structural variations and is composed of an amino acid backbone containing two lysines, and varies with the incorporation of either a phenylalanine or a tryptophan and an optional glycine. [21-23] Other linear catecholate siderophores, all produced by *Azotobacter vinelandii* include protochelin, azotochelin, and aminochelin (Figure 1.4).[24-26]

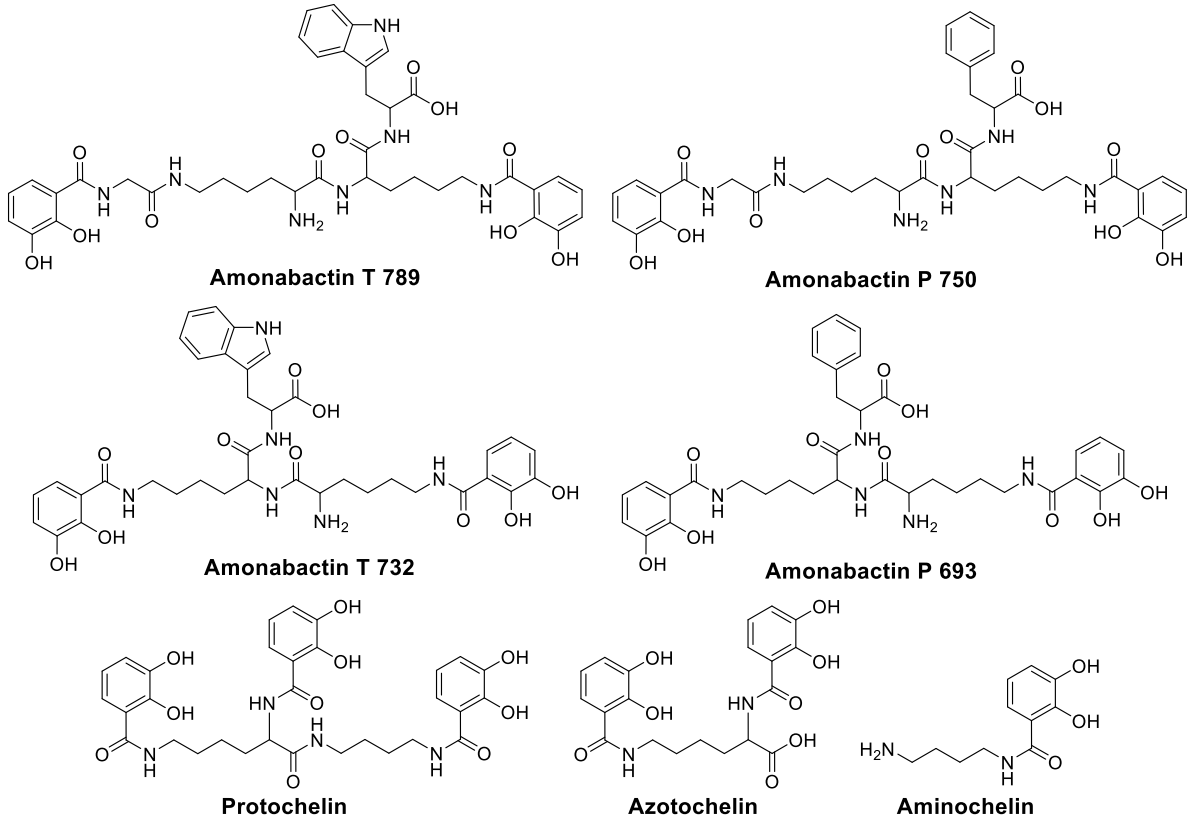

Figure 1.4. Examples of other types of linear catecholate siderophores.

1.2.2. Hydroxamate Siderophores

The hydroxamate functional group is a bidentate ligand produced by the hydroxylation and acylation of a primary amine.[27] Desferrioxamines are a well-studied family of siderophores, with the hydroxamate moiety composed of units of succinic acid and a monohydroxylated diamine (N-hydroxycadaverine or N-hydroxyputrescine). This siderophore can either be linearized or cyclized. Hexadentate Fe(III)-coordination of desferrioxamine is provided by three hydroxamate moieties, but the siderophore itself can have from two to four hydroxamate functional groups.[28-30] Most common hydroxamates in peptidic siderophores are formed through the hydroxylation and acylation of the side chain amine in ornithine. First the ornithine is N^5-hydroxylated by a flavin-dependent monooxygenase.[31] Then an acyltransferase

catalyzes the formation of δ-N-acyl-N-hydroxyornithine, forming either a δ-N-acetyl-N-hydroxyornithine (AcOHOrn) or δ-N-formyl-N-hydroxyornithine (fOHOrn). Known peptidic siderophores containing the hydroxamate moiety include amphibactins, produced by *Alcanivorax borkumensis* SK2 and by several *Vibrio* species.[32-34] At this point, the modified ornithine residue can also undergo cyclization of the δ-N-hydroxyornithine to form cyclic hydroxyornithine (cOHOrn). Delftibactin produced by *Delftia acidovorans* contains an ornithine the undergoes N^5-hydroxylation and cyclization.[35]

1.2.3. β-Hydroxyaspartate Siderophores

β-Hydroxyaspartate (β-OHAsp) is found in many peptidic siderophores and provides bidentate OO' coordination to Fe(III).[36] The first siderophore structurally characterized containing a β-OHAsp Fe(III)-binding group was pseudobactin, a member of the pyoverdine siderophore family produced by *Pseudomonas* B10.[37] Examples of β-OHAsp siderophores include acidobactins,[38] alterobactins,[39] delftibactin,[35] and malleobactins.[40, 41] Other examples include β-OHAsp siderophores that are acylated and have been isolated from both marine and terrestrial bacteria. Some acyl peptidic siderophores with the β-OHAsp Fe(III)-binding group include aquachelins,[32] loihichelins,[42] marinobactins,[43] crochelins[44] and variobactins.[38]

β-OHAsp siderophores are synthesized by NRPS and a key step in the formation of this residue is the hydroxylation of aspartic acid. Different from other amino acids, β-OHAsp has two chiral centers, one at the α-carbon and the other at the β-carbon and in turn creating the possibility of stereoisomers, L-*threo* (2S, 3S), D-*threo* (2R, 3R), L-*erythro* (2S, 3R), or D-*erythro* (2R, 3S) (Figure 1.5). Most β-OHAsp siderophores are either L-*threo* or D-*threo*, and

on occasion L-*erythro*, however D-*erythro* β-OHAsp residue has not yet been identified in a siderophore.

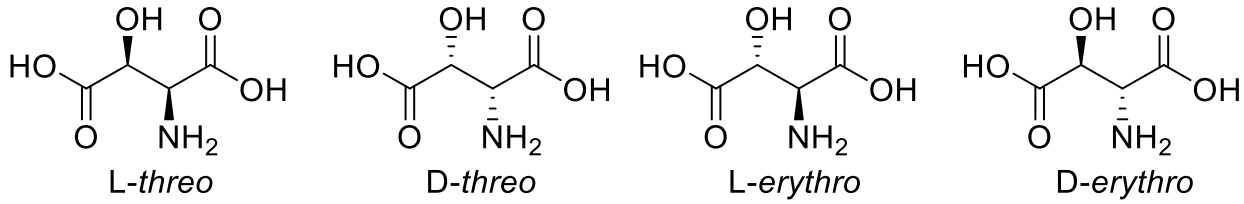

Figure 1.5. Diastereomers of β-OHAsp. Stereoisomers L-*threo*, D-*threo*, and L-*erythro* have been observed in siderophores, while D-*erythro* has not yet been observed.

1.2.4. Amphiphilic Siderophores

Another structural feature commonly found in marine siderophores is the incorporation of a lipophilic fatty acid tail attached to a hydrophilic Fe(III)-binding headgroup, resulting in an amphiphilic compound.[32] Production of amphiphilic siderophores encompasses a wide range of bacterial species ranging from marine bacteria to certain human pathogens. These amphiphilic siderophores can be hydrophobic and remain associated with the cell or can be hydrophilic and are isolated from the supernatant of harvested cultures. Amphibactins, isolated from *Alcanivorax borkumensis* SK2,[33] are hydrophobic acyl siderophores with short peptides (4 amino acids) and long fatty acyl chains ($\geq$ C16).[32, 34]

Hydrophilic siderophores contain longer peptidic headgroups but can still have fatty acid chains that range in length, hydroxylation, and degree of unsaturation. Two amphiphilic siderophores considered quite hydrophilic are aquachelins and loihichelins (Figure 1.6).[32, 42] Marinobactins produced by *Marinobacter sp.* DS40M6, have a six amino acid headgroup with a suite of varying fatty acid chain length (12-18 carbons).[32, 45] The length of the fatty acid does have an effect on hydrophobicity of the siderophore, where the longer chained marinobactins associate with the bacterial cell membrane while the shorter fatty acid chains are released into

the environment.[45] The majority of marine siderophores have been isolated as suites of amphiphiles.[32, 46-48]

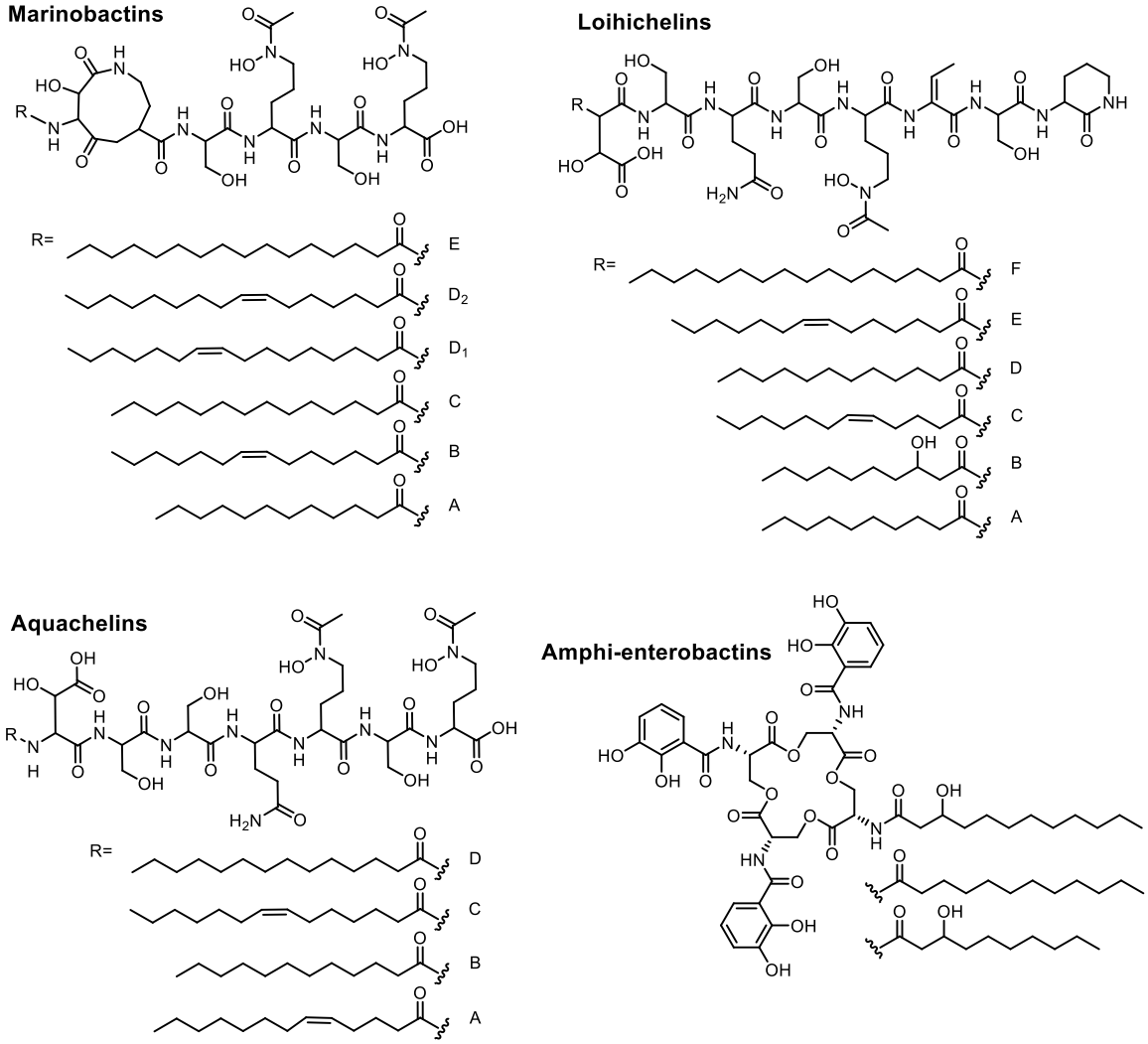

Figure 1.6. Structures of amphiphilic marine siderophores.[14, 32, 42, 48]

Amphi-enterobactin originally isolated from the marine bioluminescent bacterium *Vibrio harveyi* BAA-1116 (reclassified as *Vibrio campbellii*) is a fatty acid derivative related to enterobactin.[14] Further studies have identified that this amphiphilic siderophore is produced by a variety of microbial *Vibrio* species.[15] Like enterobactin, amphi-enterobactin is a triscatecholate siderophore, however it is framed on an expanded tetralactone core comprised

of four L-Ser residues, of which one L-Ser is appended by a fatty acid while the remaining L-Ser residues are appended by 2,3-dihydroxybenzoate (DHB).

1.3. Stability of Ferric Siderophore Complexes

The coordination chemistry properties of siderophores includes forming thermodynamically stable complexes due to the extraordinary specificity for binding Fe(III). The proton-independent Fe(III) stability constant (K_f) represents the stability of the Fe(III)-siderophore complex and are among the highest known Fe(III) stability constants.[10, 49] To offer a meaningful, more physiologically-relevant visual of complex stability, the pFe scale was developed. The pFe is defined as $-\log[Fe(H_2O)_6^{3+}]$ at a defined set of experimental conditions, where $[Fe]_{total}$ = 1 μM, [L] = 10 μM, and pH 7.4.[50] The stability constants of selected siderophores are shown in Table 1.1 below.

Table 1.1. Fe(III)-siderophore stability constants and pFe measurements of selected Fe(III)-siderophore complexes along with Fe(III)-EDTA.

Siderophore	$logK_f$	pFe^{III}
Enterobactin[10]	49.0	34.3
Bacillibactin[51]	47.6	33.1
Desferrioxamine B[52]	30.5	25
Marinobactin[53]	31.8	25.8
Acetohydroxamic acid[54]	28.3	14.8
Vibrioferrin[55]	24.02	18.4
EDTA[56]	25.2	23.4

Hexadentate siderophores form more stable complexes in comparison to bidentate or tetradentate siderophores. The proton independent stability constant of acetohydroxamic acid is K_f=$10^{28.3}$, while for desferrioxamine B it is K_f =$10^{30.5}$, in turn illustrating this effect. The proton independent Fe(III) stability constant for enterobactin is K_f = 10^{49}, making this hexadentate siderophore the most powerful ferric ion complexing agent.[10] The trilactone core

helps make it a stable complex and in turn makes it difficult for reductases to directly reduce and release the iron from the Fe(III)-enterobactin complex. Hydrolysis of the trilactone core to $(DHB\text{-}^{L}Ser)_3$ was found to substantially lower the stability complex to 10^{43}.[57] This less stable complex then allows for easier removal of iron that can then be used in other metabolic processes.

Reduction potentials of Fe(III)-siderophore complexes are quite negative. Ferric enterobactin exhibits an exceptionally low reduction potential (-1.0 V above pH 10), suggesting the ligand must first be hydrolyzed to improve the iron release process.[58] At a pH>10, ferric enterobactin has a formal reduction potential (E_f) of -986mV vs the normal hydrogen electrode, and shows a reversible one-electron wave.[58] From the pH dependence of this potential, the study estimated that at pH 7, ferric enterobactin would have a reduction potential of -750 mV.[58] Both of these values are well below the range of physiological reducing agents like NADPH, suggesting a chemical modification such as hydrolysis to the siderophore is necessary to allow iron to be released via ferric ion reduction.

1.4. Chirality of Fe(III)-Siderophore Complexes

Upon Fe(III) coordination, the metal center of the hexadentate Fe(III)-siderophore complex becomes chiral. Two enantiomers are possible: the right-handed (Δ) configuration, and the left-handed (Λ) configuration (Figure 1.7). Circular dichroism (CD) spectroscopy and X-ray crystallography are used to determine the chirality of the metal center. The overall structure of the ligand affects the chirality of the Fe(III)-center, and the smallest change can affect the chirality. The chirality of the metal center can in turn have an affect on siderophore recognition and uptake.[9, 59-61]

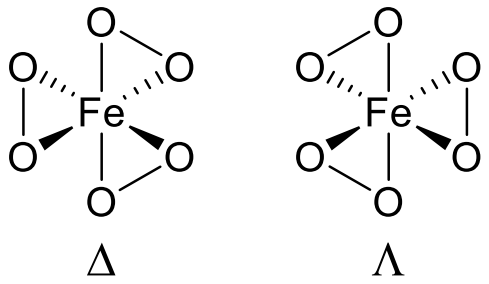

Figure 1.7. Enantiomers of Fe(III) coordinated by three bidentate ligands with either a Δ or Λ configuration.

Two well-known triscatechol siderophores, enterobactin (Ent), a trimeric macrolactone of 2,3-dihydroxybenzoate (DHB)-^{L}Ser, and bacillibactin (BB), a cyclic trimeric ester of 2,3-DHB-Gly-^{L}Thr, coordinate Fe(III) in a hexadentate fashion with the catecholate ligands. On top of the different residues in the macrolactone core, BB contains a glycine residue acting as a spacer between each L-Thr and DHB. The chirality at the metal center of these two similar siderophores are opposite of one another, where Fe(III)-Ent^{3-} adopts the Δ configuration,[62 63] while Fe(III)-BB^{3-} adopts the Λ configuration.[62] Enantioenterobactin was synthesized with D-Ser in the macrolactone core and formed the Λ complex when coordinated to Fe(III).[64] Other triscatechol siderophores containing a chiral amino acid inserted between the oligoester backbone and DHB have also adopted enantiomeric configurations at the Fe(III) site (Table 1.2). For instance, cyclic trichrysobactin a triscatechol oligoester (DHB-^{D}Lys-^{L}Ser)$_3$ produced by *Dickeya chrysanthemi* EC16,[19] and frederiksenibactin, a linear triscatechol ester (DHB-^{L}Lys-^{L}Ser)$_3$, produced by *Yersinia frederiksenii* ATCC 33641,[65] bind Fe(III) in Λ and Δ configurations, respectively.[65] Another example of siderophores forming pair opposite configurations are trivanchrobactin (DHB-^{D}Arg-^{L}Ser)$_3$ and ruckerbactin (DHB-^{L}Arg-^{L}Ser)$_3$.[66] These four siderophores contain the cationic amino acids, $^{D/L}$Lys or $^{D/L}$Arg, and are considered diastereomers. There is one other triscatechol siderophore, turnerbactin, (DHB-^{L}Orn-^{L}Ser)$_3$,[20]

with the cationic amino acid ^{L}Orn. However, a diastereomer with ^{D}Orn has not yet been reported.

Table 1.2. Stereochemistry of amino acids and the chirality around the Fe(III) metal center of selected hexadentate Fe(III)-siderophore complexes.

Siderophore	1st Loaded Amino Acid	2nd Loaded Amino Acid	Chirality
Enterobactin	L-Ser		Δ
Enantioenterobactin	D-Ser		Λ
Frederiksenibactin	L-Lys	L-Ser	Δ
Cyclic trichrysobactin	D-Lys	L-Ser	Λ
Ruckerbactin	L-Arg	L-Ser	Δ
Trivanchrobactin	D-Arg	L-Ser	Λ
Turnerbactin	L-Orn	L-Ser	Δ
Unidentified	D-Orn	L-Ser	

1.5. Biosynthesis of Siderophores

Siderophores compromised of an assortment of proteogenic and non-proteogenic amino acids depend on NRPS for biosynthesis.[67, 68] A secondary biosynthesis pathway for siderophores is a NRPS independent (NIS) pathway that assembles siderophores composed of alternating dicarboxylic acid and diamine or amino alcohol components.[69] However, the focus here will be on the NRPS dependent biosynthesis.

1.5.1. General NRPS Mediated Biosynthesis

Peptidic siderophores are assembled by a thiol-templated catalytic mechanism carried out by non-ribosomal peptide synthetases (NRPS). NRPS is a modular enzyme that uses an assembly line approach to synthesize the peptidic metabolites. [70 71] The modules that make up NRPS are each responsible for activating and incorporating a single amino acid into the growing peptide chain. The NRPS module at a minimum is composed of a condensation (C)

domain, an adenylation (A) domain, and a thiolation (T) domain (often referred to as the peptidyl carrier protein, or PCP domain) (Figure 1.8). [71] [72] The A domain is responsible for selecting the desired substrate, either a specific amino acid or a hydroxy acid, and activating it to form the corresponding amino acyl-adenylate through a reaction of the selected substrate with ATP.[73] [74] The newly formed amino acyl-adenylate is then loaded by the A domain onto the terminal thiolate of the prosthetic 4'-phosphopantetheinyl arm bound to the thiolation domain, allowing for further reactivity of the substrate.[75] Once the amino acids are covalently linked to the 4-phosphopantetheinyl arm, the condensation (C) domain catalyzes the coupling between two thiolation domain-bound substrates, forming the first amide bond.[76] This process is repeated until all residues have been incorporated and the complete product is transferred to the thioesterase (TE) domain, which catalyzes the release of the final product through hydrolysis, generating the free acid, or through intramolecular cyclization, generating a lactone.[77] [78] Once released from the assembly line, the siderophore can undergo further tailoring or be exported into the environment.

Other additional domains found in NRPS add complexity to the siderophore structure and bioactivity of the peptide. These domains provide modifications to the amino acids that are not commonly found in ribosomally produced peptides.[79] A few examples of these additional domains include domains that provide substrate modifications such as oxidation,[80] N-methylation, [81] [82] N-formylation,[72] cyclization,[72] and reduction.[72] The epimerization domain, which will be discussed in Chapter 2, is responsible for the racemization of L- to D-amino acids.[83] Other tailoring enzymes responsible for modifying the peptide before, during, or after chain elongation, are often found near the biosynthetic gene cluster of that siderophore.[84]

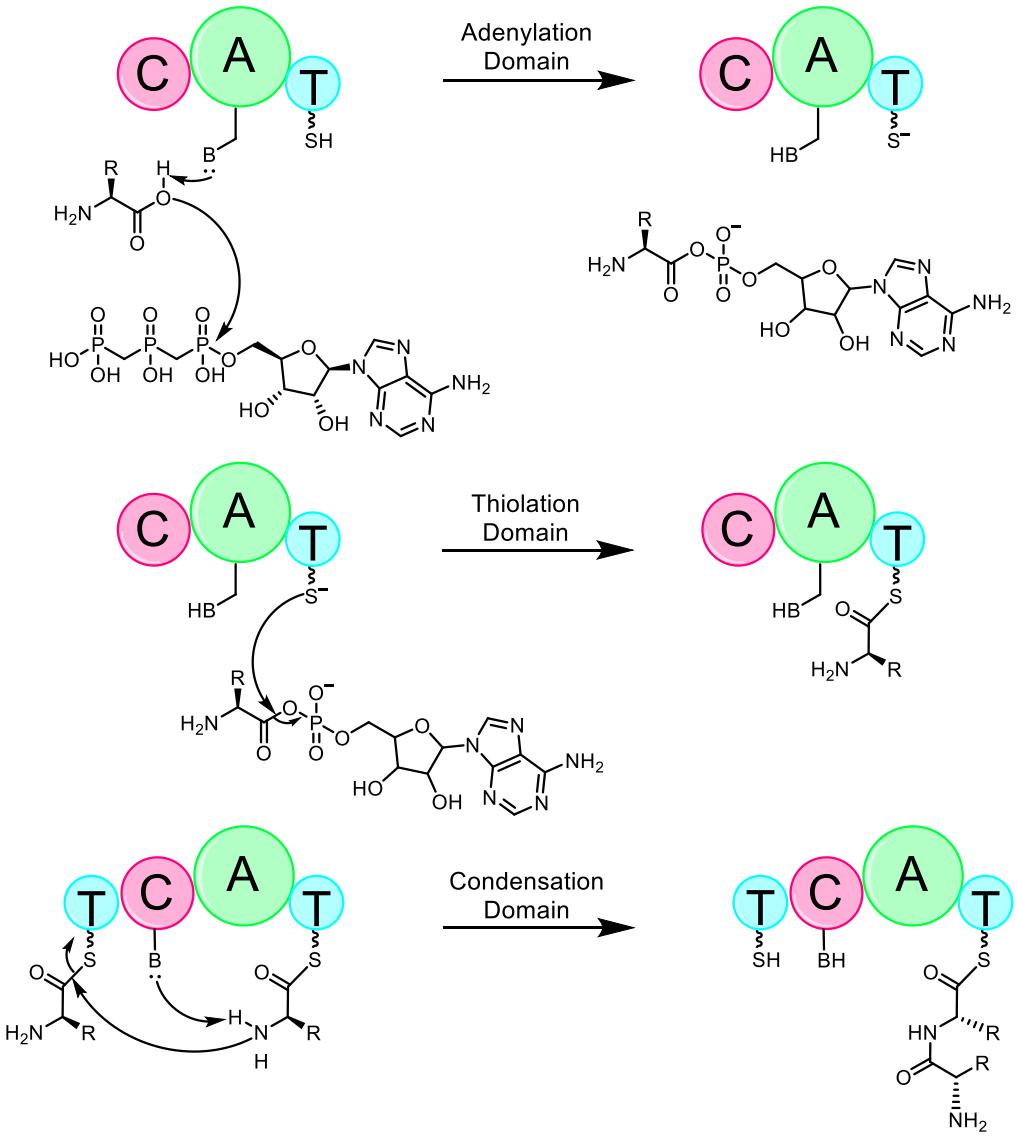

Figure 1.8. The basic enzymatic domains in a NRPS protein: A – adenylation; T – thiolation; C – condensation.

1.5.2. Biosynthetic Origins of Several Chelating Groups

1.5.2.1. 2,3-Dihydroxybenzoate (DHB)

2,3-dihydroxybenzoate (2,3-DHB) is synthesized from chorismate in a three-step biosynthesis catalyzed by three proteins, an isochorismate synthase, isochorismatase, and a

2,3-dihydro-2,3-dihydroxybenzoate dehydrogenase. [72] [85] For incorporation into a peptidyl siderophore, the synthesized 2,3-DHB needs to be activated by a DHB-AMP ligase, which is then transferred to the specified NRPS aryl carrier protein (Figure 1.9).[72] [85] In the case of enterobactin biosynthesis, EntA is the 2,3-dihydro-2,3-dihydroxybenzoate dehydrogenase, the N-terminus of EntB is an isochorismatase, and EntC is an isochorismate synthase. Once DHB is synthesized it is activated by adenylation by the protein EntE.[72] [85] The 2,3-DHB found in siderophores is made by EntABCE homologs. [72] [85]

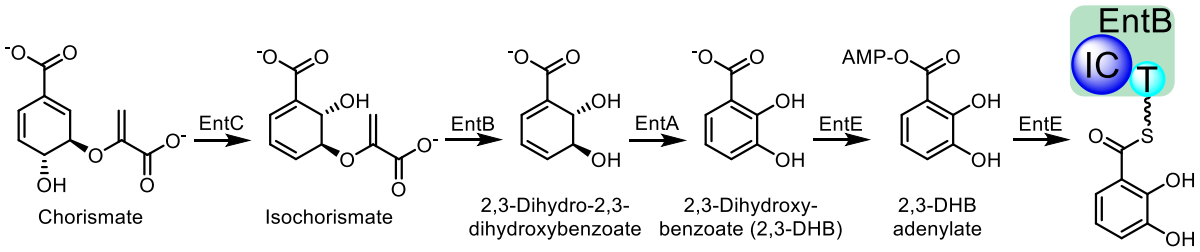

Figure 1.9. Synthesis and activation of 2,3-DHB by proteins EntABCE. IC – isochorismatase; T – thiolation domain.

1.5.2.2. β-Hydroxyaspartate

β-hydroxylation of a residue can happen to aspartic acids and histidines via a family of non-heme Fe(II)/α-ketoglutarate dependent β-hydroxylases (Figure 1.10).[86] These enzymes are thought to act on the aspartic acid or histidine when it is tethered to the thiolation domain of a NRPS, due to the homology of these enzymes to a syringomycin aspartyl β-hydroxylase.[86]

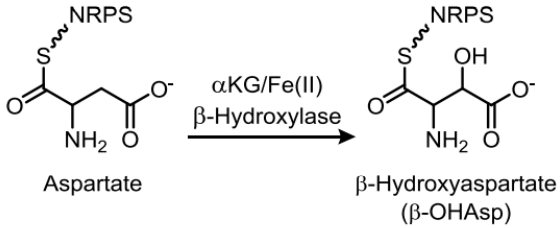

Figure 1.10. Biosynthesis of β-hydroxyaspartate.

1.5.2.3. Hydroxamate

The hydroxamate chelating group comes from the hydroxylation and acylation of a primary amine. Hydroxamates are commonly found in siderophores with the nonproteinogenic amino acid ornithine. The ornithine is N^5-hydroxylated by a flavin-dependent monooxygenase, then followed by either an acyltransferase, which catalyzes the formation of (δ-*N*-acyl-*N*-hydroxy)ornithine, either as (δ-*N*-formyl-) or (δ-*N*-acetyl-δ-*N*-hydroxy)ornithine (Figure 1.11).[31] Cyclic *N*-hydroxyornithine is formed through the lactamization of δ-*N*-hydroxyornithine (Figure 1.12).

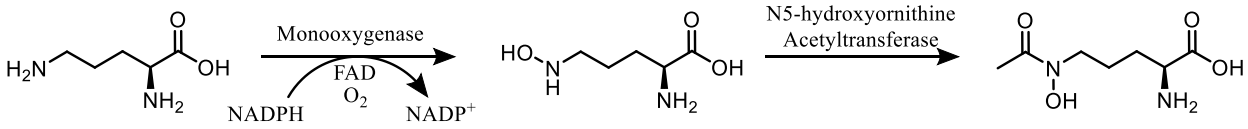

Figure 1.11. Biosynthesis of N5-acetyl-N5-hydroxyornithine via a FAD-dependent monooxygenase followed by a N5-hydroxyornithine acetyltransferase.

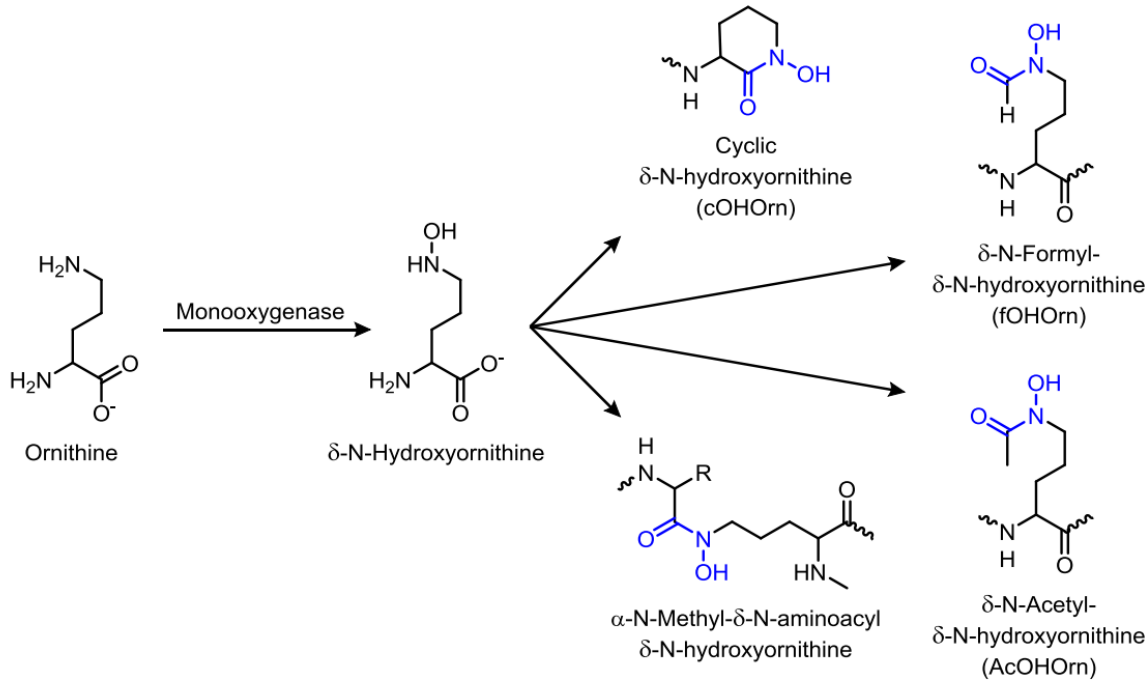

Figure 1.12. Biosynthesis of the hydroxamate chelating group in ornithine.

1.5.3. Biosynthesis of Enterobactin

The biosynthesis of enterobactin has been studied extensively.[72] Proteins involved in the biosynthesis are EntABCDEF. EntA is a 2,3-dihydro-2,3-dihydroxybenzoate dehydrogenase, the N-terminus of EntB is an isochorismatase, and EntC is an isochorismate synthase. These three proteins are involved in the synthesis of 2,3-dihydroxybenzoate (DHB) and once synthesized is activated by adenylation by the protein EntE.[72 85] EntF, the iterative NRPS is where each ester and amide bond found in enterobactin is formed. EntD is the 4'-phosphopantetheinyl transferase required in activating the T domains of EntB and EntF. For the biosynthesis of enterobactin, first the A domain in EntF recognizes and adenylates L-Ser and then transferred to the 4'-phosphopantetheinyl (P-pant) arm of the T domain. The formation of the first DHB-^{L}Ser amide bond is catalyzed by the C domain. The DHB-^{L}Ser is transferred to the thioesterase (Te) domain, and the following iteration follows. Once the trimer is formed, macrocyclization occurs and the final enterobactin product is released (Figure 1.13).

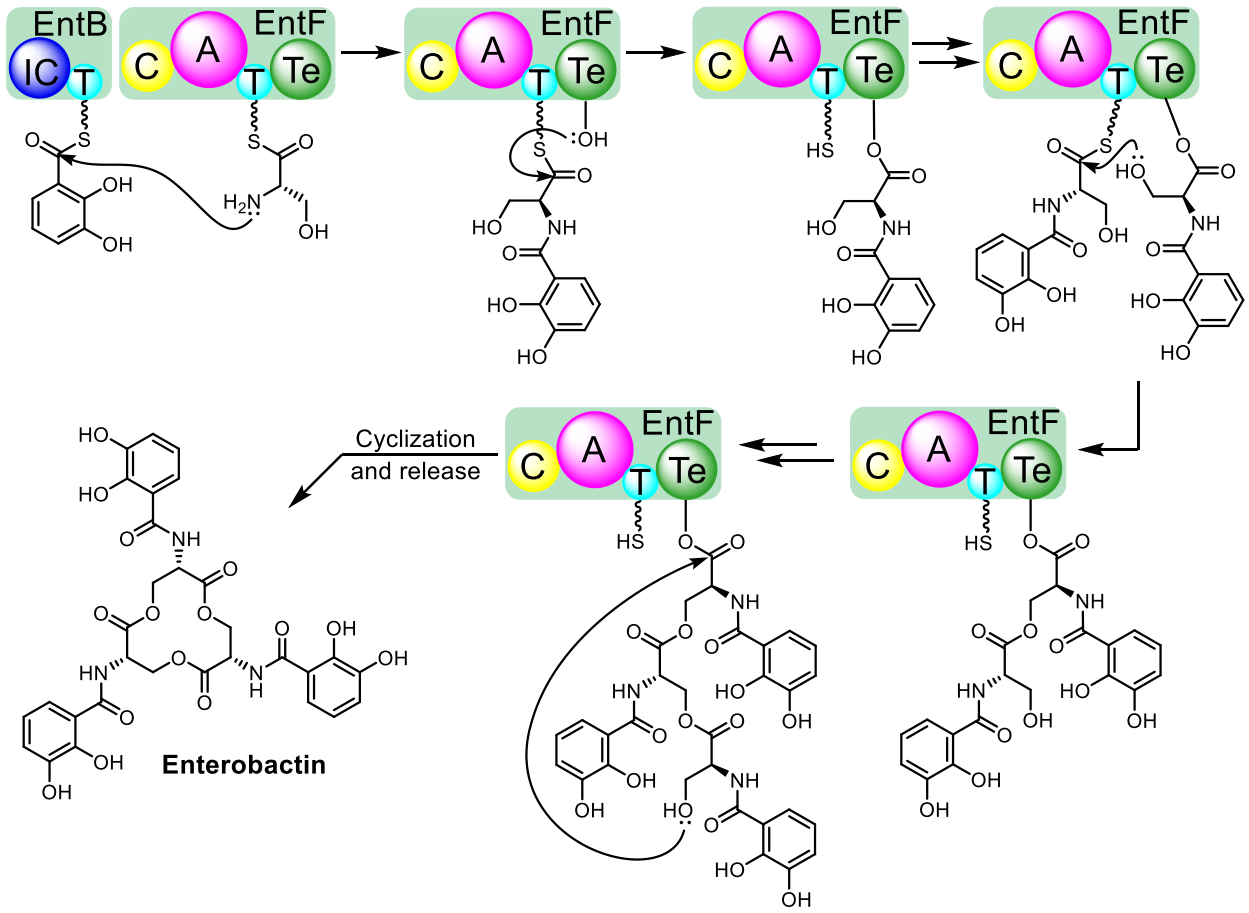

Figure 1.13. Biosynthesis of enterobactin by NRPS. C – condensation domain; A – adenylation domain; T – Thiolation domain; Te – thioesterase domain; IC – isochorismatase.

1.5.4. Biosynthesis of Amphi-enterobactin

Amphi-enterobactin was initially isolated from *Vibrio harveyi* BAA-1116, a model bacterium for quorum sensing because of its quorum-regulated bioluminescence.[87] *Vibrio harveyi* BAA-1116 contains genes homologous to the biosynthetic cluster of enterobactin (Figure 1.14), but instead produces an amphiphilic derivative of enterobactin called amphi-enterobactin (Figure 1.6).[14] Amphi-enterobactin is a triscatecholate siderophore and resembles enterobactin with three 2,3-DHB groups, however it is distinguished by an expanded tetralactone core, and is decorated by a fatty acid appended at the amine of the additional L-

Ser.[14] The 3-hydroxydodecanoate is the most prevalent fatty acid, but these fatty acid appendages can range in length (C10-C16), degree of unsaturation, and hydroxylation.[14 15]

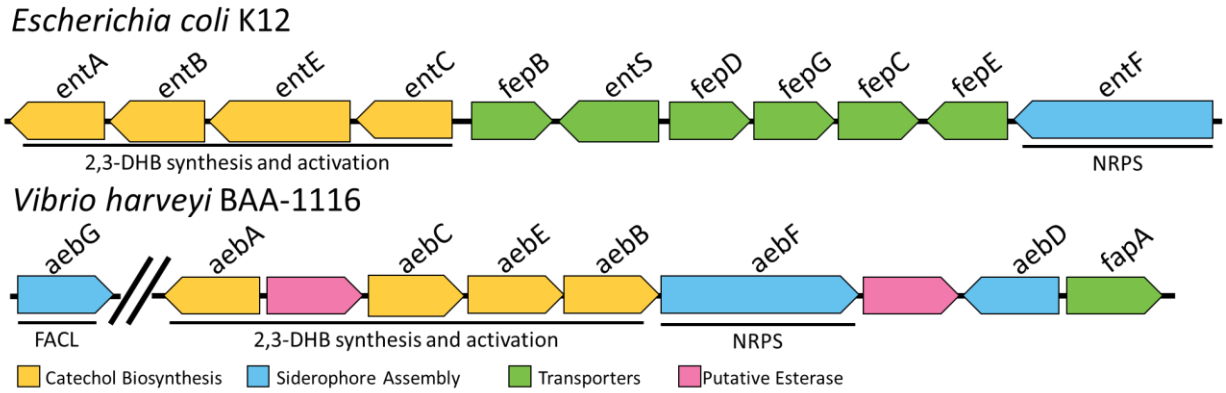

Figure 1.14. Biosynthesis gene clusters of enterobactin in *E. coli* K12 and of amphi-enterobactin in *V. harveyi* BAA-1116.

The genome of *V. harveyi* BAA-1116 contains a nonribosomal peptide synthetase (NRPS) gene cluster (*aebF*) that resembles that of enterobactin biosynthesis.[14] However, nearby this NRPS gene cluster, a gene, *aebG*, encoded for long-chain fatty acid CoA ligase (FACL) is present.[14] Along with structurally characterizing this novel siderophore, the biosynthetic genes of amphi-enterobactin were reported (Figure 1.14).[14] The proposed amphi-enterobactin biosynthetic pathway (Figure 1.15) involves six genes (*aebA-F*), where *aebF* encodes for NRPS that catalyzes amide and ester bond formation and cyclization of the lactone backbone. The *aebG* gene is responsible for activating the fatty acids to fatty acyl-CoA thioesters.[14] After activation, the fatty acyl-CoA is condensed onto L-serine as the first iteration of the NRPS. Similar to EntF, the following three iterations involve the addition of three DHB-^{L}Ser monomers to the fatty acyl-^{L}Ser bound to the thioesterase.[14] Despite the similarity of AebF to EntF, the condensation domain of AebF recognizes two donors: 2,3-DHB-P-pant-AebB and fatty acyl-CoA thioester, to catalyze the DHBA amidation and fatty acid acylation

of L-Ser-*S*-P-pant-AebF. On the other hand, the condensation domain of EntF catalyzes amide bond formation between 2,3-DHB-P-pant-EntB and L-Ser-*S*-P-pant-EntF. This unique feature of AebF, where the condensation domain recognizes two different donors, is the first demonstration of a condensation domain with this level of substrate flexibility. Studies on the amphi-enterobactin biosynthetic machinery revealed that a knockout mutation of *aebG* disturbs amphi-enterobactin biosynthesis.[14] Furthermore, the fatty acyl-CoA must be condensed in the first iteration or else recombinant AebF will not react with DHB-P-pant-AebB.[14]

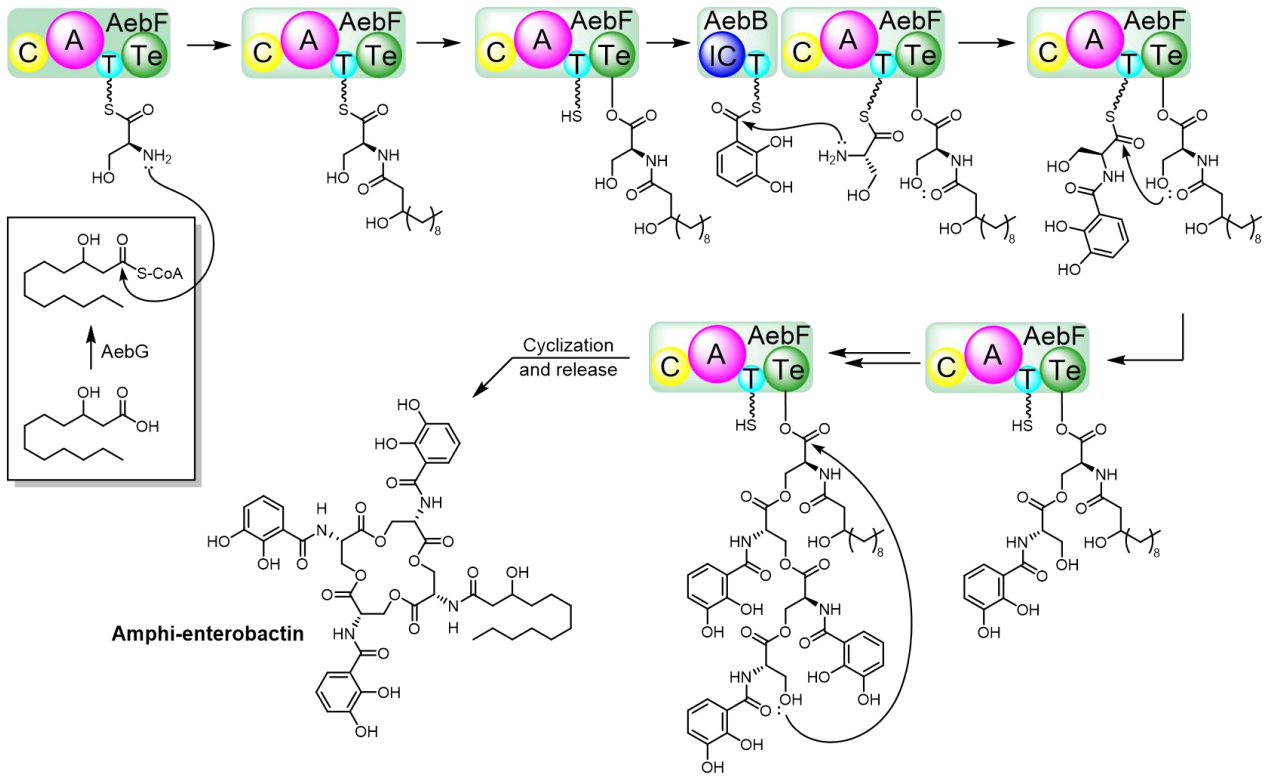

Figure 1.15. Proposed biosynthesis of amphi-enterobactins. AebG activates a fatty acid that is then condensed with L-serine as the first iteration of AebF. The next three iterations condense 2,3-DHB to L-Serine, followed by cyclization and release of the siderophore. C – condensation domain; A – adenylation domain, T – thiolation domain; Te – thioesterase domain; IC – isochorismatase.

1.6. Occasions of Premature Release of Siderophores during Biosynthesis

Premature release of siderophores during biosynthesis would occur when the nonribosomal peptide synthetase is exposed to solvent molecules and in turn hydrolytically terminating the growing siderophore (Figure 1.16). There have not been many occasions documented about siderophores being prematurely released in the environment, however a few studies have shown premature release precursors in cell-free reconstitution studies. For instance, premature release precursors were identified during a cell-free reconstitution of cyclosporine synthetase, which is believed to be caused by the absence of an essential factor to complete the overall synthesis.[88]

In a study by Guo et. al., a large number of enterobactin linear precursors were prematurely released during an *in vitro* reconstitution of the nonribosomal enterobactin synthetase. [89] The group investigated the factors influencing the cause of this premature release.[89] The study noted that previous investigations focused on a cell-free reconstitution of NRPS, a condition that differs substantially from a highly crowded intracellular environment.[90] Therefore, Guo et. al. created *in vitro* crowding conditions in attempt to mimic the intracellular environment and found that macromolecular crowding (mimicking the intracellular environment) suppresses the premature release of the linear precursors from enterobactin NRPS biosynthesis.[89] This study is the first experimental evidence of how macromolecular crowding and mimicking the intracellular environment is essential during *in vitro* reconstitution to have a normally functioning nonribosomal peptide synthetase.[89] Further studies on the structural changes of the enterobactin synthetase in a crowded environment emphasize that macromolecular crowding is an important physiological factor for normal function of NRPSs.[91] Overall, occasions of premature release of siderophores can occur, however it is highly more likely during cell-free *in vitro* reconstitution of the NRPS biosynthesis rather than spontaneous hydrolytic termination in a normal intracellular environment.

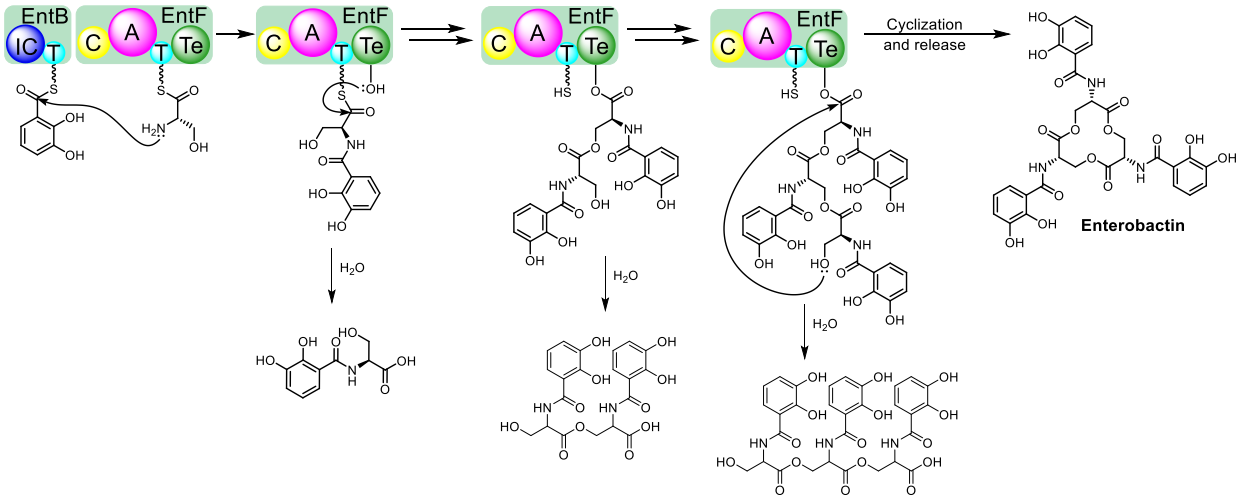

Figure 1.16. Representation of the premature release products in enterobactin biosynthesis if premature hydrolytic termination with water occurred. C – condensation domain; A – adenylation domain; T – Thiolation domain; Te – thioesterase domain; IC – isochorismatase.

1.7. Siderophore Transport and Iron Release

1.7.1. Siderophore Export

Once siderophores are biosynthesized, these natural products are actively transported into the environment. Enterobactin, for example, is first translocated into the periplasm by an active efflux pump, EntS,[92] then excreted into the environment through TolC, an outer membrane channel protein that is used by other efflux systems as well.[93] Further studies identified that deletion of *tolC* eliminates enterobactin export, while deletion of *entS* reduces enterobactin export. The biosynthesis and uptake pathways of siderophores has been well studied, but many questions still remain about siderophore export pathways.

1.7.2. Uptake of Fe(III)-Siderophore Complexes

Fe(III)-siderophore complexes are too large for diffusion through the outer membrane and need to be actively transported. The complexes follow the overall pathway of recognition by the outer membrane receptor, transport by the periplasmic binding proteins to a cytoplasmic membrane permease, typically an ATP binding cassette (ABC) transporter, and translocation into the cytoplasm (Figure 1.17). Uptake is specific to the bacterial strain and the Fe(III)-siderophore complex being transported, whether it be the native siderophore or a xenosiderophore. The following sections will cover recognition by the outer membrane receptors, key points for transport by periplasmic binding proteins and iron(III) release by either esterases or reductases.

Enterobactin produced by *Escherichia coli* is a macrolactone trimer of *N*-2,3-dihydroxy-benzoyl-L-serine that coordinates iron(III) with three 2,3-diydroxybenzoate (DHB)

catechol groups. The proton independent Fe(III) stability constant for enterobactin is $K_f = 10^{49}$, making this siderophore the most powerful ferric ion complexing agent.[10] When iron binds to enterobactin in the environment, the complex is first recognized by a TonB-dependent outer membrane receptor, FepA, and transported into the periplasm.[94 95] Then FepB, a periplasmic binding protein, transports the complex to the inner membrane via recognition of an ABC-type transporter (FepCDG) and ultimately ends up in the cytoplasm.[94 96 97]

Iron release from Fe(III)-bound enterobactin then requires a two-step process, where first the trilactone esters are enzymatically hydrolyzed by the cytoplasmic esterase Fes and then reduced by the NADPH-dependent reductase for iron release. [58 98 99] The Fes esterase hydrolyzes the lactone core of enterobactin into three molecules of 2,3-DHB, which lowers the iron stability constant and allows iron release by the YqjH-mediated reduction of Fe(III) to Fe(II).[58 100 101] The ferrous ion is now liberated and used for necessary cellular metabolic pathways.

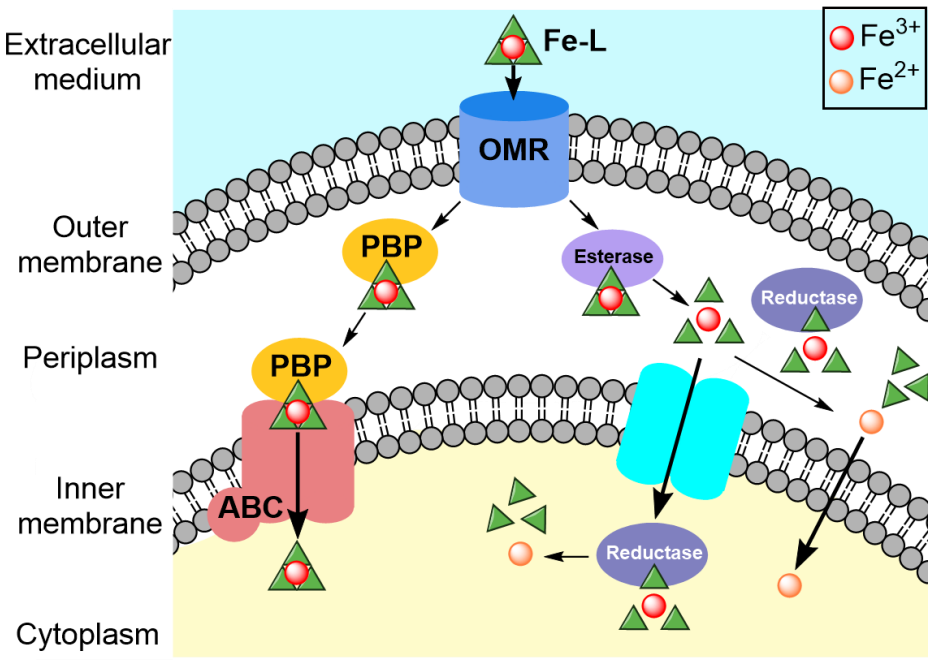

Figure 1.17. General iron-siderophore acquisition model in Gram-negative bacteria. Iron-siderophore complex is recognized by the outer membrane receptor (OMR; blue), interacts with a periplasmic binding protein (PBP, yellow), and transported into the cytoplasm via cytoplasmic ATP-binding proteins (ABC, red).

1.7.2.1. Enterobactin as a Xenosiderophore

Enterobactin is used in a strategy known as siderophore piracy as the xenosiderophore amongst microorganisms that do not contain the genes that encode for enterobactin biosynthesis. For iron release from the Fe(III)-enterobactin complex, hydrolysis by an esterase and reduction of Fe(III) to Fe(II) must occur. In *E. coli*, where enterobactin is the native siderophore, an esterase called Fes, catalyzes the hydrolysis of both apo- and ferric enterobactin ester linkages.[99] Therefore, microorganisms that do not produce enterobactin but utilize it as a xenosiderophore need to express the esterase specific for macrolactone hydrolysis.

The following bacteria use enterobactin as an xenosiderophore: *Pseudomonas aeruginosa, Vibrio anguillarum, V. cholerae, V. parahaemolyticus,* and *Campylobacter jejuni*.

[102] [103] [104] [105] [106] [107] These strains synthesize native siderophores, but also use enterobactin as an additional iron-chelating metabolite. Enterobactin is taken up by these microorganisms in diverse ways. A stark difference among these five strains is that two strains, *P. aeruginosa* and *V. anguillarum* utilize cyclic enterobactin, while the remaining three are only able to utilize the linearized enterobactin.

1.7.2.2. Outer Membrane Receptors

Outer membrane receptors are the first recognition sites of the ferric siderophore complex. Selection of siderophore uptake begins at this point and can be the rate-limiting step in the iron uptake mechanism.[108] For example, the OMR in *E. coli*, FepA, is able to recognize both Fe(III)-enterobactin and Fe(III)-enantioenterobactin.[109] FepA has been structurally characterized and crystallized (Figure 1.18).[110] Other outer membrane receptors including FhuA (ferrichrome/hydroxamates) in *E. coli*, FpvA (pyoverdine) and FptA (pyochelin) in *P. aeruginosa* have also been characterized by X-ray crystallography.[111-113] These siderophore receptor proteins consist of β-barrel domain and a plug, where the plug sits within the β-barrel domain, creating a seal when the channel is not actively transporting Fe(III)-siderophore complexes.[111-113] Within the outer membrane protein, in this case for FepA, there are two binding sites for Fe(III)-enterobactin. Recognition of the iron(III)-siderophore complex is dependent on the triscatechol functional groups and the amide linkage interacting with certain aromatic residues within the binding domain of FepA.[109]

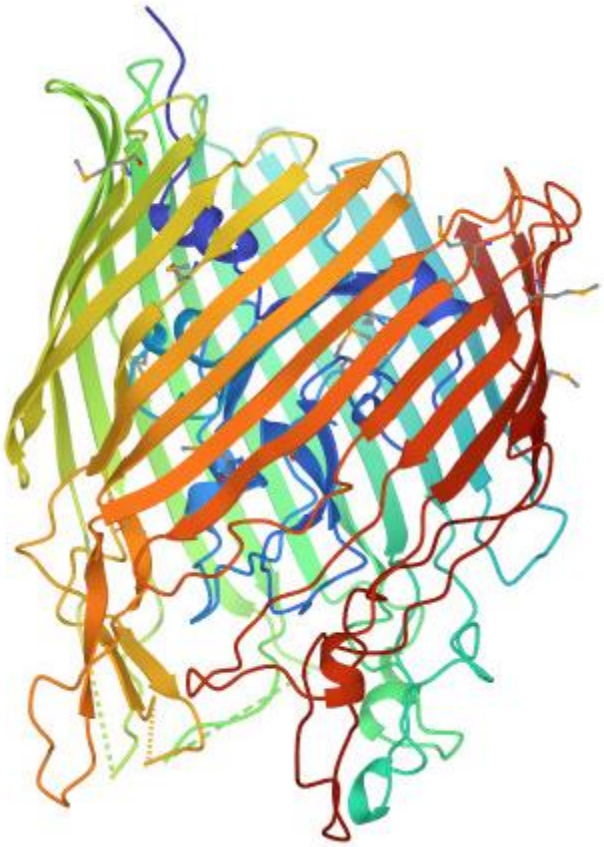

Figure 1.18. Crystal structure of the OMR FepA. The β-barrel domain is depicted in the red, orange, and green, while the plug is blue. (PDB cod 1FEP).[110]

The first step of iron(III)-siderophore uptake is the recognition and binding of the complex by its specific outer membrane receptor. Every OMR is able to recognize and transport a specific siderophore, and sometimes a structurally related siderophore, however, it will not recognize a chemically different siderophore.[114 115 116 117] For example, *Vibrio cholerae* synthesizes vibriobactin, the native triscatecholate siderophore with a nonhydrolyzable backbone to import iron, but the strain also utilizes linear derivatives of enterobactin as xenosiderophores.[118 106] The recognition and uptake of these two siderophores differs at the outer membrane receptor. Vibriobactin is transported across the outer membrane by ViuA, while the linear derivatives of enterobactin are recognized by VctA and IrgA.[119 120] This

phenomena is also predicted in *Vibrio parahaemolyticus* where genes homologous to the OMR genes in *V. cholerae*, *irgA* and *vctA*, were identified.[107] However, the study of receptor specificity has not been completed for *V. parahaemolyticus* and it is unknown if the OMRs function similarly to the ones identified in *V. cholerae*. [107] Models for Fe(III)-enterobactin acquisition as a xenosiderophore in five Gram-negative bacterial strains are shown in Figure 1.19.

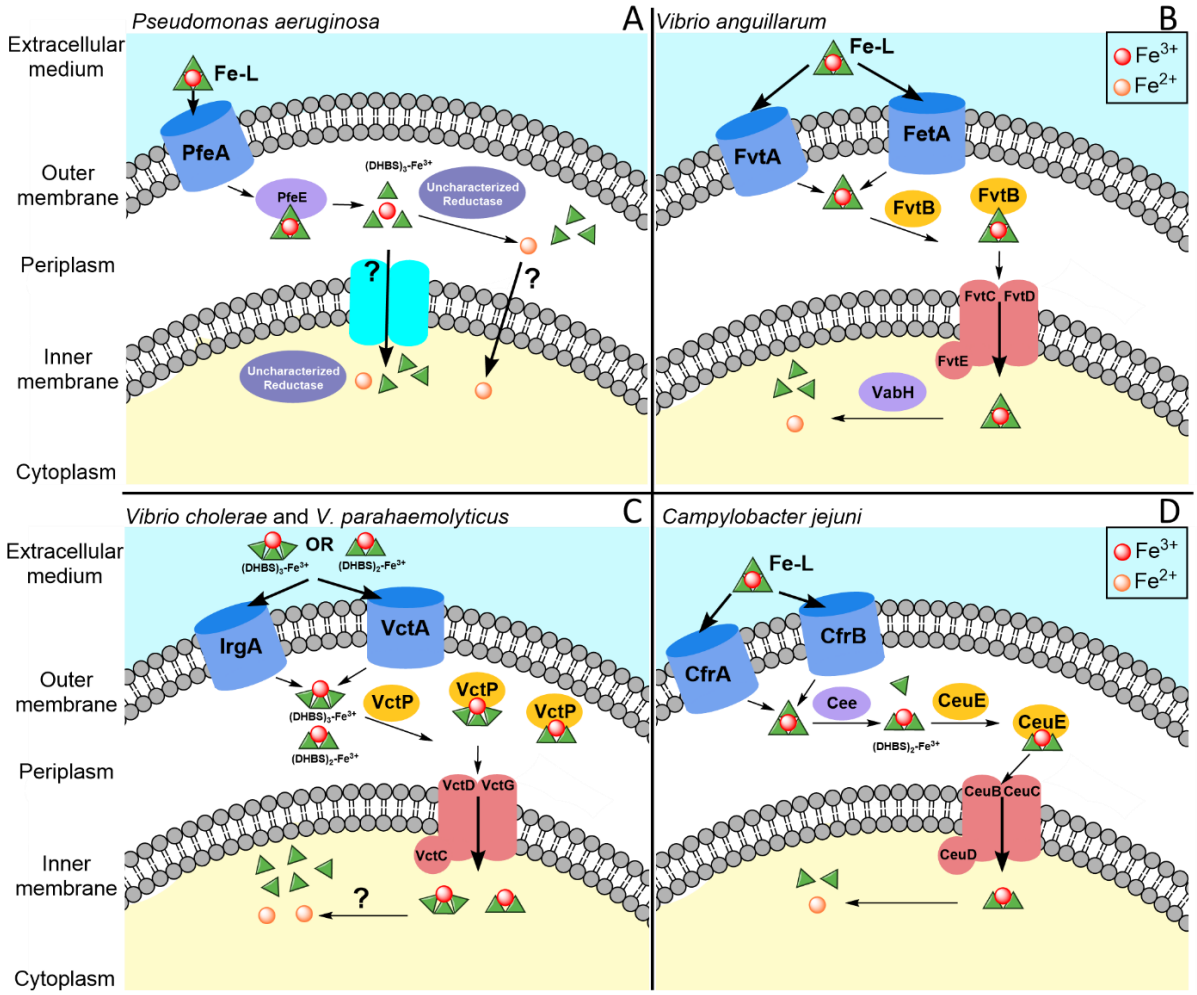

Figure 1.19. Models for Fe-ENT acquisition and release in Gram-negative bacteria. The outer membrane receptors are shown in blue, periplasmic binding proteins are shown in yellow, esterases are shown purple, and the cytoplasmic ATP-binding proteins are shown in red. Fe-L stands for Fe(III)-enterobactin. Questions marks point to unidentified/uncharacterized parts of the uptake mechanism. Uptake systems are shown for (A) *P. aeruginosa*; (B) V. *anguillarum*; (C) *V. cholerae* and *V. parahaemolyticus*; and (D) *C. jejuni*.

1.7.2.3. Periplasmic Binding Proteins

Certain OMRs have evolved to bind a variety of siderophores that have similar chemical structures. Periplasmic binding proteins on the other hand may be more specific towards certain siderophores and can be a point of exclusion. Interaction with these proteins is a key component in the iron uptake mechanism of Gram-negative bacteria. After transport into the periplasm, the Fe(III)-siderophore complex interacts with a periplasmic binding protein (PBP), which brings the complex to the ABC-transporter embedded in the inner membrane and the complex is translocated to the cytoplasm (Figure 1.17).

In *E. coli*, the periplasmic binding protein is FepB which binds to cyclic enterobactin.[94] *Pseudomonas aeruginosa* on the other hand does not have a PBP specific for Fe(III)-enterobactin because iron release occurs in the periplasm. The PBP involved in transport of enterobactin in *Vibrio cholerae*, VctB, differs in comparison to the PBPs of *E. coli* and *V. anguillarum*, in the sense that VctB recognizes only the linearized enterobactin complexes, whereas FepB (*E. coli* PBP) and FvtB (*V. anguillarum* PBP) recognizes cyclic enterobactin.[106] Since the iron transport system shows homology to *V. cholerae* the same observation is suspected in *V. parahaemolyticus*.[107]

Unlike many bacterial strains, *Campylobacter jejuni* does not produce its own siderophores, but instead depends on xenosiderophores for iron acquisition.[121] Originally, it was proposed that Fe(III)-bound cyclic enterobactin was transported into the periplasm, then recognized by the PBP CeuE, and ultimately transported into the cytoplasm. [121] [122] [123] However, further research has demonstrated that *C. jejuni* utilizes enterobactin hydrolysis products for the uptake of iron. [121] [124] [125] [126] The OMR's of *C. jejuni* are able to recognize cyclic enterobactin and transport the complex into the periplasm. The sole trilactone esterase

in *C. jejuni* is located in the periplasm.[124] Further analysis of this Fe(III) acquisition model has shown that the PBP, CeuE, binds to the enterobactin dimer hydrolysis product, $[Fe(bisDHBS)]^{2-}$ with higher affinity than $[Fe(Ent)]^{3-}$.[126]

1.7.3. Iron Release from Catechol Siderophores

Mechanisms of iron release from siderophores falls under three possible pathways: an enzymatic chemical modification, proton-assisted dissociation of the complex, or reduction via a reductase of the Fe(III) center.[99 127] Reduction of Fe(III) is a common strategy for releasing iron from the Fe(III)-siderophore complex because reduction lowers the affinity of the siderophore for Fe(II) and in turn releasing it.[128 129]

1.7.3.1. Catechol Siderophore that Require an Esterase

Fe(III)-enterobactin being a stable complex, the Fe(III) is unable to be directly reduced by a reductase and released from the complex. Instead, once Fe(III) binds to enterobactin and transported into the cell, the siderophore trilactone core is enzymatically hydrolyzed by the esterase Fes into three equivalent molecules of 2,3-DHB-Ser.[99] The reduction potential of Fe(III)-enterobactin is -750 mV at pH 7, well outside the range of physiological reducing agents such as reductases.[58] Once the trilactone backbone of Fe(III)-enterobactin is hydrolyzed, the reduction potential becomes -350 mV, now within the range of physiological reducing agents.[58, 130] The reductase involved in reducing Fe(III) bound to enterobactin is YqjH in *Escherichia coli*.[58 98 99 100] More information is covered in the following sections. Iron release has been studied for enterobactin, but other siderophores, like amphi-enterobactin, not much is known.

Fes is the most well-known esterase that hydrolyzes enterobactin. Other esterases that fall into the same class as Fes include IroD and IroE that hydrolyze salmochelin in *Salmonella enterica* and BesA that hydrolyzes bacillibactin in *Bacillus subtilis*. [98 99 96 9] In strains that take up enterobactin as an xenosiderophore, there have been three esterases identified: PfeE for *P. aeruginosa*,[131] VabH *for V. anguillarum*,[103, 132] and Cee for *C. jejuni* (Figure 1.19).[124]

The esterase in *P. aeruginosa* is located in the periplasm and once ferric-enterobactin is transported by the outer membrane into the periplasm, the siderophore is hydrolyzed by PfeE.[131] Interestingly, the gene encoding this esterase is localized next to the *pfeA* gene (encodes the OMR), and transcription of both of these genes are regulated by the presence of enterobactin.[131]

Iron(III)-enterobactin uptake in *V. anguillarum* follows the same uptake pathway as for its native siderophore vanchrobactin.[103] [104] Once the Fe(III)-bound cyclized enterobactin is transported into the cytoplasm, it undergoes a chemical modification to allow for the release of iron. It is suggested that VabH is the acting esterase involved in the hydrolysis of both the xenosiderophore enterobactin and the native siderophore vanchrobactin due to the structural similarities of the two siderophores. [103] [104]

C. jejuni has a sole trilactone esterase, Cee, located in the periplasm.[124] Cee hydrolyzes the Fe(III)-bound cyclized enterobactin and these tetradentate hydrolysis products ($Fe(bisDHBS)]^{2-}$) are then transported via the PBP, CeuE, to the ABC-transporter CeuBCD, and ultimately into the cytoplasm.[124]

1.7.3.2. Iron Release via Reductase

The essentiality of esterases has been revealed in many studies about Fes, IroD, and BesA, the three trilactone hydrolases known to hydrolyze iron(III) bound enterobactin, salmochelin, bacillibactin, respectively. [98] [99] [96] [9] However, successive events following the hydrolysis of the ferric trilactone scaffolds, specifically the process of iron release is not yet fully understood. Focusing on the ferric enterobactin complex, after hydrolysis of the complex, the formation constant of the hydrolysis product still favors complex formation over iron dissociation, thus emphasizing the need for a reductase.[127] [129] Once the ferric siderophore is hydrolyzed, the stability constant is lowered, and the reduction potential of Fe(III) falls into the same range as for ferric hydroxamate siderophores. [127] [129] These ferric hydroxamate siderophores involve a ferric reductase for iron release.[127] [129] After the reduction of Fe(III), Fe(II) is released from the complex and used in other metabolic pathways. Very little is known about Fe(III)-siderophore dissociation involving reductases and only a few siderophore pathways have been investigated. For Fe(III) release from enterobactin in *E. coli*, a NADPH-dependent reductase, YqjH, directly follows hydrolysis and catalyzes iron release from enterobactin.[100]

YqjH belongs to the ferredoxin reductase-like family but differs from a ferredoxin reductase (FNR) in that YqjH favors the flow of electrons from NADPH to ferric substrates, whereas a FNR transfers an electron from reduced ferredoxin to $NADP^+$.[100] This characteristic shows that the goal of YqjH is iron assimilation rather than NADPH generation.[100]

Another known reductase ViuB, found in *V. cholerae,* is known to reduce the Fe(III)-vibriobactin complex.[106] [119] It is identified as a siderophore-interacting protein (SIP) and belongs to the same SIP oxidoreductase family as YqjH. [106] [119] Vibriobactin is a triscatecholate

siderophore with a nonhydrolyzable backbone therefore an esterase is not necessary to promote iron release. These two known reductases already differ, where YqjH is efficient in reducing the hydrolyzed siderophore while ViuB favors the intact ferric triscatecholate complex. This differentiation is dependent on the reduction potential of the ferric complex itself and whether or not hydrolysis is first required to improve the reduction potential. A summary of the associated proteins involved in iron(III) uptake for these bacterial strains is found in Table 1.3.

Table 1.3. A summary list of siderophores used by the selected bacterial species and the associated proteins involved in iron(III) uptake.

Species and siderophore	Uptake Proteins and Esterases		Iron Release Notes
P. aeruginosa			
Native Siderophores			
Pyoverdine	OMR	FpvA [133]	Iron Released in periplasm
Pyochelin	OMR	FptA [134 135]	Iron Release Unknown
Xenosiderophore			
Enterobactin	OMR	PfeA [102]	Hydrolysis occurs in periplasm
	Periplasmic esterase	PfeE [131]	
V. anguillarum			
Native Siderophores			
Anguibactin	OMR	FatA [136]	Unknown, but suggested an NADPH-dependent ferric reductase is involved
	PBP and ABC Transporter	FatBCDE [136]	
Vanchrobactin	OMR	FvtA [137]	FvtCDE has homology to FatCDE
	PBP and ABC Transporter	FvtBCDE [137]	
	Esterase	VabH [103]	
Xenosiderophore			
Enterobactin	OMR	FvtA/FetA [104]	VabH is suggested as the acting esterase, but not yet confirmed
	PBP and ABC Transporter	FvtBCDE [104]	
	Esterase	VabH [103 104]	
V. cholerae			
Native Siderophores			
Vibriobactin	OMR	ViuA [120 119]	PBP and ABC transporters ViuPDGC and Vct PDGC recognize both vibriobactin and enterobactin
	PBP and ABC Transporter	ViuPDGC [138]	
	Reductase	ViuB [119 106]	
Xenosiderophore			
Enterobactin	OMR	IrgA & VctA [106 105]	Lacks OMR and esterase for cyclic enterobactin. OMRs IrgA and VctA only recognize linear enterobactin (dimer/trimer)
	PBP and ABC Transporter	VctPDGC [106]	
	Esterase	none	
V. parahaemolyticus			
Native Siderophores			
Vibrioferrin	OMR	PvuA [55 139]	Iron release through photolysis
	PBP and ABC Transporter	PvuBCDE [55 139]	
Xenosiderophore			
Enterobactin	OMR	IrgA, VctA, PeuA [107 140]	*Shows homology to V. cholerae. Esterase unknown, but has 74% identity to Fes
	PBP and ABC Transporter	VctPDGC* [107]	
	Esterase	Unidentified	
C. jejuni			
Xenosiderophore			
Enterobactin	OMR	CfrAB [122 141 123]	Utilizes only linear enterobactin. PBP prefers the dimer hydrolysis product.
	Esterase	Cee [124]	
	PBP	CeuE [126]	
	ABC transporter	CeuBCD [126]	
E. coli			
Native Siderophore			
Enterobactin	OMR	FepA [94 95]	Hydrolysis of ester backbone required for iron release
	PBP and ABC Transporter	FepBCDE [94]	
	Esterase	Fes [58 98 99]	
	Reductase	YqjH [100 101]	
S. enterica			
Native Siderophore			
Salmochelin	OMR	IroN [142 143 96]	Hydrolysis of salmochelin required for iron release
	PBP	IroC [142 143 96]	
	Esterase	IroD and IroE [99 12]	
B. subtilis			
Native Siderophore			
Bacillibactin	PBP and ABC Transporter	FeuABC[144]	YclQ binds petrobactin
	PBP	YclQ[145]	
	Esterase	BesA [144]	

1.8. Bioinformatic Techniques

Genome mining has become an important tool in natural product discovery and has expanded the capabilities of bioinformatic tools for genomic analysis.[146] [147] In turn, useful information is extracted from biological databases and used for sequence or structural analysis. A few techniques used for sequence analysis include BLAST, MUSCLE, and HMMR.

1.8.1. Genome Mining for NRPS Biosynthesis Pathways and Siderophore Discovery

In chemistry-driven natural product discovery, genome mining has become an important bioinformatic tool. For siderophore discovery, the NRPS biosynthetic pathway is an ideal genome mining target because of its straightforward architecture, conservation of core enzymatic features, and predictability of substrate specificities.[148] A software tool, antiSMASH, is able to identify NRPS clusters in a genome and identify the component modules and domains, and ultimately predict the substrates, which then allows for the prediction of siderophore structure.[149] The sequence analysis of the adenylation domain in NRPS can help predict the amino acid composition of the siderophore being synthesized through comparison of its Stachelhaus codes.[150] A closer prediction improves the chances of siderophore discovery and techniques like antiSMASH, BLAST, and MUSCLE pull together information for structural predictions.

1.8.2. BLAST: Pairwise Alignments

Pairwise alignment tools like BLAST (Basic Local Alignment Search Tool) to detect sequence similarity is one of the most commonly used techniques in characterizing new sequences.[151 152] It allows one to identify homologous genes or proteins based on the statistical similarity.[151] Homology is identified when the pair of sequences has a high degree of similarity, based on the percent identity output from BLAST.[152]

1.8.3. MUSCLE: Multiple Sequence Alignments

Protein sequence alignment is an important bioinformatic technique that provides information for structure prediction and critical residue identification. A multiple sequence alignment of homologous sequences allows for a visualization of conserved residues, in particular critical residues like those that reside in catalytic sites. A popular algorithm that generates alignments that was used in this work was MUSCLE (MUltiple Sequence Comparison by Log-Expectation).[153]

1.9. Conclusions

The importance of iron and the scarcity of soluble Fe(III) in most environments has pushed microbes to evolve and expand the iron acquisition strategies. The abundance and accessibility of microbial genomic information has opened and facilitated the discovery of novel siderophores as well as providing significant insight into siderophore biosynthetic and regulatory pathways. Many siderophores are synthesized by nonribosomal peptide synthetases, which allow for discovery of new siderophores through genome mining. The novel NRPS biosynthesized siderophores that are isolated and characterized provide further information on

how NRPS assembles these natural products. In turn, this new information allows for closer predictions of other novel siderophores, including the specifics like the stereochemistry of the amino acids that compose the siderophores. As the number of sequenced microbial genomes increases, we expand our ability to uncover the factors and mechanisms governing iron recognition and release from the Fe(III)-siderophore complexes.

1.10. References

1. Winkelmann, G., Microbial siderophore-mediated transport. Biochemical Society Transactions 2002, 30 (4), 691-696.
2. Boukhalfa, H.; Crumbliss, A. L., Chemical aspects of siderophore mediated iron transport. Biometals 2002, 15 (4), 325-339.
3. Sandy, M.; Butler, A., Microbial Iron Acquisition: Marine and Terrestrial Siderophores. Chemical Reviews 2009, 109 (10), 4580-4595.
4. Hider, R. C.; Kong, X., Chemistry and biology of siderophores. Natural product reports 2010, 27 (5), 637-657.
5. Crosa, J. H.; Mey, A. R.; Payne, S. M.; American Society for Microbiology., Iron transport in bacteria. ASM Press,: Washington, D.C., 2004; pp. 1 online resource (xix, 499 p. ill., charts, tables, diagrs. ASM eBooks. Restricted to UCB IP Addresses. http://www.asmscience.org/content/book/10.1128/9781555816544.
6. Cornelis, P.; Andrews, S. C., Iron uptake and homeostasis in microorganisms. Caister Academic Press: 2010.
7. Raymond, K. N.; Telford, J. R., Siderophore-Mediated Iron Transport in Microbes. In Bioinorganic Chemistry: An Inorganic Perspective of Life, Kessissoglou, D. P., Ed. Springer Netherlands: Dordrecht, 1995; pp 25-37.
8. Pollack, J. R.; Neilands, J. B., Enterobactin, an iron transport compound from Salmonella typhimurium. Biochemical and Biophysical Research Communications 1970, 38 (5), 989-992.
9. Abergel, R. J.; Zawadzka, A. M.; Hoette, T. M.; Raymond, K. N., Enzymatic Hydrolysis of Trilactone Siderophores: Where Chiral Recognition Occurs in Enterobactin and Bacillibactin Iron Transport. Journal of the American Chemical Society 2009, 131 (35), 12682-12692.
10. Loomis, L. D.; Raymond, K. N., Solution equilibria of enterobactin and metal-enterobactin complexes. Inorganic Chemistry 1991, 30 (5), 906-911.
11. May, J. J.; Kessler, N.; Marahiel, M. A.; Stubbs, M. T., Crystal structure of DhbE, an archetype for aryl acid activating domains of modular nonribosomal peptide synthetases. Proceedings of the National Academy of Sciences 2002, 99 (19), 12120.
12. Hantke, K.; Nicholson, G.; Rabsch, W.; Winkelmann, G., Salmochelins, siderophores of Salmonella enterica and uropathogenic Escherichia coli strains, are

recognized by the outer membrane receptor IroN. Proc Natl Acad Sci U S A 2003, 100 (7), 3677-82.
13. Bister, B.; Bischoff, D.; Nicholson, G. J.; Valdebenito, M.; Schneider, K.; Winkelmann, G.; Hantke, K.; Süssmuth, R. D., The structure of salmochelins: C-glucosylated enterobactins of Salmonella enterica§. Biometals 2004, 17 (4), 471-481.
14. Zane, H. K.; Naka, H.; Rosconi, F.; Sandy, M.; Haygood, M. G.; Butler, A., Biosynthesis of Amphi-enterobactin Siderophores by Vibrio harveyi BAA-1116: Identification of a Bifunctional Nonribosomal Peptide Synthetase Condensation Domain. Journal of the American Chemical Society 2014, 136 (15), 5615-5618.
15. Naka, H.; Reitz, Z. L.; Jelowicki, A. L.; Butler, A.; Haygood, M. G., Amphi-enterobactin commonly produced among Vibrio campbellii and Vibrio harveyi strains can be taken up by a novel outer membrane protein FapA that also can transport canonical Fe(III)-enterobactin. JBIC Journal of Biological Inorganic Chemistry 2018, 23 (7), 1009-1022.
16. Soengas, R. G.; Anta, C.; Espada, A.; Paz, V.; Ares, I. R.; Balado, M.; Rodríguez, J.; Lemos, M. L.; Jiménez, C., Structural characterization of vanchrobactin, a new catechol siderophore produced by the fish pathogen Vibrio anguillarum serotype O2. Tetrahedron Letters 2006, 47 (39), 7113-7116.
17. Rauscher, L.; Expert, D.; Matzanke, B. F.; Trautwein, A. X., Chrysobactin-dependent Iron Acquisition inErwinia chrysanthemi : FUNCTIONAL STUDY OF A HOMOLOG OF THE ESCHERICHIA COLIFERRIC ENTEROBACTIN ESTERASE. Journal of Biological Chemistry 2002, 277 (4), 2385-2395.
18. Sandy, M.; Han, A.; Blunt, J.; Munro, M.; Haygood, M.; Butler, A., Vanchrobactin and anguibactin siderophores produced by Vibrio sp. DS40M4. Journal of natural products 2010, 73 (6), 1038-1043.
19. Sandy, M.; Butler, A., Chrysobactin siderophores produced by Dickeya chrysanthemi EC16. Journal of natural products 2011, 74 (5), 1207-1212.
20. Han, A. W.; Sandy, M.; Fishman, B.; Trindade-Silva, A. E.; Soares, C. A. G.; Distel, D. L.; Butler, A.; Haygood, M. G., Turnerbactin, a Novel Triscatecholate Siderophore from the Shipworm Endosymbiont Teredinibacter turnerae T7901. PLoS One 2013, 8 (10), e76151.
21. Telford, J. R.; Leary, J. A.; Tunstad, L. M. G.; Byers, B. R.; Raymond, K. N., Amonabactin: Characterization of a Series of Siderophores from Aeromonas hydrophila. Journal of the American Chemical Society 1994, 116 (10), 4499-4500.
22. Telford, J. R.; Raymond, K. N., Coordination Chemistry of the Amonabactins, Bis(catecholate) Siderophores from Aeromonas hydrophila1. Inorganic Chemistry 1998, 37 (18), 4578-4583.
23. Stintzi, A.; Raymond, K. N., Amonabactin-mediated iron acquisition from transferrin and lactoferrin by Aeromonas hydrophila: direct measurement of individual microscopic rate constants. JBIC Journal of Biological Inorganic Chemistry 2000, 5 (1), 57-66.
24. Cornish, A. S.; Page, W. J., Production of the triacetecholate siderophore protochelin by Azotobacter vinelandii. Biometals 1995, 8 (4), 332-338.
25. Khodr, H.; Hider, R.; Duhme-Klair, A. K., The iron-binding properties of aminochelin, the mono(catecholamide) siderophore of Azotobacter vinelandii. JBIC Journal of Biological Inorganic Chemistry 2002, 7 (7), 891-896.

26. Bellenger, J.-P.; Arnaud-Neu, F.; Asfari, Z.; Myneni, S. C. B.; Stiefel, E. I.; Kraepiel, A. M. L., Complexation of oxoanions and cationic metals by the biscatecholate siderophore azotochelin. JBIC Journal of Biological Inorganic Chemistry 2007, 12 (3), 367-376.
27. Kakkar, R.; Grover, R.; Chadha, P., Conformational behavior of some hydroxamic acids. Org Biomol Chem 2003, 1 (12), 2200-6.
28. Ledyard, K. M.; Butler, A., Structure of putrebactin, a new dihydroxamate siderophore produced by Shewanella putrefaciens. JBIC Journal of Biological Inorganic Chemistry 1997, 2 (1), 93-97.
29. Feistner, G. J.; Stahl, D. C.; Gabrik, A. H., Proferrioxamine siderophores of Erwinia amylovora. A capillary liquid chromatographic/electrospray tandem mass spectrometric study. Organic Mass Spectrometry 1993, 28 (3), 163-175.
30. Nishio, T.; Tanaka, N.; Hiratake, J.; Katsube, Y.; Ishida, Y.; Oda, J., Isolation and structure of the novel dihydroxamate siderophore alcaligin. Journal of the American Chemical Society 1988, 110 (26), 8733-8734.
31. Ge, L.; Seah, S. Y. K., Heterologous Expression, Purification, and Characterization of an l-Ornithine N⁵-Hydroxylase Involved in Pyoverdine Siderophore Biosynthesis in Pseudomonas aeruginosa. Journal of Bacteriology 2006, 188 (20), 7205-7210.
32. Martinez, J. S.; Zhang, G. P.; Holt, P. D.; Jung, H. T.; Carrano, C. J.; Haygood, M. G.; Butler, A., Self-assembling amphiphilic siderophores from marine bacteria. Science 2000, 287 (5456), 1245-7.
33. Kem, M. P.; Zane, H. K.; Springer, S. D.; Gauglitz, J. M.; Butler, A., Amphiphilic siderophore production by oil-associating microbes. Metallomics 2014, 6 (6), 1150-1155.
34. Vraspir, J. M.; Holt, P. D.; Butler, A., Identification of new members within suites of amphiphilic marine siderophores. BioMetals 2011, 24 (1), 85-92.
35. Johnston, C. W.; Wyatt, M. A.; Li, X.; Ibrahim, A.; Shuster, J.; Southam, G.; Magarvey, N. A., Gold biomineralization by a metallophore from a gold-associated microbe. Nature Chemical Biology 2013, 9 (4), 241-243.
36. Hardy, C. D.; Butler, A., β-Hydroxyaspartic acid in siderophores: biosynthesis and reactivity. J Biol Inorg Chem 2018, 23 (7), 957-967.
37. Teintze, M.; Hossain, M. B.; Barnes, C. L.; Leong, J.; Van der Helm, D., Structure of ferric pseudobactin: a siderophore from a plant growth promoting Pseudomonas. Biochemistry 1981, 20 (22), 6446-6457.
38. Johnston, C. W.; Skinnider, M. A.; Wyatt, M. A.; Li, X.; Ranieri, M. R. M.; Yang, L.; Zechel, D. L.; Ma, B.; Magarvey, N. A., An automated Genomes-to-Natural Products platform (GNP) for the discovery of modular natural products. Nature Communications 2015, 6 (1), 8421.
39. Reid, R. T.; Livet, D. H.; Faulkner, D. J.; Butler, A., A siderophore from a marine bacterium with an exceptional ferric ion affinity constant. Nature 1993, 366 (6454), 455-458.
40. Franke, J.; Ishida, K.; Hertweck, C., Plasticity of the Malleobactin Pathway and Its Impact on Siderophore Action in Human Pathogenic Bacteria. Chemistry – A European Journal 2015, 21 (22), 8010-8014.

41. Franke, J.; Ishida, K.; Ishida-Ito, M.; Hertweck, C., Nitro versus Hydroxamate in Siderophores of Pathogenic Bacteria: Effect of Missing Hydroxylamine Protection in Malleobactin Biosynthesis. Angewandte Chemie International Edition 2013, 52 (32), 8271-8275.
42. Homann, V. V.; Sandy, M.; Tincu, J. A.; Templeton, A. S.; Tebo, B. M.; Butler, A., Loihichelins A-F, a suite of amphiphilic siderophores produced by the marine bacterium Halomonas LOB-5. Journal of natural products 2009, 72 (5), 884-888.
43. Martinez, J. S.; Zhang, G. P.; Holt, P. D.; Jung, H.-T.; Carrano, C. J.; Haygood, M. G.; Butler, A., Self-Assembling Amphiphilic Siderophores from Marine Bacteria. Science 2000, 287 (5456), 1245-1247.
44. Baars, O.; Zhang, X.; Gibson, M. I.; Stone, A. T.; Morel, F. M. M.; Seyedsayamdost, M. R., Crochelins: Siderophores with an Unprecedented Iron-Chelating Moiety from the Nitrogen-Fixing Bacterium Azotobacter chroococcum. Angewandte Chemie International Edition 2018, 57 (2), 536-541.
45. Martinez, J. S.; Butler, A., Marine amphiphilic siderophores: Marinobactin structure, uptake, and microbial partitioning. Journal of Inorganic Biochemistry 2007, 101 (11), 1692-1698.
46. Martin, J. D.; Ito, Y.; Homann, V. V.; Haygood, M. G.; Butler, A., Structure and membrane affinity of new amphiphilic siderophores produced by Ochrobactrum sp. SP18. JBIC Journal of Biological Inorganic Chemistry 2006, 11 (5), 633-641.
47. Xu, G.; Martinez, J. S.; Groves, J. T.; Butler, A., Membrane Affinity of the Amphiphilic Marinobactin Siderophores. Journal of the American Chemical Society 2002, 124 (45), 13408-13415.
48. Martinez, J. S.; Carter-Franklin, J. N.; Mann, E. L.; Martin, J. D.; Haygood, M. G.; Butler, A., Structure and membrane affinity of a suite of amphiphilic siderophores produced by a marine bacterium. Proc Natl Acad Sci U S A 2003, 100 (7), 3754-9.
49. Lewis, B. L.; Holt, P. D.; Taylor, S. W.; Wilhelm, S. W.; Trick, C. G.; Butler, A.; Luther, G. W., Voltammetric estimation of iron(III) thermodynamic stability constants for catecholate siderophores isolated from marine bacteria and cyanobacteria. Marine Chemistry 1995, 50 (1), 179-188.
50. McQueen, C. F.; Groves, J. T., A reevaluation of iron binding by Mycobactin J. JBIC Journal of Biological Inorganic Chemistry 2018, 23 (7), 995-1007.
51. Dertz, E. A.; Xu, J.; Stintzi, A.; Raymond, K. N., Bacillibactin-Mediated Iron Transport in Bacillus subtilis. Journal of the American Chemical Society 2006, 128 (1), 22-23.
52. Evers, A.; Hancock, R. D.; Martell, A. E.; Motekaitis, R. J., Metal ion recognition in ligands with negatively charged oxygen donor groups. Complexation of iron(III), gallium(III), indium(III), aluminum(III), and other highly charged metal ions. Inorganic Chemistry 1989, 28 (11), 2189-2195.
53. Zhang, G.; Amin, S. A.; Küpper, F. C.; Holt, P. D.; Carrano, C. J.; Butler, A., Ferric Stability Constants of Representative Marine Siderophores: Marinobactins, Aquachelins, and Petrobactin. Inorganic Chemistry 2009, 48 (23), 11466-11473.
54. Caudle, M. T.; Crumbliss, A. L., Dissociation kinetics of (N-methylacetohydroxamato) iron (III) complexes: A model for probing electronic and structural effects in the dissociation of siderophore complexes. Inorganic Chemistry 1994, 33 (18), 4077-4085.

55. Amin, S. A.; Green, D. H.; Küpper, F. C.; Carrano, C. J., Vibrioferrin, an Unusual Marine Siderophore: Iron Binding, Photochemistry, and Biological Implications. Inorganic Chemistry 2009, 48 (23), 11451-11458.
56. Smith, R. M.; Martell, A. E., Critical stability constants: inorganic complexes. Springer: 1976; Vol. 4.
57. Scarrow, R. C.; Ecker, D. J.; Ng, C.; Liu, S.; Raymond, K. N., Iron(III) coordination chemistry of linear dihydroxyserine compounds derived from enterobactin. Inorganic Chemistry 1991, 30 (5), 900-906.
58. Cooper, S. R.; McArdle, J. V.; Raymond, K. N., Siderophore electrochemistry: relation to intracellular iron release mechanism. Proceedings of the National Academy of Sciences 1978, 75 (8), 3551.
59. Müller, G.; Isowa, Y.; Raymond, K., Stereospecificity of siderophore-mediated iron uptake in Rhodotorula pilimanae as probed by enantiorhodotorulic acid and isomers of chromic rhodotorulate. Journal of Biological Chemistry 1985, 260 (26), 13921-13926.
60. Bergeron, R. J.; Dionis, J. B.; Elliott, G. T.; Kline, S. J., Mechanism and stereospecificity of the parabactin-mediated iron-transport system in Paracoccus denitrificans. J Biol Chem 1985, 260 (13), 7936-44.
61. Brillet, K.; Reimmann, C.; Mislin, G. L. A.; Noël, S.; Rognan, D.; Schalk, I. J.; Cobessi, D., Pyochelin Enantiomers and Their Outer-Membrane Siderophore Transporters in Fluorescent Pseudomonads: Structural Bases for Unique Enantiospecific Recognition. Journal of the American Chemical Society 2011, 133 (41), 16503-16509.
62. Bluhm, M. E.; Kim, S. S.; Dertz, E. A.; Raymond, K. N., Corynebactin and Enterobactin: Related Siderophores of Opposite Chirality. Journal of the American Chemical Society 2002, 124 (11), 2436-2437.
63. Johnstone, T. C.; Nolan, E. M., Determination of the Molecular Structures of Ferric Enterobactin and Ferric Enantioenterobactin Using Racemic Crystallography. Journal of the American Chemical Society 2017, 139 (42), 15245-15250.
64. Neilands, J. B.; Erickson, T. J.; Rastetter, W. H., Stereospecificity of the ferric enterobactin receptor of Escherichia coli K-12. Journal of Biological Chemistry 1981, 256 (8), 3831-3832.
65. Stow, P. R.; Reitz, Z. L.; Johnstone, T. C.; Butler, A., Genomics-driven discovery of chiral triscatechol siderophores with enantiomeric Fe(iii) coordination. Chemical Science 2021, 12 (37), 12485-12493.
66. Thomsen, E.; Reitz, Z. L.; Stow, P. R.; Dulaney, K.; Butler, A., Ruckerbactin Produced by Yersinia ruckeri YRB Is a Diastereomer of the Siderophore Trivanchrobactin Produced by Vibrio campbellii DS40M4. Journal of Natural Products 2022, 85 (1), 264-269.
67. Fischbach, M. A.; Walsh, C. T., Assembly-line enzymology for polyketide and nonribosomal peptide antibiotics: logic, machinery, and mechanisms. Chemical reviews 2006, 106 (8), 3468-3496.
68. Condurso, H. L.; Bruner, S. D., Structure and noncanonical chemistry of nonribosomal peptide biosynthetic machinery. Natural product reports 2012, 29 (10), 1099-1110.

69. Oves-Costales, D.; Kadi, N.; Challis, G. L., The long-overlooked enzymology of a nonribosomal peptide synthetase-independent pathway for virulence-conferring siderophore biosynthesis. Chemical Communications 2009, (43), 6530-6541.
70. Koglin, A.; Walsh, C. T., Structural insights into nonribosomal peptide enzymatic assembly lines. Natural Product Reports 2009, 26 (8), 987-1000.
71. Crosa, J. H.; Walsh, C. T., Genetics and assembly line enzymology of siderophore biosynthesis in bacteria. Microbiology and molecular biology reviews : MMBR 2002, 66 (2), 223-249.
72. Sattely, E. S.; Fischbach, M. A.; Walsh, C. T., Total biosynthesis: in vitro reconstitution of polyketide and nonribosomal peptide pathways. Natural Product Reports 2008, 25 (4), 757-793.
73. Challis, G. L.; Ravel, J.; Townsend, C. A., Predictive, structure-based model of amino acid recognition by nonribosomal peptide synthetase adenylation domains. Chemistry & Biology 2000, 7 (3), 211-224.
74. Rausch, C.; Weber, T.; Kohlbacher, O.; Wohlleben, W.; Huson, D. H., Specificity prediction of adenylation domains in nonribosomal peptide synthetases (NRPS) using transductive support vector machines (TSVMs). Nucleic Acids Res 2005, 33 (18), 5799-808.
75. Lambalot, R. H.; Gehring, A. M.; Flugel, R. S.; Zuber, P.; LaCelle, M.; Marahiel, M. A.; Reid, R.; Khosla, C.; Walsh, C. T., A new enzyme superfamily — the phosphopantetheinyl transferases. Chemistry & Biology 1996, 3 (11), 923-936.
76. Rausch, C.; Hoof, I.; Weber, T.; Wohlleben, W.; Huson, D. H., Phylogenetic analysis of condensation domains in NRPS sheds light on their functional evolution. BMC Evolutionary Biology 2007, 7 (1), 78.
77. Fischbach, M. A.; Walsh, C. T., Assembly-Line Enzymology for Polyketide and Nonribosomal Peptide Antibiotics: Logic, Machinery, and Mechanisms. Chemical Reviews 2006, 106 (8), 3468-3496.
78. Shaw-Reid, C. A.; Kelleher, N. L.; Losey, H. C.; Gehring, A. M.; Berg, C.; Walsh, C. T., Assembly line enzymology by multimodular nonribosomal peptide synthetases: the thioesterase domain of E. coli EntF catalyzes both elongation and cyclolactonization. Chemistry & Biology 1999, 6 (6), 385-400.
79. Walsh, C. T.; Chen, H.; Keating, T. A.; Hubbard, B. K.; Losey, H. C.; Luo, L.; Marshall, C. G.; Miller, D. A.; Patel, H. M., Tailoring enzymes that modify nonribosomal peptides during and after chain elongation on NRPS assembly lines. Current Opinion in Chemical Biology 2001, 5 (5), 525-534.
80. Takahashi, H.; Kumagai, T.; Kitani, K.; Mori, M.; Matoba, Y.; Sugiyama, M., Cloning and Characterization of a Streptomyces Single Module Type Non-ribosomal Peptide Synthetase Catalyzing a Blue Pigment Synthesis*. Journal of Biological Chemistry 2007, 282 (12), 9073-9081.
81. Weber, G.; Schörgendorfer, K.; Schneider-Scherzer, E.; Leitner, E., The peptide synthetase catalyzing cyclosporine production in Tolypocladium niveum is encoded by a giant 45.8-kilobase open reading frame. Current Genetics 1994, 26 (2), 120-125.
82. Gehring, A. M.; DeMoll, E.; Fetherston, J. D.; Mori, I.; Mayhew, G. F.; Blattner, F. R.; Walsh, C. T.; Perry, R. D., Iron acquisition in plague: modular logic in enzymatic biogenesis of yersiniabactin by Yersinia pestis. Chemistry & Biology 1998, 5 (10), 573-586.

83. Linne, U.; Doekel, S.; Marahiel, M. A., Portability of Epimerization Domain and Role of Peptidyl Carrier Protein on Epimerization Activity in Nonribosomal Peptide Synthetases. Biochemistry 2001, 40 (51), 15824-15834.
84. Samel, S. A.; Marahiel, M. A.; Essen, L.-O., How to tailor non-ribosomal peptide products—new clues about the structures and mechanisms of modifying enzymes. Molecular BioSystems 2008, 4 (5), 387-393.
85. Gehring, A. M.; Bradley, K. A.; Walsh, C. T., Enterobactin Biosynthesis in Escherichia coli: Isochorismate Lyase (EntB) Is a Bifunctional Enzyme That Is Phosphopantetheinylated by EntD and Then Acylated by EntE Using ATP and 2,3-Dihydroxybenzoate. Biochemistry 1997, 36 (28), 8495-8503.
86. Singh, G. M.; Fortin, P. D.; Koglin, A.; Walsh, C. T., β-Hydroxylation of the Aspartyl Residue in the Phytotoxin Syringomycin E: Characterization of Two Candidate Hydroxylases AspH and SyrP in Pseudomonas syringae. Biochemistry 2008, 47 (43), 11310-11320.
87. Lilley, B. N.; Bassler, B. L., Regulation of quorum sensing in Vibrio harveyi by LuxO and Sigma-54. Molecular Microbiology 2000, 36 (4), 940-954.
88. Zocher, R.; Nihira, T.; Paul, E.; Madry, N.; Peeters, H.; Kleinkauf, H.; Keller, U., Biosynthesis of cyclosporin A: partial purification and properties of a multifunctional enzyme from Tolypocladium inflatum. Biochemistry 1986, 25 (3), 550-3.
89. Guo, Z.-F.; Jiang, M.; Zheng, S.; Guo, Z., Suppression of Linear Side Products by Macromolecular Crowding in Nonribosomal Enterobactin Biosynthesis. Organic Letters 2008, 10 (4), 649-652.
90. Zimmerman, S. B., Macromolecular crowding effects on macromolecular interactions: Some implications for genome structure and function. Biochimica et Biophysica Acta (BBA) - Gene Structure and Expression 1993, 1216 (2), 175-185.
91. Guo, Z.-F.; Jiang, M.; Zheng, S.; Guo, Z., Structural change of the enterobactin synthetase in crowded solution and its relation to crowding-enhanced product specificity in nonribosomal enterobactin biosynthesis. Bioorganic & Medicinal Chemistry Letters 2010, 20 (13), 3855-3858.
92. Furrer, J. L.; Sanders, D. N.; Hook-Barnard, I. G.; McIntosh, M. A., Export of the siderophore enterobactin in Escherichia coli: involvement of a 43 kDa membrane exporter. Molecular Microbiology 2002, 44 (5), 1225-1234.
93. Bleuel, C.; Große, C.; Taudte, N.; Scherer, J.; Wesenberg, D.; Krauß, G. J.; Nies, D. H.; Grass, G., TolC Is Involved in Enterobactin Efflux across the Outer Membrane of Escherichia coli. Journal of Bacteriology 2005, 187 (19), 6701-6707.
94. Stephens, D. L.; Choe, M. D.; Earhart, C. F., Escherichia coli periplasmic protein FepB binds ferrienterobactin. Microbiology 1995, 141 (7), 1647-1654.
95. Ecker, D. J.; Matzanke, B. F.; Raymond, K. N., Recognition and transport of ferric enterobactin in Escherichia coli. Journal of Bacteriology 1986, 167 (2), 666.
96. Zhu, M.; Valdebenito, M.; Winkelmann, G.; Hantke, K., Functions of the siderophore esterases IroD and IroE in iron-salmochelin utilization. Microbiology 2005, 151 (7), 2363-2372.
97. Neumann, W.; Sassone-Corsi, M.; Raffatellu, M.; Nolan, E. M., Esterase-Catalyzed Siderophore Hydrolysis Activates an Enterobactin–Ciprofloxacin Conjugate and Confers Targeted Antibacterial Activity. Journal of the American Chemical Society 2018, 140 (15), 5193-5201.

98. Brickman, T. J.; McIntosh, M. A., Overexpression and purification of ferric enterobactin esterase from Escherichia coli. Demonstration of enzymatic hydrolysis of enterobactin and its iron complex. Journal of Biological Chemistry 1992, 267 (17), 12350-12355.
99. Lin, H.; Fischbach, M. A.; Liu, D. R.; Walsh, C. T., In Vitro Characterization of Salmochelin and Enterobactin Trilactone Hydrolases IroD, IroE, and Fes. Journal of the American Chemical Society 2005, 127 (31), 11075-11084.
100. Miethke, M.; Hou, J.; Marahiel, M. A., The Siderophore-Interacting Protein YqjH Acts as a Ferric Reductase in Different Iron Assimilation Pathways of Escherichia coli. Biochemistry 2011, 50 (50), 10951-10964.
101. Gasser, V.; Kuhn, L.; Hubert, T.; Aussel, L.; Hammann, P.; Schalk, I. J., The Esterase PfeE, the Achilles' Heel in the Battle for Iron between Pseudomonas aeruginosa and Escherichia coli. International Journal of Molecular Sciences 2021, 22 (6), 2814.
102. Gasser, V.; Baco, E.; Cunrath, O.; August, P. S.; Perraud, Q.; Zill, N.; Schleberger, C.; Schmidt, A.; Paulen, A.; Bumann, D.; Mislin, G. L.; Schalk, I. J., Catechol siderophores repress the pyochelin pathway and activate the enterobactin pathway in Pseudomonas aeruginosa: an opportunity for siderophore-antibiotic conjugates development. Environ Microbiol 2016, 18 (3), 819-32.
103. Balado, M.; Osorio, C. R.; Lemos, M. L., A gene cluster involved in the biosynthesis of vanchrobactin, a chromosome-encoded siderophore produced by Vibrio anguillarum. Microbiology 2006, 152 (12), 3517-3528.
104. Naka, H.; Crosa, J. H., Identification and characterization of a novel outer membrane protein receptor FetA for ferric enterobactin transport in Vibrio anguillarum 775 (pJM1). BioMetals 2012, 25 (1), 125-133.
105. Mey, A. R.; Wyckoff, E. E.; Oglesby, A. G.; Rab, E.; Taylor, R. K.; Payne, S. M., Identification of the Vibrio cholerae enterobactin receptors VctA and IrgA: IrgA is not required for virulence. Infection and immunity 2002, 70 (7), 3419-3426.
106. Wyckoff, E. E.; Allred, B. E.; Raymond, K. N.; Payne, S. M., Catechol Siderophore Transport by Vibrio cholerae. Journal of bacteriology 2015, 197 (17), 2840-2849.
107. Tanabe, T.; Funahashi, T.; Shiuchi, K.; Okajima, N.; Nakao, H.; Miyamoto, K.; Tsujibo, H.; Yamamoto, S., Characterization of Vibrio parahaemolyticus genes encoding the systems for utilization of enterobactin as a xenosiderophore. Microbiology 2012, 158 (8), 2039-2049.
108. Usher, K. C.; Özkan, E.; Gardner, K. H.; Deisenhofer, J., The plug domain of FepA, a TonB-dependent transport protein from Escherichia coli, binds its siderophore in the absence of the transmembrane barrel domain. Proceedings of the National Academy of Sciences 2001, 98 (19), 10676-10681.
109. Cao, Z.; Qi, Z.; Sprencel, C.; Newton, S. M. C.; Klebba, P. E., Aromatic components of two ferric enterobactin binding sites in Escherichia coli FepA. Molecular Microbiology 2000, 37 (6), 1306-1317.
110. Buchanan, S. K.; Smith, B. S.; Venkatramani, L.; Xia, D.; Esser, L.; Palnitkar, M.; Chakraborty, R.; van der Helm, D.; Deisenhofer, J., Crystal structure of the outer membrane active transporter FepA from Escherichia coli. Nature Structural Biology 1999, 6 (1), 56-63.

111. Ferguson, A. D.; Coulton, J. W.; Diederichs, K.; Welte, W.; Braun, V.; Fiedler, H.-P., Crystal structure of the antibiotic albomycin in complex with the outer membrane transporter FhuA. Protein Science 2000, 9 (5), 956-963.
112. Cobessi, D.; Celia, H.; Folschweiller, N.; Schalk, I. J.; Abdallah, M. A.; Pattus, F., The crystal structure of the pyoverdine outer membrane receptor FpvA from Pseudomonas aeruginosa at 3.6 angstroms resolution. Journal of molecular biology 2005, 347 (1), 121-134.
113. Cobessi, D.; Celia, H.; Pattus, F., Crystal structure at high resolution of ferric-pyochelin and its membrane receptor FptA from Pseudomonas aeruginosa. Journal of molecular biology 2005, 352 (4), 893-904.
114. Hoegy, F.; Lee, X.; Noel, S.; Rognan, D.; Mislin, G. L. A.; Reimmann, C.; Schalk, I. J., Stereospecificity of the siderophore pyochelin outer membrane transporters in fluorescent pseudomonads. J Biol Chem 2009, 284 (22), 14949-14957.
115. Hoegy, F.; Gwynn, M. N.; Schalk, I. J., Susceptibility of Pseudomonas aeruginosa to catechol-substituted cephalosporin is unrelated to the pyochelin–Fe transporter FptA. Amino Acids 2010, 38 (5), 1627-1629.
116. Greenwald, J.; Nader, M.; Celia, H.; Gruffaz, C.; Geoffroy, V.; Meyer, J.-M.; Schalk, I. J.; Pattus, F., FpvA bound to non-cognate pyoverdines: molecular basis of siderophore recognition by an iron transporter. Molecular Microbiology 2009, 72 (5), 1246-1259.
117. Mislin, G. L. A.; Hoegy, F.; Cobessi, D.; Poole, K.; Rognan, D.; Schalk, I. J., Binding Properties of Pyochelin and Structurally Related Molecules to FptA of Pseudomonas aeruginosa. Journal of Molecular Biology 2006, 357 (5), 1437-1448.
118. Wyckoff, E. E.; Mey, A. R.; Payne, S. M., Iron acquisition in Vibrio cholerae. BioMetals 2007, 20 (3), 405.
119. Butterton, J. R.; Calderwood, S. B., Identification, cloning, and sequencing of a gene required for ferric vibriobactin utilization by Vibrio cholerae. Journal of bacteriology 1994, 176 (18), 5631-5638.
120. Butterton, J. R.; Stoebner, J. A.; Payne, S. M.; Calderwood, S. B., Cloning, sequencing, and transcriptional regulation of viuA, the gene encoding the ferric vibriobactin receptor of Vibrio cholerae. J Bacteriol 1992, 174 (11), 3729-38.
121. Naikare, H.; Butcher, J.; Flint, A.; Xu, J.; Raymond, K. N.; Stintzi, A., Campylobacter jejuni ferric–enterobactin receptor CfrA is TonB3 dependent and mediates iron acquisition from structurally different catechol siderophores†. Metallomics 2013, 5 (8), 988-996.
122. Xu, F.; Zeng, X.; Haigh, R. D.; Ketley, J. M.; Lin, J., Identification and characterization of a new ferric enterobactin receptor, CfrB, in Campylobacter. Journal of bacteriology 2010, 192 (17), 4425-4435.
123. Stahl, M.; Butcher, J.; Stintzi, A., Nutrient Acquisition and Metabolism by Campylobacter jejuni. Front Cell Infect Microbiol 2012, 2 (5).
124. Zeng, X.; Mo, Y.; Xu, F.; Lin, J., Identification and characterization of a periplasmic trilactone esterase, Cee, revealed unique features of ferric enterobactin acquisition in Campylobacter. Molecular Microbiology 2013, 87 (3), 594-608.
125. Raines, D. J.; Moroz, O. V.; Wilson, K. S.; Duhme-Klair, A.-K., Interactions of a Periplasmic Binding Protein with a Tetradentate Siderophore Mimic. Angewandte Chemie International Edition 2013, 52 (17), 4595-4598.

126. Raines, D. J.; Moroz, O. V.; Blagova, E. V.; Turkenburg, J. P.; Wilson, K. S.; Duhme-Klair, A.-K., Bacteria in an intense competition for iron: Key component of the Campylobacter jejuni iron uptake system scavenges enterobactin hydrolysis product. Proceedings of the National Academy of Sciences 2016, 113 (21), 5850.
127. Harrington, J. M.; Crumbliss, A. L., The redox hypothesis in siderophore-mediated iron uptake. BioMetals 2009, 22 (4), 679-689.
128. Fontecave, M.; Covès, J.; Pierre, J.-L., Ferric reductases or flavin reductases? Biometals 1994, 7 (1), 3-8.
129. Schröder, I.; Johnson, E.; de Vries, S., Microbial ferric iron reductases. FEMS Microbiology Reviews 2003, 27 (2-3), 427-447.
130. O'Brien, I. G.; Gibson, F., The structure of enterochelin and related 2,3-dihydroxy-N-benzoyne conjugates from Eschericha Coli. Biochimica et Biophysica Acta (BBA) - General Subjects 1970, 215 (2), 393-402.
131. Perraud, Q.; Moynié, L.; Gasser, V.; Munier, M.; Godet, J.; Hoegy, F.; Mély, Y.; Mislin, G. L. A.; Naismith, J. H.; Schalk, I. J., A Key Role for the Periplasmic PfeE Esterase in Iron Acquisition via the Siderophore Enterobactin in Pseudomonas aeruginosa. ACS Chemical Biology 2018, 13 (9), 2603-2614.
132. Balado, M.; Osorio, C. R.; Lemos, M. L., Biosynthetic and regulatory elements involved in the production of the siderophore vanchrobactin in Vibrio anguillarum. Microbiology (Reading) 2008, 154 (Pt 5), 1400-1413.
133. Ganne, G.; Brillet, K.; Basta, B.; Roche, B.; Hoegy, F.; Gasser, V.; Schalk, I. J., Iron Release from the Siderophore Pyoverdine in Pseudomonas aeruginosa Involves Three New Actors: FpvC, FpvG, and FpvH. ACS Chemical Biology 2017, 12 (4), 1056-1065.
134. Michel, L.; Bachelard, A.; Reimmann, C., Ferripyochelin uptake genes are involved in pyochelin-mediated signalling in Pseudomonas aeruginosa. Microbiology (Reading) 2007, 153 (Pt 5), 1508-1518.
135. Braud, A.; Hannauer, M.; Mislin, G. L.; Schalk, I. J., The Pseudomonas aeruginosa pyochelin-iron uptake pathway and its metal specificity. J Bacteriol 2009, 191 (11), 3517-25.
136. Naka, H.; Actis, L. A.; Crosa, J. H., The anguibactin biosynthesis and transport genes are encoded in the chromosome of Vibrio harveyi: a possible evolutionary origin for the pJM1 plasmid–encoded system of Vibrio anguillarum? MicrobiologyOpen 2013, 2 (1), 182-194.
137. Naka, H.; Liu, M.; Crosa, J. H., Two ABC transporter systems participate in siderophore transport in the marine pathogen Vibrio anguillarum 775 (pJM1). FEMS Microbiol Lett 2013, 341 (2), 79-86.
138. Wyckoff, E. E.; Valle, A. M.; Smith, S. L.; Payne, S. M., A multifunctional ATP-binding cassette transporter system from Vibrio cholerae transports vibriobactin and enterobactin. J Bacteriol 1999, 181 (24), 7588-96.
139. Tanabe, T.; Funahashi, T.; Nakao, H.; Miyoshi, S.; Shinoda, S.; Yamamoto, S., Identification and characterization of genes required for biosynthesis and transport of the siderophore vibrioferrin in Vibrio parahaemolyticus. J Bacteriol 2003, 185 (23), 6938-49.

140. Tanabe, T.; Kato, A.; Shiuchi, K.; Miyamoto, K.; Tsujibo, H.; Maki, J.; Yamamoto, S.; Funahashi, T., Regulation of the Expression of the Vibrio parahaemolyticus peuA Gene Encoding an Alternative Ferric Enterobactin Receptor. PLoS One 2014, 9 (8), e105749.
141. Miller, C. E.; Williams, P. H.; Ketley, J. M., Pumping iron: mechanisms for iron uptake by Campylobacter. Microbiology 2009, 155 (10), 3157-3165.
142. Bäumler, A. J.; Tsolis, R. M.; van der Velden, A. W. M.; Stojiljkovic, I.; Anic, S.; Heffron, F., Identification of a new iron regulated locus of Salmonella typhi. Gene 1996, 183 (1), 207-213.
143. Bäumler, A. J.; Norris, T. L.; Lasco, T.; Voigt, W.; Reissbrodt, R.; Rabsch, W.; Heffron, F., IroN, a Novel Outer Membrane Siderophore Receptor Characteristic of <em>Salmonella enterica</em&gt. Journal of Bacteriology 1998, 180 (6), 1446.
144. Miethke, M.; Klotz, O.; Linne, U.; May, J. J.; Beckering, C. L.; Marahiel, M. A., Ferri-bacillibactin uptake and hydrolysis in Bacillus subtilis. Molecular Microbiology 2006, 61 (6), 1413-1427.
145. Zawadzka, A. M.; Kim, Y.; Maltseva, N.; Nichiporuk, R.; Fan, Y.; Joachimiak, A.; Raymond, K. N., Characterization of a Bacillus subtilis transporter for petrobactin, an anthrax stealth siderophore. Proceedings of the National Academy of Sciences 2009, 106 (51), 21854-21859.
146. Weber, T., In silico tools for the analysis of antibiotic biosynthetic pathways. International Journal of Medical Microbiology 2014, 304 (3), 230-235.
147. Medema, M. H.; Fischbach, M. A., Computational approaches to natural product discovery. Nature Chemical Biology 2015, 11 (9), 639-648.
148. Ziemert, N.; Alanjary, M.; Weber, T., The evolution of genome mining in microbes – a review. Natural Product Reports 2016, 33 (8), 988-1005.
149. Blin, K.; Wolf, T.; Chevrette, M. G.; Lu, X.; Schwalen, C. J.; Kautsar, S. A.; Suarez Duran, H. G.; de Los Santos, E. L. C.; Kim, H. U.; Nave, M.; Dickschat, J. S.; Mitchell, D. A.; Shelest, E.; Breitling, R.; Takano, E.; Lee, S. Y.; Weber, T.; Medema, M. H., antiSMASH 4.0-improvements in chemistry prediction and gene cluster boundary identification. Nucleic acids research 2017, 45 (W1), W36-W41.
150. Stachelhaus, T.; Mootz, H. D.; Marahiel, M. A., The specificity-conferring code of adenylation domains in nonribosomal peptide synthetases. Chemistry & biology 1999, 6 (8), 493-505.
151. Pearson, W. R., An Introduction to Sequence Similarity ("Homology") Searching. Current Protocols in Bioinformatics 2013, 42 (1), 3.1.1-3.1.8.
152. Johnson, M.; Zaretskaya, I.; Raytselis, Y.; Merezhuk, Y.; McGinnis, S.; Madden, T. L., NCBI BLAST: a better web interface. Nucleic Acids Res 2008, 36 (Web Server issue), W5-9.
153. Edgar, R. C., MUSCLE: multiple sequence alignment with high accuracy and high throughput. Nucleic Acids Research 2004, 32 (5), 1792-1797.

2. Two Siderophores Produced by *Marinomonas Mediterranea* MMB-1: Acinetobactin and Mediterraneabactin – A Diastereomer of Turnerbactin

2.1. Introduction

Bacteria produce low molecular weight secondary metabolites called siderophores to obtain iron necessary for growth. Siderophores bind Fe(III) with high affinity and these Fe(III)-siderophore complexes are taken up by the cell. This iron is then used as a cofactor by many enzymes involved in cellular processes. Siderophores are biosynthesized by either non-ribosomal peptide synthetase (NRPS)-dependent process or the NRPS-independent synthetase, i.,e., the so-called NIS process. Siderophores are classified by their functional binding groups, typically catechols, hydroxamic acids, and α -hydroxycarboxylic acids, although other Fe(III)-binding groups are known in siderophores. The chirality around the metal center of the Fe(III)-siderophore complex plays in important role in recognition, acquisition, and extraction of iron from the complex.[1 2]

Two well-known triscatechol siderophores, enterobactin (Ent), a trimeric macrolactone of 2,3-dihydroxybenzoate (DHB)-^{L}Ser, and bacillibactin (BB), a cyclic trimeric ester 2,3-DHB-Gly-^{L}Thr, coordinate Fe(III) in a hexadentate fashion with the catechol ligands. On top of the different residues in the macrolactone core, BB contains a glycine residue between each L-Thr and DHB. The chirality at the metal center of these two similar siderophores are enantiomers, where Fe(III)-Ent^{3-} adopts the Δ configuration,[3 4] while Fe(III)-BB^{3-} forms the Λ configuration.[3] Other triscatechol siderophores containing a chiral amino acid inserted between

the oligoester backbone and DHB have also adopted enantiomeric configurations at the Fe(III) site. For instance, cyclic trichrysobactin, a triscatechol oligoester (DHB-^{D}Lys-^{L}Ser)$_3$, produced by *Dickeya chrysanthemi* EC16,[5] and frederiksenibactin, a linear triscatechol ester (DHB-^{L}Lys-^{L}Ser)$_3$, produced by *Yersinia frederiksenii* ATCC 33641,[6] bind Fe(III) in Λ and Δ configurations, respectively.[6] Another pair of diastereomers that form opposite configurations are trivanchrobactin (DHB-^{D}Arg-^{L}Ser)$_3$ and ruckerbactin (DHB-^{L}Arg-^{L}Ser)$_3$.[7] These four siderophores are pairs of diastereomers containing either cationic amino acids, $^{D/L}$Lys or $^{D/L}$Arg. However, the ^{D}Orn diastereomer to turnerbactin, another triscatechol ester (DHB-^{L}Orn-^{L}Ser)$_3$,[8] has not yet been reported.

Marinomonas mediterranea MMB-1 is a marine bacterium isolated from the Mediterranean Sea.[9] [10] It has an interesting feature not seen in other species of this genus, where the bacterium synthesizes melanin pigments from *L*-tyrosine.[11] Siderophore production in *M. mediterranea* MMB-1 has not been studied until now.

While analysis of the mediterraneabactin gene cluster of *M. mediterranea* MMB-1 did not initially lead to the predicted structure of mediterraneabactin (DHB-^{D}Orn-^{L}Ser)$_3$, two siderophores were discovered fortuitously. Mediterraneabactin is a diastereomer of turnerbactin, (DHB-^{L}Orn-^{L}Ser)$_3$. We report herein the structural characterization of mediterraneabactin (1), a related biscatecholamide compound, (2), monocatecholamide compound (3), and acinetobactin (4) (Figure 2.1). The cyclic mediterraneabactin product was not detected or isolated. The stereochemistry of the Fe(III)-mediterraneabactin complex was compared to its diastereomer Fe(III)-turnerbactin. Acinetobactin, originally isolated from *Acinetobacter baumannii* ATCC 19606 was also isolated from *M. mediterranea* MMB-1, where it is the first instance this siderophore is produced in a marine bacterium.

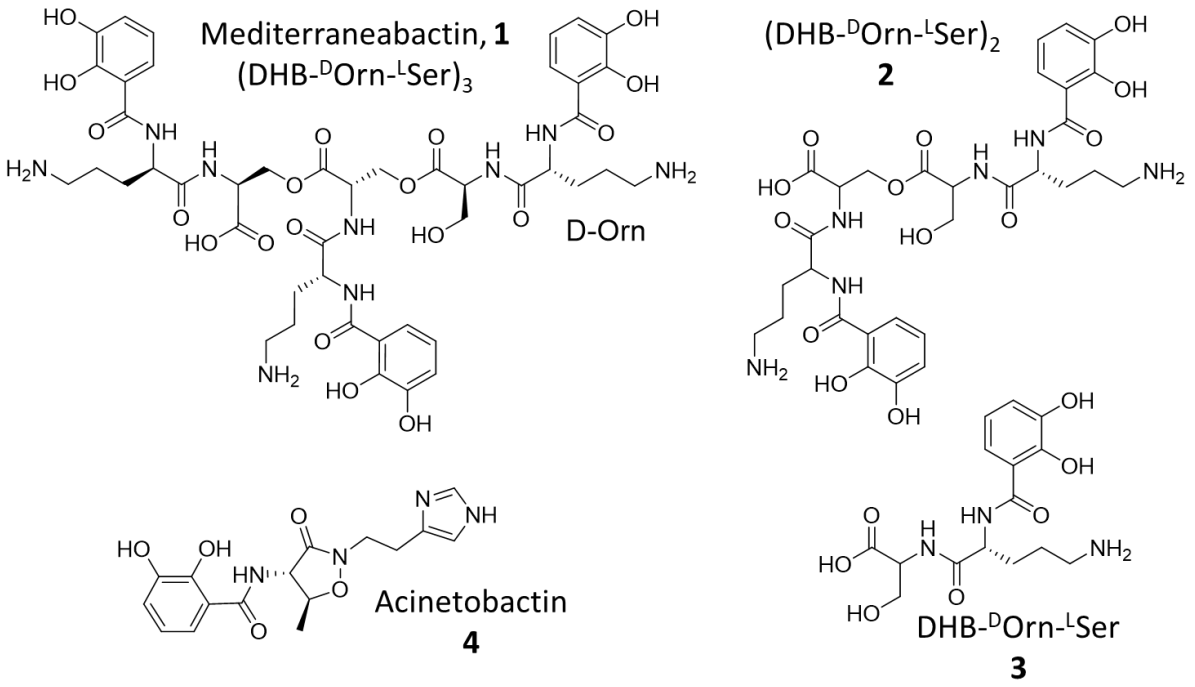

Figure 2.1. Structures of siderophores identified in *Marinomonas mediterranea* MMB-1: Mediterraneabactin (1), biscatecholamide compound (2), monocatecholamide compound (3), and acinetobactin (4).

2.2. Statement of Chapter Objectives

The purpose of this study was to use a genome mining approach to isolate and structurally characterize the siderophores produced by *Marinomonas mediterranea* MMB-1. This marine bacterium has been found to produce a new triscatechol amide siderophore, mediterraneabactin (1), a related biscatecholamide compound, (2), a related monocatecholamide compound (3), and acinetobactin (4). Mediterraneabactin is a diastereomer of the siderophore, turnerbactin. A related but distinct biosynthetic gene cluster (BGC) of turnerbactin (DHB-^{L}Orn-^{L}Ser)$_3$, was identified in the genome of the bacterium *Marinomonas mediterranea* MMB-1. Isolation of the siderophore from *M. mediterranea*

MMB-1 revealed the triscatechol oligoester (DHB-^{D}Orn-^{L}Ser)$_3$. The mediterraneabactin structure was elucidated through mass spectrometry, amino acid analysis, and circular dichroism spectroscopy (CD). CD spectroscopy established that Fe(III)-mediterraneabactin and Fe(III)-turnerbactin are formed in opposite enantiomeric configuration at the Fe(III) site. The cyclic mediterraneabactin product was not detected. Acinetobactin, a siderophore and virulence factor, originally produced by *A. baumannii* ATCC 19606 was also isolated from *M. mediterranea* MMB-1 and structurally characterized through 1D NMR analysis and mass spectrometry. Overall, the analysis of the genome sequence revealed that *M. mediterranea* MMB-1 possesses two biosynthesis gene clusters: one cluster with high similarity to genes encoding turnerbactin in *Teredinibacter turnerae* T7901, while the other cluster with high similarity to the BGC for acinetobactin.

2.3. Materials and Methods

2.3.1. General Experimental Procedures

UV-visible absorption spectra were obtained on an Agilent Cary 300 UV Vis spectrophotometer. Electronic circular dichroism spectra were measured on a Jasco J-1500 circular dichroism spectropolarimeter. Mass spectrometry analysis was carried out on a Waters Xevo G2-XS QTof with positive mode electrospray ionization coupled to an ACQUITY UPLC H-Class system with a Waters BEH C18 column. Culture extracts were analyzed with a linear gradient of 0% to 30% CH_3CN (0.1% formic acid) in ddH_2O (0.1% formic acid) over 10 minutes. For MSMS analysis, a collision energy profile of 20, 25, 30 kEV was employed. Using MassLynx 4.1, chromatograms for masses of interest were generated and molecular ion peaks quantified by integration (ApexTrack algorithm). The absorbance of the eluent was

monitored at 215 nm. NMR spectroscopy was performed on a Bruker Advanced NEO 500 MHz, with a Prodigy BBO cryoprobe. Chemical shifts were referenced through residual solvent peaks [^{1}H (DMSO-*d*$_6$) 2.50 ppm, ^{13}C (DMSO-*d*$_6$) 39.51 ppm].

2.3.2. Genome Mining and Gene Cluster Annotation

The genome of *Marinomonas mediterranea* MMB-1 was accessed through NCBI and analyzed with the NRPS cluster-predicting software PRISM and antiSMASH.[12] [13] Genes within the siderophore cluster and their corresponding amino acid sequences were analyzed using BLAST and the PFAM database to predict function of proteins encoded by the cluster.

2.3.3. Bacterial Growth and Siderophore Isolation

Marinomonas mediterranea MMB-1, obtained from ATCC (ATCC 700492), was cultured in artificial seawater medium (ASW) containing 15 g NaCl, 0.75 g KCl, 0.2 $MgSO_4 \cdot 7H_2O$, 0.1 g $CaCl_2 \cdot 2H_2O$, 1 g NH_4Cl, 5 g sodium succinate, and 3 g $Na_2HPO_4 \cdot 7H_2O$ per liter of doubly deionized water. The medium was adjusted to pH 7.0 and autoclaved. A one-liter culture was grown on an orbital shaker (180 rpm) at 25℃ for 7 days. The presence of potential siderophores were monitored with the Fe(III)- CAS solution assay for a color change.[14] The cultures were harvested at 6,000 rpm for 30 minutes at 4℃ and the supernatant was kept for further siderophore extraction. The supernatant was incubated with Amberlite XAD-4 resin for 3-4 hours at ambient temperature with mild agitation. The siderophores were eluted from the resin with 90% methanol and concentrated by rotary evaporation.

Eluent was initially purified by semi-preparative HPLC on a YMC 20x250 mm C18-AQ column, with a linear gradient of 10% MeOH in ddH_2O (+0.1% trifluoroacetic acid) to

80% MeOH in ddH_2O (+0.1% trifluoroacetic acid) over 40 minutes. Samples were ultrapurified on the same column with a gradient of 10% MeOH in ddH_2O (+0.1% trifluoroacetic acid) to 40% MeOH in ddH_2O (+0.1% trifluoroacetic acid) over 40 minutes for mediterraneabactin, which eluted at 31.5 minutes. Acinetobactin was ultrapurified with a gradient of 20% MeOH in ddH_2O (+0.1% trifluoroacetic acid) to 60% MeOH in ddH_2O (+0.1% trifluoroacetic acid) over 40 minutes and eluted at 25.1 minutes. The eluent was continuously monitored (215 nm and 310 nm). Purified samples were lyophilized and stored at -20℃.

Extracts were analyzed through positive ion mode ESI-MS on a Waters Xevo G2-XS QTof coupled to a Waters Acquity H-Class UPLC system. A Waters BEH C18 column was used with a gradient of 0-100% water/acetonitrile (both with 0.1% w/v formic acid). Using MassLynx 4.1, chromatograms for masses of interest were generated and molecular ion peaks quantified by integration (ApexTrack algorithm). The absorbance of the eluent was monitored at 215 nm.

2.3.4. Amino Acid Analysis of Mediterraneabactin with Marfey's Reagent

Purified apo mediterraneabactin (0.61 mg) was dissolved in 6 M HCl, sealed in an ampoule, and heated at 120℃ for 17 hours to hydrolyze the siderophore. Hydrolysis using HI is commonly used to reduce any modified amino acids like N5-hydroxyornithine or N5-acetyl-N5-hydroxyornithine. Since the ornithine in mediterraneabactin is not modified, HCl is sufficient for hydrolysis. The hydrolysis mixture was evaporated to dryness to remove HCl and redissolved in doubly deionized water. Two additional cycles of evaporation and dissolution in ddH_2O was repeated. Amino acid standards were prepared by dissolving D-Orn (≥98%), L-Orn (≥98%), D-Ser (≥98%), and L-Ser (≥99%) in ddH_2O at 1 mg/mL. The

hydrolyzed siderophore samples and amino acid standards were then derivatized with 1-fluoro-2-4-dinitrophenyl-5-L-alanine amide (Marfey's reagent) by using standard procedures.[15] Derivatized hydrolysis products were separated by HPLC on a YMC 4.6x250mm C18-AQ column with a gradient from 10% to 45% CH_3CN in triethylamine in phosphoric acid over 45 minutes. Derivatized hydrolysis products were co-injected with Marfey's derivatized amino acid standards to determine the stereochemistry of the amino acids in mediterraneabactin. The stereochemical assignment was made by comparison with the retention times of Marfey's derivatized amino acid standards of D- and L- ornithine and D- and L- serine (Sigma-Aldrich) using the method described above.

2.3.5. Electronic Circular Dichroism Spectroscopy of Fe(III) Siderophore Complexes

The absolute configurations of Fe(III)-mediterraneabactin and Fe(III)-turnerbactin were evaluated by ECD spectroscopy. The ferric complexes of the diastereomers were prepared in a citrate-phosphate buffer (50 mM, pH 7.40) by mixing a solution of $FeCl_3$ [2.53 mM, 50 mM HCl (aq)] with 1.0 equivalent of the desired apo-ligand. Fe(III)-complex formation was tracked by UV-visible spectroscopy by following the absorbance at 498 nm. Full CD spectra of the iron complexes and blank (50 mM citrate-phosphate buffer) were obtained using the following parameters: 400-600 nm; 2 s D.I.T., 1 nm bandwidth, and 100 nm s^{-1}scan speed and recorded on a Jasco J-1500 CD spectropolarimeter.

2.4. Results

2.4.1. Analysis of the Mediterraneabactin Gene Cluster for Siderophore Biosynthesis

Through bioinformatics and genome mining approaches applied to microbial genome sequences, a distinct NRPS gene cluster surrounded by siderophore iron transport genes was revealed (Figure 2.2). Proteins with closest similarity to the gene products of this cluster are shown in Table 2.1. This biosynthetic gene cluster shows similarity to the *tnb* locus encoding biosynthesis of turnerbactin in *Teredinibacter turnerae* T7901 (Figure 2.1, Table 2.1 - 2.2).[8] Homologs of *tnb*CEBA encoding the biosynthesis and activation of 2,3-DHB for turnerbactin were identified in *M. mediterranea* MMB-1. TnbC isomerizes chorismate into isochorismate, then TnbB hydrolyzes isochorismate into 2,3-dihydro-DHB, which is oxidized by TnbA to DHB. TnbE activates and transfers DHB to TnbB. These genes are also homologous to the entCEBA genes involved in the biosynthesis of DHB for enterobactin. The full annotation of the mediterraneabactin siderophore gene cluster in *M. mediterranea* MMB-1 with proposed gene names is found in Table 2.3 with the graphical representation shown in Figure 2.3.

Focusing on the NRPS in *M. mediterranea* MMB-1, it is a two-module protein consistent with a triscatechol siderophore (Figure 2.2). The Stachelhaus code of the first adenylation domain did not have a strong prediction on incorporation of a certain amino acid residue. The adenylation domain in the second module predicted incorporation of Ser (Figure 2.2b). Both of the NRPS in *M. mediterranea* MMB-1 and *T. turnerae* T7901 are composed of two modules, however the distinction between the two NRPS occurs in the first module, where an epimerization domain is present in the BGC for mediterraneabactin, responsible for

converting ^{L}AA to ^{D}AA, while this domain is absent in the BGC for turnerbactin. The presence of the epimerization domain in *M. mediterranea* MMB-1 then predicts the production of a siderophore composed of (DHB-^{D}AA-^{L}Ser)$_3$, with similarities to turnerbactin.

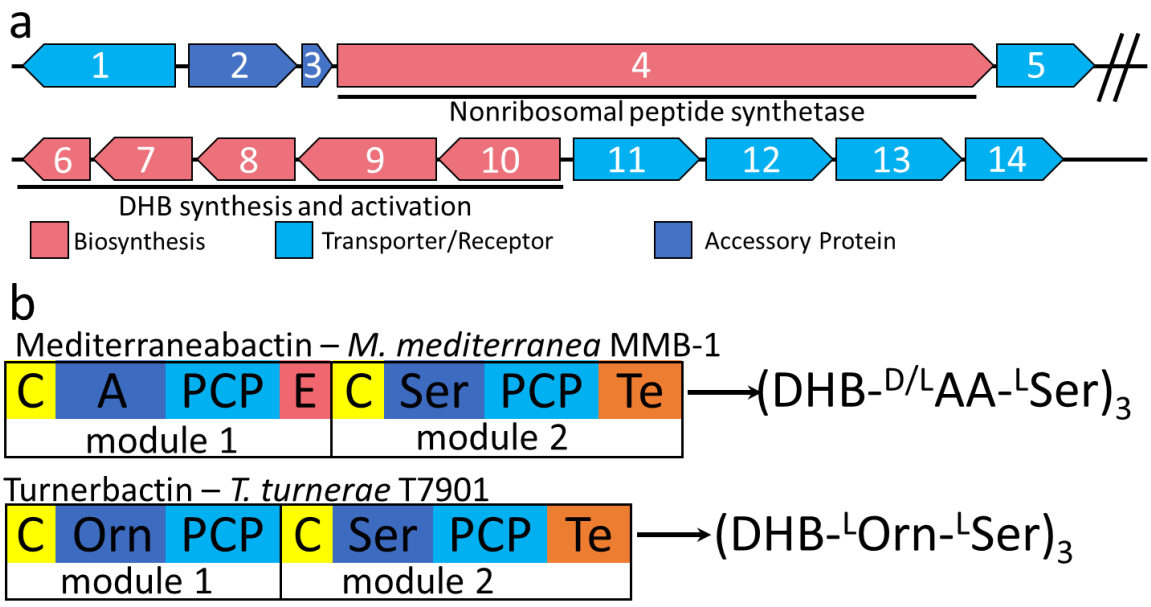

Figure 2.2. Biosynthetic gene cluster of two diastereomers of (DHB-$^{D/L}$Orn-^{L}Ser)$_3$ found in *M. mediterranea* MMB-1 and in *T. turnerae* T7901. (a) The genetic organization of the mediterraneabactin biosynthetic gene cluster. (b) NRPS domain architecture involved in the biosynthesis of the triscatechol siderophores mediterraneabactin and turnerbactin. The adenylation domain is represented by the selected amino acid, in this case ornithine for *T. turnerae* T7901 and unknown for *M. mediterranea* MMB-1.

Table 2.1 Annotation of mediterraneabactin gene cluster in *Marinomonas mediterranea* MMB-1, including predicted protein functions based on sequence analysis using Pfam and BLAST. The sequence similarity of each gene to the corresponding homolog from the turnerbactin gene cluster (*Teredinibacter turnerae* T7901) is indicated. I: identity, P: positives.

Ref Seq in *M. mediterranea* MMB-1	**Protein Size**	**Proposed function**	**Ref Seq homolog in *Teredinibacter turnerae* T7901**	**Homolog gene in *T. turnerae* T7901**	**I/P %**
WP_013660531.1	689	TonB-dependent receptor	WP_015817255.1		24/44
WP_013660532.1	485	Enterochelin esterase	WP_015816819.1		28/41
WP_013660533.1	69	MbtH family protein	WP_015818593.1		48/63
WP_013660534.1	3,014	NRPS	WP_041590315.1 (*tnbF*)	*tnbF*	47/60
WP_013660535.1	440	Enterobactin transporter EntS	WP_015819712.1	*tnbS*	49/68
WP_013661956.1	388	isochorismate synthase	WP_015819844.1 (*tnbC*)	*tnbC*	44/59
WP_013661955.1	571	(2,3-dihydroxybenzoyl) adenylate synthase	WP_187148814.1 (*tnbE*)	*tnbE*	51/67
WP_013661954.1	301	isochorismatase family protein	WP_015816823.1 (*tnbB*)	*tnbB*	50/70
WP_013661953.1	285	2,3-dihydro-2,3-dihydroxybenzoate dehydrogenase	WP_015818365.1 (*tnbA*)	*tnbA*	47/63
WP_013660114.1	405	efflux RND transporter periplasmic adaptor subunit	WP_015817978.1	*tnbD*	37/57
WP_013660115.1	1,035	Multidrug efflux RND transporter permease subunit	WP_015817325.1		51/71

Table 2.2. The sequence similarity of the mediterraneabactin biosynthetic genes to the corresponding homolog from the enterobactin gene cluster (*Escherichia coli* K12) is indicated as percent identity.

Ref Seq	Protein Size	Proposed function	Homolog in *E. coli* K12	Homolog gene name in *E. coli* K12	I %
WP_013660531.1	689	TonB-dependent receptor			
WP_013660532.1	485	Enterochelin esterase	PSF24345.1	*fes*	35.04
WP_013660533.1	69	MbtH family protein	WP_249568728.1		40.00
WP_013660534.1	3,014	NRPS	WP_249568727.1	*entF*	42.67
WP_013660535.1	440	Enterobactin transporter EntS	WP_090082098.1	*entS*	48.32
WP_013661956.1	388	isochorismate synthase	WP_249568723.1	*entC*	40.92
WP_013661955.1	571	(2,3-dihydroxybenzoyl) adenylate synthase	WP_249568770.1	*entE*	52.59
WP_013661954.1	301	isochorismatase family protein	WP_249568722.1	*entB*	51.85
WP_013661953.1	285	2,3-dihydro-2,3-dihydroxybenzoate dehydrogenase	WP_249568721.1	*entA*	52.42
WP_013661952.1	232	4'-phosphopantetheinyl transferase superfamily protein	WP_249568730.1	*entD*	31.07
WP_013660114.1	405	efflux RND transporter periplasmic adaptor subunit			
WP_013660115.1	1,035	Multidrug efflux RND transporter permease subunit			

Table 2.3. Full annotation of the mediterraneabactin siderophore gene cluster in *M. mediterranea* MMB-1 with proposed gene names

Proposed Gene name	Number	Protein accession number	Location	Proposed Function	Protein Size
fmbA	1	WP_013660531.1	1,512,611 - 1,514,680	TonB-dependent receptor	689 aa
mbsH	2	WP_013660532.1	1,514,921 - 1,516,378	Enterochelin esterase	485 aa
mbsI	3	WP_013660533.1	1,516,392 - 1,516,601	MbtH family protein	69 aa
mbsF[a]	4	WP_013660534.1	1,516,664 - 1,525,708	NRPS	3,014 aa
mbsS	5	WP_013660535.1	1,525,724 - 1,527,046	Enterobactin transporter EntS	440 aa
mbsD	6	WP_013661952.1	3,094,545..3,095,243	4'-phosphopantetheinyl transferase superfamily protein	232 aa
mbsA	7	WP_013661953.1	3,095,304..3,096,161	2,3-dihydro-2,3-dihydroxybenzoate dehydrogenase	285 aa
mbsB	8	WP_013661954.1	3,096,161..3,097,066	isochorismatase	301 aa
mbsE	9	WP_013661955.1	3,097,171..3,098,886	(2,3-dihydroxybenzoyl)adenylate synthase	571 aa
mbsC	10	WP_013661956.1	3,098,883..3,100,049	Isochorismate synthase	388 aa
fmbB	11	WP_013661957.1	3,100,290..3,101,345	fepB; Fe2+-enterobactin ABC transporter substrate binding protein	351 aa
fmbC	12	WP_013661958.1	3,101,332..3,102,381	Fe(3+)-siderophore ABC transporter permease	349 aa
fmbD	13	WP_013661959.1	3,102,392..3,103,432	iron chelate uptake ABC transporter family permease subunit	346 aa
fmbE	14	WP_013661960.1	3,103,445..3,104,227	ABC transporter ATP-binding protein	260 aa

[a]Proposed gene names for the mediterraneabactin biosynthetic gene cluster reflect literature precedent and homology to other triscatechol biosynthetic gene clusters using the mnemonic *mbs* for **m**editerraneabactin **b**io**s**ynthesis genes and the mnemonic *fmb* for **f**erric **m**editerranea**b**actin.

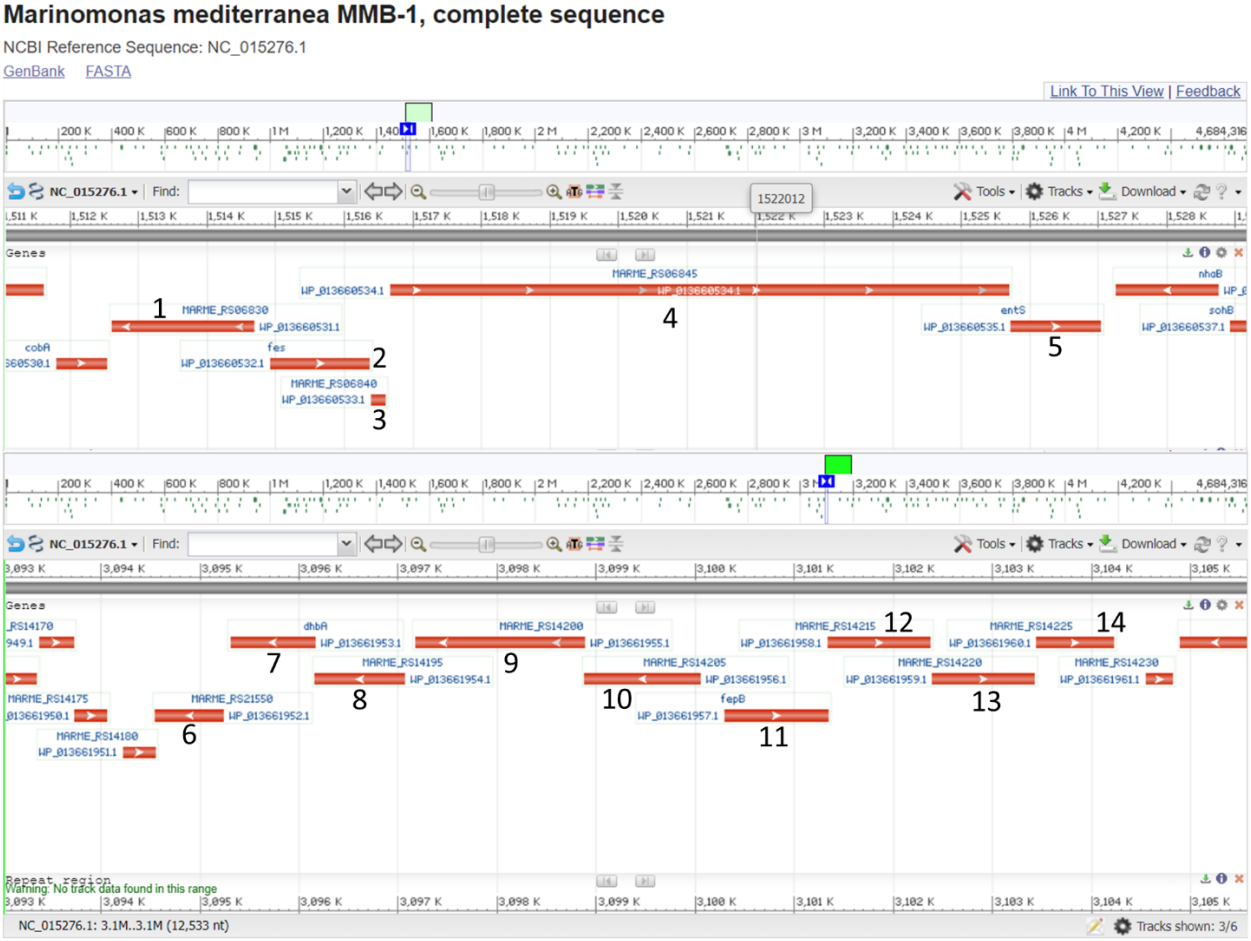

Figure 2.3. Graphical representation of the mediterraneabactin gene cluster within the *Marinomonas mediterranea* MMB-1 genome generated from the National Center for Biotechnology Information (NCBI) website.

2.4.2. Isolation and Structural Characterization of Mediterraneabactin

Siderophores from *M. mediterranea* MMB-1 were extracted and purified from a low-iron minimal medium. The CAS assay was used to track the siderophores throughout the purification process.[14] RP-HPLC revealed a total of five peaks displaying CAS activity (Figure 2.4). The following sections will cover each siderophore individually. Four of the five peaks (1-4) are related to the siderophore mediterraneabactin.

2.4.2.1. Structural Characterization of the Triscatechol Mediterraneabactin

UPLC-ESIMS determined the mass of the molecular ion $[M+H]^+$: (DHB-Orn-Ser)$_3$ (**1**), *m/z* 1030.4014, corresponding to a molecular formula $C_{45}H_{60}N_9O_{19}$ (calculated 1030.4000). This mass is similar to that of turnerbactin, isolated from *T. turnerae* T7901.[8] We have named this new siderophore mediterraneabactin.

ESI tandem mass spectrometry (ESI-MS/MS) analysis of compounds **1** – **3** are summarized in Table 2.4. The analysis revealed fragments in agreement with a DHB-Orn-Ser core structure, which has been previously observed in the siderophore turnerbactin.[8] Loss of the catechol was identified for compounds **1** – **3** by the fragment with a *m/z* 137.07 (b_1) (Figures 2.6, 2.9, 2.11, and 2.12). The MSMS analysis of mediterraneabactin (**1**) shown in Figure 2.6, shows that the loss of the catechol gave rise to the 2-DHB-3-Orn-3-Ser fragment, *m/z* 894.36 (y_1). For fragmentation between Orn and Ser in **1** formed the DHB-Orn fragment *m/z* 251.11 (b_2) and the 2-DHB-2-Orn-3-Ser fragment, *m/z* 780.30 (y_2). Signals originating from the cleavage of the serine esters were identified in mediterraneabactin as *m/z* 675.25, *m/z* 338.14, and *m/z* 693.27. Internal fragments of this compound, summarized in Table 2.4 are also observed further confirming this structure. The structure of mediterraneabactin with the fragment masses are depicted in Figure 2.7. The mass of the fragments that are correlated with the loss of various constituents of the siderophore are indicated in Table 2.4. Fragment losses refer to the parent ion identified in the table. All of these fragment losses are observed in the MSMS of each compound.

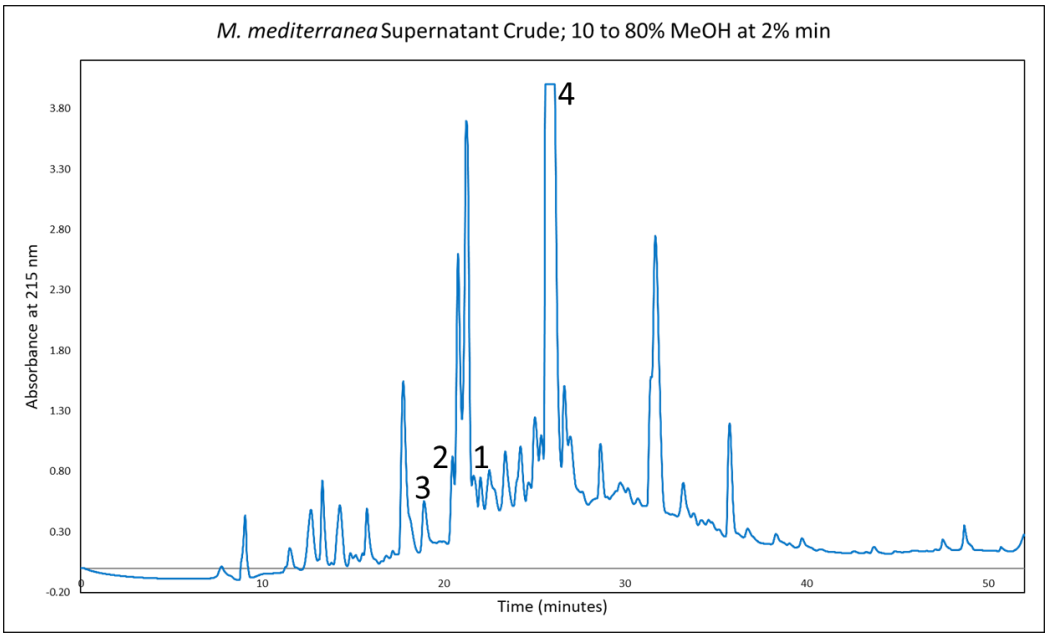

Figure 2.4. HPLC of the MeOH XAD-4 extract from the supernatant of a *M. mediterranea* MMB-1 culture. ESI-MS of peaks **1** – **3** are shown in Figure 2.5-2.8.

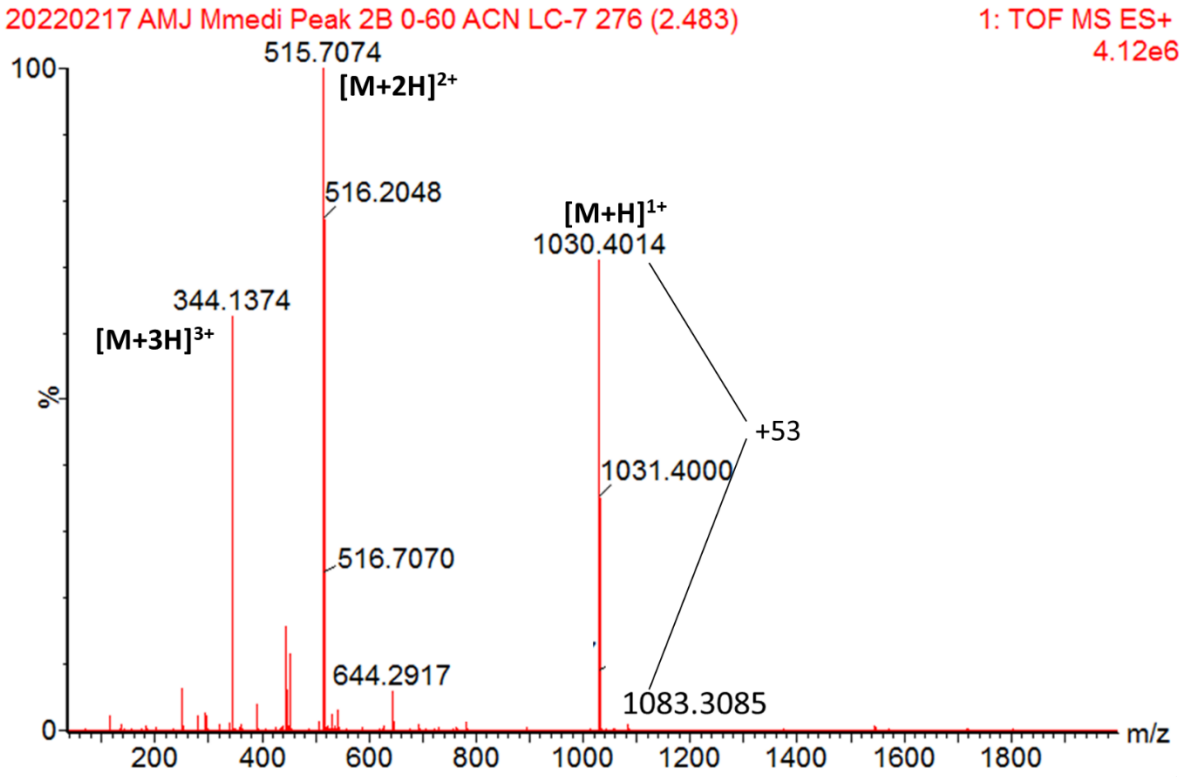

Figure 2.5. HR-ESI-MS spectrum of mediterraneabactin (**1**), *m/z* 1030.4014 $[M+H]^{1+}$. Calculated exact mass for mediterraneabactin $[M+H]^{1+}$ is *m/z* 1030.4000 ($C_{45}H_{60}N_9O_{19}$).

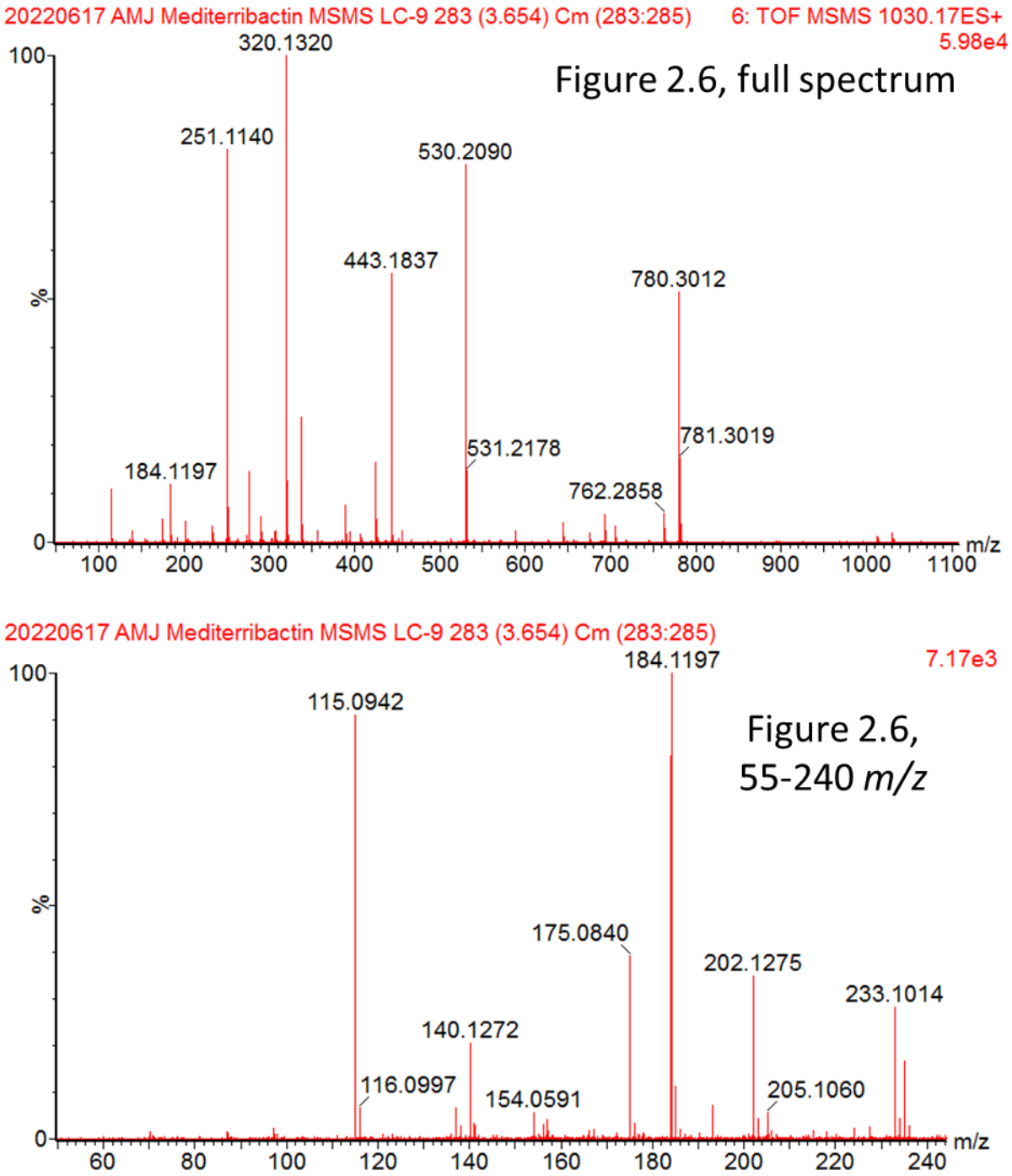

Figure 2.6. ESI-MSMS spectrum of mediterraneabactin (**1**) (*m/z* 1030.40; $C_{45}H_{60}N_9O_{19}$), with selected regions zoomed in for clarity. Collision energy profile of 20, 25, and 30 kEV employed for optimal fragmentation.

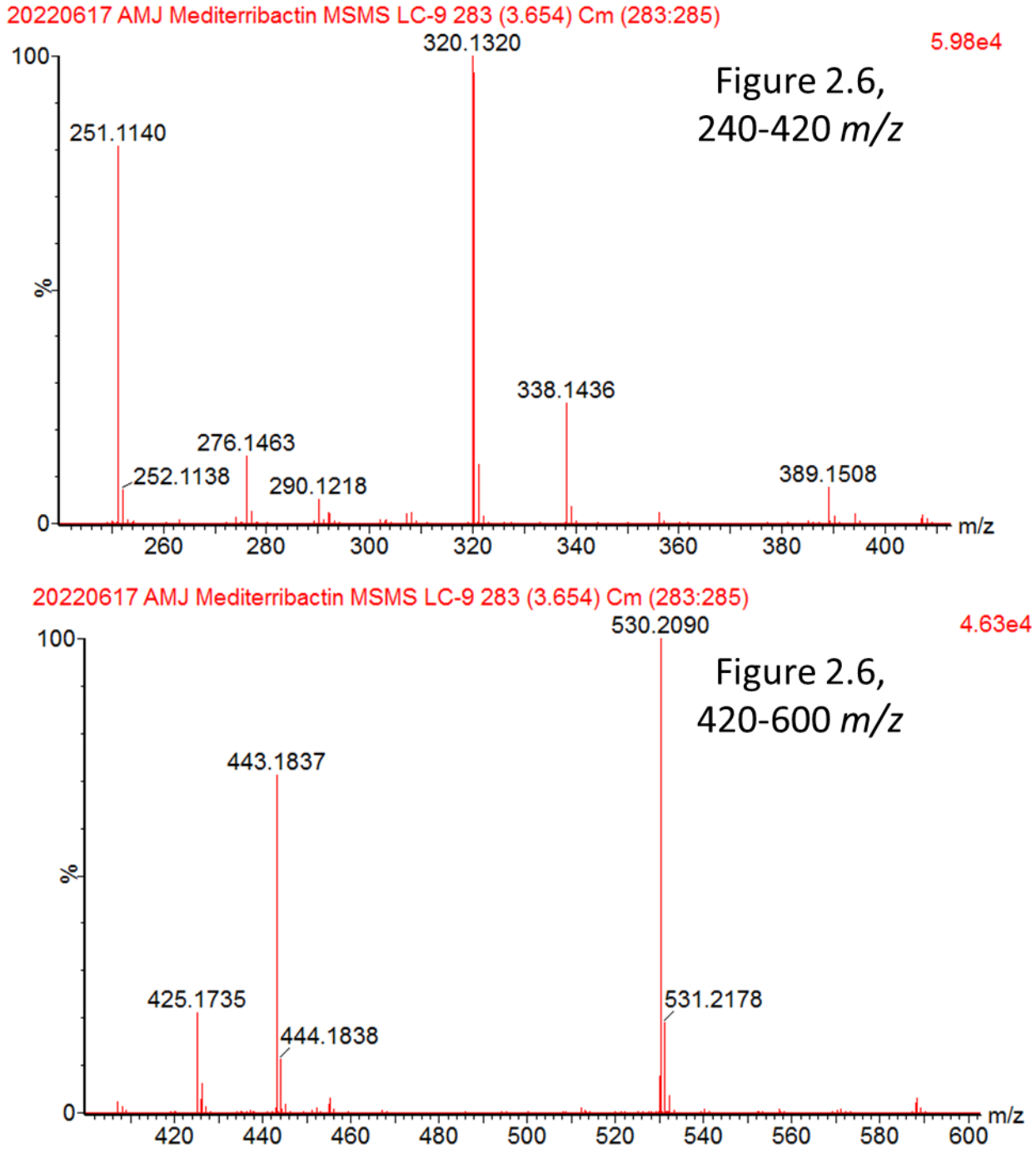

Figure 2.6. continued

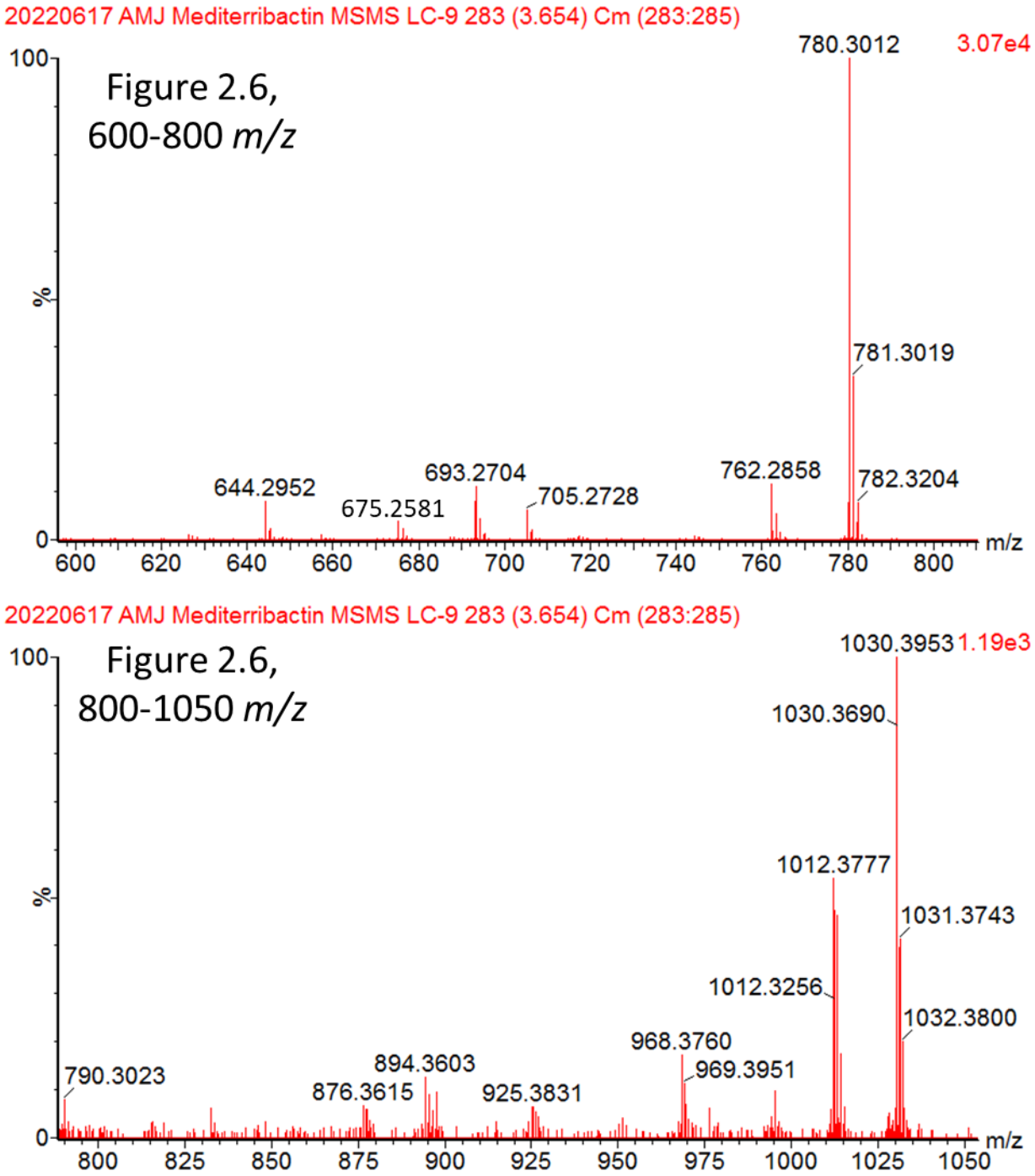

Figure 2.6. Continued

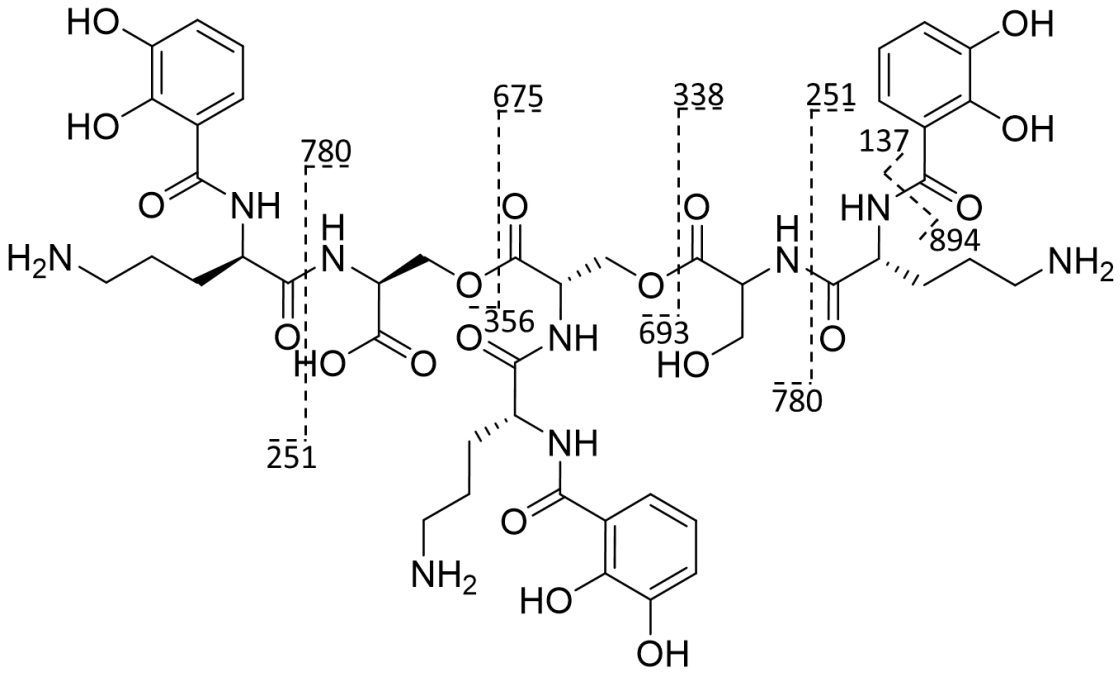

Fragment	b_1	y_1	b_2	y_2	1’	2’	1	2
m/z	137.07	894.36	251.11	780.30	338.14	693.27	675.25	356.15

Figure 2.7. Structure of mediterraneabactin (1), with b/y fragment masses.

Table 2.4. Molecular Ions and Common Mass Fragments of Mediterraneabactin (**1**), (**2**), (**3**), compared to Turnerbactin

Turnerbactin $[M+H]^+$	Mediterraneabactin (1) $[M+H]^+$	$(DHB\text{-}Orn\text{-}Ser)_2$ (2) $[M+H]^+$	(DHB-Orn-Ser) (3) $[M+H]^+$	Modified $(DHB\text{-}Orn\text{-}Ser)_3$ $[M+H]^+$	Fragment
1030.4	1030.4	693.3	356.1	1012.4	Parent ion
780.3	780.3			762.3	Loss of DHB-Orn
693.3	693.3	675.2		675.2	Loss of DHB-Orn-Ser
530.2	530.2				Loss of DHB-Orn x2
443.2	443.2	443.2		425.2	Loss of DHB-Orn-Ser & DHB-Orn
356.1	356.1	356.1		338.1	Loss of DHB-Orn-Ser x2
251.1	251.1	251.1	251.1	251.1	DHB-Orn
115.1	115.1	115.1	115.1	115.1	Orn

2.4.2.2. Structural Characterization of the Biscatechol, Monocatechol, and a Triscatechol Compound Related to Mediterraneabactin

Structural characterization was also completed of the related biscatechol unit (**2**), monocatechol unit (**3**), and a modified triscatechol compound related to mediterraneabactin. The ESI-MS of compounds **2** and **3** revealed molecular ions $[M+H]^+$ at *m/z* 693.2744, corresponding to a molecular formula of $C_{30}H_{41}N_6O_{13}$ (calculated 693.2732) and *m/z* 356.1537, corresponding to a molecular formula of $C_{15}H_{22}N_3O_7$ (calculated 356.1457). The modified triscatechol compound related to mediterraneabactin was also identified, with a molecular ion $[M+H]^+$ at *m/z* 1012.4167, corresponding to a molecular formula $C_{45}H_{58}N_9O_{18}$ (calculated 1012.3899), 18 amu less than mediterraneabactin.

ESI-MS/MS of these three compounds are depicted in Figures 2.9, 2.11, and 2.12. The molecular ions and some of common mass fragments of mediterraneabactin are summarized in Table 2.4 and the *b/y* fragment masses are shown along with the corresponding structures in Figures 2.10 and 2.13. The fragment characteristic of Orn, with the ion *m/z* 115.09 is evident in the mass spectra of biscatechol unit (**2**), monocatechol unit (**3**), and a modified triscatechol compound. Further analysis of the *b/y* fragments showed that the loss of the catechol was identified for these three compounds by the fragment with a *m/z* 137.07 (b_1) (Figures 2.9, 2.11, and 2.12). For compound **3**, the monomer unit of mediterraneabactin, the loss of catechol gave rise to the Orn-Ser fragment, *m/z* 220.13 (y_1), while for compound **2**, the dimer of mediterraneabactin, the loss of the catechol gave rise to the 1-DHB-2-Orn-2-Ser fragment, *m/z* 557.27 (y_1). Fragmentation between Ser-Orn for **3** produces the DHB-Orn fragment with *m/z* 251.11 (b_2) and Ser fragment *m/z* 106.05 (y_2). Fragmentation between Ser-Orn for **2** produces the DHB-Orn fragment with *m/z* 251.11 (b_2) and the 1-DHB-1-Orn-2-Ser fragment with *m/z*

443.17 (y_2). Signals originating from the cleavage of the serine ester in **2** were identified as *m/z* 338.13 and *m/z* 356.14. Other common mass fragments seen in **2** include the loss of DHB-Orn with *m/z* 443.17, and the loss of DHB-Orn-Ser with *m/z* 356.14 (Figure 2.10).

For the modified triscatechol compound, there are two possible structures, a dehydro-alanine triscatechol compound, or cyclized mediterraneabactin. The loss of catechol in a dehydro-alanine compound would give rise to the 2-DHB-3-Orn-2-Ser-1-(Dehydro-Ser) fragment with *m/z* 876, however, this fragment is not observed in the ESI-MS/MS analysis. Fragmentation between Orn and Ser formed the DHB-Orn fragment with *m/z* 251.10 (b_2) and the 2-DHB-2-Orn-2-Ser-1-(Dehydro-Ser) with *m/z* 762.31 (y_2). One signal originating from the cleavage of the serine esters in the modified triscatechol was identified as *m/z* 657.23. Internal fragments of this compound, summarized in Table 2.4 are also observed. Due to the overlap of similar fragments in the dehydro-alanine and cyclized mediterraneabactin compound, it is difficult to differentiate between the two compounds by ESI-MSMS. The distinguishing fragment for the dehydro-alanine triscatechol compound that would need to be observed is *m/z* 876 to identify the presence of this compound. This fragment is not seen, but the absence of this mass is not definitive evidence for the cyclic compound. Overall, the molecular ion $[M+H]^+$ at *m/z* 1012.4167 could be a dehydro-alanine triscatechol compound or cyclized mediterraneabactin. In the case of turnerbactin, the cyclic form was not observed, while the dehydro-turnerbactin was isolated and structurally characterized.[8]

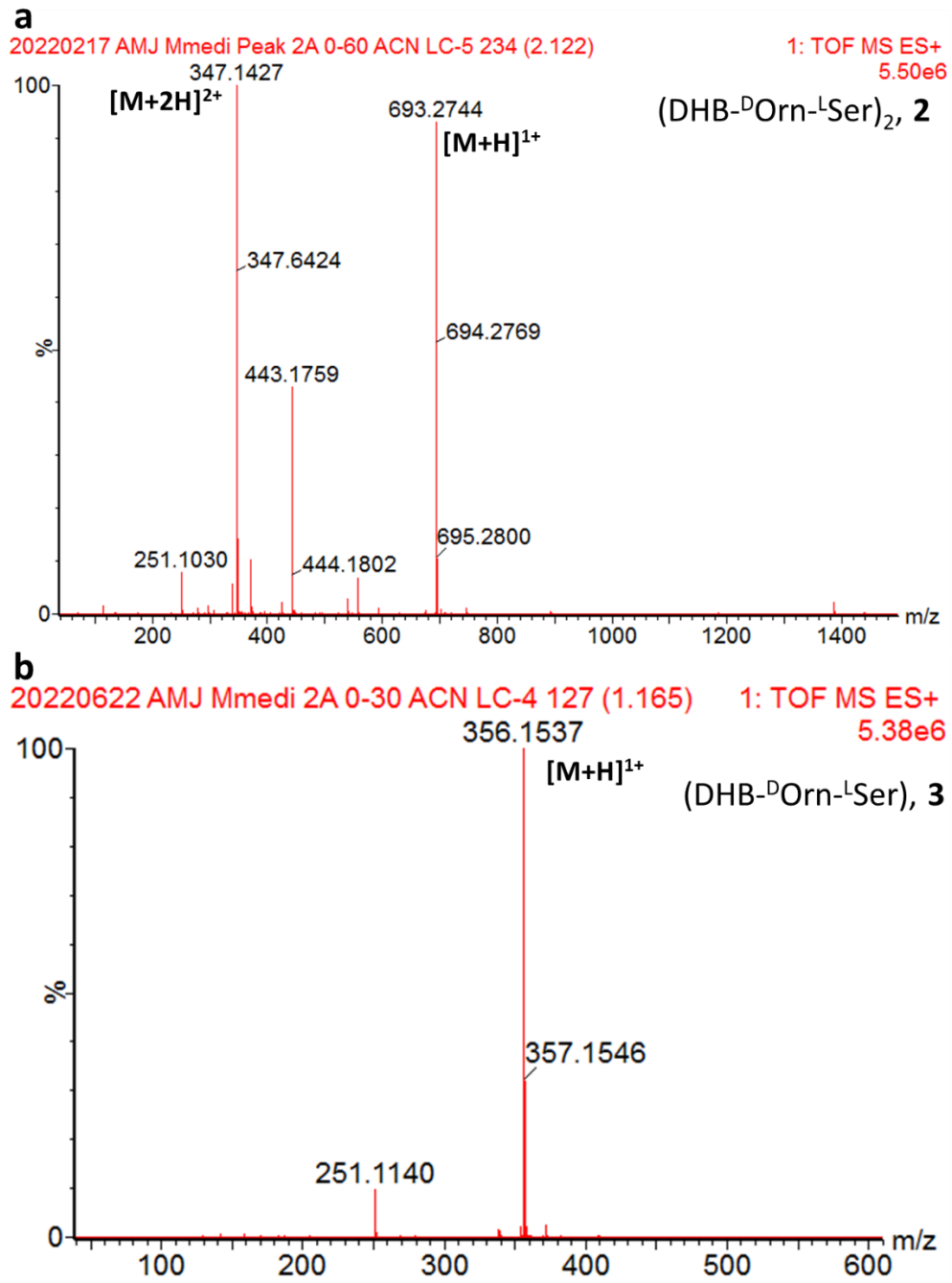

Figure 2.8. (a) HR-ESI-MS spectrum of dimer unit (DHB-^{D}Orn-^{L}Ser)$_2$ associated with mediterraneabactin, *m/z* 693.2744 ($C_{30}H_{41}N_6O_{13}$). (b) HR-ESI-MS spectrum of the monomer unit (DHB-^{D}Orn-^{L}Ser) associated with mediterraneabactin, *m/z* 356.1537 ($C_{15}H_{22}N_3O_7$).

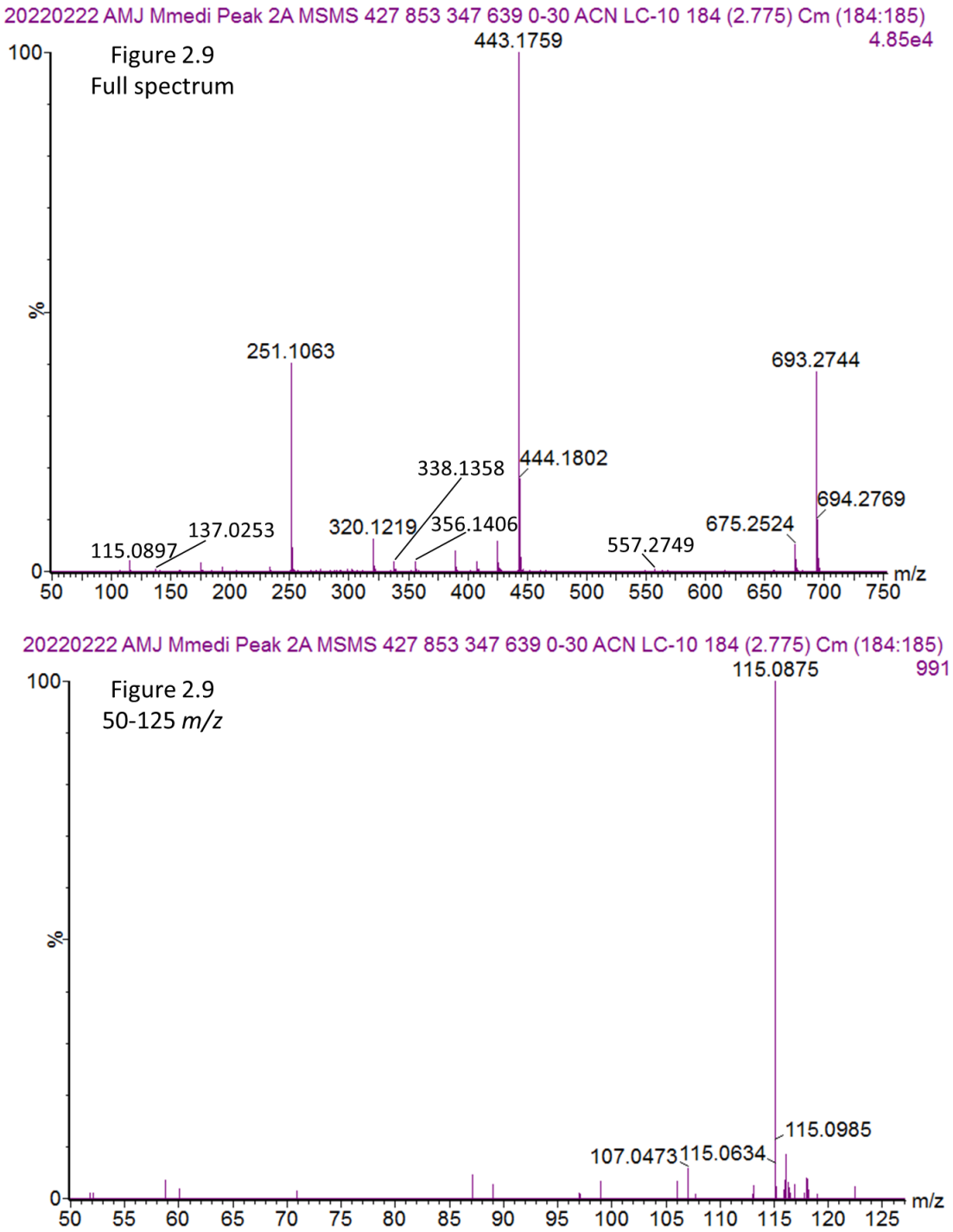

Figure 2.9. ESI-MSMS spectrum of mediterraneabactin dimer unit (DHB-^{D}Orn-^{L}Ser)$_2$ (*m/z* 693.2744), with selected regions zoomed in for clarity. Collision energy profile of 20, 25, and 30 kEV employed for optimal fragmentation.

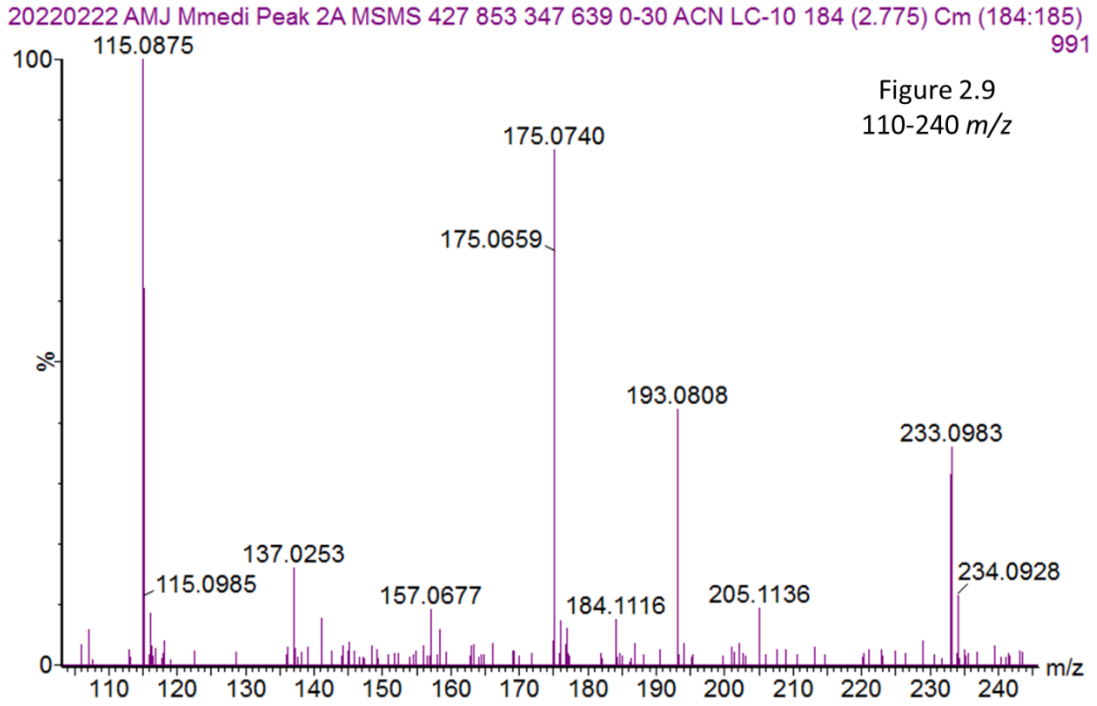

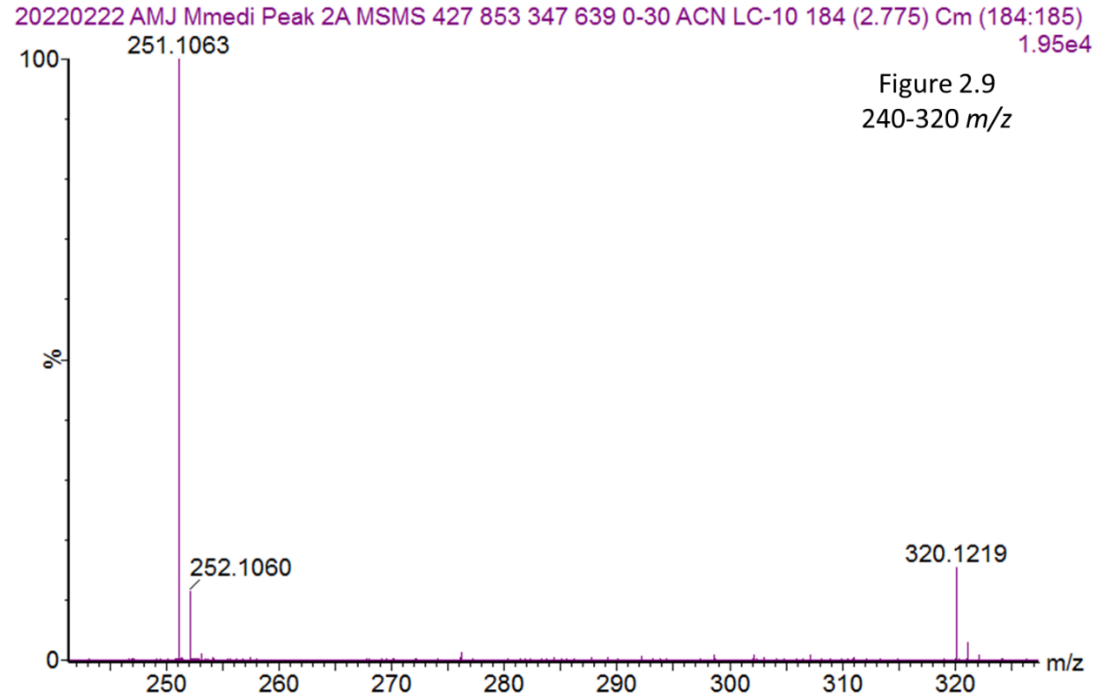

Figure 2.9. Continued

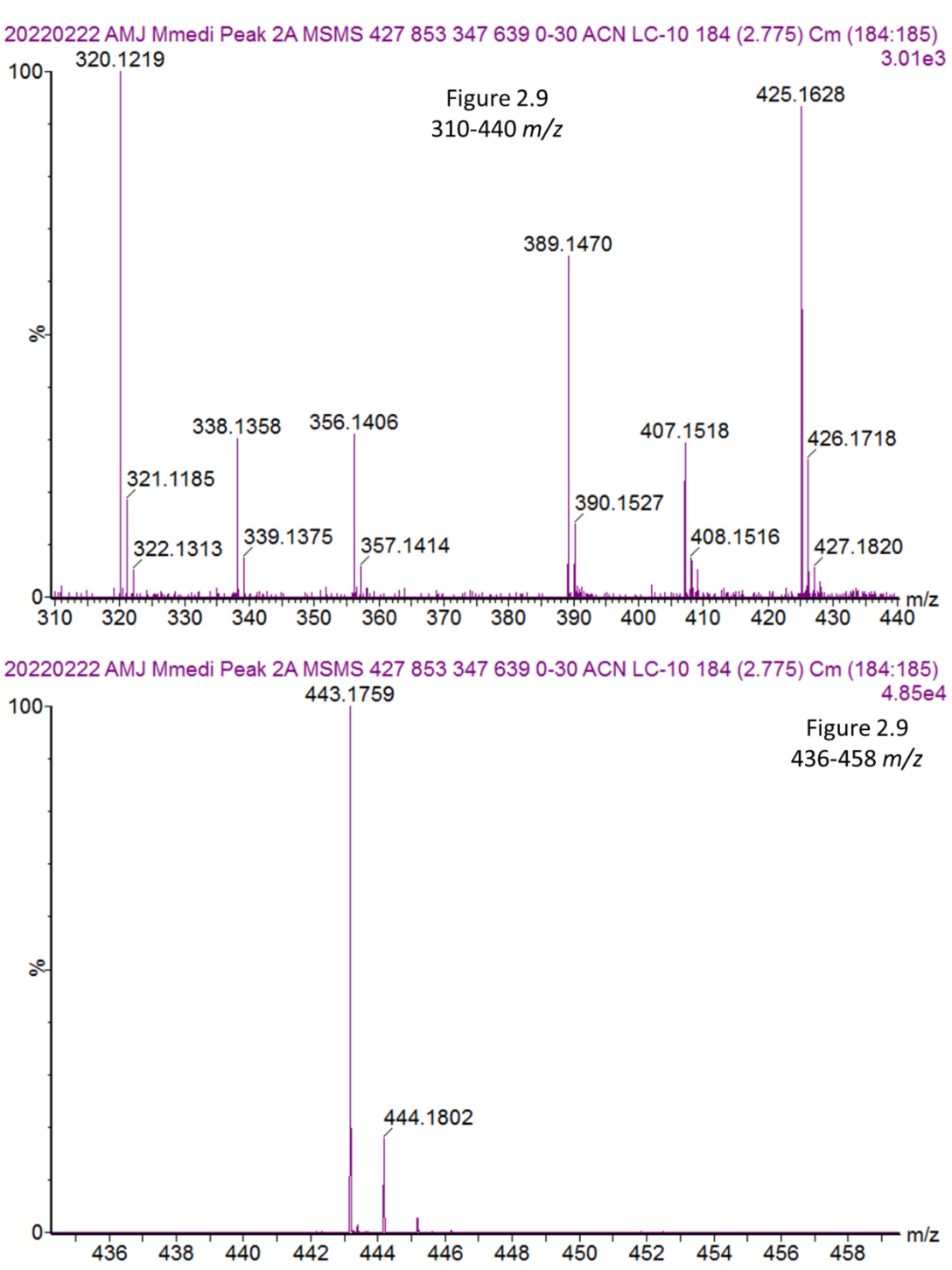

Figure 2.9. Continued

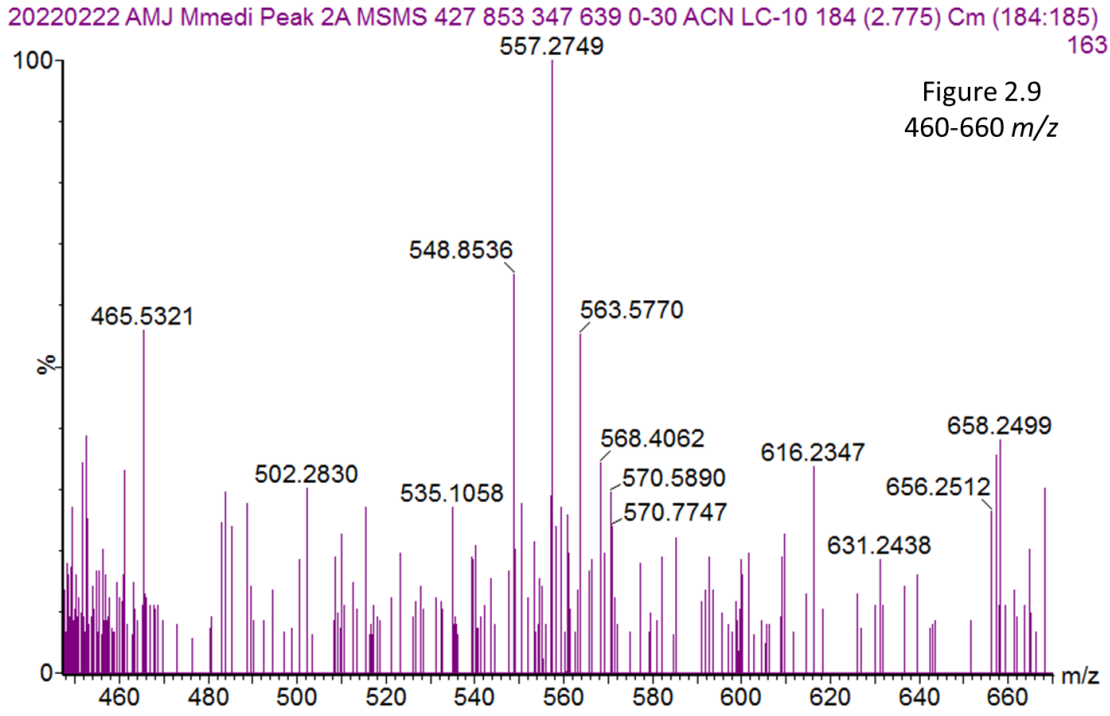

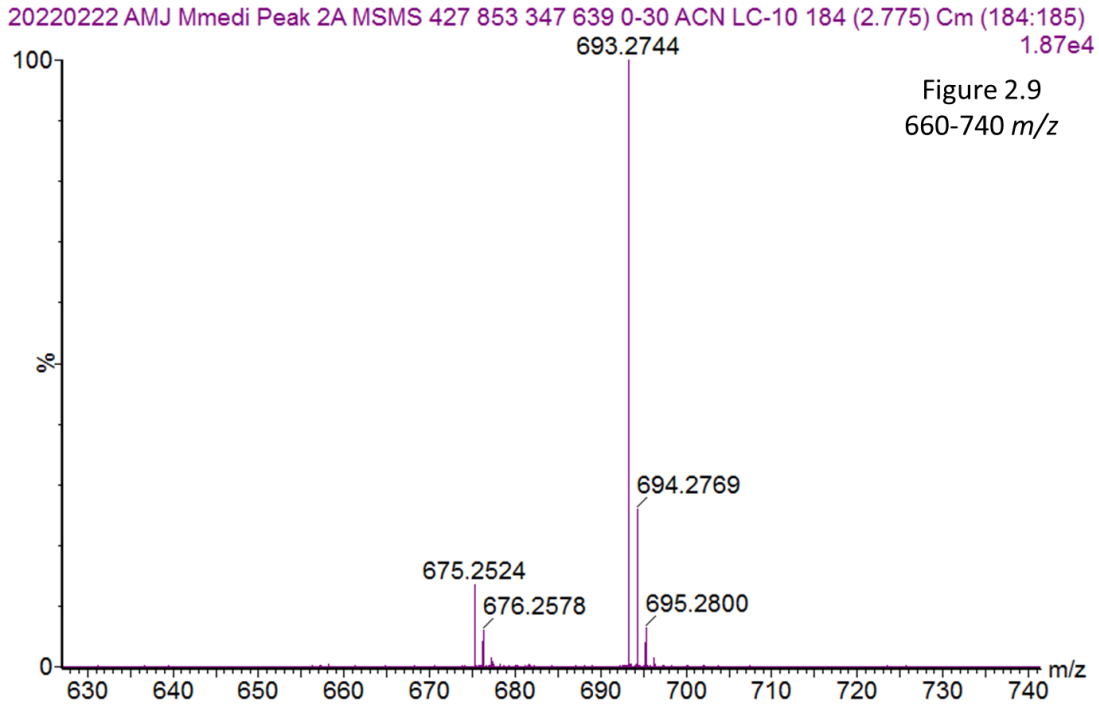

Figure 2.9. Continued

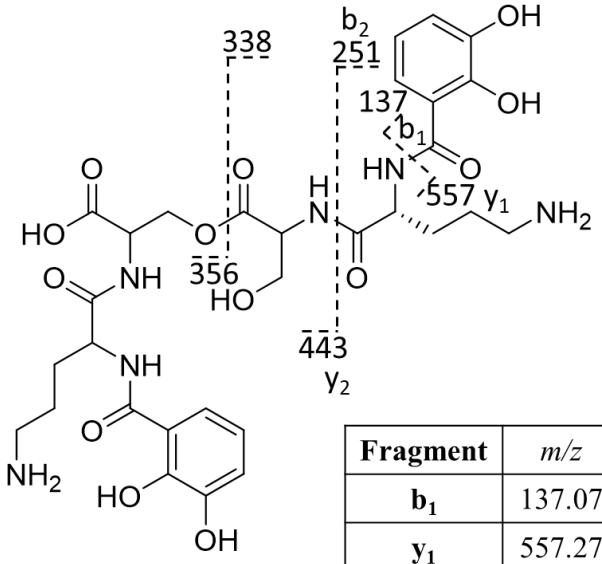

(DHB-^{D}Orn-^{L}Ser)$_2$, **2**
m/z 693.27 [M+H]$^+$

Fragment	*m/z*
$\mathbf{b_1}$	137.07
$\mathbf{y_1}$	557.27
$\mathbf{b_2}$	251.11
$\mathbf{y_2}$	443.17
1'	338.14
2'	356.14

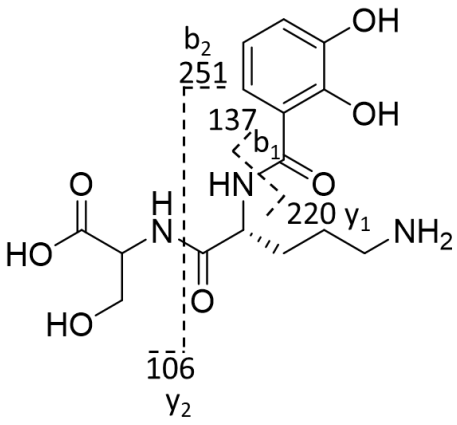

(DHB-^{D}Orn-^{L}Ser), **3**
m/z 356.15 [M+H]$^+$

Fragment	*m/z*
$\mathbf{b_1}$	137.07
$\mathbf{y_1}$	220.13
$\mathbf{b_2}$	251.11
$\mathbf{y_2}$	106.05

Figure 2.10. Structure of mediterraneabactin dimer unit (DHB-^{D}Orn-^{L}Ser)$_2$ (**2** - left), and monomer unit (DHB-^{D}Orn-^{L}Ser) (**3** – right) with b/y fragments.

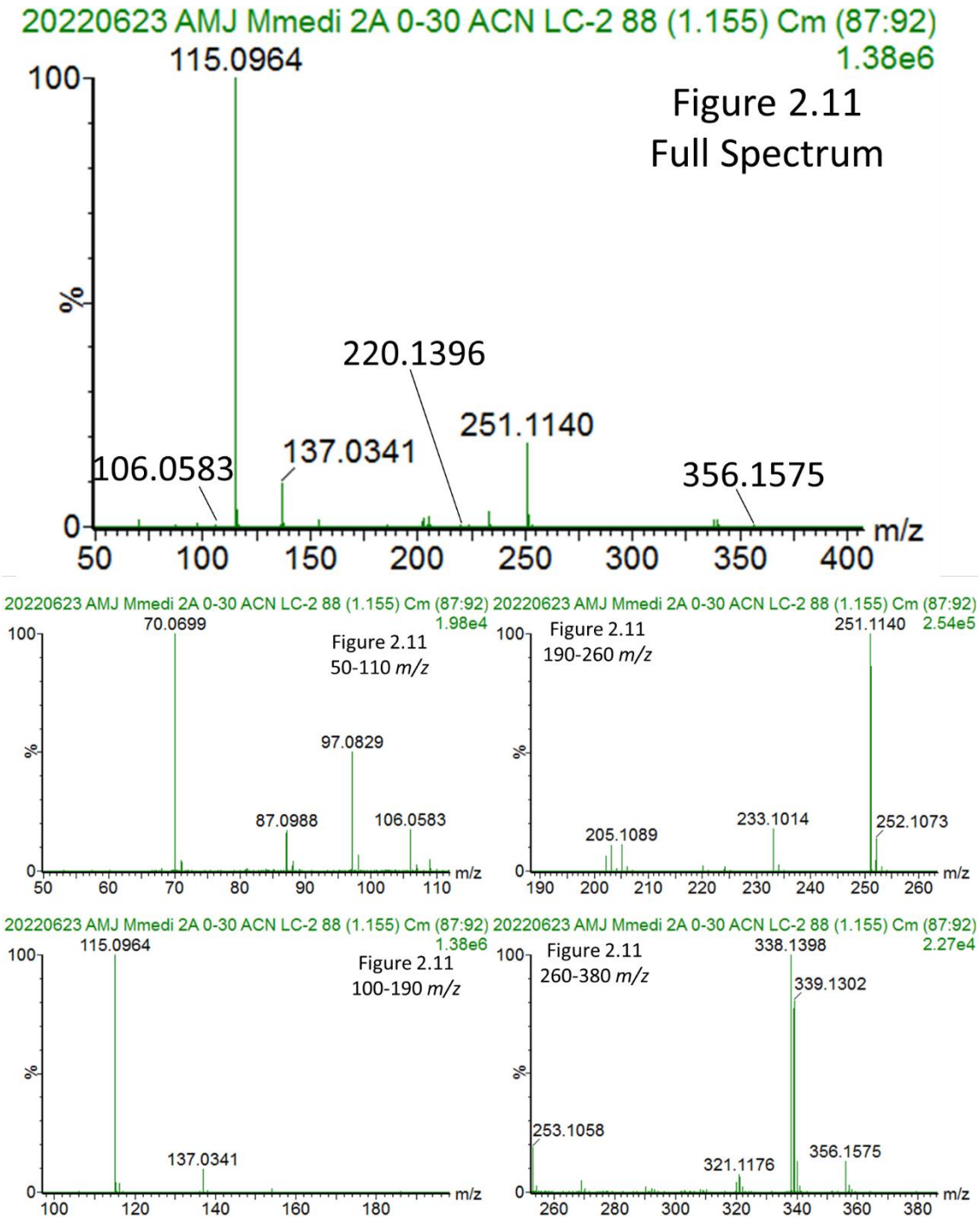

Figure 2.11. ESI-MSMS of the monomer unit (DHB-Orn-Ser) with a parent mass of *m/z* 356.1 $[M+H]^+$ ($C_{15}H_{22}N_3O_7$) with selected regions zoomed in for clarity. Collision energy profile of 20, 25, and 30 kEV employed for optimal fragmentation.

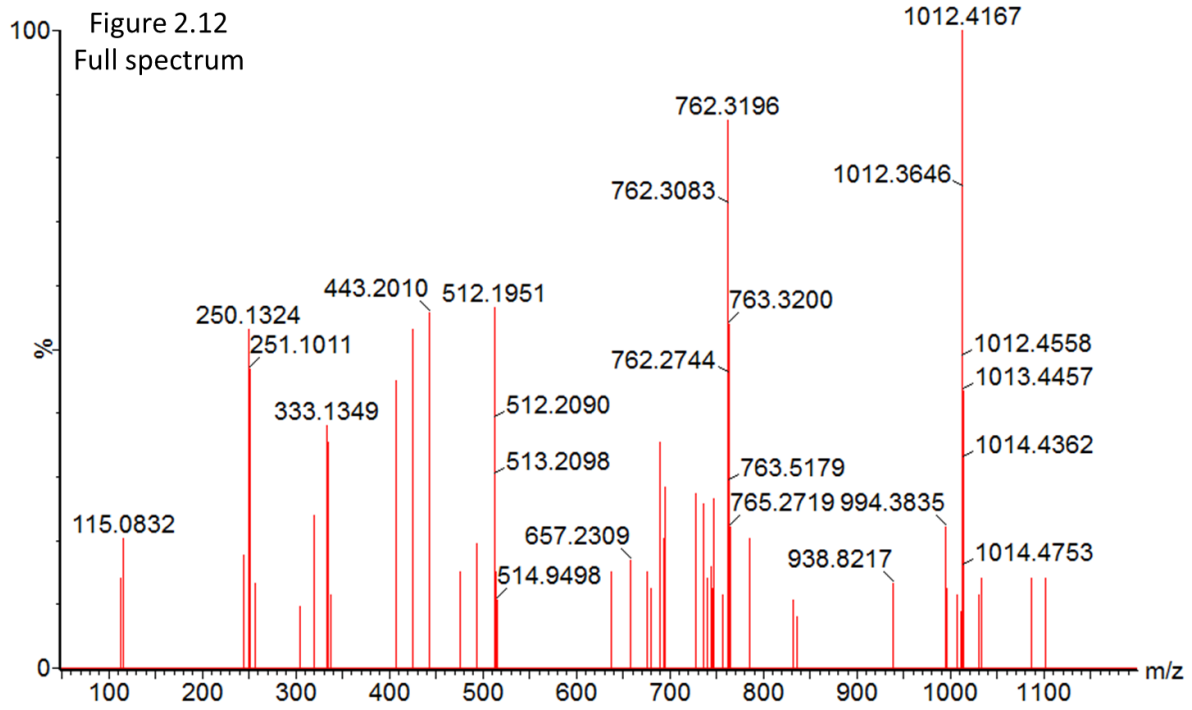

Figure 2.12. ESI-MSMS of the compound with a parent mass of *m/z* 1012.41 $[M+H]^+$, 18 amu less than mediterraneabactin (*m/z* 1030.40 $[M+H]^+$) $(DHB\text{-}Orn\text{-}Ser)_3$ ($C_{45}H_{58}N_9O_{18}$), selected regions zoomed in for clarity. Collision energy profile of 20, 25, and 30 kEV employed for optimal fragmentation.

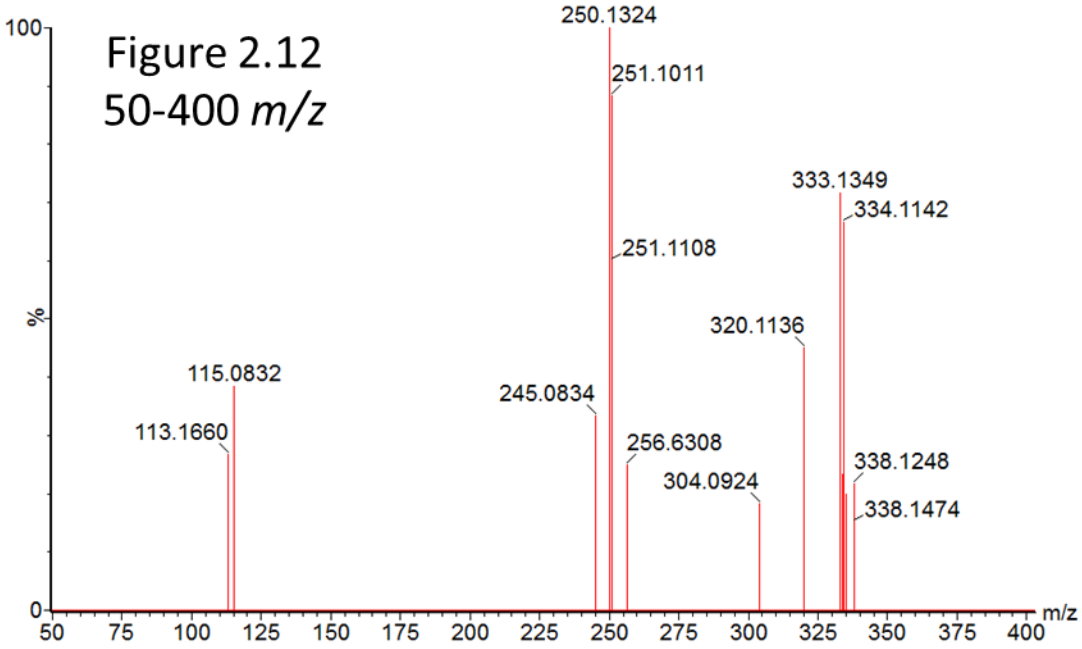

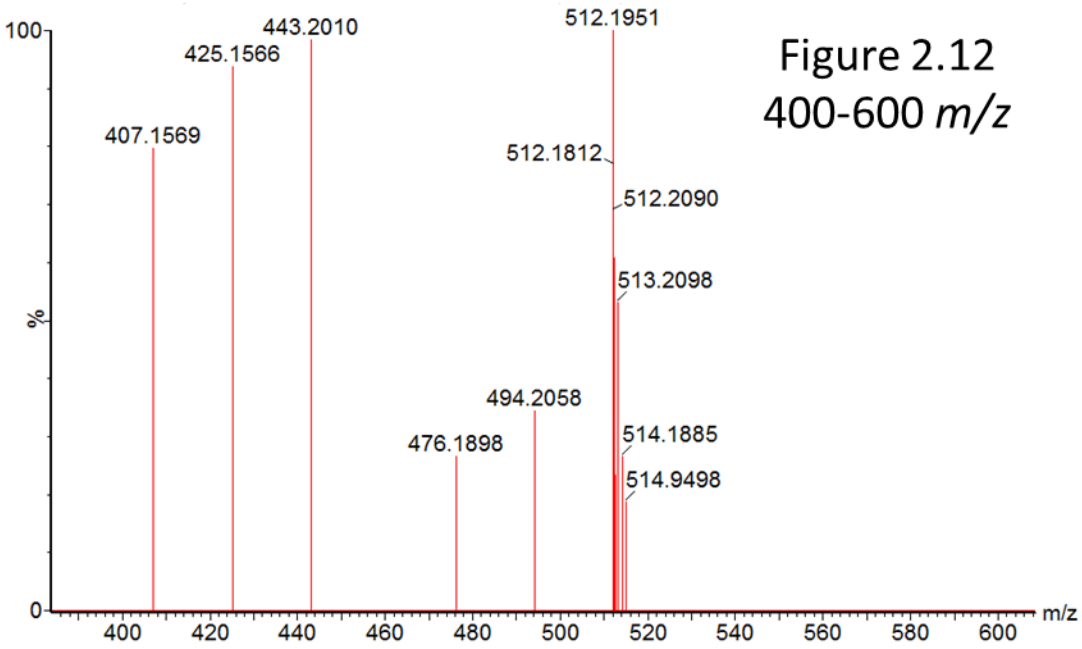

Figure 2.12. Continued

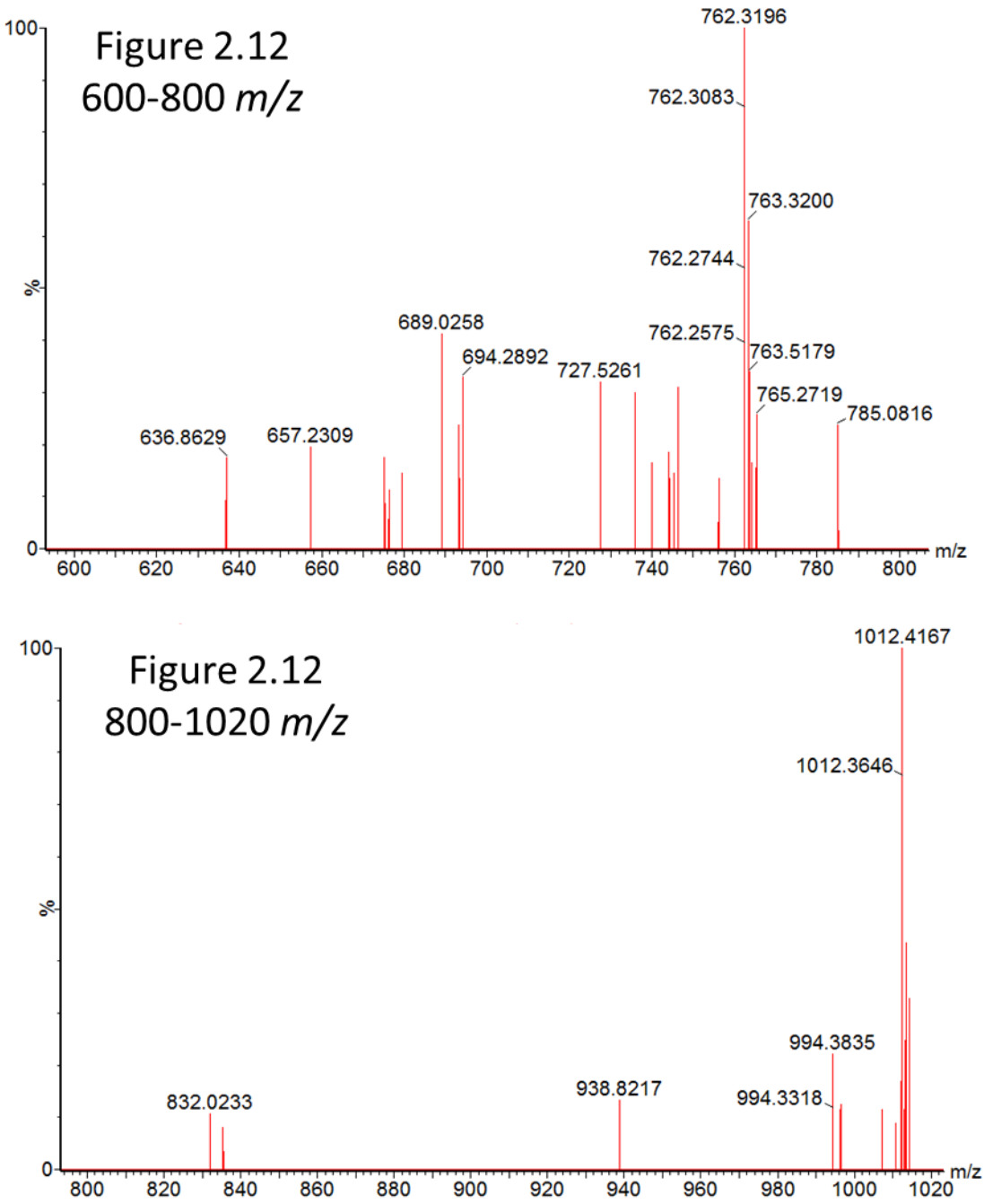

Figure 2.12. Continued

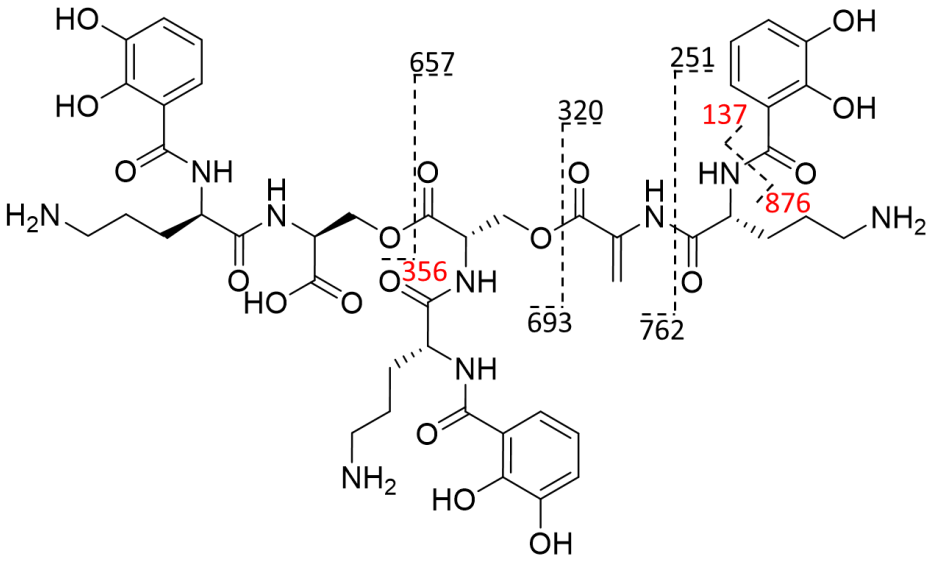

Fragment	b_1	y_1	b_2	y_2	1'	2'	1	2
m/z	137.07	875.33	251.11	762.31	320.11	693.28	657.23	356.15

Figure 2.13. Possible structure of compound with a parent mass of *m/z* 1012.41 $[M+H]^+$, 18 amu less than mediterraneabactin, with key peptide fragment masses (fragment with *m/z* in red was not observed).

2.4.3. Chiral Amino Acid Analysis of Mediterraneabactin

The mediterraneabactin gene cluster (Figure 2.2) contains an epimerization domain within the NRPS assembly line. Given the placement of the epimerization domain, incorporation of ^{D}Orn is expected. Chiral amino acid analysis reveals the difference in structure of mediterraneabactin (**1**) and turnerbactin (Figure 2.14). This amino acid analysis of mediterraneabactin established the presence of D-ornithine and L-serine. Mediterraneabactin was acid hydrolyzed and subsequently derivatized with Marfey's reagent (1-fluoro-2,4-dinitrophenyl-5-L-alanine amide, FDAA).[15] This chiral derivatizing reagent, FDAA, allows for the differentiation between D- and L- isomers of amino acids and is very important in siderophore characterization especially when differentiating between two siderophores where the only difference is one chiral amino acid.

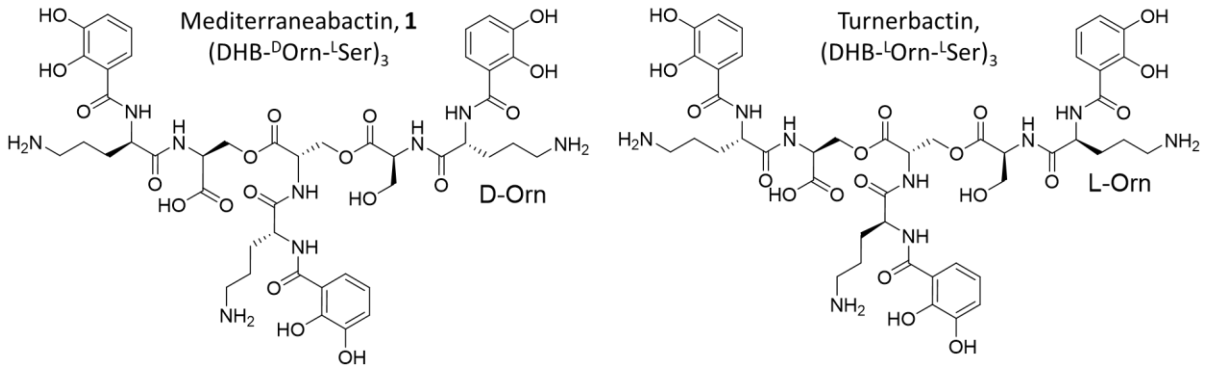

Figure 2.14. Structure comparison of mediterraneabactin produced by *M. mediterranea* MMB-1 to its diastereomer turnerbactin, produced by *T. turnerae* T7901.

Possible FDAA-derivatives of the hydrolysis products of mediterraneabactin are shown in Figure 2.15. Figure 2.16a -e presents the HPLC chromatograms of Marfey's assay for the HCl hydrolysis products of mediterraneabactin. The derivatized samples were compared to chiral amino acid standards prepared the same way (Figure 2.17ab). Assignments were confirmed by co-injection of the derivatized siderophore sample with amino acid standards. Retention times (minutes) of the FDAA-derivatized amino acids used as standards were ^{D}Ser (25.48, mono α-derivative), ^{L}Ser (23.67, mono α-derivative), ^{D}Orn(19.28, mono α-derivative; 23.16, mono δ-derivative, and 41.92, bis-derivative), ^{L}Orn (19.50, mono α-derivative; 23.16, mono δ-derivative, 44.76, bis-derivative). Retention times (minutes) of FDAA-derivatized hydrolysis products of mediterraneabactin were ^{D}Orn (18.79, mono α-derivative; 23.08, mono δ-derivative, and 41.61, bis-derivative) and ^{L}Ser (24.20, mono α-derivative).

HPLC separation of the FDAA-derivatized amino acids in the presence of added FDAA-derivatized standards of ^{D}Orn, ^{L}Orn, ^{D}Ser, and ^{L}Ser established the presence of ^{D}Orn and ^{L}Ser in mediterraneabactin. Therefore, this chiral amino acid analysis confirms the

genomic prediction of ^{D}Orn and ^{L}Ser in mediterraneabactin, (DHB-^{D}Orn-^{L}Ser)$_3$, making it the diastereomeric siderophore to turnerbactin, (DHB-^{L}Orn-^{L}Ser)$_3$.

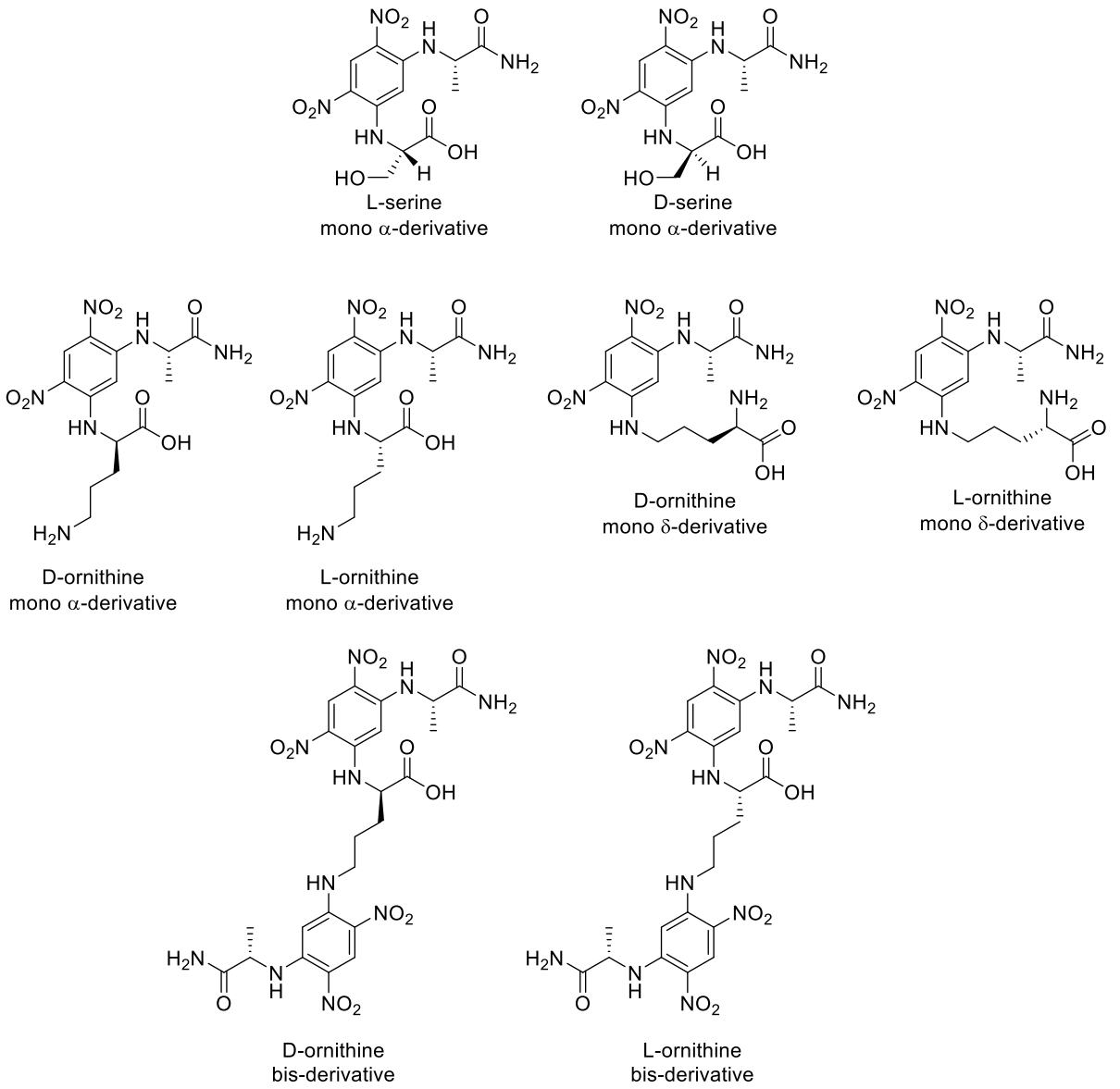

Figure 2.15. Possible FDAA-derivatives of amino acids serine and ornithine resulting in the hydrolysis of mediterraneabactin siderophores.

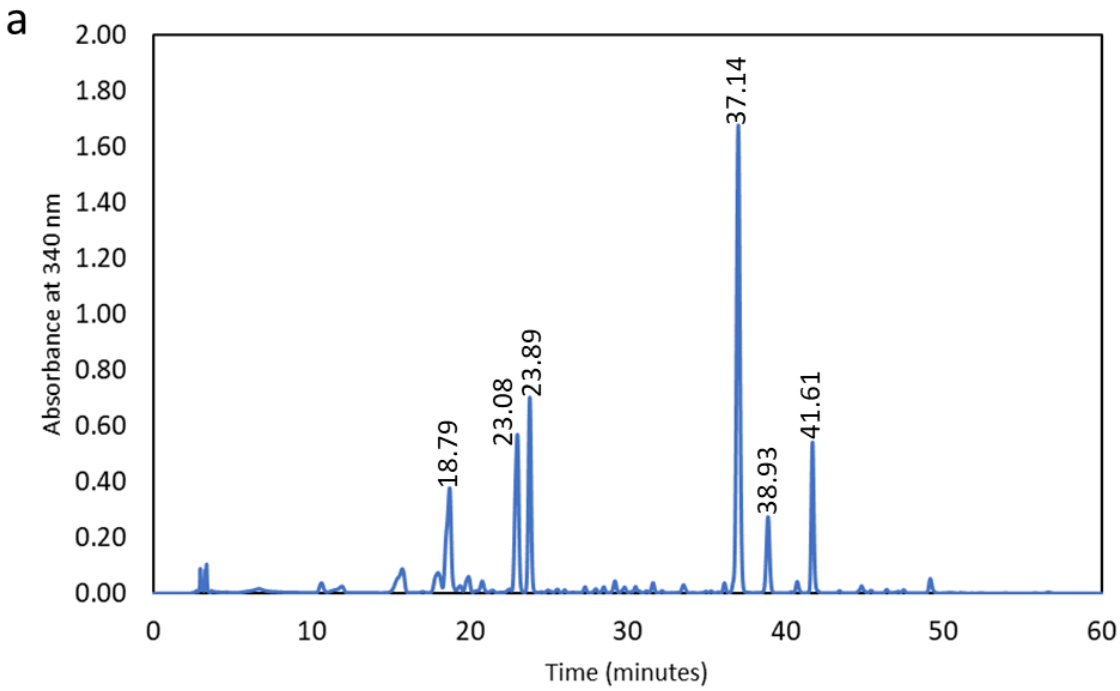

Figure 2.16. HPLC chromatograms of Marfey's assay for HCl hydrolysis product of mediterraneabactin. (a). Mediterraneabactin. (b) Mediterraneabactin co-injected with D-ornithine (c) Mediterraneabactin co-injected with L-ornithine (d) Mediterraneabactin co-injected with D-serine (e) Mediterraneabactin co-injected with L-serine. Derivatized amino acids from HCl hydrolysis product of mediterraneabactin was separated by HPLC on a YMC 4.6x250mm C18-AQ column with a gradient from 10% to 45% CH_3CN in triethylamine in phosphoric acid over 45 minutes at a flow rate of 1.0 ml/min. The absorbance was monitored at 340 nm. Retention times are assigned as follows: D-ornithine (18.79, 23.08, 41.61), L-ornithine (19.37, 23.08, 44.62), D-serine (25.48), L-serine (23.89), FDAA (37.14), unidentified peak (38.93). Retention times varied slightly from one run to another.

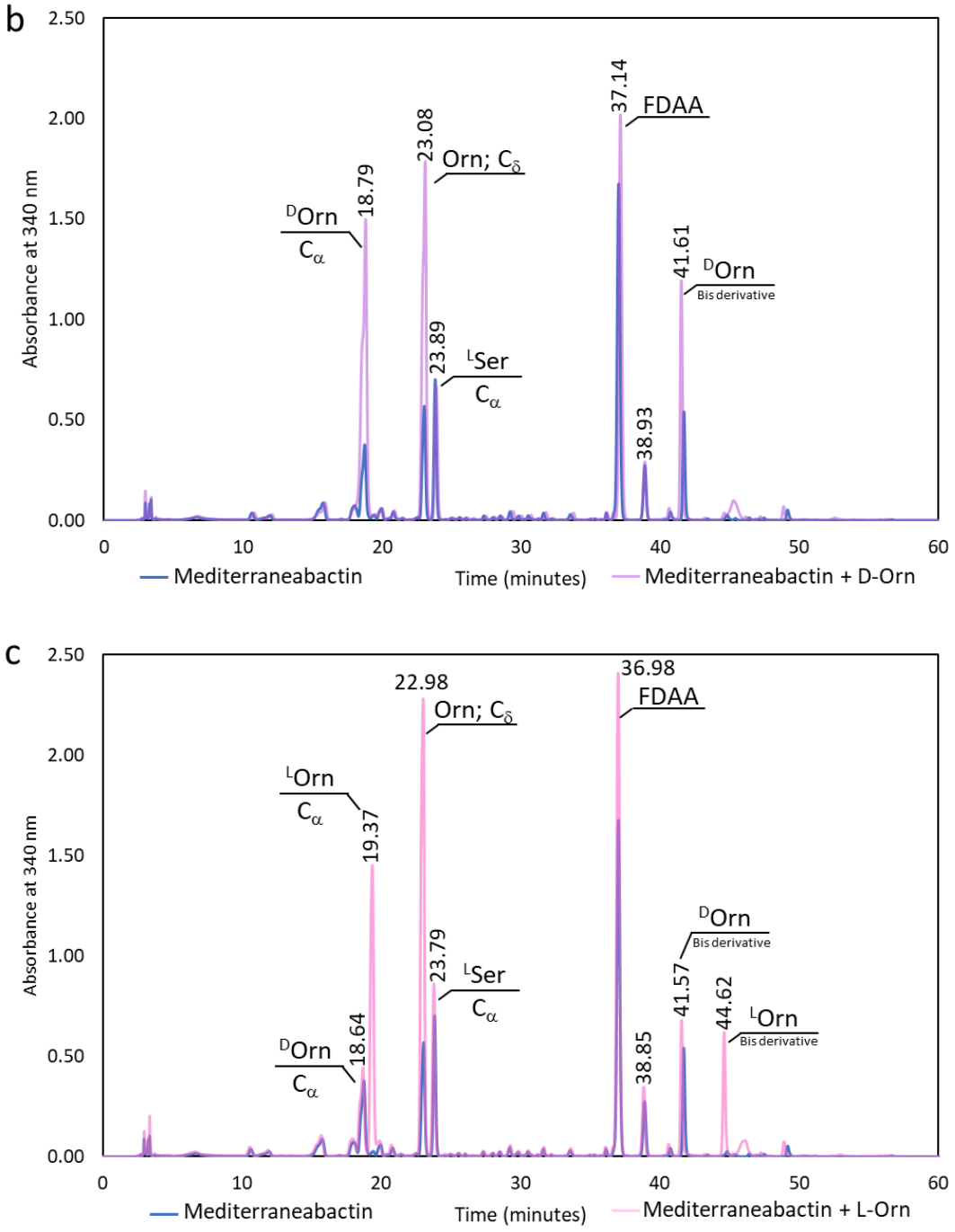

Figure 2.16. Continued

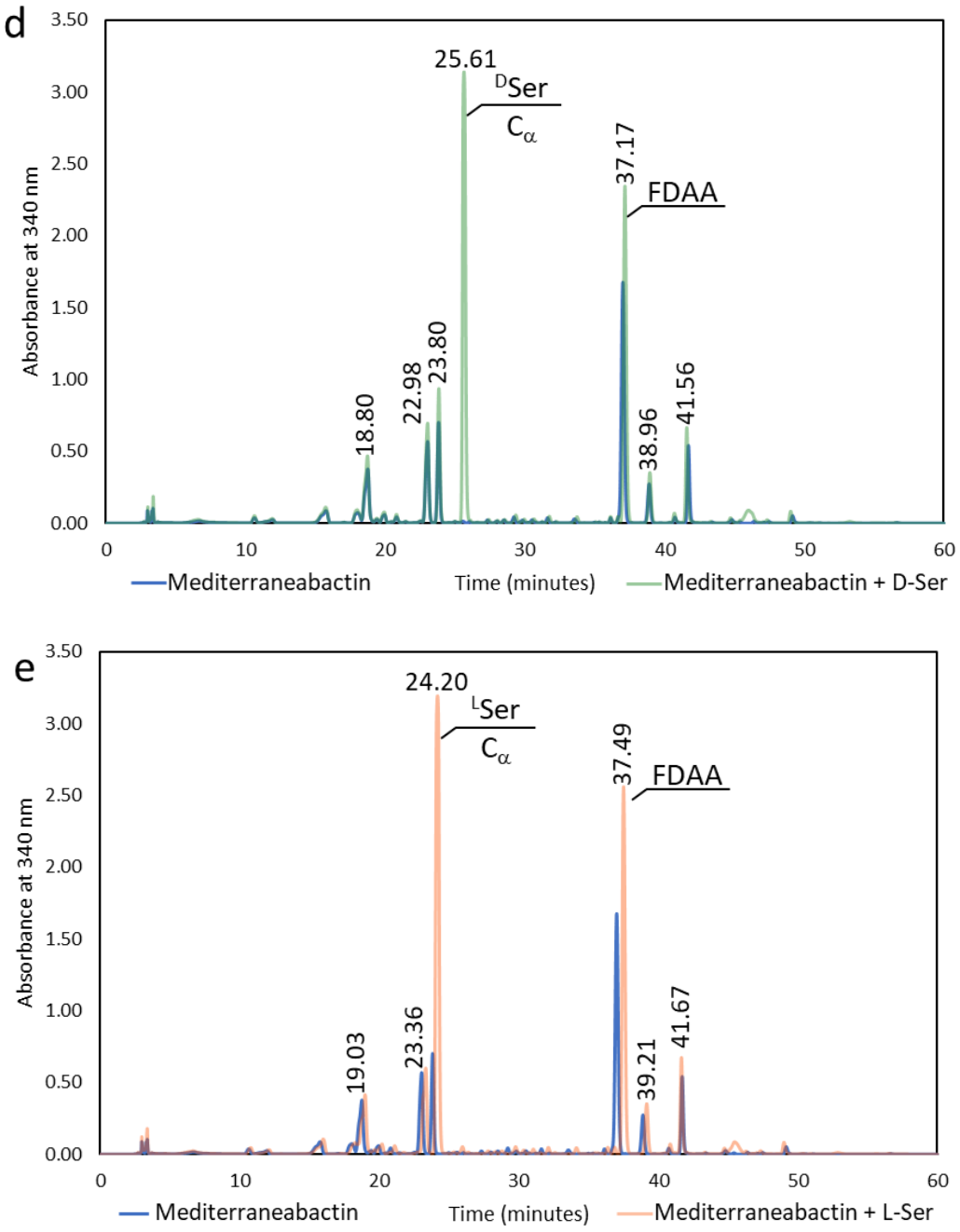

Figure 2.16. Continued

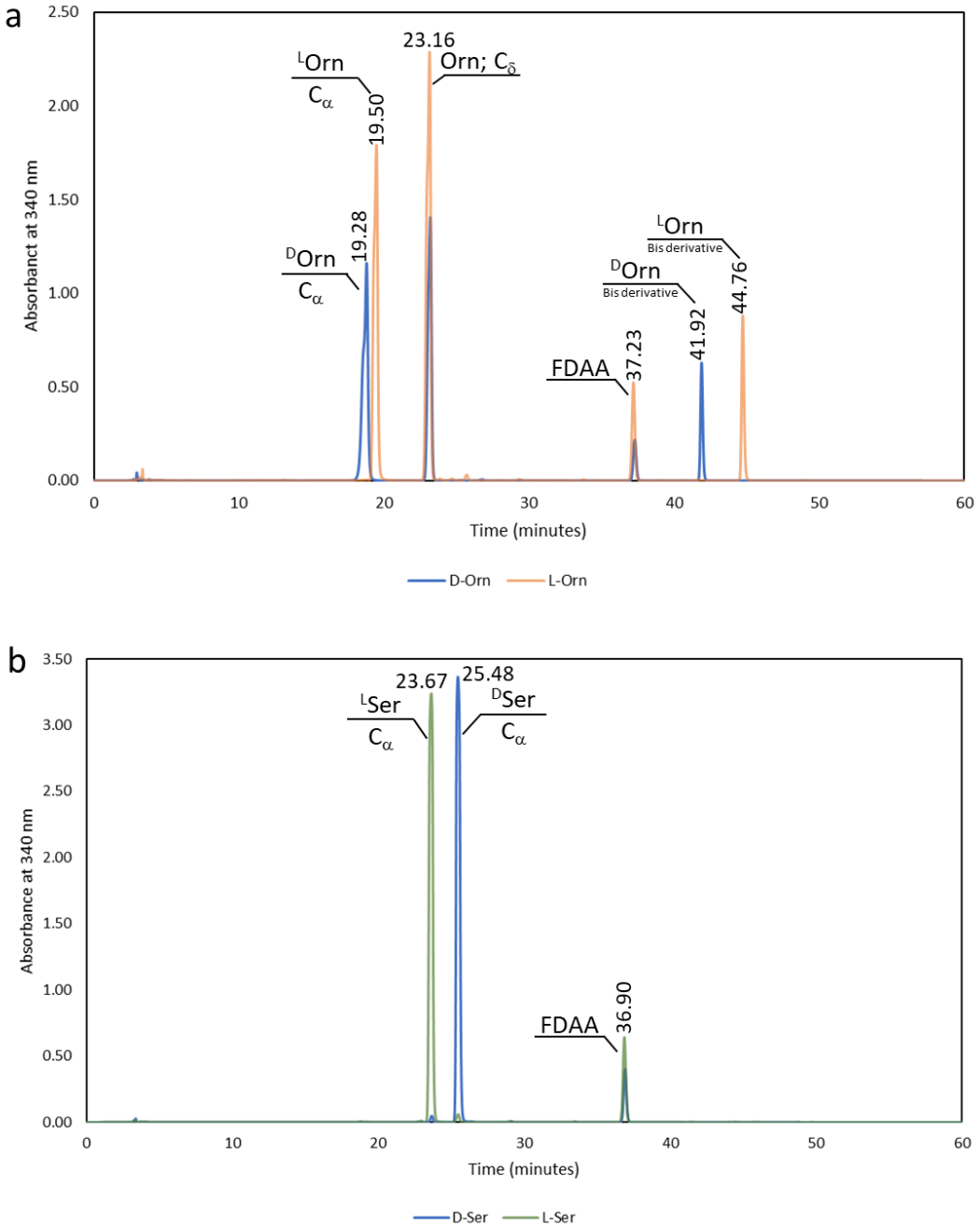

Figure 2.17. HPLC chromatograms of Marfey's assay amino acid standards to use in comparison of the HCl hydrolysis product of mediterraneabactin. (a). D-Ornithine and L-Ornithine Standards (b) D-Serine and L-Serine Standards Derivatized amino acids were separated by HPLC on a YMC 4.6x250mm C18-AQ column with a gradient from 10% to 45% CH_3CN in triethylamine in phosphoric acid over 45 minutes at a flow rate of 1.0 ml/min. The absorbance was monitored at 340 nm. Retention times are assigned as follows: D-ornithine (19.28, 23.16, 41.92), L-ornithine (19.50, 23.16, 44.76), D-serine (25.48), L-serine (23.89), FDAA (37.23). Retention times varied slightly from one run to another.

2.4.4. Chirality of Fe(III)-Mediterraneabactin and Fe(III)-Turnerbactin

A tris bidentate catechol siderophore will form an octahedral metal complex and can result in either the Λ or the Δ configuration. The diastereomeric counter to Fe(III)-trivanchrobactin is Fe(III)-ruckerbactin with ^{L}Arg and adopts the Δ configuration.[7] Similar results are observed with ^{D}Lys in Fe(III)-cyclic trichrysobactin directing the formation of the Λ configuration, while ^{L}Lys in Fe(III)-frederiksenibactin adopts the Δ configuration.[6] On top of the trend already presented, enterobactin, a macrolactone of (DHB-^{L}Ser)$_3$, adopts the Δ configuration,[1] while the synthetic enantiomer of enterobactin (DHB-^{D}Ser)$_3$ adopts the Λ configuration.[4] These three sets of diastereomeric counters demonstrate the D-amino acids direct the chirality of the Fe(III) complex toward the Λ configuration, while the L-amino acids direct toward the Δ configuration. Now, the question arises whether ^{D}Orn in mediterraneabactin affects the chirality at the Fe(III) center in Fe(III)-mediterraneabactin in the same manner that ^{D}Arg in Fe(III)-trivanchrobactin forms the Λ configuration.[7] Electronic circular dichroism (ECD) spectroscopy was utilized to identify the chirality of Fe(III)-mediterraneabactin in comparison to Fe(III)-turnerbactin and how the diastereomeric amino acids, ^{D}Orn and ^{L}Orn affect the chirality. The ECD spectra of Fe(III)-mediterraneabactin and Fe(III)-turnerbactin both display four bands and are inverted in sign from each other (Figure 2.18, Table 2.5). The ECD spectra of the two Fe(III)-bound diastereomeric siderophores appear as near images of each other, where Fe(III)-mediterraneabactin adopts the Λ configuration and Fe(III)-turnerbactin the Δ configuration, after comparison to the CD spectra of Fe(III)-enterobactin and Fe(III)-bacillibactin.[3 4]. This result indicates an opposite configurational preference around iron due to the opposite chirality of the amino acid ornithine. The opposing

chirality for the ferric complexes is likely due to the stereochemistry of the Orn residue adjacent to the catecholamide. We observe that the siderophores with the D-amino acid takes on the Λ configuration, in this case Fe(III)-mediterraneabactin, Fe(III)-trivanchrobactin, and Fe(III)-cyclic trichrysobactin. The siderophores with the L-amino acid adjacent to the catecholamide all take on the Δ configuration, Fe(III)-turnerbactin, Fe(III)-ruckerbactin, Fe(III)-frederiksenibactin and Fe(III)-enterobactin (DHB-^{L}Ser)$_3$.

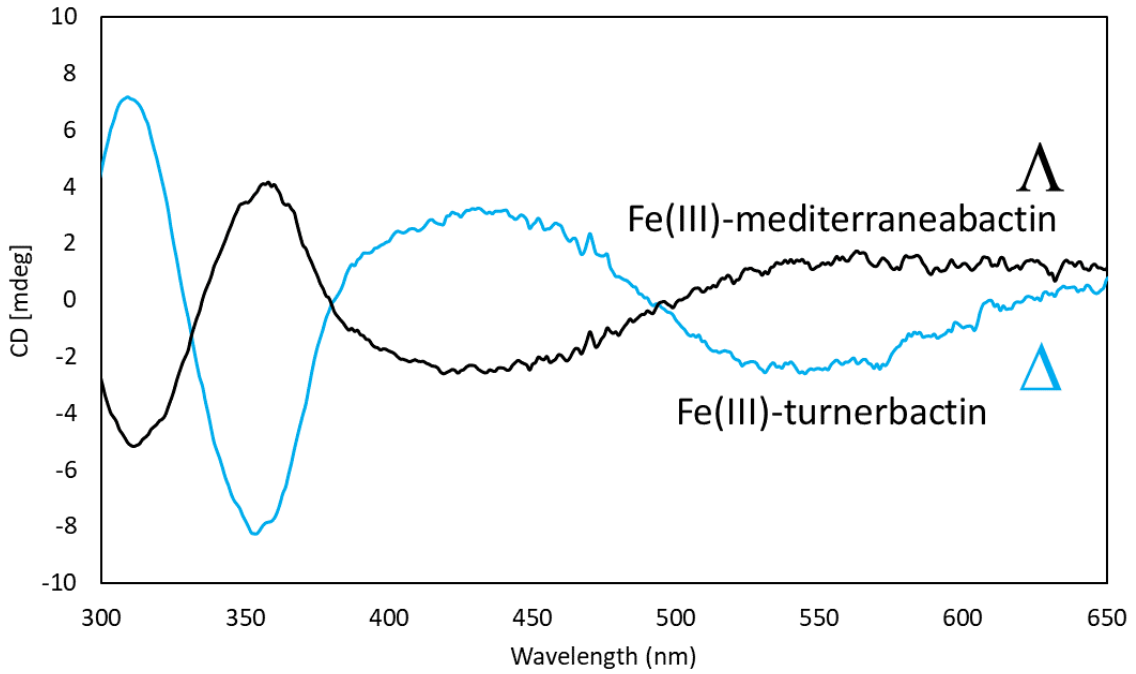

Figure 2.18. ECD spectra of Fe(III)-mediterraneabactin and Fe(III)-turnerbactin. Conditions: approximately 50 μM Fe(III)-mediterraneabactin (citrate-phosphate buffer, pH 7.4), and 50 μM Fe(III)-turnerbactin (citrate-phosphate buffer, pH 7.4).

Table 2.5. Comparison of the molar ellipticity of the transitions in Fe(III)-mediterraneabactin and Fe(III)-turnerbactin.

	$\pi \rightarrow \pi^*, \Delta\varepsilon$	$\pi \rightarrow \pi^*, \Delta\varepsilon$	LMCT, $\Delta\varepsilon$	LMCT, $\Delta\varepsilon$
Mediterraneabactin	311 nm, (-6.01)	360 nm (2.89)	434 nm (-3.18)	565 nm (0.56)
Turnerbactin	309 nm, (6.39)	354 nm (-9.67)	431 nm (2.61)	563 nm (-3.44)

2.4.5. Analysis of the Acinetobactin Gene Cluster for Siderophore Biosynthesis

The acinetobactin gene cluster in *A. baumannii* ATCC 19606 responsible for the biosynthesis, export, and uptake of acinetobactin was identified in studies by Yamamoto and Actis.[16 17 18] Analysis of the *M. mediterranea* MMB-1 genome with antiSMASH[12] does not reveal a biosynthetic gene cluster associated with acinetobactin. However, according to *in silico* predictions using BLAST comparisons to the acinetobactin BGC in *A. baumannii* ATCC 19606 (Table 2.6), we identified a cluster of genes within *M. mediterranea* MMB-1 with over 45% identity to the acinetobactin biosynthesis genes (Figure 2.19-20). A total of 18 genes are involved in the biosynthesis, export, and uptake of acinetobactin in *A. baumannii* ATCC 19606. In *M. mediterranea* MMB-1, 16 out of the 18 genes were identified. The two genes that were not identified in *M. mediterranea* MMB-1 are *basH*, which encodes an acinetobactin biosynthesis thioesterase and *bauF*, an acinetobactin utilization protein. Interestingly, the genes 13-15, and 17 (Table 2.6), with similarity to *basB*, *basE*, *basF*, and *basI* respectively, are found further downstream from the cluster, and are the same genes in the BGC for mediterraneabactin.

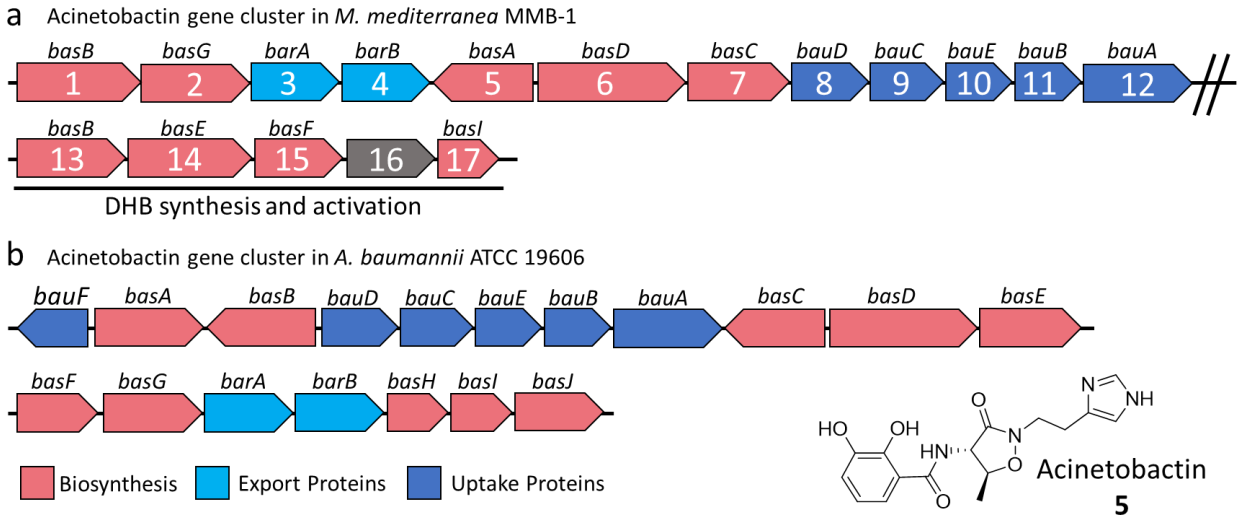

Figure 2.19. Biosynthetic gene clusters of acinetobactin identified in (a) *Marinomonas mediterranea* MMB-1 in comparison to the BGC in (b) *Acinetobacter baumannii* ATCC 19606.

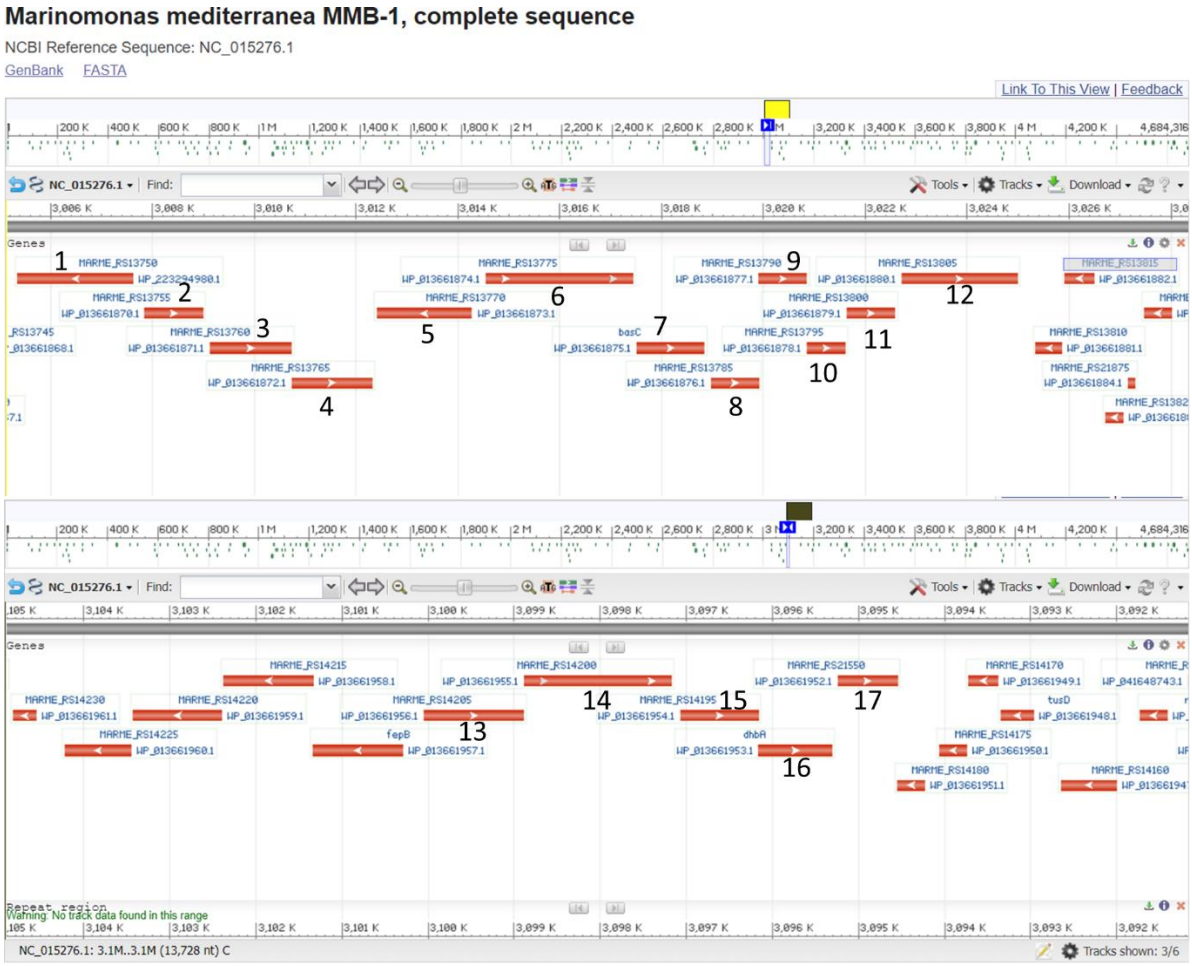

Figure 2.20. Graphical representation of the acinetobactin gene cluster within *M. mediterranea* MMB-1. Genome generated from the National Center for Biotechnology Information (NCBI) website.

Table 2.6. Annotation of acinetobactin gene cluster in *Marinomonas mediterranea* MMB-1, including predicted protein functions based on sequence analysis using Pfam and BLAST. The sequence similarity of each gene to the corresponding homolog from the acinetobactin gene cluster (*A. baumannii* ATCC 19606) is indicated.

Homolog in *A. baumanii* ATCC 19606 NZ_CP045110.1	**Gene Name***	**I%**	**Number**	**Location**	***M. mediterranea* MMB-1** NC_015276.1	**Protein Size**	**Proposed function in *M. mediterranea* MMB-1**
WP_000939830.1	*basB*	46.90%	1	3,005,347..3,007,629	WP_223294980.1	760 aa	condensation domain-containing protein
WP_000603884.1	*basG*	71.51%	2	3,007,844..3,008,995	WP_013661870.1	383 aa	histidine decarboxylase
WP_001281550.1	*barA*	55.22%	3	3,009,123..3,010,733	WP_013661871.1	536 aa	ABC transporter ATP-binding protein/permease
WP_001090097.1	*barB*	58.60%	4	3,010,730..3,012,319	WP_013661872.1	592 aa	ABC transporter ATP-binding protein/permease
WP_000910263.1	*basA*	51.83%	5	3,012,398..3,014,278	WP_013661873.1	626 aa	AMP-binding protein
WP_001177731.1	*basD*	46.19%	6	3,014,544..3,017,441	WP_013661874.1	965 aa	Condensation domain-containing protein
WP_000717764.1	*basC*	66.44%	7	3,017,500..3,018,846	WP_013661875.1	448 aa	Putative histamine N-monooxygenase
WP_001210788.1	*bauD*	70.61%	8	3,018,968..3,019,909	WP_013661876.1	313 aa	iron chelate uptake ABC transporter family permease subunit
WP_001223275.1	*bauC*	63.67%	9	3,019,906..3,020,856	WP_013661877.1	316 aa	iron chelate uptake ABC transporter family permease subunit
WP_000582118.1	*bauE*	71.71%	10	3,020,853..3,021,611	WP_013661878.1	252 aa	ATP-binding cassette domain-containing protein
WP_001104129.1	*bauB*	62.50%	11	3,021,624..3,022,592	WP_013661879.1	322 aa	siderophore ABC transporter substrate-binding protein
WP_001073039.1	*bauA*	49.58%	12	3,022,703..3,024,991	WP_013661880.1	762 aa	TonB-dependent siderophore receptor
WP_000983818.1	*basJ*	38.26%	13	3,098,883..3,100,049	WP_013661956.1	388 aa	isochorismate synthase
WP_000744376.1	*basE*	51.44%	14	3,097,171..3,098,886	WP_013661955.1	571 aa	(2,3-dihydroxybenzoyl)adenylate synthase
WP_001018262.1	*basF*	52.35%	15	3,096,161..3,097,066	WP_013661954.1	301 aa	isochorismatase
	NA**		16	3,095,304..3,096,161	WP_013661953.1	285 aa	2,3-dihydro-2,3-dihydroxybenzoate dehydrogenase
WP_001093099.1	*basI*	28.98%	17	3,094,545..3,095,243	WP_013661952.1	232 aa	4'-phosphopantetheinyl transferase superfamily protein

*Color coding of gene name is associated with Figure 2.18. Salmon color represents the biosynthesis genes; light blue the genes encoding export proteins; navy blue – the genes encoding uptake proteins; gray – gene within the BGC that does not have a homolog in *A. baumannii* ATCC 19606. * NA, not applicable (no homolog in the *A. baumannii* ATCC 19606 acinetobactin locus).

2.4.6. Isolation And Structural Characterization of Acinetobactin

Further isolation of siderophores from the supernatant extract of *M. mediterranea* MMB-1, reveals a compound with a molecular ion mass of *m/z* 347.14 ($[M+H]^+$). The structure was elucidated by ESIMSMS, ^1H NMR spectroscopy, identifying it as acinetobactin, previously isolated and the most studied siderophore in the human pathogen *A. baumannii* ATCC 19606. Acinetobactin is a virulence factor for the pathogenic strain and is composed of 2,3-dihydroxybenzoic acid, L-threonine, and N-hydroxyhistamine and features two key motifs, a catechol oxazoline and a histamine connected by a hydroxamate bridge. MSMS analysis displays the same fragmentation as those reported for acinetobactin produced by *A. baumannii* ATCC 19606 (Figure 2.21).[19] Structure analysis via NMR further confirmed the production of acinetobactin (Figure 2.22-23, Table 2.7).

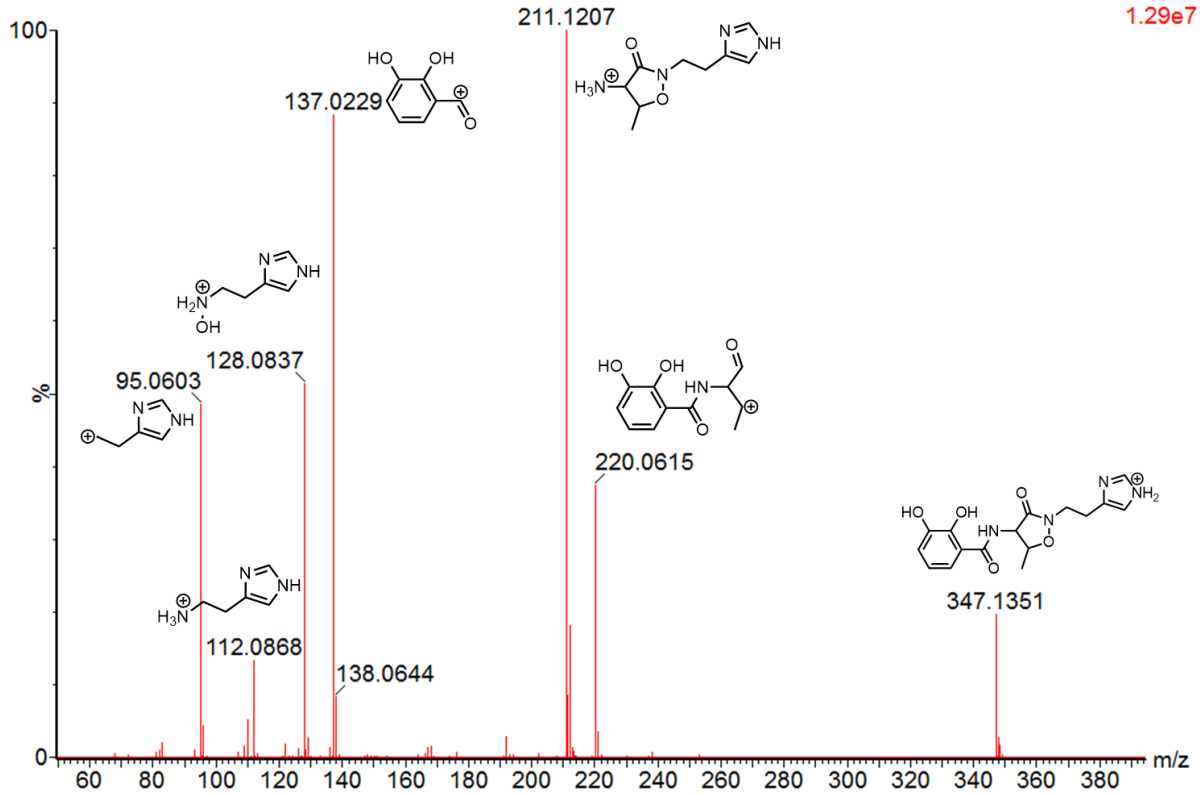

Figure 2.21. ESI-MSMS of the isolated acinetobactin compound with a molecular ion mass *m/z* 347.13 $[M+H]^+$ ($C_{16}H_{19}N_4O_3$). Fragments of acinetobactin associated with the mass fragments are drawn.

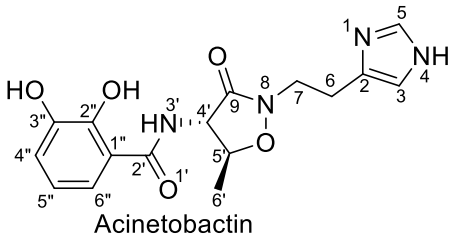

Figure 2.22. Structure of acinetobactin.

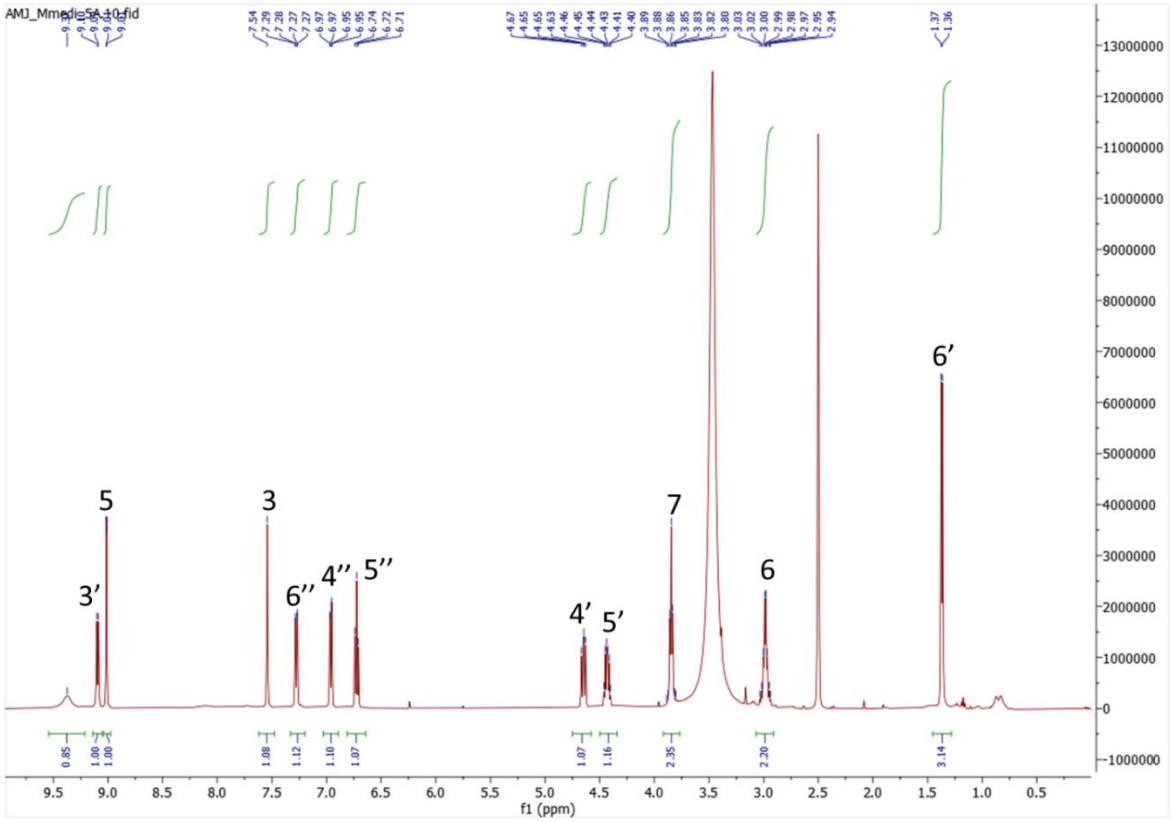

Figure 2.23. ^{1}H NMR spectrum (500 MHz) of acinetobactin in DMSO-d_6. Signals are assigned in **Table 2.7.**

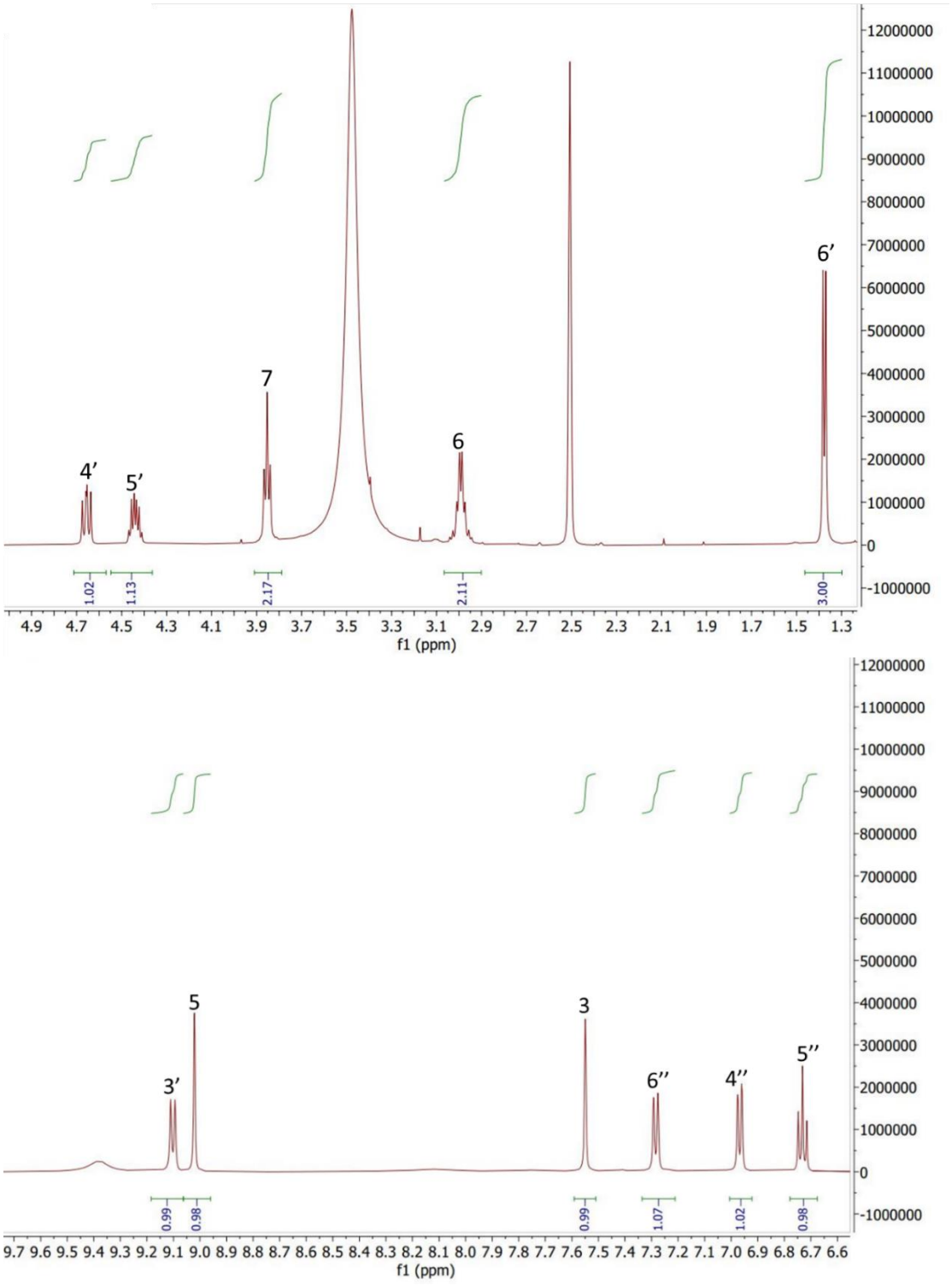

Figure 2.23. Continued ^{1}H NMR of acinetobactin, expansion of 1.3 ppm – 4.9 ppm and the 6.6 ppm – 9.8 ppm region for clarity.

Table 2.7. NMR characterization data (500 MHz) of acinetobactin in DMSO-d6.

Atom Position	^{1}H (ppm), multiplets in Hz
2	-
3	7.54 (s, 1H)
5	9.01 (s, 1H)
6	3.03 - 2.94 (m, 2H)
7	3.89-3.80 (t, 2H)
9	-
2’	-
3’	9.10 (d, 1H)
4’	4.65 (dd, 1H)
5’	4.46 - 4.40 (m, 1H)
6’	1.36 (d, 3H)
1’’	-
2’’	-
3’’	-
4’’	6.95 (d, 1H)
5’’	6.74 – 6.71(m, 1H)
6’’	7.30 – 7.25 (d, 1H)

2.5. Discussion

In conclusion, we have predicted and structurally characterized the tris catechol siderophore mediterraneabactin as the linear oligoester (DHB-^{D}Orn-^{L}Ser)$_3$, along with the biscatechol **2,** (DHB-^{D}Orn-^{L}Ser)$_2$, and monocatechol **3** (DHB-^{D}Orn-^{L}Ser) compounds. Mediterraneabactin is identified as the diastereomer to turnerbactin, (DHB-^{L}Orn-^{L}Ser)$_3$, produced by the shipworm endosymbiont *Teredinibacter turnerae* T7901,[8] based on the Marfey’s amino acid analysis establishing ^{D}Orn in mediterraneabactin and ^{L}Orn in turnerbactin. Circular dichroism spectroscopy shows Fe(III)-mediterraneabactin adopts the Λ configuration, while Fe(III)-turnerbactin adopts the Δ configuration. These results establish the chirality of the amino acid appended to 2,3-DHB in these siderophores influences the configuration at the Fe(III) center, where the siderophores containing D-amino acids adopt the

Λ configuration. In this case, the siderophores with D-amino acids are Fe(III)-mediterraneabactin, (DHB-^{D}Orn-^{L}Ser)$_3$, Fe(III)-trivanchrobactin,[7 20] (DHB-^{D}Arg-^{L}Ser)$_3$, and Fe(III)-cyclic trichrysobactin,[5 6] (DHB-^{D}Lys-^{L}Ser)$_3$. The diastereomeric siderophores, Fe(III)-turnerbactin,[8] (DHB-^{L}Orn-^{L}Ser)$_3$, Fe(III)-ruckerbactin,[7] (DHB-^{L}Arg-^{L}Ser)$_3$, and Fe(III)-frederiksenibactin,[6] (DHB-^{L}Lys-^{L}Ser)$_3$ all adopt the Δ configuration.

The BGCs for mediterraneabactin in *M. mediterranea* MMB-1 and turnerbactin in *T. turnerae* T7901 show homology. The BGC of *M. mediterranea* MMB-1 encodes a two-module NRPS consistent with a triscatechol siderophore, and it was established that the first module containing the epimerization domain loads a ^{D}Orn onto the growing siderophore, making it a diastereomer of turnerbactin with ^{L}Orn. The presence of the epimerase domain is also seen in the BGC of cyclic trichrysobactin (DHB-^{D}Lys-^{L}Ser)$_3$ in *D. chrysanthemi* EC16, and trivanchrobactin (DHB-^{D}Arg-^{L}Ser)$_3$ in *V. campbellii* DS40M4, thus producing the diastereomeric siderophores of frederiksenibactin (DHB-^{L}Lys-^{L}Ser)$_3$ in *Y. frederiksenii* ATCC 3364 and ruckerbactin (DHB-^{D}Arg-^{L}Ser)$_3$ in *Y. ruckeri* YRB.[6 7]

The production of siderophores in *M. mediterranea* MMB-1 has not been identified until now. Along with mediterraneabactin being produced, acinetobactin, a major siderophore produced by the opportunistic pathogen *Acinetobacter baumannii* ATCC 19606,[19] has been structurally characterized. The two siderophores, turnerbactin and acinetobactin, were originally produced by unrelated pathogens, *T. turnerae* T7901 and *A. baumannii* ATCC 19606, respectively. This fact highlights the "usability" of a single copy of genes for multiple siderophores and the interchange of the siderophores between different bacteria. A different bacterial strain, *Aeromonas salmonicida* subsp. *salmonicida* produces acinetobactin and amonabactin and the synthesis of both of these siderophores depends on a single copy of genes

encoding the synthesis of DHB.[21] [22] *Vibrio* sp. DS40M4 on the other hand produces the triscatechol amide siderophore, trivanchrobactin, and anguibactin, but it was not identified whether the same genes encoding the synthesis of DHB are used in the synthesis of the siderophores.[20]

With the discovery of mediterraneabactin (D-Orn), we have now identified the full combinatoric suite of triscatechol siderophores framed on a tri-L-Ser core with selected amino acids: D/L-Orn, D/L-Arg, and D/L-Lys (Figure 2.24) The pairings of these diastereomeric siderophores indicate the importance of chirality around the Fe(III)-center to the siderophore mediated microbial iron-uptake pathways. For example, the esterases, BesA and Fes that hydrolyze Fe(III)-bacillibactin and Fe(III)-enterobactin, respectively, have shown instances of stereospecificity.[1] Chiral recognition occurs at the point of iron(III) release, where BesA and Fes are unable to cleave the enantiomer of enterobactin with a tri-D-serine lactone and in turn do not promote growth. [1] Overall, this complete combinatoric suite of triscatechol siderophores shows the importance of chirality in the siderophore-mediated microbial iron-uptake pathway.

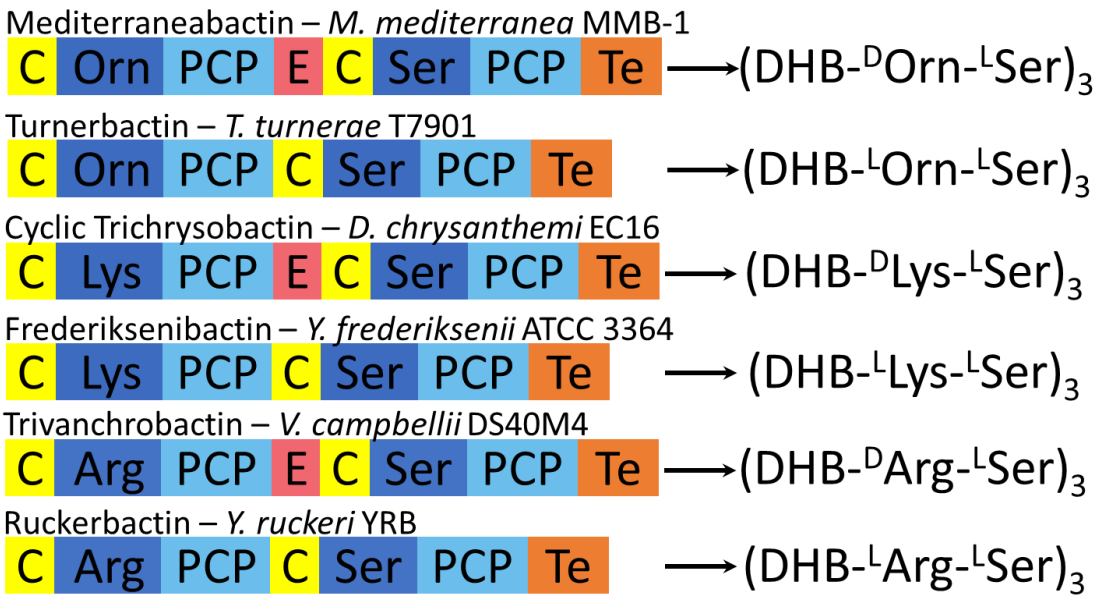

Figure 2.24. NRPS organization for mediterraneabactin, turnerbactin, cyclic trichrysobactin, frederiksenibactin, trivanchrobactin, and ruckerbactin. C: condensation domain; PCP: peptidyl carrier protein, E: epimerase domain, TE: thioesterase domain, and the adenylation domain, represented by the selected amino acid for each NRPS.

2.6. References

1. Abergel, R. J.; Zawadzka, A. M.; Hoette, T. M.; Raymond, K. N., Enzymatic Hydrolysis of Trilactone Siderophores: Where Chiral Recognition Occurs in Enterobactin and Bacillibactin Iron Transport. *Journal of the American Chemical Society* **2009,** *131* (35), 12682-12692.
2. Neilands, J. B.; Erickson, T. J.; Rastetter, W. H., Stereospecificity of the ferric enterobactin receptor of *Escherichia coli* K-12. *Journal of Biological Chemistry* **1981,** *256* (8), 3831-3832.
3. Bluhm, M. E.; Kim, S. S.; Dertz, E. A.; Raymond, K. N., Corynebactin and Enterobactin: Related Siderophores of Opposite Chirality. *Journal of the American Chemical Society* **2002,** *124* (11), 2436-2437.
4. Johnstone, T. C.; Nolan, E. M., Determination of the Molecular Structures of Ferric Enterobactin and Ferric Enantioenterobactin Using Racemic Crystallography. *Journal of the American Chemical Society* **2017,** *139* (42), 15245-15250.
5. Sandy, M.; Butler, A., Chrysobactin siderophores produced by *Dickeya chrysanthemi* EC16. *Journal of natural products* **2011,** *74* (5), 1207-1212.
6. Stow, P. R.; Reitz, Z. L.; Johnstone, T. C.; Butler, A., Genomics-driven discovery of chiral triscatechol siderophores with enantiomeric Fe(III) coordination. *Chemical Science* **2021,** *12* (37), 12485-12493.
7. Thomsen, E.; Reitz, Z. L.; Stow, P. R.; Dulaney, K.; Butler, A., Ruckerbactin Produced by *Yersinia ruckeri* YRB Is a Diastereomer of the Siderophore Trivanchrobactin Produced by *Vibrio campbellii* DS40M4. *Journal of Natural Products* **2022,** *85* (1), 264-269.
8. Han, A. W.; Sandy, M.; Fishman, B.; Trindade-Silva, A. E.; Soares, C. A. G.; Distel, D. L.; Butler, A.; Haygood, M. G., Turnerbactin, a Novel Triscatecholate Siderophore from the Shipworm Endosymbiont *Teredinibacter turnerae* T7901. *PLoS One* **2013,** *8* (10), e76151.
9. Solano, F.; Garcia, E.; Perez, D.; Sanchez-Amat, A., Isolation and Characterization of Strain MMB-1 (CECT 4803), a Novel Melanogenic Marine Bacterium. *Appl Environ Microbiol* **1997,** *63* (9), 3499-506.
10. Solano, F.; Sanchez-Amat, A., Note: Studies on the phylogenetic relationships of melanogenic marine bacteria: Proposal of *Marinomonas mediterranea* sp. nov. *International Journal of Systematic and Evolutionary Microbiology* **1999,** *49* (3), 1241-1246.
11. López-Serrano, D.; Solano, F.; Sanchez-Amat, A., Identification of an operon involved in tyrosinase activity and melanin synthesis in *Marinomonas mediterranea*. *Gene* **2004,** *342* (1), 179-87.
12. Blin, K.; Wolf, T.; Chevrette, M. G.; Lu, X.; Schwalen, C. J.; Kautsar, S. A.; Suarez Duran, H. G.; de Los Santos, E. L. C.; Kim, H. U.; Nave, M.; Dickschat, J. S.; Mitchell, D. A.; Shelest, E.; Breitling, R.; Takano, E.; Lee, S. Y.; Weber, T.; Medema, M. H., antiSMASH 4.0-improvements in chemistry prediction and gene cluster boundary identification. *Nucleic acids research* **2017,** *45* (W1), W36-W41.
13. Skinnider, M. A.; Dejong, C. A.; Rees, P. N.; Johnston, C. W.; Li, H.; Webster, A. L.; Wyatt, M. A.; Magarvey, N. A., Genomes to natural products PRediction Informatics for Secondary Metabolomes (PRISM). *Nucleic Acids Res* **2015,** *43* (20), 9645-62.

14. Schwyn, B.; Neilands, J. B., Universal chemical assay for the detection and determination of siderophores. *Analytical Biochemistry* **1987,** *160* (1), 47-56.
15. Marfey, P., Determination ofD-amino acids. II. Use of a bifunctional reagent, 1,5-difluoro-2,4-dinitrobenzene. *Carlsberg Research Communications* **1984,** *49* (6), 591.
16. Mihara, K.; Tanabe, T.; Yamakawa, Y.; Funahashi, T.; Nakao, H.; Narimatsu, S.; Yamamoto, S., Identification and transcriptional organization of a gene cluster involved in biosynthesis and transport of acinetobactin, a siderophore produced by *Acinetobacter baumannii* ATCC 19606T. *Microbiology* **2004,** *150* (8), 2587-2597.
17. Dorsey, C. W.; Beglin, M. S.; Actis, L. A., Detection and Analysis of Iron Uptake Components Expressed by *Acinetobacter baumannii* Clinical Isolates. *Journal of Clinical Microbiology* **2003,** *41* (9), 4188-4193.
18. Dorsey, C. W.; Tomaras, A. P.; Connerly, P. L.; Tolmasky, M. E.; Crosa, J. H.; Actis, L. A., The siderophore-mediated iron acquisition systems of *Acinetobacter baumannii* ATCC 19606 and *Vibrio anguillarum* 775 are structurally and functionally related. *Microbiology* **2004,** *150* (11), 3657-3667.
19. Yamamoto, S.; Okujo, N.; Sakakibara, Y., Isolation and structure elucidation of acinetobactin., a novel siderophore from *Acinetobacter baumannii*. *Archives of Microbiology* **1994,** *162* (4), 249-254.
20. Sandy, M.; Han, A.; Blunt, J.; Munro, M.; Haygood, M.; Butler, A., Vanchrobactin and anguibactin siderophores produced by *Vibrio* sp. DS40M4. *Journal of natural products* **2010,** *73* (6), 1038-1043.
21. Balado, M.; Souto, A.; Vences, A.; Careaga, V. P.; Valderrama, K.; Segade, Y.; Rodríguez, J.; Osorio, C. R.; Jiménez, C.; Lemos, M. L., Two Catechol Siderophores, Acinetobactin and Amonabactin, Are Simultaneously Produced by *Aeromonas salmonicida* subsp. *salmonicida* Sharing Part of the Biosynthetic Pathway. *ACS Chemical Biology* **2015,** *10* (12), 2850-2860.
22. Balado, M.; Segade, Y.; Rey, D.; Osorio, C. R.; Rodríguez, J.; Lemos, M. L.; Jiménez, C., Identification of the Ferric-Acinetobactin Outer Membrane Receptor in *Aeromonas salmonicida* subsp. salmonicida and Structure–Activity Relationships of Synthetic Acinetobactin Analogues. *ACS Chemical Biology* **2017,** *12* (2), 479-493.

3. Amphi-enterobactin Production in *Vibrio* species: Origin of catechol-based fragments

Sections of this chapter were published in: Jelowicki, A.M., Butler, A. On the origin of amphi-enterobactin fragments produced by Vibrio campbellii species. J. Biol. Inorg. Chem. **27**, 565-572 (2022). https://doi.org/10.1007/s00775-022-01949-0

3.1. Introduction

Iron is a cofactor required by many enzymes involved in essential cellular processes. However, obtaining iron becomes challenging due to the low solubility of iron (III). One strategy that bacteria have evolved to obtain iron is the biosynthesis of siderophores, low molecular weight organic compounds that bind Fe(III) with high affinity. These Fe(III)-siderophore complexes are taken up by the cell through outer membrane receptor proteins.

Amphi-enterobactin (Fig. 3.1)[1], was initially isolated from *Vibrio campbellii* ATCC BAA-1116 (formerly *V. harveyi* BAA-1116), a model bacterium for quorum sensing because of its quorum-regulated bioluminescence.[2] Enterobactin, utilized by many bacterial species, is a macrolactone of *tris*-(*N*-2,3-dihydroxybenzoyl-L-serine) that coordinates iron(III) with three 2,3-dihydroxybenzoyl (DHB) catechol groups. Amphi-enterobactin is a triscatecholate siderophore resembling enterobactin, although distinguished by an expanded tetralactone core, and decorated by a fatty acid appended at the amine of the additional L-Ser.[1] Multiple strains of *V. campbellii* and *V. harveyi* have been shown to produce a suite of amphi-enterobactins with varying fatty acyl groups.[1, 3] These fatty acid appendages can range in length (C10-C16),

degree of unsaturation, and hydroxylation.[1, 3, 4] *V. campbellii* CAIM 519T produced the full suite (C10-C16) amphi-enterobactins in greater amounts than *V. campbellii* BAA-1116.[3]

V. campbellii BAA-1116 contains a set of genes homologous to the biosynthetic gene cluster (BGC) of enterobactin, *entA-F* (Figure 3.1), yet instead of enterobactin, the strain produces amphi-enterobactin (Figure 3.1a).[1] In addition to the amphi-enterobactin *aebA-F genes*, the gene *aebG* encoding a long-chain fatty acid Co-A ligase (FACL) is located nearby this BGC.[1] The biosynthesis of 2,3-dihydroxybenzoic acid (2,3-DHBA) is carried out by AebABCE. Zane *et. al*.[1] established that the biosynthesis of amphi-enterobactin begins by appending an AebG-activated fatty acid to L-Ser loaded on AebF (Figure. 3.1b). FACL enzymes are known to activate fatty acids to fatty acyl-CoA thioesters before integrating with the nonribosomal peptides.[5, 6] Thus, this FACL initiates the biosynthetic process of amphi-enterobactin by appending the FA to the first loaded L-Ser residue on AebF NRPS. AebF continues its bifunctional activity of catalyzing the formation of amide bonds between DHB and another L-Ser, respectively. The thioesterase domain of AebF ultimately catalyzes the release of amphi-enterobactin through intramolecular cyclization, generating the macrolactone and releasing amphi-enterobactin from the NRPS.[1]

Several bacterial strains, *V. campbellii* BAA-1116, *Burkholderia cepacian* K56-2, and *V. vulnificus* MO6-24/O have been shown to engage in quorum-sensing regulation of siderophore production, where high cell density leads to an accumulation of quorum sensing molecules, which with the Fe(II)-Fur complex decreases siderophore production [2, 4, 7, 8]. A recent report explored the link between quorum sensing, siderophore production, and iron uptake in *V. campbellii* BAA-1116[4]. The study reported the presence of amphi-enterobactin-related soluble fragments, particularly 2,3-dihydroxybenzoic acid (DHBA) and 2,3-

dihydroxybenzoyl-L-serine (DHB-Ser), along with linearized amphi-enterobactin fragments as confirmed by spectrometry [4]. DHBA and DHB-Ser were found to be more abundant in comparison to amphi-enterobactin. McRose *et al* [4] propose two possible sources of DHBA and DHB-Ser: premature release from the biosynthetic pathway or degradation of amphi-enterobactins. Because of the accumulation of DHBA and DHB-Ser found in the supernatant of *V. campbellii* BAA-1116, the study suggested an inefficient amphi-enterobactin biosynthetic process. [4]

Amphi-enterobactin hydrolysis products composed of two L-Ser residues, one 2,3-dihydroxybenzoate (2,3-DHB) group, and a fatty acid, have been reported previously. [1, 4] In this report, we use a shorthand notation for these fragments, based on a binary code [9, 10], where the number **[1]** depicts L-Ser appended by the fatty acid, and **[0]** represents the L-Ser appended by DHB. In a 2-Ser-1-DHB-FA fragment where the fatty acid is appended to the C-terminal L-Ser, the binary code is **[01]**. If the fatty acid is appended to the N-terminal L-Ser, the binary code is **[10].** The same designation is followed for 3-Ser-2-DHB-FA, where the fatty acid can be appended to the terminal L-Ser **[001],** the internal L-Ser **[010],** or the N-terminal L-Ser **[100].** This binary nomenclature was originally used to describe the isomers of desferrioxamine B and was adapted here to denote the position of the FA. [9, 10]

We have investigated the origin of the amphi-enterobactin fragments present in the culture supernatant of *V. campbellii* CAIM 519 in greater detail. Fragments associated with premature release during biosynthesis could only be **[01], [001],** and **[0001],** where the fatty acid is appended to the C-terminal Ser. If premature release from the NRPS is the only source of the hydrolysis products, we would only see these three fragments. However, if hydrolysis of the fully formed amphi-enterobactin macrolactone occurs, a mixture of fragments will be

observed, including **[10]**, **[100]** and **[1000]** which would have a unique tandem MS signature, described below, that would not be present in fragments **[01], [001],** and **[0001]**.

We report herein a mass fragmentation analysis that establishes these amphi-enterobactin hydrolysis fragments arise from the full siderophore, although we cannot rule out premature release. The amphi-enterobactin macrolactone siderophore is in fact produced as supported by the tandem MS analysis of the hydrolysis products.

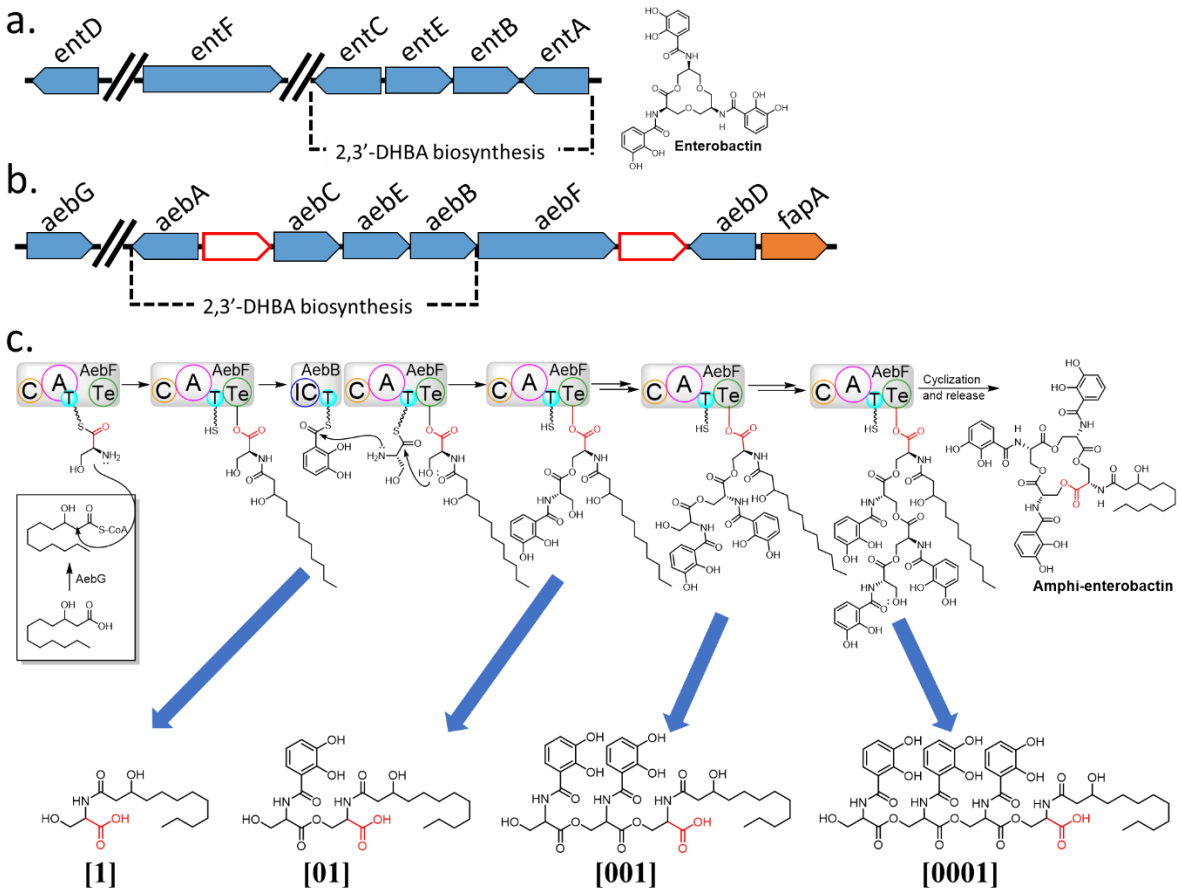

Figure 3.1. Biosynthesis of amphi-enterobactin. a. The entABCDEF biosynthetic gene cluster. b. The aebABCDEF biosynthetic gene cluster first identified in *Vibrio harveyi* BAA-1116 [1]. Genes involved in siderophore biosynthesis and transport are represented by blue and orange arrows, respectively. White arrows represent hypothetical proteins whose function has not yet been determined. c. Biosynthesis of amphi-enterobactin catalyzed by NRPS AebF. The potential points of pre-release of fragments in the biosynthesis of amphi-enterobactin are indicated (blue arrows). Each potential early release product has the fatty acid appended to the amine of a C-terminal L-Ser. C, condensation domain; A, adenylation domain; T, thiolation domain; TE, thioesterase domain.

3.2. Statement of Chapter Objectives

Amphi-enterobactin is an amphiphilic siderophore isolated from a variety of microbial *Vibrio* species. Like enterobactin, amphi-enterobactin is a triscatecholate siderophore, however it is framed on an expanded tetralactone core comprised of four L-Ser residues, of which one

L-Ser is appended by a fatty acid and the remaining L-Ser residues are appended by 2,3-dihydroxybenzoate (DHB). Fragments of amphi-enterobactin composed of 2-Ser-1-DHB-FA and 3-Ser-2-DHB-FA have been identified in the supernatant of *Vibrio campbellii* species. The origin of these fragments has not been determined, although two distinct isomers could exist for 2-Ser-1-DHB-FA and three distinct isomers could exist for 3-Ser-2-DHB-FA. The fragments of amphi-enterobactin could originate from hydrolysis of the amphi-enterobactin macrolactone, or from premature release due to an inefficient biosynthetic pathway. Unique masses in the tandem MS analysis establish that certain fragments isolated from the culture supernatant must originate from hydrolysis of the amphi-enterobactin macrolactone, while others cannot be distinguished from premature release during biosynthesis or hydrolysis of amphi-enterobactin. Further genomic investigations identify two potential putative esterases that may be involved in the hydrolysis of amphi-enterobactin. A bioinformatic analysis of the putative esterase sequences were conducted to elucidate further information about the involvement in hydrolysis of the macrolactone.

Siderophore production in *Vibrio natriegens* CCUG 16371 was also studied to identify the production of amphi-enterobactin. *V. natriegens* CCUG 16371 has the fastest growth rate of any known organism[11] and contains a similar biosynthetic gene cluster to that of amphi-enterobactin producing species. The goal of working with *V. natriegens* CCUG 16371 was to identify if this strain produces siderophores.

3.3. Materials And Methods

3.3.1. General Experimental Procedures

A Varian Cary-Bio 300 UV-visible spectrophotometer was used to monitor microbial growth at 600 nm. Analytical HPLC was used to analyze both the supernatant and cell pellet extracts from *V. campbellii* CAIM 519 to identify the production of both the amphi-enterobactin macrolactone and hydrolysis products. Mass spectrometry analysis was carried out on a Waters Xevo G2-XS QTof with positive mode electrospray ionization coupled to an ACQUITY UPLC H-Class system with a Waters BEH C18 column.

3.3.2. Cultivation of *Vibrio campbellii* CAIM 519 and Siderophore Isolation

V. campbellii CAIM 519 was cultured in low-iron artificial seawater medium containing casamino acids (10 g/L), NH_4Cl (19 mM), $Na_2HPO_4 \cdot 7H_2O$ (4.6 mM), $MgSO_4 \cdot 7H_2O$ (50 mM), $CaCl_2$ (10 mM), trace metal grade NaCl (0.5 M), glycerol (41 mM), HEPES buffer (10 mM; pH 7.4), $NaHCO_3$ (2 mM), biotin (8.2 μM), niacin (1.6 μM), thiamin (0.33 μM), 4-aminobenzoic acid (1.46 μM), pantothenic acid (0.21 μM), pyridoxine hydrochloride (5 μM), cyanocobalamin (0.07 μM), riboflavin (0.5 μM), and folic acid (0.5 μM). Two-liter cultures were grown in acid-washed 4L Erlenmeyer flasks on an orbital shaker (180 rpm) at room temperature (OD_{600}) while monitoring the growth until the culture reached stationary phase.

The cultures were harvested by centrifugation (6000 rpm, 30 minutes, 4°C). The supernatant was decanted and the cell pellet was resuspended in methanol (25 mL/pellet), transferred into 50 mL conical tubes, and shaken overnight at 180 rpm, 4°C. The methanol

extract was centrifuged (6000 rpm, 10 minutes, 4℃), filtered through a 0.22 μm membrane, and concentrated under vacuum to one-third the original volume.

Both the supernatant and the cell pellet extracts were purified with XAD resin. The cell pellet extract was diluted with 4 times the volume with doubly deionized water (Milli-Q IQ). The supernatant and cell pellet extract were incubated with Amberlite XAD-2 resin for 4 hours at 120 rpm, 25℃. After 4 hours, the XAD resin was washed with 2 L of doubly deionized water. From the cell pellet extract, siderophores were eluted with 90% methanol. From the supernatant, siderophores were eluted with 80% methanol. The eluent was concentrated under vacuum to dryness and dissolved in 5 mL of methanol.

3.3.3. Cultivation of *Vibrio natriegens* CCUG 16371 and Siderophore Isolation

Vibrio natriegens were cultured separately in low-iron artificial seawater medium (2L) containing casamino acids (10 g/L), NH_4Cl (1 g/L), glycerol phosphate (1 g/L), $MgSO_4$ (12.35 g/L), $CaCl_2$ (1.45 g/L), trace metal grade NaCl (16.55 g/L), KCl (0.75 g/L), glycerol (41 mM), HEPES buffer (10 mM; pH 7.4), $NaHCO_3$ (2 mM), biotin (8.2 μM), niacin (1.6 μM), thiamin (0.33 μM), 4-aminobenzoic acid (1.46 μM), pantothenic acid (0.21 μM), pyridoxine hydrochloride (5 μM), cyanocobalamin (0.07 μM), riboflavin (0.5 μM), and folic acid (0.5 μM). Two-liter cultures were grown in acid-washed 4L Erlenmeyer flasks on an orbital shaker (180 rpm) at room temperature (OD_{600}) while monitoring the growth until the culture reached stationary phase.

The cultures were harvested by centrifugation (6000 rpm, 30 minutes, 4℃). The supernatant was decanted and the cell pellet was resuspended in methanol (25 mL/pellet), transferred into 50 mL conical tubes, and shaken overnight at 180 rpm, 4℃. The methanol

extract was centrifuged (6000 rpm, 10 minutes, 4℃), filtered through a 0.22 μm membrane, and concentrated under vacuum to one-third the original volume.

Both the supernatant and cell pellet extracts were purified with XAD resin as mentioned in the section above for the cultivation of *V. campbellii* CAIM 519.

3.3.4. UPLC-MS And MS/MS Analysis of Extracts

Extracts were analyzed through positive ion mode ESI-MS on a Waters Xebo G2-XS QTof coupled to a Waters Acquity H-Class UPLC system. The extracts of the culture supernatant were analyzed with a linear gradient of 0-100% CH_3CN (0.1% formic acid), while the cell pellet extracts were analyzed with a linear gradient of 50-100% CH_3CN (0.1% formic acid) in ddH_2O (0.1% formic acid) over 10 minutes. For MSMS analysis, a collision energy profile of 20, 25, 30 kEV was employed. Using MassLynx 4.1, chromatograms for masses of interest were generated and molecular ion peaks quantified by integration (ApexTrack algorithm).

3.3.5. Genome Mining of Amphi-Enterobactin Producers for Putative Esterases

Homologs of the amphi-enterobactin biosynthetic gene cluster were found with tblastn (NCBI webserver)[12] using the putative esterases AebH and AebI, found embedded in the amphi-enterobactin biosynthetic gene cluster, as a query against *Vibrio* species. Amino acid sequences of the putative esterases from *V. campbellii* CAIM 519T, *V. harveyi* BAA-1116, *V. natriegens*, and *V. owensii* were retrieved from NCBI RefSeq[13] and aligned to the erythromycin esterase EreA ([WP_032084014.1]) using MUSCLE (EMBL-EBI webserver).[14] [15]

3.3.6. SignalP Program used to Predict Presence of Signal Peptides

SignalP-5.0 was used to determine the presence of signal peptide sequences in the putative esterases. The amino acid sequences of the putative esterases AebH and AebI, found embedded in the amphi-enterobactin biosynthetic gene cluster, were pasted into the main server of SignalP-5.0 in FASTA format and processed.[16] Outputs were analyzed by the probabilities reported for SP(Sec/SPI) / LIPO(Sec/SPII) / TAT(Tat/SPI), depending on the type of signal peptide predicted, CS (the cleavage site), and OTHER (the probability the sequence does not have a signal peptide.

3.3.7. Circular Dichroism Spectroscopic Measurements of Amphi-enterobactin

The ferric complex of amphi-enterobactin was prepared from a methanol stock solution of the free ligand (0.25 mM, 403.2 μL) with iron trichloride (2.419 mM, 41.34 μL) and MOPS (pH 7.4, 100 μL). The solutions were diluted with water to yield a final Fe(III)-L concentration of 0.1 mM. The spectra of the iron complex and blank (10 mM MOPS) were obtained in quartz cuvettes (1 cm path length) and recorded on a Varian Cary-Bio 300 UV-visible spectrophotometer. Full circular dichroism spectra were acquired with the following parameters: 4 s D.I.T., 1 nm bandwidth, 50 nm/s scanning speed with a total of 3 accumulations using a Jasco J-1500 CD spectrophotometer.

3.4. Results and Interpretation

3.4.1. Origin of the Amphi-Enterobactin Fragments: Premature Release During Biosynthesis or Macrolactone Ester Hydrolysis

While it has been established that *Vibrio campbellii* CAIM 519T produces a suite of amphi-enterobactins, with fatty acids ranging from C_{10} to C_{14} which are either saturated or monohydroxylated [3], fragments of these amphi-enterobactins are also present in the culture supernatant of *V. campbellii* CAIM 519T (Figures 3.2-3.5). We have turned to tandem MS to investigate whether selected fragments originate from hydrolysis of the amphi-enterobactin macrolactone siderophore.

The four circled peaks (A-D) in the UPLC chromatogram (Fig. 3.2) correlate with masses of amphi-enterobactin fragments identified in the supernatant. The species eluting at 4.3 min, labeled Peak A reveals a protonated mass of *m/z* 499 $[M+H]^+$, which matches the composition of the amphi-enterobactin fragment with a C10:0-OH fatty acid, referred to as 2-Ser-1-DHB-$FA^{C10:0-OH}$. Peak C (*m/z* 527), eluting at 5.1 minutes, is analogous to Peak A although with a C12:0-OH fatty acid, i.e., 2-Ser-1-DHB-$FA^{C12:0-OH}$. Two structural isomers are possible with each of these compositions, depending on the positions of the fatty acid and 2,3-DHB in reference to the serine ester backbone; the fatty acid may be appended to either the C-terminal L-Ser, depicted by the binary code **[01]**, or the N-terminal L-Ser, depicted by **[10]** (Fig. 3.4 and 3.5).

The species eluting at 4.6 minutes and 5.4 minutes are associated with Peak B and Peak D, respectively (Figure 3.2). Peak B reveals a protonated molecular mass of *m/z* 722 $[M+H]^+$, consistent with the composition 3-Ser-2-DHB-FA^{C10-OH}, and peak D (*m/z* 750) is associated

with the equivalent C12:0-OH fatty acid derivative. Three structural isomers exist for 3-Ser-2-DHB-FA (Figure 3.4 and 3.5) in which the fatty acid may be appended to the C-terminal L-Ser **[001]**, the internal L-Ser **[010]**, or the N-terminal L-Ser **[100]**. The structural variability of isomers **[001]**, **[010]** and **[100]** prompted further considerations for the origin of these fragments.

The protonated molecular masses at *m/z* 945.33 $[M+H]^+$ and *m/z* 973.35 $[M+H]^+$ in the UPLC-MS is consistent with production of the 4-Ser-3-DHB-FA isomers for the $C_{10:0\text{-}OH}$ and $C_{12:0\text{-}OH}$ fatty acids, respectively. Four potential isomers could be formed, i.e., **[0001]**, **[0010]**, **[0100]**, and **[1000]**, however due to the trace quantity produced, tandem MS characterization was not carried out. The complete set of isomers along with the associated binary nomenclature is shown in Fig. 3.4 and 3.5.

Biosynthesis of amphi-enterobactin is initiated during fatty acyl-CoA thioester acylation of L-Ser-S-P-pant-AebF [1]. Thus, the carboxyl group interacting with the thioesterase domain throughout the amphi-enterobactin biosynthesis will always be appended to the fatty acid that was loaded onto L-Ser. Premature release of amphi-enterobactin fragments along the biosynthetic pathway could potentially occur at the thioesterase domain of the NRPS, releasing a fragment with the fatty acid appended to the C-terminal Ser, as in **[01]**, **[001]**, or **[0001]** (Figure 3.1c).

Structural variation within fragments increases if hydrolysis products arise from the fully formed amphi-enterobactin macrolactone. While this set of fragments may contain the fatty acid appended to the C-terminal Ser, as in the premature release fragments **[01]**, **[001]**, or **[0001]**, other fragments with the fatty acid appended at each of the other Ser residues in the

oligoserine backbone may be formed as well. Depending on the site of macrolactone hydrolysis, all of the structures in Figure 3.4 and 3.5 may be considered hydrolysis products from amphi-enterobactin.

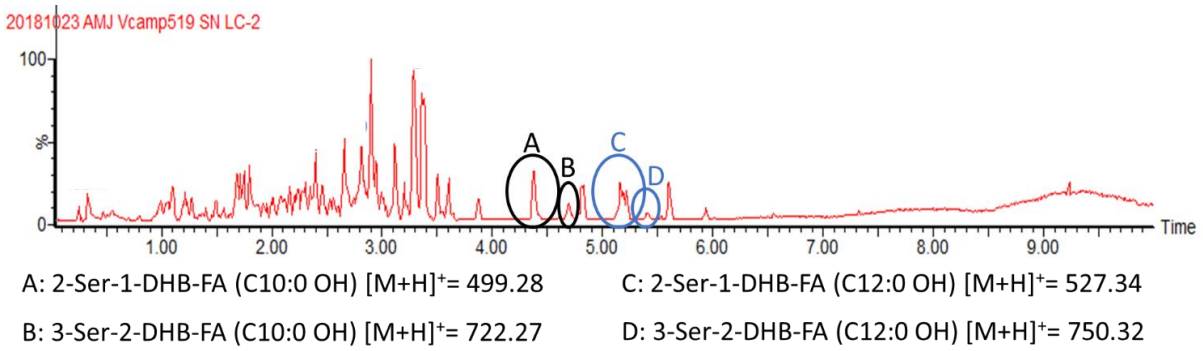

Figure 3.2. LC-MS of the *Vibrio campbellii* CAIM 519T supernatant. Peaks A-D correlate to masses of predicted amphi-enterobactin fragments.

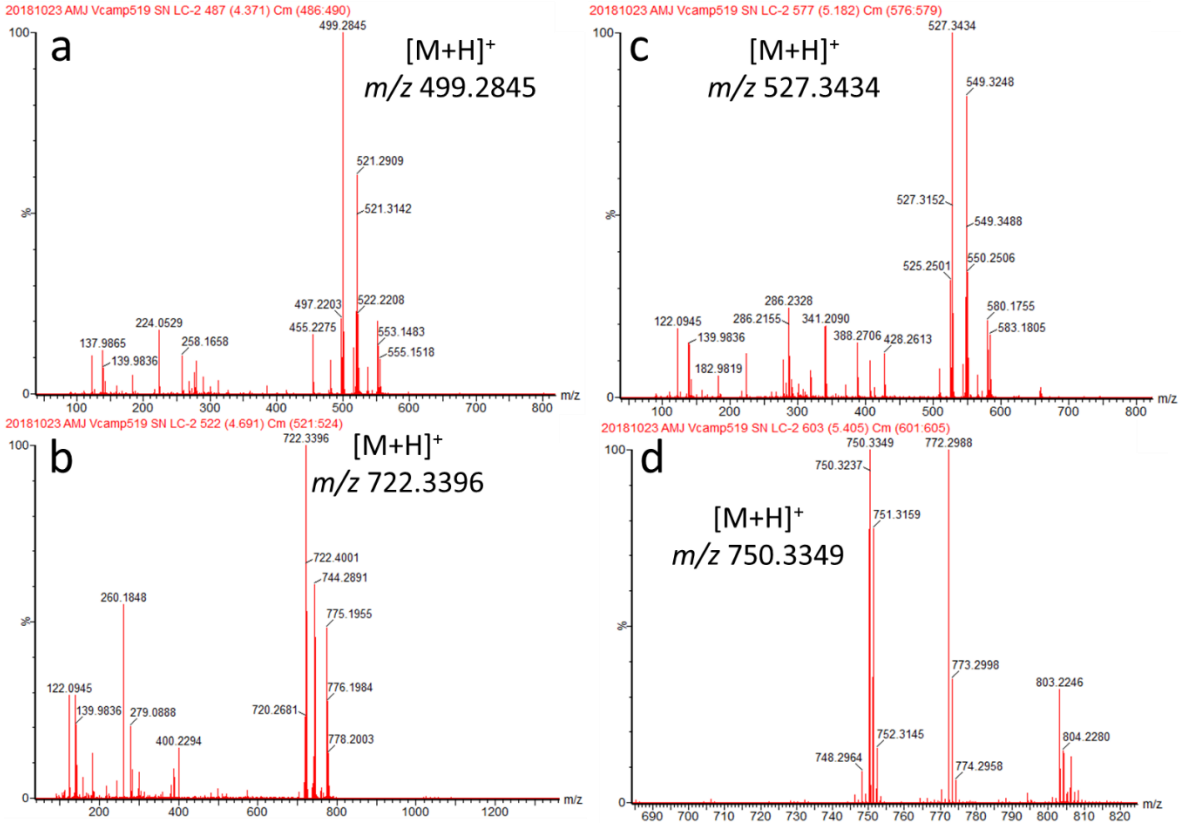

Figure 3.3. MS spectra of Peaks A-D in *V. campbellii* CAIM 519T that correlate to masses of predicted amphi-enterobactin fragments**.**

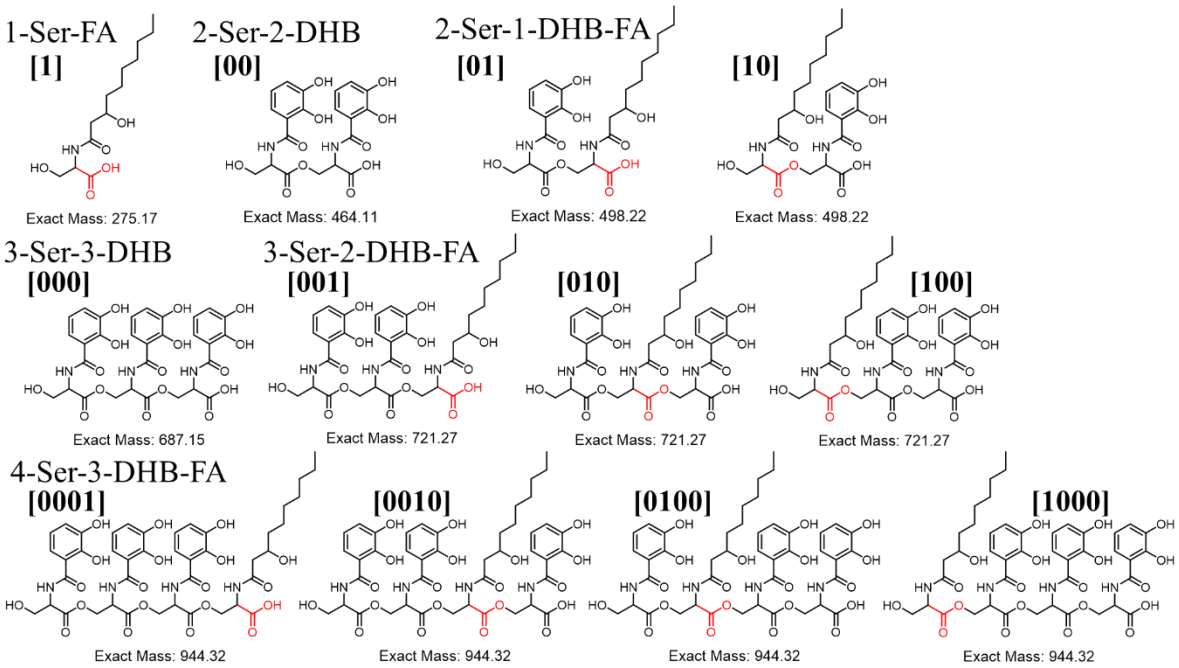

Figure 3.4. The possible hydrolysis fragments from amphi-enterobactin with a C10:0-OH fatty acid. Compounds [01], [001], [0001] are the only structural possibilities for premature release during biosynthesis. A mixture of the compounds shown here, would suggest breakdown by an esterase. The carboxylate of ^{L}Ser appended by the FA during biosynthesis is shown in red. This carboxyl would be tethered to the thioesterase domain during biosynthesis.[1]

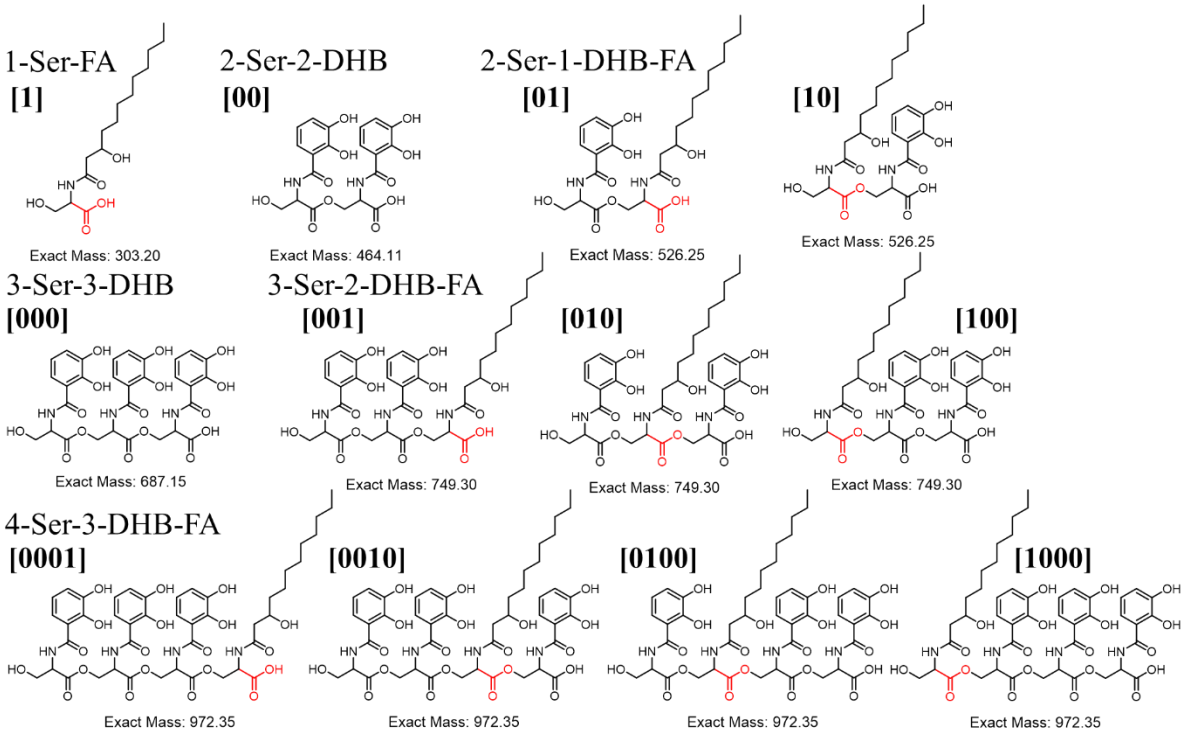

Figure 3.5. The possible hydrolysis fragments from amphi-enterobactin with a C12:0-OH fatty acid tail. Compounds [01], [001], [0001] are the only structural possibilities for premature release. A mixture of compounds shown here, suggest breakdown by an esterase or by molecular hydrolysis. The carboxylate of L-Ser appended by the FA during biosynthesis is shown in red. This carboxyl would be tethered to the thioesterase domain.

3.4.2. Structural Differentiation Among the 2-Ser-1-DHB-FA Fragments of Amphi-enterobactin in *V. campbellii* CAIM 519T

Three distinct di-Ser hydrolysis fragments can be formed from dual ester hydrolysis of the amphi-enterobactin macrolactone, only two of which would have a 2-Ser-1-DHB-FA motif, **[10]** and **[01]** (Figs. 3.6, and 3.4-3.5 for the $C_{10\text{-}OH}$ and $C_{12\text{-}OH}$ fatty acids, respectively). The third hydrolysis fragment would lack the fatty acid as 2-Ser-2-DHB, **[00]** (Fig. 3.6). Tandem mass spectrometry analysis can be used to differentiate between structures **[01]** and **[10]** based on unique MS/MS signature fragments (Figs. 3.7 and 3.8). Focusing first on the $C_{10\text{-}OH}$ 2-Ser-1-DHB-FA (*m/z* 499.28 $[M+H]^+$) in *V. campbellii* CAIM 519T,the fragment with a protonated mass of *m/*z 196 $[M+H]^+$ is specific to **[01]**, while structure **[10]** would have a fragment with a protonated mass of *m/*z 230 $[M+H]^+$.

The ESI-MS/MS spectrum of the product with a protonated mass of *m/z* value 499.28 $[M+H]^+$ (**2-Ser-1-DHB-FA$^{C10:0\text{-}OH}$**) shows fragments at both *m/z* 196 and *m/z* 230 (Fig. 3.7). The same pattern is observed for **2-Ser-1-DHB- FA$^{C12:0\text{-}OH}$** (*m/*z 527.34 $[M+H]^+$) although with analogous fragments at *m/z* 196 and *m/z* 258 (Fig. 3.8). The mixture of both unique fragments is evidence that the amphi-enterobactin macrolactone is produced and is hydrolyzed to **[01]** and **[10]**, although the presence of both **[01]** and **[10]** does not rule out premature release during the biosynthesis as the origin of some **[01]**.

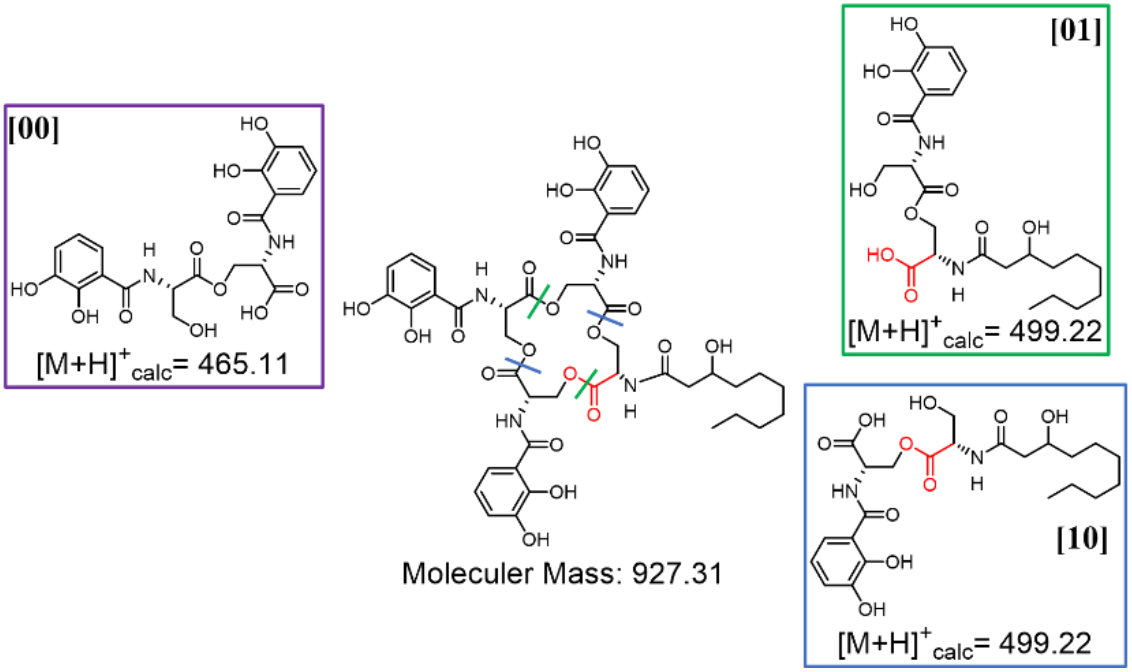

Figure 3.6. The possible di-Ser$^{C10:0-OH}$ fragments produced from ester hydrolysis of amphi-enterobactin. Esters hydrolyzed directly opposite one another form the di-Ser fragments, [00], [01], and [10].

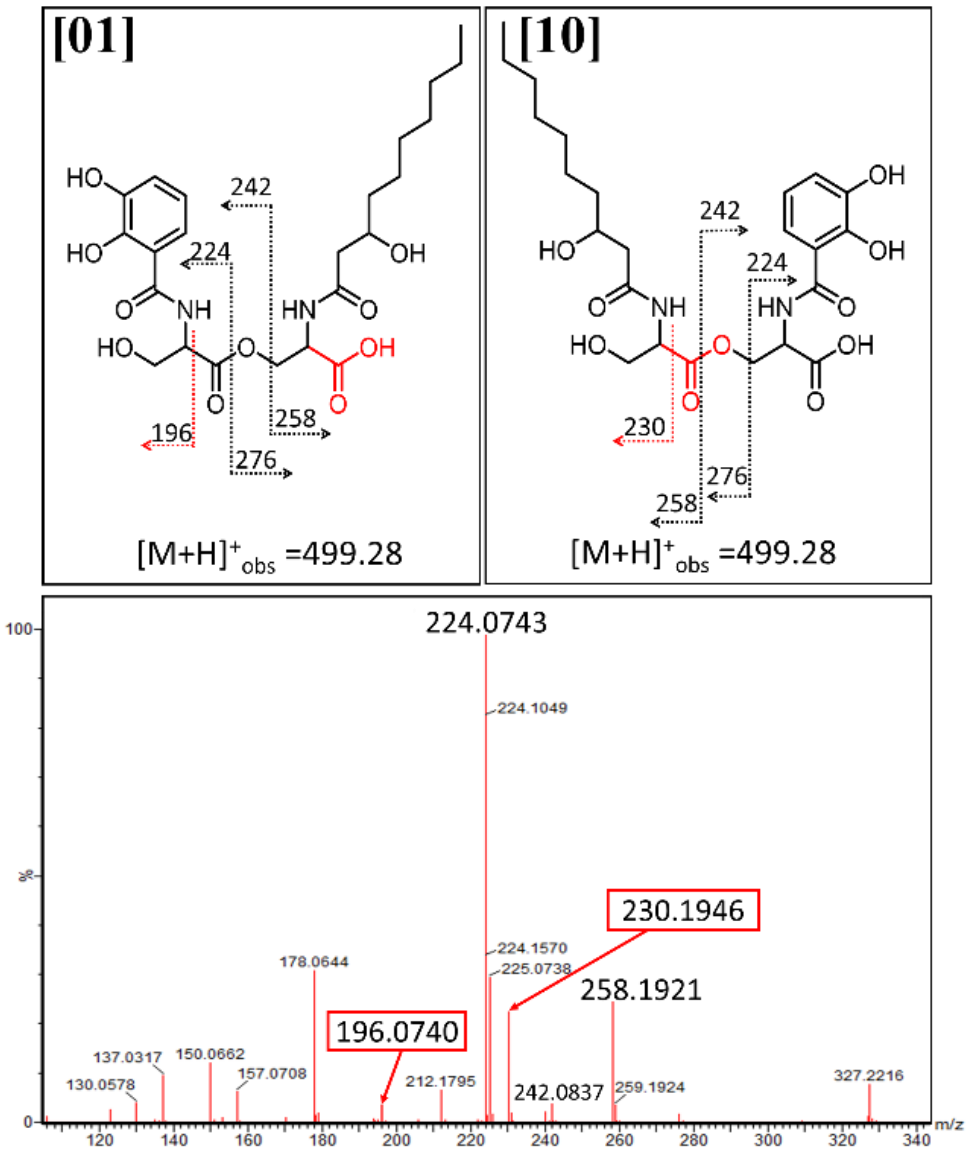

Figure 3.7. MS-MS of m/z 499.28 for differentiation between [01] and [10] in *V. campbellii* CAIM 519T. A fragment ion of m/z 196 is consistent with premature release, while a fragment ion of m/z 230 is consistent with the hydrolysis of the amphi-enterobactin macrolactone.

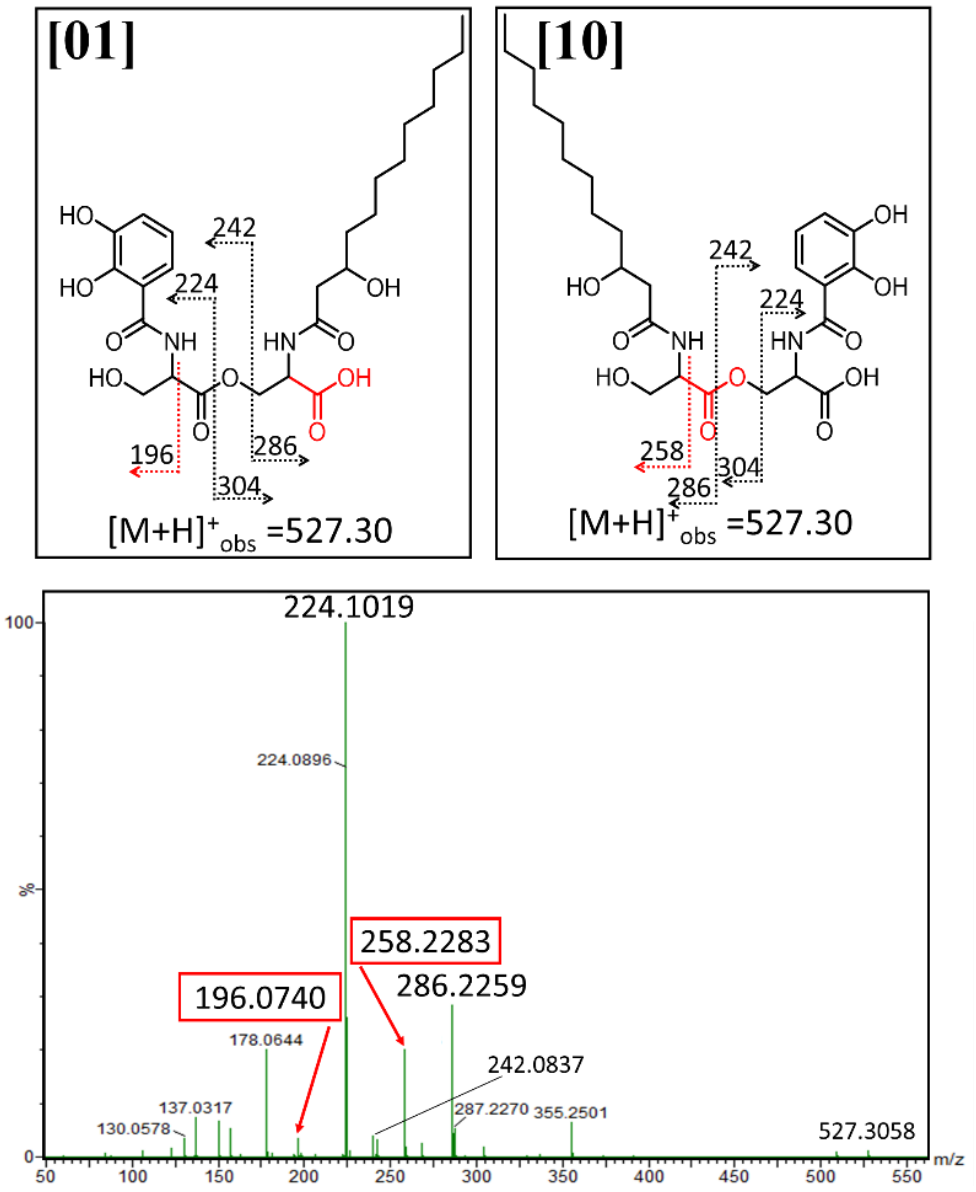

Figure 3.8. Tandem MS of m/z 527.30 for differentiation between [01] and [10] in *V. campbellii* CAIM 519T. A fragment ion of m/z 196 could result from premature release during biosynthesis or from hydrolysis of the amphi-enterobactin macrolactone, while a fragment ion of m/z 258 is consistent only with the hydrolysis of the amphi-enterobactin macrolactone.

3.4.3. Structural Differentiation among the 3-Ser-2-DHB-FA Fragments of Amphi-enterobactin in *V. campbellii* CAIM 519T

Along with **2-Ser-1-DHB-FA**, **3-Ser-2-DHB-FA** compounds were also observed. Four distinct tri-Ser hydrolysis fragments could be formed from dual hydrolysis of adjacent esters within the amphi-enterobactin macrolactone, only three of which would have a 3-Ser-2-DHB-FA motif, **[100]**, **[010]** and **[001]** (Figs. 3.9 and 3.4-3.5 for the $C_{10\text{-}OH}$ and $C_{12\text{-}OH}$ fatty acids, respectively). The fourth hydrolysis fragment would lack the fatty acid, with 3-Ser-3-DHB, **[000]** (Fig. 3.9), which is the equivalent of linear enterobactin.

Distinguishing among the three **3-Ser-2-DHB-FA$^{C10\text{-}OH}$** structural isomers (Fig. 3.10) structures by tandem MS becomes more complex in comparison to the 2-Ser-1-DHB-FA structural isomer analysis. Premature release during biosynthesis would produce the 3-Ser-2-DHB-FA$^{C10:0\text{-}OH}$ isomer **[001]**, whereas all three isomers, **[100]**, **[010]** and **[001]** would be produced from hydrolysis of the amphi-enterobactin macrolactone. The fragmentation at the N-terminal L-Ser is again the differentiating point among the isomers. Isomer [**100]** would result in a unique MS/MS fragment at *m/z* 230 $[M+H]^+$. Unfortunately, both **[001]** and **[010]** isomers would produce a fragment with *m/z* 196 $[M+H]^+$ in the same location, making these two isomers indistinguishable.

Tandem mass spectral analysis was carried out on the products with a protonated molecular mass of *m/z* 722.27 $[M+H]^+$, consistent with **3-Ser-2-DHB-FA$^{C10\text{-}OH}$** (Fig. 3.10) and 750.38 $[M+H]^+$, consistent with **3-Ser-2-DHB-FA$^{C12\text{-}OH}$** (Fig. 3.11). Tandem MS shows both of the fragments at *m/z* 196 and *m/z* 230. The *m/z* 230 ion confirms the presence of **[100]**, which can only arise from an amphi-enterobactin macrolactone hydrolysis product. The ion fragment at *m/z* 196 was identified by tandem MS and could arise from both **[001]** and **[010]**.

These two products cannot be distinguished by tandem MS. However, a mixture of the 3-Ser-2-DHB-FA products is present in both the C10:0 – OH and C12:0 – OH compounds. The mixture of both fragments is evidence that amphi-enterobactin is produced and is hydrolyzed to [**100]**, and one of both of **[010]** and **[001]**, although the presence of all three isomers does not rule out the co-occurrence of premature release during biosynthesis.

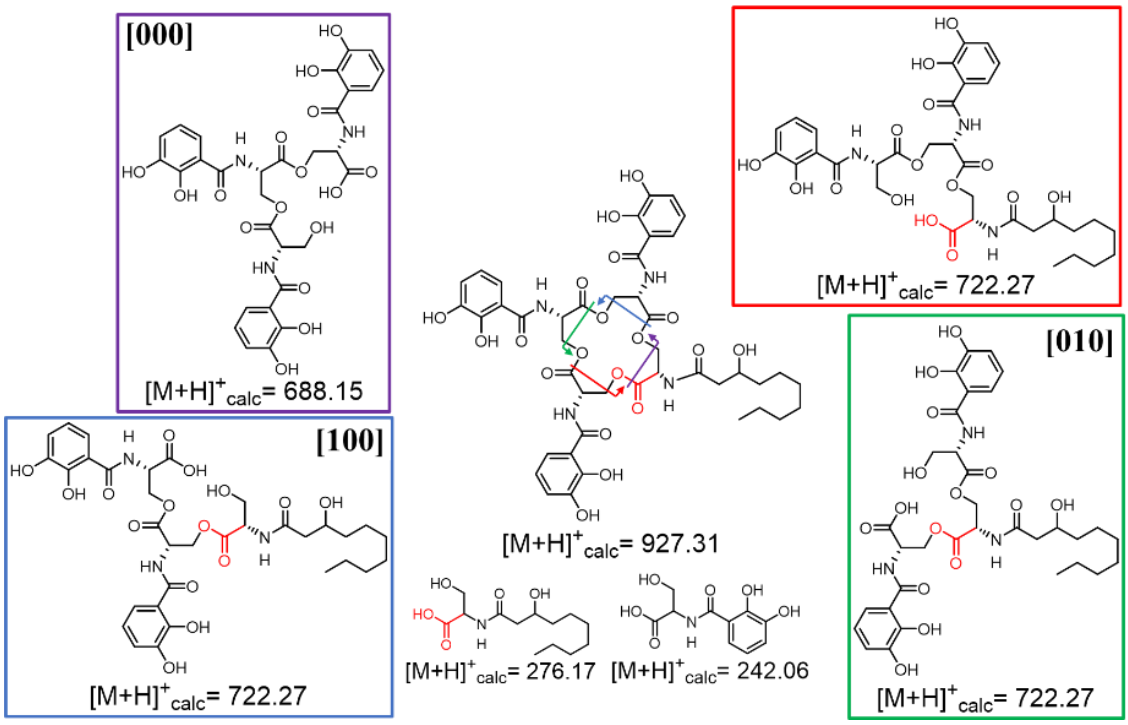

Figure 3.9. The possible tri-Ser$^{C10\text{-}OH}$ fragments produced from ester hydrolysis of amphi-enterobactin. Hydrolysis at two adjacent esters within the amphi-enterobactin macrolactone would form the tri-Ser fragments, [000], [001], [010] and [100].

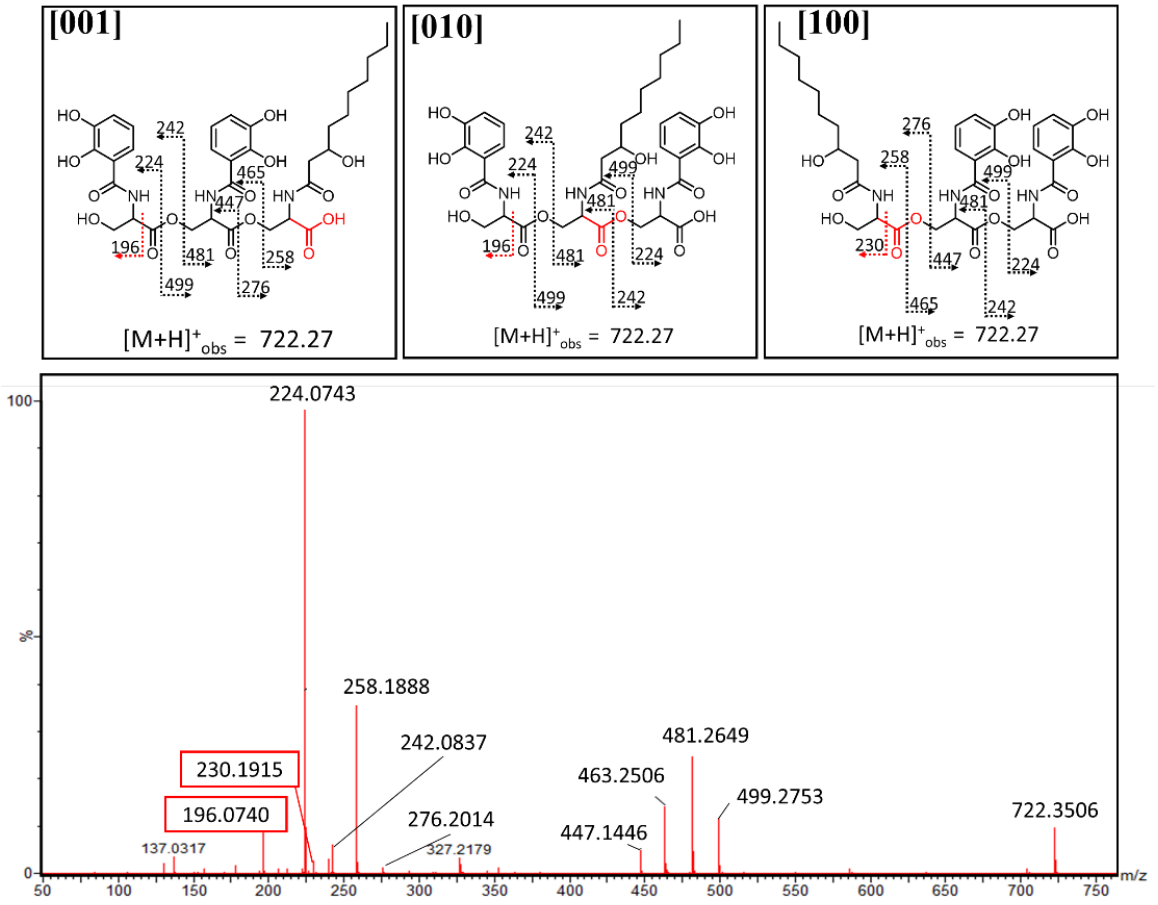

Figure 3.10. Tandem MS of m/z 722.27 for potential differentiation among the [001], [010] and [100] isomers in *V. campbellii* CAIM 519T. A fragment ion of m/z 196 is consistent with premature release, while a fragment ion of m/z 230 is consistent with the hydrolysis of the amphi-enterobactin macrolactone.

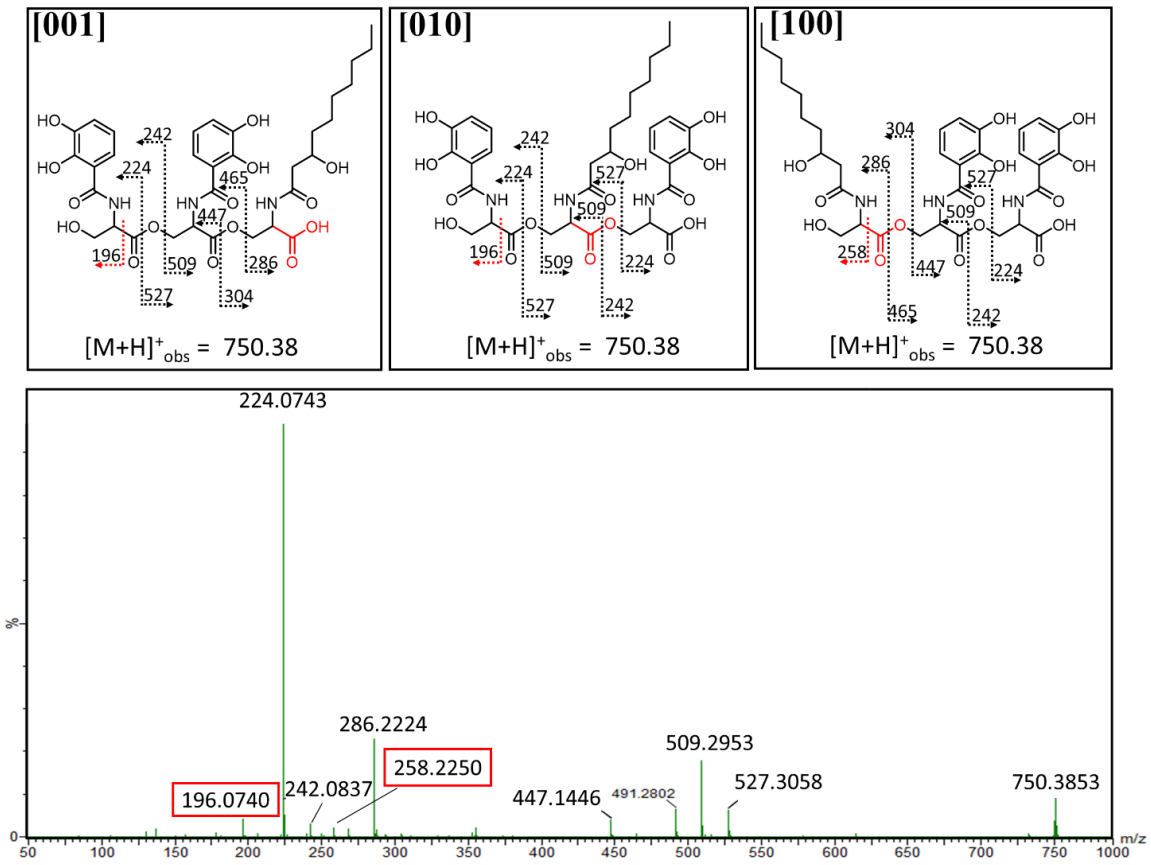

Figure 3.11. Tandem MS of m/z 750.38 for potential differentiation among the [001], [010] and [100] isomers in *V. campbellii* CAIM 519T. A fragment ion of m/z 196 could result from premature release during biosynthesis or from hydrolysis of the amphi-enterobactin macrolactone, while a fragment ion of m/z 258 is consistent only with the hydrolysis of the amphi-enterobactin macrolactone.

3.4.4. *Vibrio natriegens* CCUG 16371 Contains the Amphi-enterobactin Biosynthetic Gene Cluster Identified Through Genome Mining

In *Vibrio natriegens* CCUG 16371, the putative amphi-enterobactin biosynthetic cluster includes six genes (*aebA-F*) predicted to encode proteins that are homologous to the previously characterized amphi-enterobactin biosynthetic genes and the well-characterized enterobactin biosynthetic machinery (Figure 3.12, Table 3.1-3.2). Based on the homology to the *V. campbellii* BAA-1116 (Table 3.2) amphi-enterobactin synthetase proteins, it is proposed that *Vibrio natriegens* CCUG 16371 will produce the suite of amphi-enterobactin siderophores. All of the genes in *V. natriegens* CCUG 16371 that may be involved in the biosynthesis of amphi-enterobactin show high sequence similarity to the amphi-enterobactin biosynthesis genes identified in *Vibrio campbellii* ATCC BAA-1116. The *V. natriegens* CCUG 16371 genome also contains a long chain fatty acid CoA ligase (FACL) in close proximity to the predicted amphi-enterobactin biosynthetic gene cluster. These enzymes have been shown to be involved in the biosynthesis of acylated peptides by activating the fatty acids to fatty acyl-CoA thioesters which are then incorporated into acylated nonribosomal peptides. [5 6]

Vibrio natriegens CCUG 16371 is an emerging marine bacterium as it is the fastest growing non-pathogenic bacterium and is suggested to become the new alternative chassis organism to *Escherichia coli* for synthetic biology and biotechnology.[11 17] However, little is still known about the genetics that are responsible for the record setting replication rate of *V. natriegens* CCUG 16371. Siderophore production may have an impact on this fast growth rate.

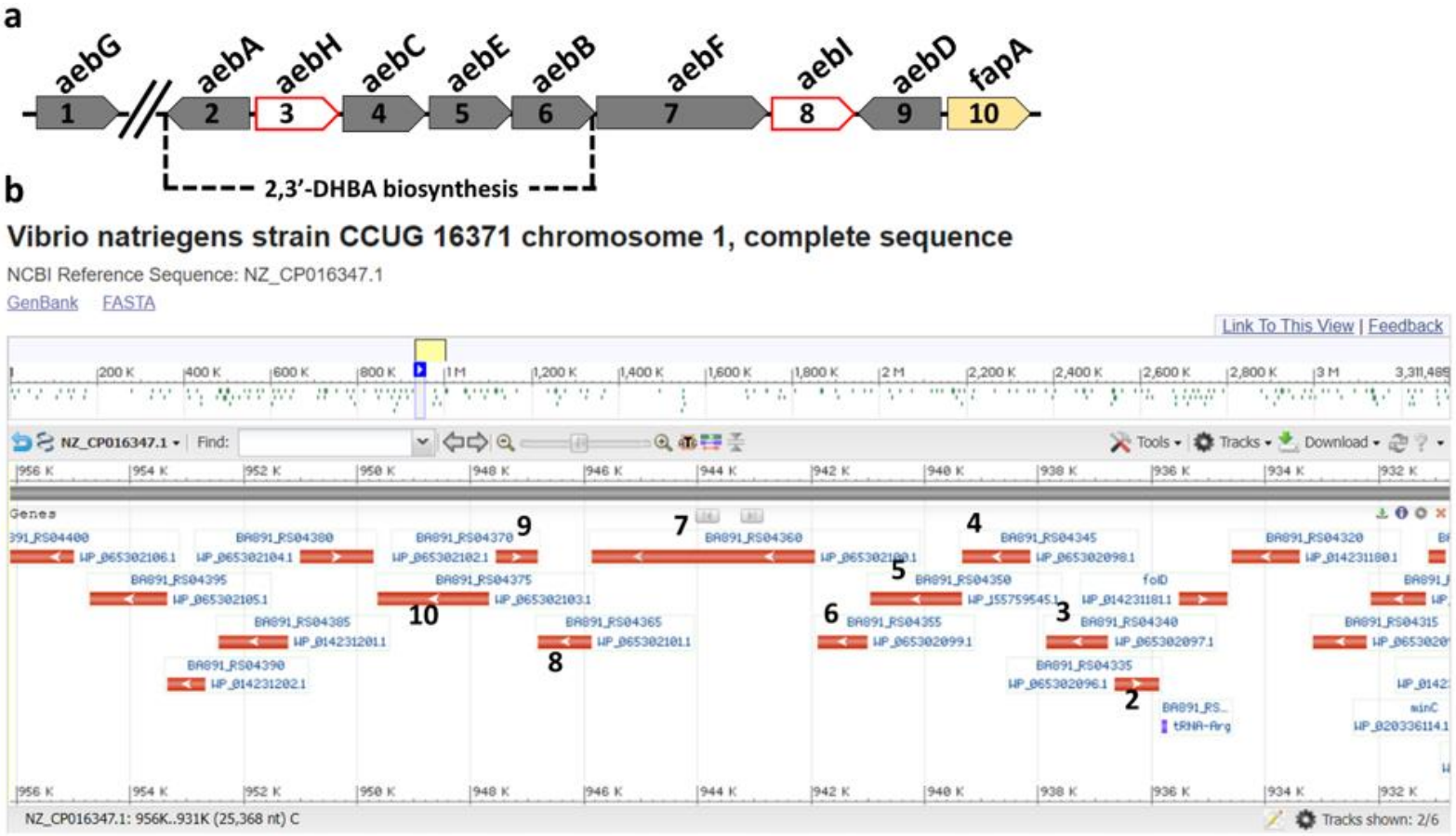

Figure 3.12. The genetic organization of the putative amphi-enterobactin biosynthetic gene cluster in *V. natriegens* CCUG 16371. a) Genes involved in siderophore biosynthesis and transport are represented by gray and yellow arrows, respectively. White arrows represent hypothetical proteins whose function has not yet been determined. b) Graphical representation of the aeb gene cluster within *V. natriegens* CCUG 16371 genome generated from the National Center for Biotechnology (NCBI) website.

Table 3.1. Annotation of the amphi-enterobactin biosynthetic gene cluster in *Vibrio natriegens* CCUG 16371

Number	Gene name	Protein accession number	Location	Proposed Function	Protein Size
1	aebG	WP_065302093.1	925,858..927,549	Long-chain-fatty-acid ligase	563
2	aebA	WP_065302096.1	935,868..936,659	2,3-dihydro-2,3-dihydroxybenzoate dehydrogenase	263
3	"aebH"	WP_065302097.1	936,761..937,858	Hypothetical protein	365
4	aebC	WP_081280996.1	938,133..939,347	Isochorismate synthase	406
5	aebE	WP_155759545.1	939,344..940,963	(2,3-dihydroxybenzoyl)adenylate synthase	539
6	aebB	WP_065302099.1	941,015..941,893	Isochorismatase/aryl carrier for DHBA	292
7	aebF	WP_065302100.1	941,927..945,874	NRPS	1,315
8	"aebI"	WP_065302101.1	945,867..946,811	Hypothetical protein	314
9	aebD	WP_065302102.1	946,826..947,554	4'-Phosohopantetheinyl transferase	242
10	fapA	WP_065302103.1	947,674..949,635	TonB-dependent receptor	653

Table 3.2. Comparison of amino acid sequences of *V. natriegens* CCUG 16371 with *V. campbellii* ATCC BAA-1116, a known amphi-enterobactin producer, and *E. coli* JML 217, a known enterobactin producer.[a]

Gene name	ORF predicted function	Protein Size (# of aa)	Identity to *V. campbellii* ATCC BAA-1116	Identity to *E. coli* JML217
aebG[b]	Long-chain-fatty-acid ligase	563	95.74%	75.72%
aebA	2,3-dihydro-2,3-DHB dehydrogenase	263	80.99%	40.31%
"aebH"	Hypothetical protein	365	71.78%	N/A
aebC	Isochorismate synthase	406	86.42%	38.95%
aebE	2,3-DHB-AMP ligase	539	79.04%	47.08%
aebB	Isochorismatase/aryl carrier for DHBA	292	80.74%	46.23%
aebF	NRPS	1,315	87.83%	35.92%
"aebI"	Hypothetical protein	314	64.77%	N/A
aebD	4'-Ppant transferase	242	55.28%	31.61%
fapA	TonB-dependent receptor	653	80.40%	26.49%

[a] Comparison of amino acid sequences with sequences in public databases were performed using the BLAST program and the NCBI website (http://blast.ncbi.nlm.nih.gov/Blast.cgi);[18] [b] Letter designations correspond to linear gene map depicted in Figure 3.12.

3.4.5. Bacterial Growth and Siderophore Production in *V. natriegens* CCUG 16371

V. natriegens CCUG 16371 was streaked onto CAS agar plates to determine if the bacterium produced siderophores. After two days of growth on the CAS agar plate, yellow hallows appeared around the bacterial colonies, indicating siderophore production is occurring as *V. natriegens* CCUG 16371 grows.

To isolate siderophores, *V. natriegens* CCUG 16371 was grown in iron-limited minimal media. The culture reached stationary phase after approximately 20 hours of growth at room temperature. When the culture was combined with liquid CAS solution, a color change from blue to pink occurred, indicating that *Vibrio natriegens* CCUG 16371 was producing siderophores.

Amphi-enterobactin is a cell-associated siderophore and is extracted from the bacterial cell pellet. Working with a new strain, both the bacterial cell pellet and the supernatant were both screened for siderophore production. After harvesting the bacterial culture, the cell-free supernatant displayed CAS activity, while the cell pellet did not display CAS activity.

3.4.6. MS/MS Analysis of the Amphi-enterobactin Fragments found in the Supernatant of *V. natriegens* CCUG 16371

The supernatant of *V. natriegens* CCUG 16371 on the other hand contains masses, labeled peaks (A-D), which correlate with masses of amphi-enterobactin fragments (Figure 3.13 and Fig. 3.14). The species eluting at 4.3 minutes, labeled Peak A reveals a protonated mass of *m/z* 499 $[M+H]^+$, which matches the composition of the amphi-enterobactin fragment with a C10:0-OH fatty acid, referred to as 2-Ser-1-DHB-$FA^{C10:0-OH}$. Peak C (*m/z* 527), eluting

at 5.1 minutes, is analogous to Peak A although with a C12:0-OH fatty acid, i.e., 2-Ser-1-DHB-$FA^{C12:0-OH}$. Similarly to the amphi-enterobactin fragments found in the supernatant of *V. campbellii* CAIM 519T, two structural isomers are possible with each of these compositions, depending on the positions of the fatty acid and 2,3-DHB in reference to the serine ester backbone; the fatty acid may be appended to either the C-terminal L-Ser, depicted by the binary code **[01]**, or the N-terminal L-Ser, depicted by **[10]**.

The species eluting at 4.6 minutes and 5.4 minutes are associated with Peak B and Peak D, respectively (Figure 3.13). Peak B reveals a protonated molecular mass of *m/z* 722 $[M+H]^+$, consistent with the composition 3-Ser-2-DHB-$FA^{C10:0-OH}$, and peak D (*m/z* 750) is associated with the equivalent C12:0-OH fatty acid derivative. Three structural isomers exist for 3-Ser-2-DHB-FA (Fig. 3.4 and 3.5) in which the fatty acid may be appended to the C-terminal L-Ser **[001]**, the internal L-Ser **[010]**, or the N-terminal L-Ser **[100]**.

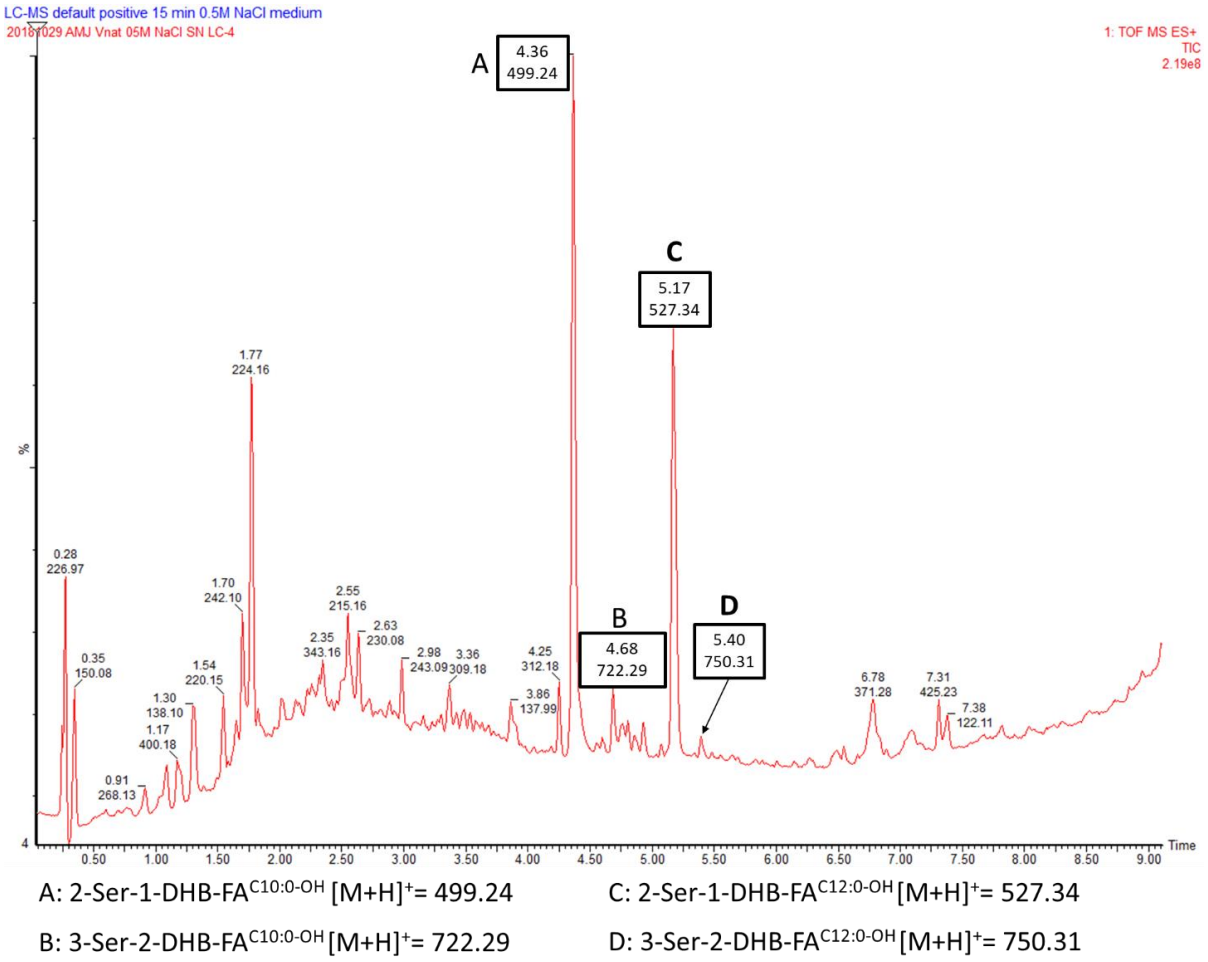

Figure 3.13. LC-MS of the *Vibrio natriegens* CCUG 16371 supernatant. Peaks A-D correlate to masses of predicted amphi-enterobactin fragments.

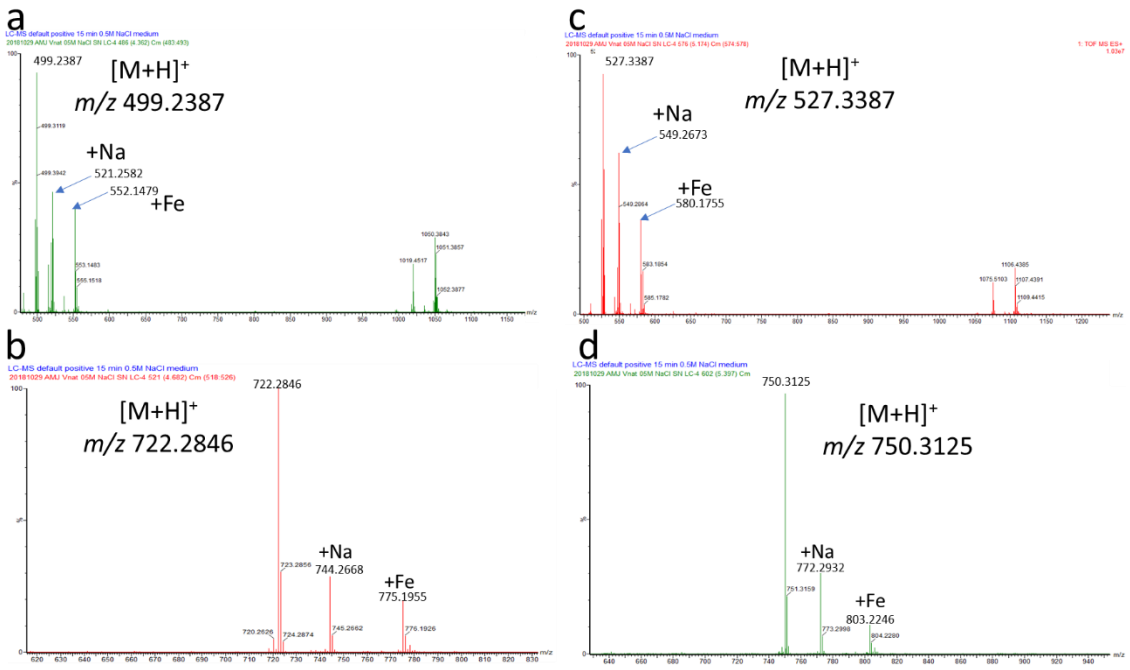

Figure 3.14. MS spectra of Peaks A-D that correlate to masses of predicted amphi-enterobactin fragments in *V. natriegens* CCUG 16371, as seen in the chromatogram.

Four masses were identified in the supernatant of *V. natriegens* CCUG 16371 that correlate with masses of amphi-enterobactin fragments. The first is a protonated mass of *m/z* 499 $[M+H]^+$, which matches the composition of the amphi-enterobactin fragment with a C10:0-OH fatty acid is referred to as 2-Ser-1-DHB-$FA^{C10:0-OH}$.

Mass fragmentation analysis establishes the presence of amphi-enterobactin hydrolysis fragments and suggest that they arise from the full siderophore, although premature release cannot be ruled out. Again, tandem mass spectrometry analysis can be used to differentiate between structures **[01]** and **[10]** based on the unique MS/MS signature fragments – *m/z* 196 $[M+H]^+$ specific to **[01]** and *m/z* 230 $[M+H]^+$ specific to **[10]**.

The ESI-MS/MS spectrum of the product with a protonated mass of *m/z* 499 $[M+H]^+$ (2-Ser-1-DHB-$FA^{C10:0-OH}$) shows fragments at both *m/z* 196 and *m/z* 230 (Figure 3.15). The same pattern is observed for the product with a protonated mass of *m/z* 527 $[M+H]^+$ (2-Ser-1-

DHB-FA$^{C12:0-OH}$), although with analogous fragments at *m/z* 196 and *m/z* 258 (Figure 3.16). The mixture of both unique fragments is evidence that the amphi-enterobactin macrolactone is produced and hydrolyzed to **[01]** and **[10]**. However, the presence of both **[01]** and **[10]** does not rule out premature release during the biosynthesis as the origin of some of **[01]**.

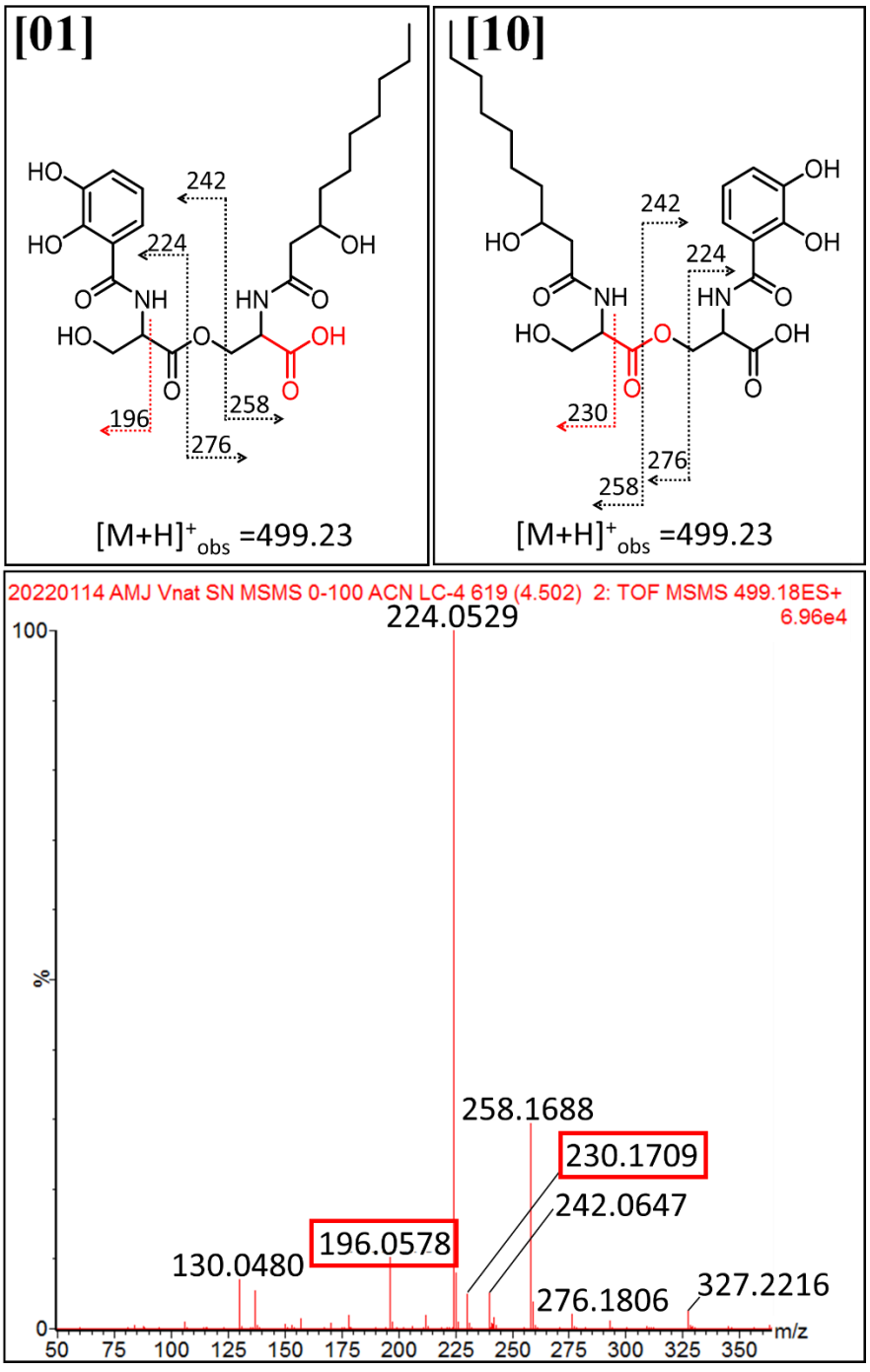

Figure 3.15. MS/MS of *m/z* 499.23 in *V. natriegens* CCUG 16371 for differentiation between **[01]** and **[10]**. A fragment ion of *m/z* 196 is consistent with premature release, while a fragment ion of *m/z* 230 is consistent with the hydrolysis of amphi-enterobactin macrolactone.

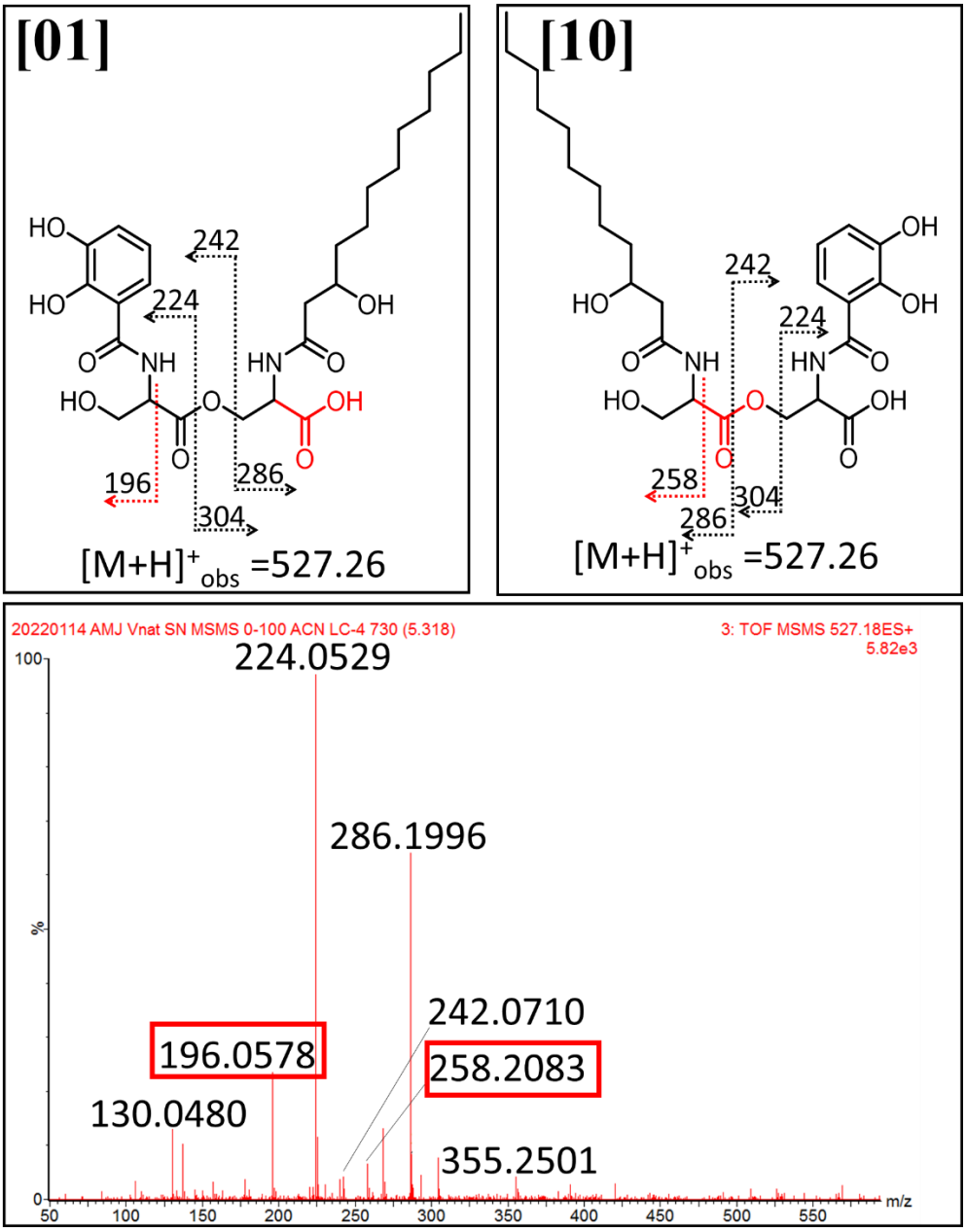

Figure 3.16. MS/MS of *m/z* 527.26 in *V. natriegens* CCUG 16371 for differentiation between **[01]** and **[10]**. A fragment ion of *m/z* 196 is consistent with premature release, while a fragment ion of *m/z* 258 is consistent with the hydrolysis of amphi-enterobactin macrolactone.

Along with 2-Ser-1-DHB-FA, 3-Ser-2-DHB-FA compounds were also observed. Four distinct tri-Ser hydrolysis fragments could be formed from dual hydrolysis of adjacent esters within the amphi-enterobactin macrolactone, only three of which would have a 3-Ser-2-DHB-FA motif, **[100]**, **[010]**, **[001]** (Figure 3.9 and 3.4). The fourth hydrolysis fragment that would lack the fatty acid, 3-Ser-3-DHB, **[000]**. Only two of the tri-Ser hydrolysis fragments were observed, fragments with the protonated mass of *m/z* 722.28 $[M+H]^+$ **(3-Ser-2-DHB-FA$^{C10:0-OH}$)** and *m/z* 750.31 $[M+H]^+$ **(3-Ser-2-DHB-FA$^{C12:0-OH}$)** (Fig. 3.13). However, due to the trace quantity of the fragment with the protonated mass of *m/z* 750.31 $[M+H]^+$, tandem MS characterization was only carried out on the fragment with the protonated mass of *m/z* 722.28 $[M+H]^+$.

Tandem mass spectral analysis was carried out on the product with a protonated molecular mass of *m/z* 722.28 $[M+H]^+$, consistent with **3-Ser-2-DHB-FA$^{C10:0-OH}$** (Figure 3.17). Tandem MS shows both of the fragments at *m/z* 196 and *m/z* 230. The *m/z* 230 ion confirms the presence of **[100]**, which can only arise from an amphi-enterobactin macrolactone hydrolysis product. The ion fragment at *m/z* 196 was also identified by tandem MS and could arise from both **[001]** and **[010]**. The mixture of both fragments is evidence that in *V. natriegens* CCUG 16371 amphi-enterobactin is produced and is hydrolyzed to **[100]**, and one of both of **[010]** and **[001]**, although the presence of all three isomers does not rule out the co-occurrence of premature release during biosynthesis.

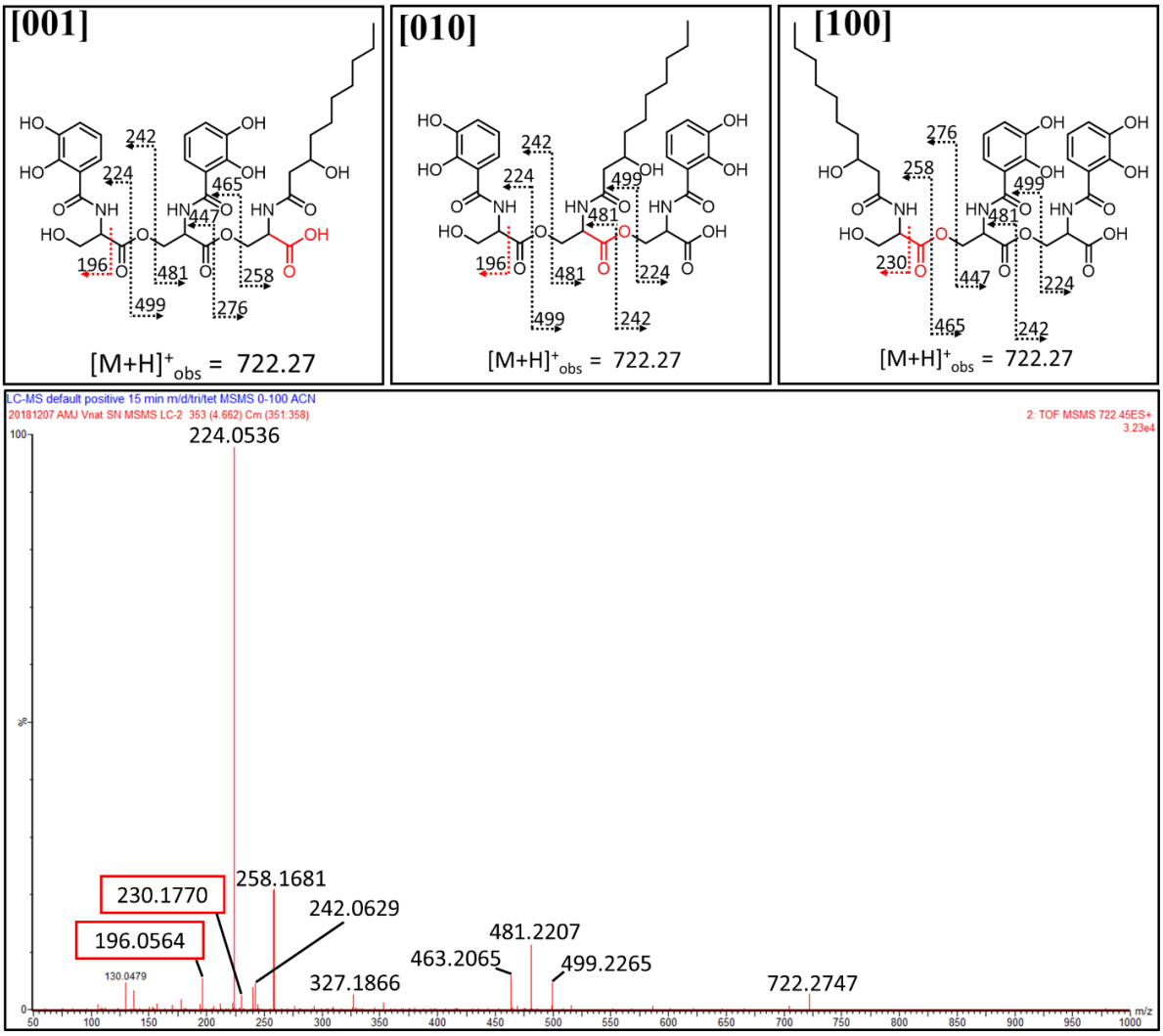

Figure 3.17. Tandem MS of *m/z* 722.27 for potential differentiation among the **[001]**, **[010]**, **[100]** isomers in *V. natriegens* CCUG 16371. A fragment ion of *m/z* 196 is consistent with premature release, while a fragment ion of *m/z* 230 is consistent with the hydrolysis of the amphi-enterobactin macrolactone.

3.4.7. Bioinformatic Analyses for Putative Esterases Found in the Biosynthetic Gene Cluster of *V. campbellii* CAIM 519T and *V. natriegens* CCUG 16371

A BLAST search of *fes* within the genomes of *V. campbellii* CAIM 519T and *V. natriegens* CCUG 16371 did not detect any homologs of this macrolactone esterase. However, a more comprehensive sequence analysis search of the AebH and AebI peptide sequence using HMM scan through EMBL-EBI found distant homology to the EreA-like superfamily.[15] EreA is an erythromycin esterase from *E. coli* that enzymatically hydrolyzes the macrolactone ring of erythromycin. [19] [20] [21] The distant homology to a macrolactone esterase suggests that these hypothetical proteins found within the amphi-enterobactin biosynthetic gene cluster may have similar functionality in cleaving the macrolactone core of amphi-enterobactin.

Partial sequence alignment of AebH and AebI found within both *V. campbellii* CAIM 519T and *V. natriegens* CCUG 16371 with the erythromycin esterases, EreA and EreB (from *E. coli*) revealed that the strictly conserved residues (E43, H46, and E74) in EreA and EreB are conserved in AebI, while AebH has the H46 and E74 conserved residues (Figure 3.18).[19] Site-directed mutagenesis of E74A in EreA and EreB abolished the functional activity of the erythromycin esterase, establishing this conserved residue as important in esterase activity.[19] SignalP, a machine learning model that detects signal peptides (Teufel et al.),[22] was used to predict the cellular localization of the hypothetical proteins.[22] AebH has both a putative signal peptide and cleavage site suggesting a periplasmic localization, while AebI is predicted to reside in the cytoplasm. This sequence analysis of the hypothetical proteins AebH and AebI in both *V. campbellii* CAIM 519T and *V. natriegens* CCUG 16371 suggests AebH and AebI may be esterases and thus function in hydrolyzing the macrolactone ring of amphi-enterobactin.

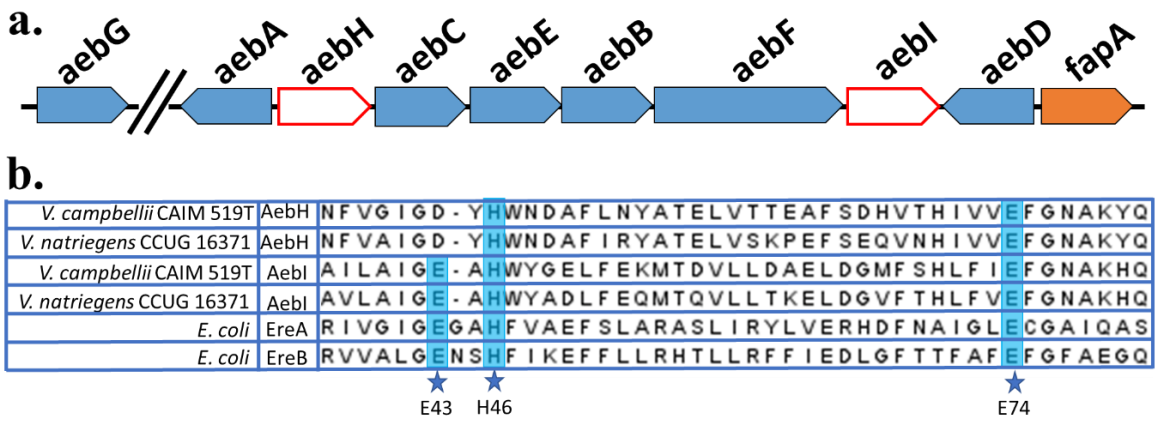

Figure 3.18. Location and comparison of genes aebH and aebI in *V. campbellii* CAIM 519T and *V. natriegens* CCUG 16371. a. Amphi-enterobactin gene cluster. White arrows have been named aebH (esterase 1) and aebI (esterase 2). b. Partial sequence alignment of AebH and AebI in both *V. campbellii* CAIM 519T and *V. natriegens* CCUG 16371 with E. coli's EreA and EreB active site residues. Stars active site residues and the blue boxes indicate the residues conserved among the six proteins.

3.4.7.1. Presence of Amphi-Enterobactin Genes in other *Vibrio* Species

Thode *et al.* compiled and visualized gene clusters for the biosynthesis of siderophores in *Vibrionaceae*.[23] The study identified four *Vibrio* species potentially responsible for producing amphi-enterobactin. *Vibrio harveyi* and *V. campbellii* have already been characterized as amphi-enterobactin producers, while *V. natriegens* and *V. owensii* have not yet been confirmed as amphi-enterobactin producers. However, there is evidence of amphi-enterobactin fragments in *V. natriegens* CCUG 16371 indicating that the macrolactone is produced however has not yet been isolated. The putative esterase sequences of these four *Vibrio* species were used to construct an HMM. Among the 88 strains with matching esterase sequences, all strains had the EreA/EreB esterase active site residues conserved (Figure 3.19).

Exploring the bacterial strains containing a positive match, one of the species, *Aeromonas veronii* CN17A0102, a gram-negative human pathogen, has only one protein homologous to one of the putative esterases found in *Vibrio campbellii* ATCC BAA-1116. A

more thorough search around this homologous esterase gene showed genes similar to the amphi-enterobactin biosynthesis genes.

A BLAST comparison evaluated the homology of the genes found adjacent to the one putative esterase (Table 3.3). AebF and AebG in *V. campbellii* ATCC BAA-1116 is identical to the gene in *A. veronii* CN17A0102 suggesting that this strain may produce amphi-enterobactin. The genes found in *Aeromonas veronii* CN17A0102 were aligned to the amphi-enterobactin gene cluster in *V. campbellii* ATCC BAA-1116 (Figure 3.20). SignalP predicted cytoplasmic localization of the putative esterase in *A. veronii* CN17A0102, similar to AebI from *V. campbellii* ATCC BAA-1116. The putative esterase in *A. veronii* CN17A0102 is adjacent to AebF in the gene cluster, just like in *V. campbellii* ATCC BAA-1116. The presence of the amphi-enterobactin biosynthetic machinery suggests that *Aeromonas veronii* CN17A0102 should produce amphi-enterobactin, however only contains one putative esterase involved in amphi-enterobactin hydrolysis. These results indicate certain species may have redundant putative amphi-enterobactin esterases and that at some point bacterial species branched from two to one esterase.

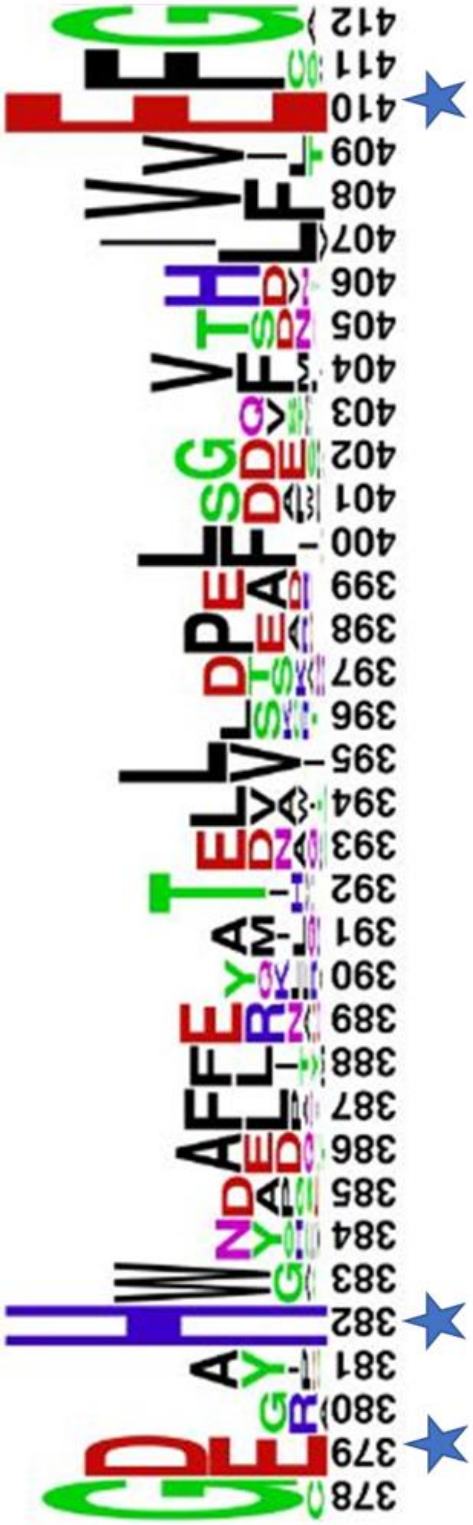

Figure 3.19. Sequence logo constructed from 88 strains that matched the putative esterase sequence alignment of both AebH and AebI. Blue stars indicate conserved active site residues of EreA (E43, H46, E74) and the putative esterases.

Table 3.3. BLAST comparison results between *Aeromonas veronii* CN17A0102 and the amphi-enterobactin biosynthesis genes of *V. campbellii* ATCC BAA-1116.

Gene name	E-value	Identities	Positives
aebG	0.0	414/562 (74%)	483/562 (85%)
aebA	$2e^{-58}$	107/261 (41%)	140/261 (53%)
aebH / Esterase #1	$3e^{-23}$	63/214 (29%)	100/214 (46%)
aebC	$1e^{-80}$	152/384 (40%)	211/384 (54%)
aebE	$2e^{-164}$	259/541 (48%)	334/541 (61%)
aebB	$3e^{-96}$	140/298 (47%)	189/298 (63%)
aebF	0.0	1329/1329 (100%)	1329/1329 (100%)
aebI / Esterase #2	$3e^{-36}$	94/295 (32%)	144/295 (48%)
aebD	n/a	n/a	n/a
fapA	$2e^{-125}$	239/671 (36%)	362/671 (53%)

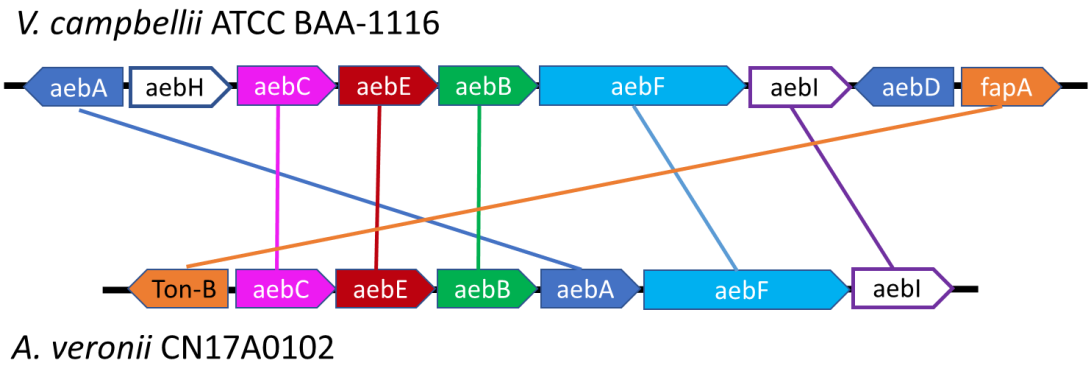

Figure 3.20. Visual representation of the position of homologous amphi-enterobactin biosynthesis genes found in *A. veronii* CN17A0102.

3.4.7.2. Signal Peptides Found in Putative Esterase Peptide Sequence (Cytoplasmic versus Periplasmic)

Signal peptides (SPs) are short amino acid sequences found in the amino terminus that carry information for protein secretion and protein target location, particularly the destination the protein is delivered.[24] The presence of a signal peptide prompts the cell to translocate the protein if needed. A signal peptide is does not consist of a strict consensus sequence, but rather is composed of three main regions: 1) N-region: the positively-charged domain; 2) H-region: the hydrophobic central region; and 3) C-region: the neutral, polar cleavage site.[25] Proteins without signaling regions are maintained in the cytoplasm, while those with signal peptides are translocated to the periplasm.[16]

The SignalP 5.0 server predicts the presence of signal peptides in proteins. This server produces an output containing the highest probability. The protein can have a Sec signal peptide (Sec/SPI), a Lipoprotein signal peptide (Sec/SPII), a Tat signal peptide (Tat/SPI), or no signal peptide at all (other).[16] If a signal peptide is reported, the position of the cleavage site is also reported.[16]

Using the SignalP server, the amino acid sequences of both AebH and AebI were studied and compared to IroE, an enterobactin esterase, identified as a periplasmic protein due to the presence of a signal peptide. The X-axis of the graph is the amino acid sequence labeled numerically from the N-terminus and the Y-axis depicts the probability of the protein containing the peptide sequence.

AebI is predicted to have cytoplasmic localization due to the lack of a signal peptide (Figure 3.21). As seen in the signal peptide analysis, AebI has a high probability, 0.9968 for OTHER, suggesting that this sequence does not contain a signal peptide.

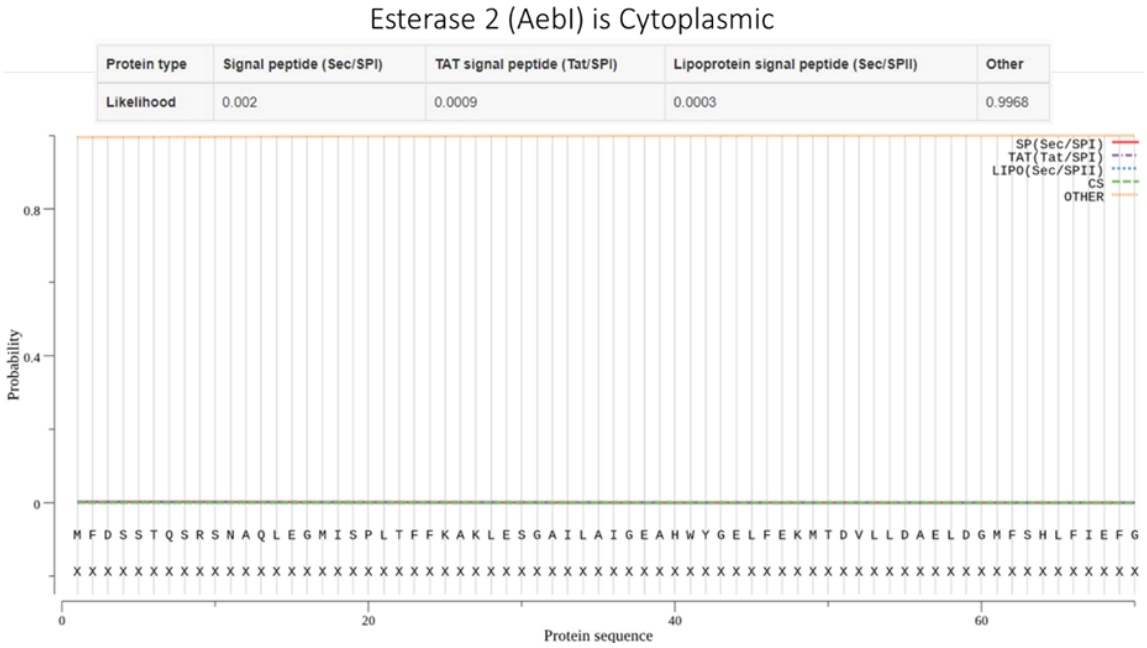

Figure 3.21. Signal peptide probability prediction for AebI. Visual representation of the prediction probabilities at each position and the signal peptide type. CS, cleavage site.

AebH on the other hand does contain a signal peptide, however it is a lipoprotein signal peptide. Analysis of the probability output (Figure 3.22) indicates that the lipoprotein signal peptide has the highest probability for residues 1-22. A cleavage signal is observed right after at residue 23. The signal peptide (Sec/SPI) probability is 0.0023, while the lipoprotein signal (Sec/SPII) is 0.9973.

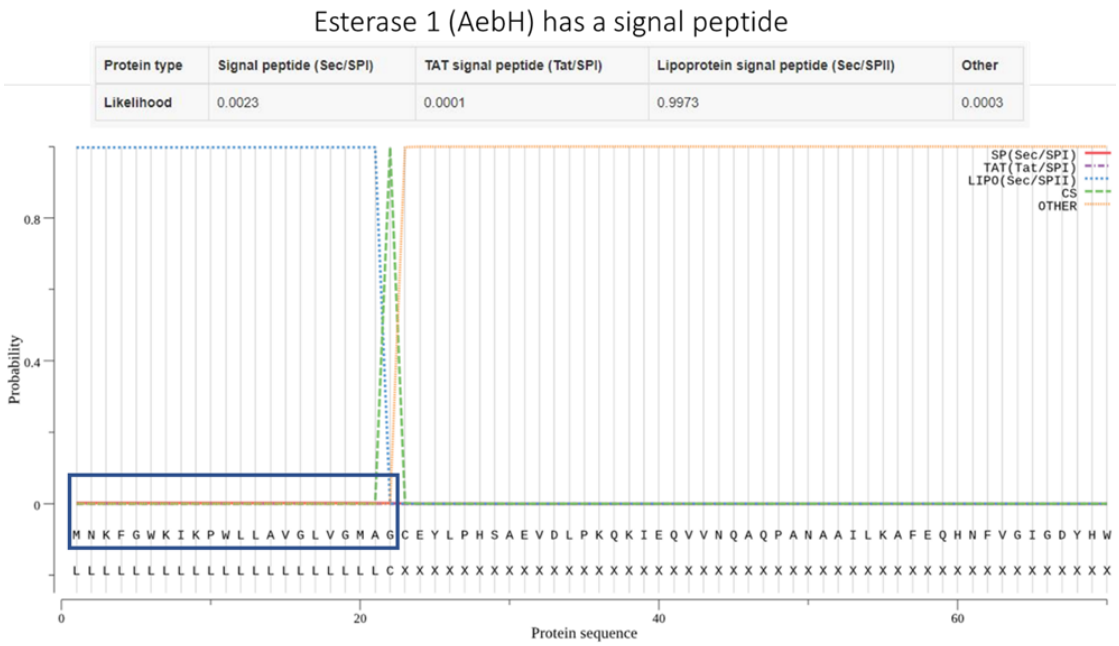

Figure 3.22. Signal peptide probability prediction for AebH. Visual representation of the prediction probabilities at each position and the signal peptide type. CS, cleavage site.

LipoP 1.0 is a program used for the prediction of lipoproteins and for discerning between lipoprotein signal peptides, other signal peptides, and N-terminal membrane helices in Gram-negative bacteria. This method is described in *Prediction of lipoprotein signal peptides in Gram-negative bacteria* by Sierakowska *et al*. [26] The first line of the output summarizes the best prediction of where the cleavage site is to occur and the second line gives the cut-off used. The columns represent the sequence ID, the type of prediction where Best means the highest scoring class, margin gives the difference between the best and second-best score, class gives the score of other classes, and signal lines contain predicted cleavage sites. The next column is feature type where SpI means signal peptide, SpII is lipoprotein signal peptide, TMH is N-terminal transmembrane helix, and CYT is cytoplasmic. Figure 3.24 shows the output information for AebH, where we see a score of 3.6844 and a cleavage site between residues 22-23, which matches with output from the SignalP-5.0 server. The LipoP 1.0 Server

provides further confirmation that AebH though containing a signal peptide is more likely a lipoprotein.

Lipoproteins are hydrophobic extracellular polypeptides that bind noncovalently to lipids and transport through an aqueous environment. Knowing that amphi-enterobactin contains a fatty acid chain and is hydrophobic, AebH may have lipoprotein functionality when interacting with amphi-enterobactin. It remains unclear how a lipoprotein would relate to putative esterase activity, however, AebH does contain a signal peptide indicating that it is transported to the periplasm. In gram-negative bacteria, lipoproteins are typically attached to the cytoplasmic membrane, the extracellular or peripheral side of the outer membrane. Meaning that lipoproteins interact with the membrane, where it was hypothesized that amphi-enterobactin may also interact with the membrane. The function of AebH still remains unknown.

```
# WP_041853222.1 SpII score=3.64844 margin=3.465957 cleavage=22-23 Pos+2=E
# Cut-off=-3
WP_041853222.1  LipoP1.0:Best   SpII    1       1       3.64844
WP_041853222.1  LipoP1.0:Margin SpII    1       1       3.465957
WP_041853222.1  LipoP1.0:Class  TMH     1       1       0.182483
WP_041853222.1  LipoP1.0:Class  CYT     1       1       -0.200913
WP_041853222.1  LipoP1.0:Class  SpI     1       1       -0.306593
WP_041853222.1  LipoP1.0:Signal CleavII 22      23      3.64844 # VGMAG|CEYLP Pos+2=E
WP_041853222.1  LipoP1.0:Signal CleavI  32      33      -1.35622        # HSAEV|DLPKQ
WP_041853222.1  LipoP1.0:Signal CleavI  30      31      -1.78318        # LPHSA|EVDLP
```

Figure 3.23. Lipoprotein peptide signal prediction for AebH.

3.4.8. Chirality of Fe(III)-Amphi-Enterobactin

Amphi-enterobactin was purified by HPLC to remove contaminants. ESI-MS confirmed the structure to be the 4-L-serine-3-DHB-FA (C12:0 OH) amphi-enterobactin with a *m/z* value of 955. Circular dichroism (CD) measurements were obtained for the iron(III) complex of amphi-enterobactin. Similarly, like Δ-Fe(III)-enterobactin complex, the ferric amphi-enterobactin complex also has a Δ configuration (Figure 3.24 and Table 3.4). The CD band at 270 nm corresponds to the carbonyl amide in the ligand, which the CD spectrum of Fe(III)-amphi-enterobactin contains. Ferric amphi-enterobactin also shows at band at 310 nm representative of the chiral lactone scaffold, however in this case it is the tetralactone scaffold while other siderophores like enterobactin and salmochelin contain a trilactone scaffold. Ultimately in the CD spectrum one is looking for the bands arising from ligand-to-metal charge transfer (LMCT) transitions, and in the case of amphi-enterobactin, they are the ferric catechol transitions observed at around 435 nm and between 500 and 550 nm. These transitions are sensitive to the chirality at the metal center.[27] The tetralactone scaffold and fatty acyl chain in amphi-enterobactin do not influence a change in chirality at the metal center when comparing enterobactin's trilactone scaffold and lack of fatty acid tail. In all, the chirality of ferric amphi-enterobactin has been determined Δ. This configuration is the same for ferric enterobactin, established by Karpishin, et. al.[28] It will be interesting to see how microbial recognition is affected, even though we see the same chiralities, will the structure be the ultimate deciding factor. For comparison purposes, the Fe(III)-amphi-enterobactin CD spectrum was compared to the published CD spectra in Abergel et. al.[29] of the following iron complexes: enterobactin, D-enterobactin, Ser-Gly-Cam, D-Ser-Gly-Cam, and bacillibactin.

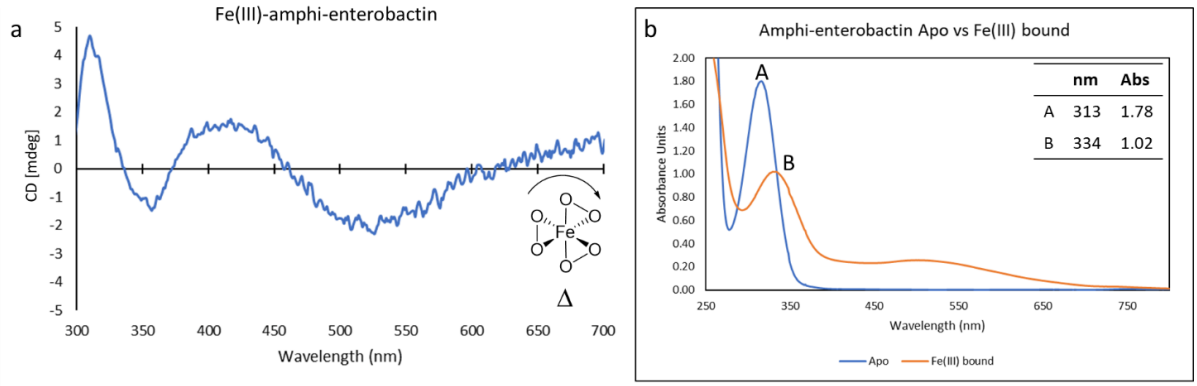

Figure 3.24. (A) Circular dichroism spectrum of 100 μM Fe(III)-bound amphi-enterobactin in MOPS buffer (pH 7.4). (b) UV-visible absorbance of apo- vs Fe(III)-amphi-enterobactin.

Table 3.4. Circular dichroism result of Fe(III)-amphi-enterobactin.

	LMCT transitions	
	λ_{max}	$\Delta\epsilon$
Ligand	(nm)	$[M^{-1}cm^{-1}]$
Amphi-enterobactin	526	-2.29

3.5. Discussion

In summary, tandem MS analysis of the hydrolysis fragments of amphi-enterobactin in the culture supernatant of both *V. campbellii* CAIM 519T and *V. natriegens* CCUG 16371 establish that isomers **[10]** and **[100]** must arise from hydrolysis of the macrolactone amphi-enterobactin siderophore as opposed to prerelease of di-Ser or tri-Ser fragments during biosynthesis. Evidence for the **[10]** and **[100]** hydrolysis fragments is given by the unique MS/MS fragment at *m/z* 230 $[M+H]^+$ arising from the $C_{10:0\ OH}$ derivatives (Figs. 3.7 and 3.10) and *m/z* 258 $[M+H]^+$ arising from the $C_{12:0\ OH}$ derivatives (Figs. 3.8 and 3.11). These fragments establish amphi-enterobactin is fully formed and then hydrolyzed. Identification of products uniquely associated with prerelease, e.g., **[1]**, **[01]**, **[001]**, and **[0001]** is not possible since the fragments may also arise from hydrolysis of the amphi-enterobactin macrolactone.

Future experiments involving an *in vitro* analysis of the biosynthesis proteins for amphi-enterobactin could provide insight into the potential for premature release of incomplete fragments along the biosynthetic pathway for amphi-enterobactin. Previous results from reconstructing enterobactin synthetase activity reveal a pH dependence for the formation of enterobactin hydrolysis products [30]. At pH 7.5, enterobactin was the only product synthesized and released, while pH 8.8, the bis-catechol, bis L-Ser fragment, $(DHB\text{-}L\text{-}Ser)_2$ was observed. This $(DHB\text{-}L\text{-}Ser)_2$ intermediate was a result of premature release of the incompletely synthesized enterobactin from EntF at pH 8.8 rather than hydrolysis of enterobactin itself. As a control, when the synthesized enterobactin is incubated in pH 8.8 Tris-HCl buffer, enterobactin hydrolyzes to the DHB-Ser linear trimer, and no monomer or dimer. This study suggests that premature hydrolysis is pH dependent, and that at physiological pH, *in vitro*, no early release occurs.[30]

Campylobacter jejuni, a bacterial strain that does not itself produce siderophores, contains a siderophore uptake system able to recognize and take up Fe(III)-siderophores produced by other bacterial species [31]. Further analysis of this uptake system identified the periplasmic binding protein, CeuE, involved in the uptake of Fe(III)-enterobactin showed a preference for binding to the Fe(III)-complex of the tetradentate hydrolysis product of enterobactin, $[Fe(III)\text{-}(DHB\text{-}L\text{-}Ser)_2]^{2-}$, **[00]** [32]. The study rationalizes that utilizing the enterobactin hydrolysis products provides *C. jejuni* a competitive advantage because it avoids the metabolic costs associated with siderophore production. *C. jeuni* is able to recognize Fe(III)-enterobactin, but for the iron complex to enter the cytoplasm, the siderophore is hydrolyzed by the trilactone esterase Cee to form $[Fe(III)\text{-}(DHB\text{-}L\text{-}Ser)_2]^{-}$ [33].

During the NRPS mediated biosynthesis, the release of the siderophore is catalyzed by the thioesterase domain either through hydrolysis, leading to a linear siderophore, or through an intramolecular nucleophilic attack, leading to the cyclized siderophore [34]. For hydrolysis to occur, water becomes the competing nucleophile and in turn releases a linear siderophore. The presence of linearized amphi-enterobactin has not yet been identified, but this does not eliminate the option that hydrolysis can still occur at any point during the biosynthesis.

Thus overall, only the **[01]**, **[001]** and **[0001]** the DHB-L-Ser fragments could originate from premature release during biosynthesis of amphi-enterobactin due to an inefficient biosynthetic pathway. The **[10]** and **[100]** fragments must arise from hydrolysis of the fully formed amphi-enterobactin macrolactone, which could occur enzymatically by a Fes-type esterase or non-enzymatically. The other possible fragment within the 3-Ser-3-DHB-FA series, **[010]**, is indistinguishable in the tandem MS analysis from the premature-release fragment; thus, without sufficient quantity of each fragment for NMR structural characterization, it is not possible to determine their origin. If fragments are prematurely released during biosynthesis, it suggests that the NRPS pathway for amphi-enterobactin is inefficient and not dependable. Further investigations may shed light on the fidelity of the NRPS-catalyzed biosynthesis of amphi-enterobactin and the prevalence of incomplete synthesis of NRPS natural products.

3.6. References

1. Zane, H. K.; Naka, H.; Rosconi, F.; Sandy, M.; Haygood, M. G.; Butler, A., Biosynthesis of Amphi-enterobactin Siderophores by *Vibrio harveyi* BAA-1116: Identification of a Bifunctional Nonribosomal Peptide Synthetase Condensation Domain. *Journal of the American Chemical Society* **2014,** *136* (15), 5615-5618.
2. Lilley, B. N.; Bassler, B. L., Regulation of quorum sensing in *Vibrio harvey*i by LuxO and Sigma-54. *Molecular Microbiology* **2000,** *36* (4), 940-954.
3. Naka, H.; Reitz, Z. L.; Jelowicki, A. L.; Butler, A.; Haygood, M. G., Amphi-enterobactin commonly produced among *Vibrio campbellii* and *Vibrio harveyi* strains can be taken up by a novel outer membrane protein FapA that also can transport canonical Fe(III)-enterobactin. *JBIC Journal of Biological Inorganic Chemistry* **2018,** *23* (7), 1009-1022.
4. McRose, D. L.; Baars, O.; Seyedsayamdost, M. R.; Morel, F. M. M., Quorum sensing and iron regulate a two-for-one siderophore gene cluster in *Vibrio harveyi*. *Proceedings of the National Academy of Sciences* **2018,** *115* (29), 7581.
5. Kraas, F. I.; Helmetag, V.; Wittmann, M.; Strieker, M.; Marahiel, M. A., Functional dissection of surfactin synthetase initiation module reveals insights into the mechanism of lipoinitiation. *Chem Biol* **2010,** *17* (8), 872-80.
6. Imker, H. J.; Krahn, D.; Clerc, J.; Kaiser, M.; Walsh, C. T., N-acylation during glidobactin biosynthesis by the tridomain nonribosomal peptide synthetase module GlbF. *Chem Biol* **2010,** *17* (10), 1077-83.
7. Lewenza, S.; Sokol, P. A., Regulation of ornibactin biosynthesis and N-acyl-L-homoserine lactone production by CepR in *Burkholderia cepacia*. *J Bacteriol* **2001,** *183* (7), 2212-8.
8. Wen, Y.; Kim, I. H.; Son, J.-S.; Lee, B.-H.; Kim, K.-S., Iron and quorum sensing coordinately regulate the expression of vulnibactin biosynthesis in *Vibrio vulnificus*. *J Biol Chem* **2012,** *287* (32), 26727-26739.
9. Telfer, T. J.; Gotsbacher, M. P.; Soe, C. Z.; Codd, R., Mixing Up the Pieces of the Desferrioxamine B Jigsaw Defines the Biosynthetic Sequence Catalyzed by DesD. *ACS Chemical Biology* **2016,** *11* (5), 1452-1462.
10. Nolan, K. P.; Font, J.; Sresutharsan, A.; Gotsbacher, M. P.; Brown, C. J. M.; Ryan, R. M.; Codd, R., Acetyl-CoA-Mediated Post-Biosynthetic Modification of Desferrioxamine B Generates N- and N-O-Acetylated Isomers Controlled by a pH Switch. *ACS Chemical Biology* **2022,** *17* (2), 426-437.
11. Weinstock, M. T.; Hesek, E. D.; Wilson, C. M.; Gibson, D. G., *Vibrio natriegens* as a fast-growing host for molecular biology. *Nature Methods* **2016,** *13* (10), 849-851.
12. Johnson, M.; Zaretskaya, I.; Raytselis, Y.; Merezhuk, Y.; McGinnis, S.; Madden, T. L., NCBI BLAST: a better web interface. *Nucleic Acids Res* **2008,** *36* (Web Server issue), W5-9.
13. Haft, D. H.; DiCuccio, M.; Badretdin, A.; Brover, V.; Chetvernin, V.; O'Neill, K.; Li, W.; Chitsaz, F.; Derbyshire, M. K.; Gonzales, N. R.; Gwadz, M.; Lu, F.; Marchler, G. H.; Song, J. S.; Thanki, N.; Yamashita, R. A.; Zheng, C.; Thibaud-Nissen, F.; Geer, L. Y.; Marchler-Bauer, A.; Pruitt, K. D., RefSeq: an update on prokaryotic genome annotation and curation. *Nucleic Acids Res* **2018,** *46* (D1), D851-d860.

14. Edgar, R. C., MUSCLE: multiple sequence alignment with high accuracy and high throughput. *Nucleic Acids Research* **2004,** *32* (5), 1792-1797.
15. Madeira, F.; Park, Y. M.; Lee, J.; Buso, N.; Gur, T.; Madhusoodanan, N.; Basutkar, P.; Tivey, A. R. N.; Potter, S. C.; Finn, R. D.; Lopez, R., The EMBL-EBI search and sequence analysis tools APIs in 2019. *Nucleic acids research* **2019,** *47* (W1), W636-W641.
16. Almagro Armenteros, J. J.; Tsirigos, K. D.; Sønderby, C. K.; Petersen, T. N.; Winther, O.; Brunak, S.; von Heijne, G.; Nielsen, H., SignalP 5.0 improves signal peptide predictions using deep neural networks. *Nature Biotechnology* **2019,** *37* (4), 420-423.
17. Hoff, J.; Daniel, B.; Stukenberg, D.; Thuronyi, B. W.; Waldminghaus, T.; Fritz, G., *Vibrio natriegens*: an ultrafast-growing marine bacterium as emerging synthetic biology chassis. *Environmental Microbiology* **2020,** *22* (10), 4394-4408.
18. Altschul, S. F.; Madden, T. L.; Schäffer, A. A.; Zhang, J.; Zhang, Z.; Miller, W.; Lipman, D. J., Gapped BLAST and PSI-BLAST: a new generation of protein database search programs. *Nucleic Acids Research* **1997,** *25* (17), 3389-3402.
19. Morar, M.; Pengelly, K.; Koteva, K.; Wright, G. D., Mechanism and Diversity of the Erythromycin Esterase Family of Enzymes. *Biochemistry* **2012,** *51* (8), 1740-1751.
20. Ounissi, H.; Courvalin, P., Nucleotide sequence of the gene ereA encoding the erythromycin esterase in Escherichia coli. *Gene* **1985,** *35* (3), 271-278.
21. Arthur, M.; Autissier, D.; Courvalin, P., Analysis of the nucleotide sequence of the ereB gene encoding the erythromydn esterase type II. *Nucleic Acids Research* **1986,** *14* (12), 4987-4999.
22. Teufel, F.; Almagro Armenteros, J. J.; Johansen, A. R.; Gíslason, M. H.; Pihl, S. I.; Tsirigos, K. D.; Winther, O.; Brunak, S.; von Heijne, G.; Nielsen, H., SignalP 6.0 predicts all five types of signal peptides using protein language models. *Nature Biotechnology* **2022**.
23. Thode, S. K.; Rojek, E.; Kozlowski, M.; Ahmad, R.; Haugen, P., Distribution of siderophore gene systems on a *Vibrionaceae* phylogeny: Database searches, phylogenetic analyses and evolutionary perspectives. *PLoS One* **2018,** *13* (2), e0191860.
24. Owji, H.; Nezafat, N.; Negahdaripour, M.; Hajiebrahimi, A.; Ghasemi, Y., A comprehensive review of signal peptides: Structure, roles, and applications. *European Journal of Cell Biology* **2018,** *97* (6), 422-441.
25. von Heijne, G., The signal peptide. *The Journal of Membrane Biology* **1990,** *115* (3), 195-201.
26. Juncker, A. S.; Willenbrock, H.; von Heijne, G.; Brunak, S.; Nielsen, H.; Krogh, A., Prediction of lipoprotein signal peptides in Gram-negative bacteria. *Protein Science* **2003,** *12* (8), 1652-1662.
27. Karpishin, T. B.; Gebhard, M. S.; Solomon, E. I.; Raymond, K. N., Spectroscopic studies of the electronic structure of iron(III) tris(catecholates). *Journal of the American Chemical Society* **1991,** *113* (8), 2977-2984.
28. Karpishin, T. B.; Dewey, T. M.; Raymond, K. N., Coordination chemistry of microbial iron transport. 49. The vanadium(IV) enterobactin complex: structural, spectroscopic, and electrochemical characterization. *Journal of the American Chemical Society* **1993,** *115* (5), 1842-1851.
29. Abergel, R. J.; Zawadzka, A. M.; Hoette, T. M.; Raymond, K. N., Enzymatic Hydrolysis of Trilactone Siderophores: Where Chiral Recognition Occurs in Enterobactin and

Bacillibactin Iron Transport. *Journal of the American Chemical Society* **2009,** *131* (35), 12682-12692.
30. Gehring, A. M.; Mori, I.; Walsh, C. T., Reconstitution and Characterization of the *Escherichia coli* Enterobactin Synthetase from EntB, EntE, and EntF. *Biochemistry* **1998,** *37* (8), 2648-2659.
31. Naikare, H.; Butcher, J.; Flint, A.; Xu, J.; Raymond, K. N.; Stintzi, A., *Campylobacter jejuni* ferric–enterobactin receptor CfrA is TonB3 dependent and mediates iron acquisition from structurally different catechol siderophores†. *Metallomics* **2013,** *5* (8), 988-996.
32. Raines, D. J.; Moroz, O. V.; Blagova, E. V.; Turkenburg, J. P.; Wilson, K. S.; Duhme-Klair, A.-K., Bacteria in an intense competition for iron: Key component of the *Campylobacter jejun*i iron uptake system scavenges enterobactin hydrolysis product. *Proceedings of the National Academy of Sciences* **2016,** *113* (21), 5850-5855.
33. Zeng, X.; Mo, Y.; Xu, F.; Lin, J., Identification and characterization of a periplasmic trilactone esterase, Cee, revealed unique features of ferric enterobactin acquisition in *Campylobacter*. *Molecular Microbiology* **2013,** *87* (3), 594-608.
34. Tseng, C. C.; Bruner, S. D.; Kohli, R. M.; Marahiel, M. A.; Walsh, C. T.; Sieber, S. A., Characterization of the Surfactin Synthetase C-Terminal Thioesterase Domain as a Cyclic Depsipeptide Synthase. *Biochemistry* **2002,** *41* (45), 13350-13359.

4. Investigations of the Putative Esterases that Produce Hydrolyzed Amphi-Enterobactin in *Vibrio* Species

Sections of this chapter were published in: Naka, H., Reitz, Z.L., Jelowicki, A.M. Butler, A., Haygood, M.G. Amphi-enterobactin commonly produced among *Vibrio campbellii* and *Vibrio harveyi* strains can be taken up by a novel outer membrane protein FapA that also can transport canonical Fe(III)-enterobactin. *J Biol Inorg Chem* 23, 1009–1022 (2018). https://doi.org/10.1007/s00775-018-1601-5

4.1. Introduction

The marine bacteria *Vibrio harveyi* and *Vibrio campbellii* are phenotypically closely related and share similar gene sequences.[1] It has been previously shown that *V. campbellii* BAA-1116 and HY01 (formerly *V. harveyi* [1, 2]) produce two siderophores, anguibactin and amphi-enterobactin.[3] [4] Thode et al. compiled and visualized gene clusters for the biosynthesis of siderophores in *Vibrionaceae* [5] It was reported that homologs of the amphi-enterobactin biosynthetic gene cluster can be found in the genome sequences of *V. campbellii* and *V. harveyi*.[5] However, their analysis does not provide information on whether these amphi-enterobactin biosynthetic genes are found in only certain strains or widespread among *V. campbellii* and *V. harveyi* strains.

The suite of amphi-enterobactins was initially isolated from *Vibrio campbellii* ATCC BAA-1116 (formerly *V. harveyi* BAA-1116).[3] As previously mentioned, amphi-enterobactin is a triscatecholate siderophore resembling enterobactin, although distinguished by an expanded tetralactone core, and decorated by a fatty acid appended at the amine of the additional L-Ser.[3] Along with amphi-enterobactin, its hydrolysis products composed of two L-Ser residues, on 2,3-dihydroxybenzoate (2,3-DHB) group, and a fatty acid, have been reported

previously (Figure 4.1).[3, 6] These hydrolysis products have been analyzed by ESI-MS/MS, establishing these amphi-enterobactin hydrolysis fragments arise from the full siderophore. The amphi-enterobactin macrolactone siderophore is in fact produced as supported by the tandem MS analysis of the hydrolysis product.[7]

For enterobactin, salmochelin, and bacillibactin, esterases have been identified that are responsible for cytoplasmic iron release.[8 9 10 11] Fes is the esterase that catalyzes the hydrolysis of apo- and Fe(III)-enterobactin ester linkages, in turn producing dihydroxybenzoyl-L-serine.[9] The tris-(hydroxybenzoyl)-L-serine-Fe(III) complex now has a substantially reduced stability constant for Fe(III) and in turn releasing the iron from the Fe(III)-siderophore complex. The mechanism of iron release from Fe(III)-siderophores still has many questions.

An esterase for the hydrolysis of amphi-enterobactin has not yet been identified. The genomes of amphi-enterobactin producing strains, in this case *V. campbellii* and *V. harveyi,* were analyzed to discover an esterase that could selectively hydrolyze amphi-enterobactin. Even though amphi-enterobactin and enterobactin are similar in structure, a homolog of Fes was not identified in the *V. campbellii* and *V. harveyi* species.

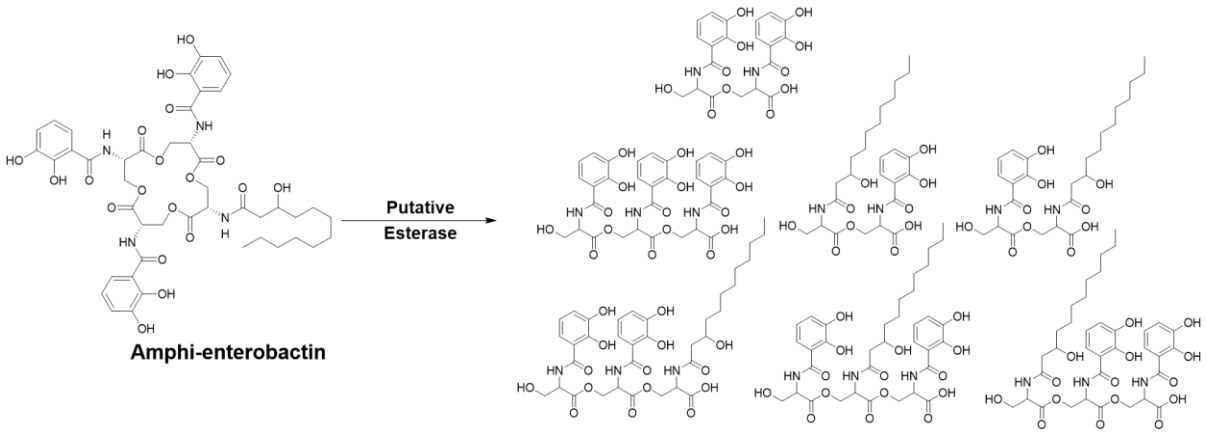

Figure 4.1. The amphi-enterobactins produced by *V. campbellii* and *V. harveyi*, along with the amphi-enterobactin hydrolysis product hypothesized to be a product of an esterase.

Siderophore-mediated iron acquisition needs to be understood to provide information on the mechanism of iron release. Iron acquisition begins with Fe(III) chelation, forming the Fe(III)-siderophore complex. Once the Fe(III)-siderophore complex forms, it is recognized by a specific outer membrane receptor (OMR), and transported across the cellular membrane by the TonB-ExbB-ExbD system and energy is imparted by the proton motive force.[12] [13] [14] Dependent on the Gram stain result of the bacterium, the complex will then be either in the periplasm or the cytoplasm. In a Gram-negative bacterium, the complex will be recognized by a periplasmic binding protein (PBP) and delivered to a cytoplasmic membrane permease known as an ATP binding cassette (ABC) transporter, and the Fe(III)-siderophore complex is transported into the cytosol.[15]

Recognition of this iron(III)-siderophore complex is specific to the bacterial strain and the siderophore it is taken up, whether it be the native siderophore or a xenosiderophore. This additional Fe(III)-xenosiderophore uptake further diversifies the proteins involved in transporting the complex from the environment into the cytosol. Many bacterial strains produce native siderophores but have the ability to take up xenosiderophores produced by other microorganisms. The challenge of acquiring iron is improved by the use of xenosiderophores as it provides the microorganism with the advantage of taking up a variety of siderophores without the metabolic cost associated with siderophore biosynthesis. Bacterial genomes have also shown to contain more siderophore uptake genes in comparison to siderophore biosynthetic genes.[16] A larger variety of siderophore uptake genes improves the chances of recognizing different Fe(III)-siderophore complexes, which in turn increases the opportunities of acquiring iron.

Much less is known about the mechanism of iron release from the Fe(III)-siderophore complex than the mechanisms of iron-siderophore acquisition.[17] [18] The location the Fe(III)-siderophore complex and how iron is released from the complex varies with each siderophore. Certain siderophores with a macrolactone backbone are chemically modified through an enzyme hydrolysis, producing fragments with reduced ferric stability constants.[19] Other pathways of iron(III) release involve a reductase reducing the Fe(III) within a ferric siderophore complex; and proton-assisted Fe(III)-release in a reduced pH environment.

Overall, transport from the external environment into the cytosol of the bacterial cell requires several key proteins, including the outer membrane receptor, the periplasmic binding protein, and the ABC-transporter (Figure 1.19). Iron(III) release on the other hand is dependent on the structure and whether an esterase is needed to chemically modify the structure or just the reductase to promote iron release. We will be covering the key proteins involved in recognizing and transporting enterobactin as a xenosiderophore in a few key bacterial species.

4.2. Statement of Chapter Objectives

Several strains of two closely related bacteria, *V. campbellii* and *V. harveyi*, were studied to identify how widespread the amphi-enterobactin biosynthetic genes are among these strains and understand siderophore-mediated iron(III) transport mechanisms.

Electrospray ionization mass spectrometry revealed that various *V. campbellii* and *V. harveyi* strains produce a suite of amphi-enterobactins with various fatty acid appendages, including several novel amphi-enterobactins. These results establish that amphi-enterobactin production is a common phenotype among *V. campbellii* and *V. harveyi* strains. Along with amphi-enterobactin, its hydrolysis products have been reported and analyzed. As previously

mentioned, the mass fragmentation analysis established these amphi-enterobactin hydrolysis fragments arise from the full siderophore, suggesting that an enzyme catalyzed hydrolysis is involved in the production of the fragments.

The secondary goal is to identify the function of the hypothetical esterase genes and how they play a role in the formation of amphi-enterobactin hydrolysis products. Gene deletion experiments show that the genes encoding putative esterases, *aebH* and *aebI*, may play a role in the formation of these hydrolyzed amphi-enterobactin products. Identifying an amphi-enterobactin esterase would provide another example of how modifying the structure of a siderophore can change the physical properties.

Lastly, it is important to understand the key proteins involved in recognizing and transporting siderophores. Microorganisms have adapted their receptor and transport proteins to compete with other strains. The goal is through genome mining identify the differences in the uptake pathway of Fe(III), with a particular focus on enterobactin as a xenosiderophore and identify the necessary residues involved in recognition/transport of this and similar Fe(III)-catecholate complexes.

4.3. Materials and Methods

4.3.1. General Experimental Procedures

A Varian Cary-Bio 300 UV-visible spectrophotometer was used for UV measurements to monitor growth. Analytical HPLC was used to analyze both the supernatant and cell pellet extracts from *V. campbeliii* CAIM 519 to identify the production of both the breakdown products and the cyclized amphi-enterobactins. Mass spectrometry analysis was carried out on

a Waters Xevo G2-XS QTof with positive mode electrospray ionization coupled to an ACQUITY UPLC H-Class system with a Waters BEH C18 column.

4.3.2. Bacterial Strains of Amphi-Enterobactin Producers and Culture Conditions

Bacterial strains used in this study are listed in Table 4.1. Strains were grown in a low-iron artificial seawater medium containing casamino acids (10 g/L), NH4Cl (19 mM), disodium hydrogen phosphate (4.6 mM), $MgSO_4 \cdot 7H_2O$ (50 mM), $CaCl_2$(10 mM), trace metal grade NaCl (0.3 M), KCl (10 mM), glycerol (41 mM), HEPES buffer (10 mM; pH 7.4), $NaHCO_3$ (2 mM), biotin (8.2 μM), niacin (1.6 μM), thiamin (0.33 μM), 4-aminobenzoic acid (1.46 μM), pantothenic acid (0.21 μM), pyridoxine hydrochloride (5 μM), cyanocobalamin (0.07 μM), riboflavin (0.5 μM), and folic acid (0.5 μM).[3] Cultures were grown at 100 mL scale in 250-mL acid-washed erlenmeyer flasks on an orbital shaker (180 rpm). After 48 hours, cultures were harvested by centrifugation (5400 RCF, 15 min).

The cell pellet was resuspended in ethanol (30 mL per pellet) and shaken overnight at 4 °C. The ethanol extract was centrifuged briefly (13,000 rpm, 5 min) and filtered through a 0.22-μm membrane. Siderophores were extracted with XAD resin. The cell pellet was diluted 4 times the volume with doubly deionized water (Milli-Q IQ) and incubated with Amberlite XAD-2 resin for one hour at 120 rpm, 25℃. Afterwards, the XAD resin was washed with doubly deionized water and the siderophores were eluted with 90% methanol. The eluent was concentrated under vacuum to dryness and dissolved in 5 mL of 50% methanol.

Table 4.1. Strains containing the amphi-enterobactin biosynthetic gene cluster that were tested for amphi-enterobactin production.

Strains	Characteristics	Reference or source
V. campbellii strains		
HY01	Dead, luminescing shrimp isolate	Ref. 20
HY01ΔaebF		
42A	Healthy coral (*Mussismilia hispida*) isolate	Ref. 21
CAIM 115	Shrimp (*Litopenaeus sp.*) hemolymph isolate	Ref. 21
CAIM 198	Shrimp (*Litopenaeus sp.*) hepatopancreas isolate	Ref. 21
CAIM 519T	Seawater isolate *V. campbellii* type strain ATCC 25920	Ref. 22
DS40M4	Seawater isolate	Ref. 23
V. harveyi strains		
CAIM 148	Diseased shrimp (*Panaeus sp.*) hemolymph isolate	Ref. 21
CAIM 513T	Dead, luminescing amphipod (*Talorchestia sp.*) isolate *V. harveyi* type strain ATCC 14126	Ref. 24
CAIM 1075	Oyster (*Crassostrea gigas*) isolate	Ref. 21
CAIM 1792	Diseased shrimp (*Litopenaeus vannamei*) lesion isolate	Ref. 25

4.3.3. Detection of Amphi-enterobactin by Electrospray Ionization Mass Spectrometry

The eluent was concentrated under vacuum to dryness and dissolved in 5 mL of 50% methanol. Extracts were analyzed through positive ion mode ESI–MS on a Waters Xevo G2-XS QTof coupled to a Waters Acquity H-Class UPLC system. A Waters BEH C18 column was used with a gradient of 50–90 or 100% acetonitrile/water (both with 0.1% w/v formic acid). Using MassLynx 4.1, chromatograms for masses of interest were generated and molecular ion peaks quantified by integration (ApexTrack algorithm).

4.3.4. Knockout Mutant of A1Q_1382 And A1Q_1377

The knockout mutants of A1Q_1382 (Δ*est1*) and A1Q1377 (Δ*est2*), associated with the putative esterases AebH and AebI, respectively, were kindly constructed and sent to us by our collaborators Dr. Hiroaki Naka and Professor Margo Haygood. Double knockout mutants of the *angR* gene (A1Q_2165) responsible for the production of anguibactin, and the putative esterase genes were also constructed (Figure 4.2). Four mutants in total were constructed and tested for amphi-enterobactin production: WTΔ*est1*, Δ*angR*Δ*est1*, WTΔ*est2*, and Δ*angR*Δ*est2*.

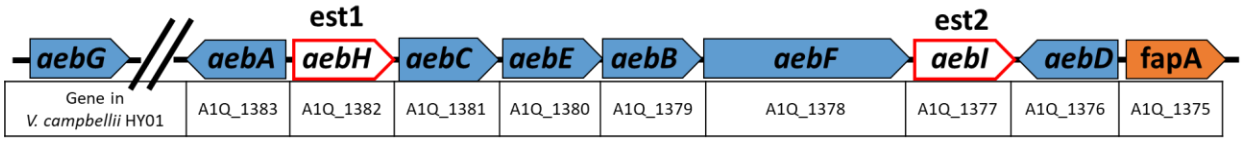

Figure 4.2. Amphi-enterobactin biosynthetic gene cluster and the gene locus tags in *Vibrio campbellii* HY01 associated with each gene. Genes *aebH* and *aebI* were knocked out for this study.

4.3.5. Siderophore Production of Deletion Mutants and Complements in *Vibrio Campbellii* HY01

Our collaborators, Dr. Hiroaki Naka and Dr. Margo Haygood constructed deletion mutants and complement strains in *Vibrio campbellii* HY01 (Table 4.2). The deletion and complement mutant strains, along with wild-type *Vibrio campbellii* HY01 were grown in AB medium. The medium was pre-made and stored at room temperature until use. One liter of AB medium contains 2.0 g/L casamino acids, vitamin free (0.2% w/v final), 12.3 g/L MgSO4·7H2O (50 mM final), 17.5 g/L NaCl (0.3 M), pH adjusted to 7.5 and sterilized by autoclaving. After sterilization, the following sterile ingredients were added to give the following final concentrations: 1 mM L-arginine, 1% (v/v) glycerol, and 10 mM potassium phosphate buffer (pH 7.0). The medium was supplemented with 1 mM IPTG and 10 μg/mL chloramphenicol. The strains were grown in 100 mL of the medium on a rotary shaker at 180 rpm, 30℃, for 24 hours. The cultures were harvested at 6,000 rpm for 30 minutes at 4℃ and the supernatants were incubated with amberlite XAD-2 resin for 2 hours at room temperature with mild agitation. The cell pellet was resuspended in 20 mL of methanol and shaken over night at 180 rpm, 4℃. The cell pellet was filtered and incubated with 100 mL of ddH2O and amberlite XAD-2 resin for 2 hours at room temperature. Siderophores were eluted from the resin with 90% methanol and concentrated by rotary evaporation. The extracts were analyzed by UPLC-MS.

Table 4.2. Strains and plasmids constructed by Dr. Hiroaki Naka (OHSU, Portland Oregon) were used in this study.

Strains and plasmids	Characteristics	Short-Hand Notation	Source
V. campbellii strains			
HY01	Dead, luminescing shrimp isolate		Ref. 20
HNVC-1	HY01 (pMMB208)	WT+emp	This study
HNVC-2	Δest1(pMMB208)	Δest1+emp	This study
HNVC-3	Δest1(pMMB208-est1)	Δest1+est1	This study
HNVC-4	Δest2(pMMB208)	Δest2+emp	This study
HNVC-5	Δest2(pMMB208-est2)	Δest2+est2	This study
HNVC-6	Δest1Δest2(pMMB208)	Δest1Δest2+emp	This study
HNVC-7	Δest1Δest2(pMMB208-est1)	Δest1Δest2+est-1	This study
HNVC-8	Δest1Δest2(pMMB208-est2)	Δest1Δest2+est2	This study
Plasmid			
pMMB208	A broad-host-range expression vector; Cm^r *InQ laclq* Ptac; polylinker from M13mp19		Ref. 26

4.3.6. Genome Mining of Proteins Involved in Xenosiderophore Enterobactin Uptake

The genomes of bacteria identified to use enterobactin as a xenosiderophore were accessed through NCBI. The amino acid sequences of enterobactin outer membrane receptors (FepA), periplasmic binding proteins (FepB), and esterase (Fes) were retrieved from NCBI RefSeq[27] and used in BLAST and the PFAM database to construct a percent identity comparison table.[28] [27] The amino acid sequences of the OMRs, PBPs, and esterases were aligned to FepA, FepB, and Fes, respectively, using MUSCLE (EMBL-EBI webserver). [29] [30]

4.4. Results

4.4.1. *Vibrio* Strains Producing Amphi-enterobactin

Sections 4.4.1 and 4.4.2 contain my results that appear in the collaborative publication "Amphi-enterobactin commonly produced among *Vibrio campbellii* and *Vibrio harveyi* strains can be taken up by a novel outer membrane protein FapA that also can transport canonical Fe(III)-enterobactin, by Naka, H., Reitz, Z.L., Jelowicki, A.M., Butler, A., Haygood, M.G. [31]

Thode *et al.* compiled and visualized gene clusters for the biosynthesis of siderophores in *Vibrionaceae*.[5] The study identified four *Vibrio* species potentially responsible for producing amphi-enterobactin. A couple strains of *Vibrio harveyi* and *V. campbellii* have already been characterized as amphi-enterobactin producers. The analysis from Thode *et al.*, however did not confirm that the amphi-enterobactin biosynthetic genes are found widespread or if the genes are only found in specific strains among *V. campbellii* and *V. harveyi*.

Amphi-enterobactin genes were identified in all eleven of the species below (Table 4.3), however, production of amphi-enterobactin needed to be evaluated. The goal of identifying the production of amphi-enterobactin in these strains is to further understand siderophore-mediated iron transport mechanisms and identify the versatility of amphi-enterobactin among other marine bacteria.

Table 4.3. Distribution of amphi-enterobactin biosynthesis and transport genes in *V. harveyi* and *V. campbellii* strains used in the following experiments.

Strain	Species	Former species	Amphi-enterobactin genes		
			aebF	*aebG*	*fapA*
HY01	*V. campbellii*	*V. harveyi*	+	+	+
BAA-1116	*V. campbellii*	*V. harveyi*	+	+	+
42A	*V. campbellii*		+	+	+
CAIM 115	*V. campbellii*		+	+	+
CAIM 198	*V. campbellii*		+	+	+
CAIM 519	*V. campbellii*		+	+	+
DS40M4	*V. campbellii*	*Vibrio sp.*	+	+	+
CAIM 148	*V. harveyi*		+	+	+
CAIM 513	*V. harveyi*		+	+	+
CAIM 1075	*V. harveyi*		+	+	+
CAIM 1792	*V. harveyi*		+	+	+

+, presence; -, absence. The genes *aebF* and *aebG* are essential for amphi-enterobactin biosynthesis while the *fapA* gene is essential for ferric-amphi-enterobactin uptake

Strains were grown in a low-iron artificial seawater medium for 48 hours. Ethanolic cell pellet extracts were analyzed through positive ion mode ESI – MS to identify production of amphi-enterobactin. Amphi-enterobactins are usually produced as a suite of siderophores comprised of three 2,3-dihydroxybenzoyl-L-serine residues and one acyl-L-serine of varying chain lengths. The attached fatty acid in amphi-enterobactin varies in length (C10-C14), degree of unsaturation, and whether or not the fatty acid is hydroxylated. Zane et. al. previously identified and structurally characterized a total of seven macrolactone amphi-enterobactins (Table 4.4).[3]

Table 4.4. Masses and structure composition of previously identified amphi-enterobactins.[3]

	Mass (*m/z*)	Composition	Fatty Acid Tail
1	927	4-Ser-3-DHB-FA	C10:0 OH
2	953	4-Ser-3-DHB-FA	C12:1 OH
3	955	4-Ser-3-DHB-FA	C12:0 OH
4	981	4-Ser-3-DHB-FA	C14:1 OH
5	937	4-Ser-3-DHB-FA	C12:1
6	939	4-Ser-3-DHB-FA	C12:0
7	965	4-Ser-3-DHB-FA	C14:1

The presence of these amphi-enterobactins were tested after growth of the various *Vibrio campbellii* and *V. harveyi* strains. All of the strains tested showed production of a suite of amphi-enterobactins with varying fatty acid appendages. Not all seven were consistently produced amongst each strain (Table 4.5).

For each strain, the bottom trace in Figure 4.3 is an ESI-MS total ion count (TIC) over time. Using MassLynx 4.1, chromatograms for masses of interest were generated, shown stacked above the TIC and the masses of interest shown to the right of each trace (Figure 4.3 a-k and Figure 4.4). Molecular ion peaks were quantified by integration (ApexTrack algorithm). Integrated masses are labeled on each trace with, elution time, base peak, and integration, from top to bottom respectively. The amount of amphi-enterobactins produced varies among different strains. From Table 4.5, it is observed that *V. campbellii* CAIM 519 has the highest abundance of amphi-enterobactin, among the ten strains tested, producing all eleven amphi-enterobactins identified (C10:0 OH; C12:1 OH; C12:0 OH; C10:0; C14:1 OH; C12:1; C14:0 OH; C12:0; C14:1; C14:0; and C16:1). *V. campbellii* HY01 on the other hand shows lowest abundance of amphi-enterobactins, producing only four out of the eleven possible structures, C12:0; C14:1; C14:0; and C16:1, all of which are the non-hydroxylated. *V. harveyi* CAIM 513 and CAIM 1792 also have low relative abundance of amphi-enterobactins, again producing the same four structures as *V. campbellii* HY01.

Table 4.5. Relative abundance of amphi-enterobactins among *Vibrio campbellii* and *V. harveyi* strains.

Strain	Fatty acid tail: Species	10:0 OH *m/z* 927	12:1 OH *m/z* 953	12:0 OH *m/z* 955	10:0[a] *m/z* 911	14:1 OH *m/z* 981	12:1 *m/z* 937	14:0 OH[a] *m/z* 983	12:0 *m/z* 939	14:1 *m/z* 965	14:0[a] *m/z* 967	16:1[a] *m/z* 993
HY01	*V. campbellii*	–	–	–	–	–	–	–	+	+	+	+
HY01ΔaebF	*V. campbellii*	–	–	–	–	–	–	–	–	–	–	–
42A	*V. campbellii*	–	–	–	–	–	–	–	+++	++	+++	+
CAIM 115	*V. campbellii*	–	–	–	–	–	–	–	++	++	+	+
CAIM 198	*V. campbellii*	++	+	++++	++	++	+++	++	++++	++++	++++	+++
CAIM 519	*V. campbellii*	+++	++	+++++	+++	+++	++++	++	+++++	+++++	++++	++++
DS40M4	*V. campbellii*	–	+	++	+	+	++	+	++++	+++	+++	++
CAIM 148	*V. harveyi*	–	–	–	–	–	+	–	+++	++	++	++
CAIM 513	*V. harveyi*	–	–	–	–	–	–	–	+	+	+	*
CAIM 1075	*V. harveyi*	–	–	++	+	–	+	+	+++	++	++	++
CAIM 1792	*V. harveyi*	–	–	–	–	–	–	–	++	++	+	+

UPLC/ESI-MS molecular ion counts were integrated and normalized to an OD of 1.0. +++++, $>10^6$ normalized counts; ++++, $>10^5$ normalized counts; +++, $>10^4$ normalized counts; ++, $>10^3$ normalized counts; +, $>10^2$ normalized counts; *,$<10^2$ normalized counts; –, not detected above background

Integrations are shown in Figs. 4.3a-k and 4.4

[a]Fatty acid tails newly reported in Ref. 31 and in section 4.4.2.

a. *V. campbellii* HY01

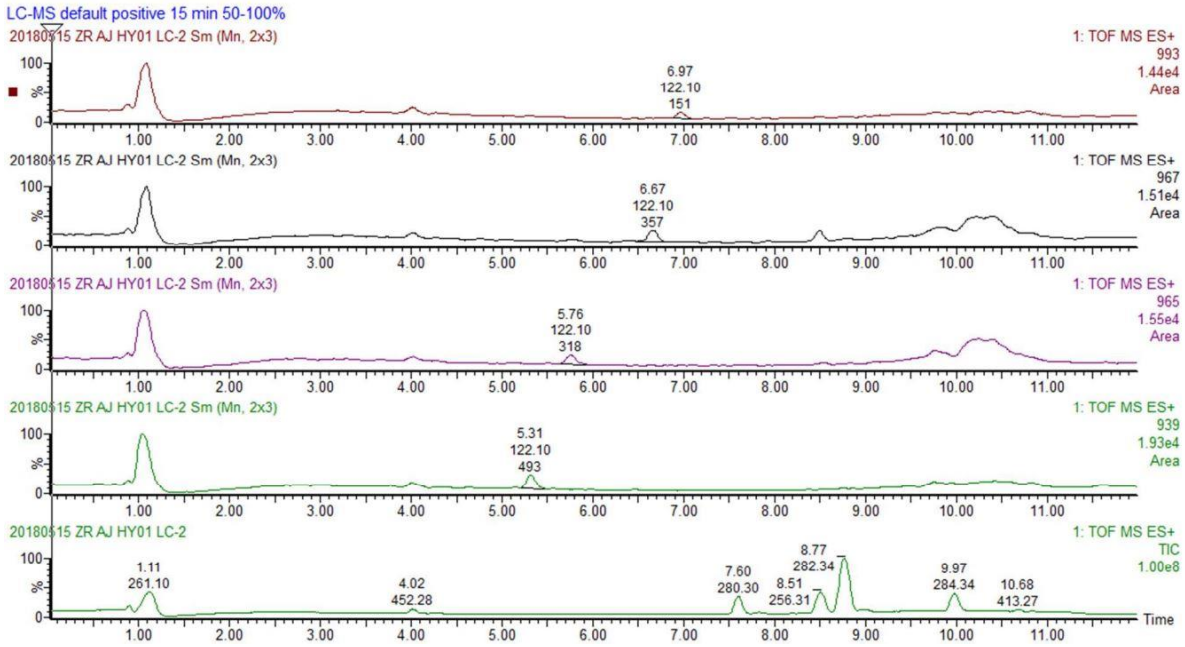

Figure 4.3. a-k: UPLC/ESI-MS analysis of *Vibrio* species. Ethanolic cell pellet extracts were analyzed through positive ion mode ESI-MS on a Waters Xevo G2-XS QTof coupled to a Waters Acquity H-Class UPLC system. A Waters BEH C18 column was used with an acetonitrile/water (both with 0.1% w/v formic acid) gradient shown at the top of each stacked trace. For each strain, the bottom trace is an ESI-MS total ion count (TIC) over time. TIC peaks are labeled with the elution time (top) and base peak (bottom). Chromatograms for masses of interest were generated with MassLynx 4.1, shown stacked above the TIC. The mass of interest is shown to the right of each trace. Molecular ion peaks were quantified by integration (ApexTrack algorithm). Integrated masses are labeled with, from top to bottom, elution time, base peak, and integration. Species not detected are not shown, with the exception of the negative control HY01 ΔaebF (stacked trace **b**).

b. *V. campbellii* HY01Δ*aebF*

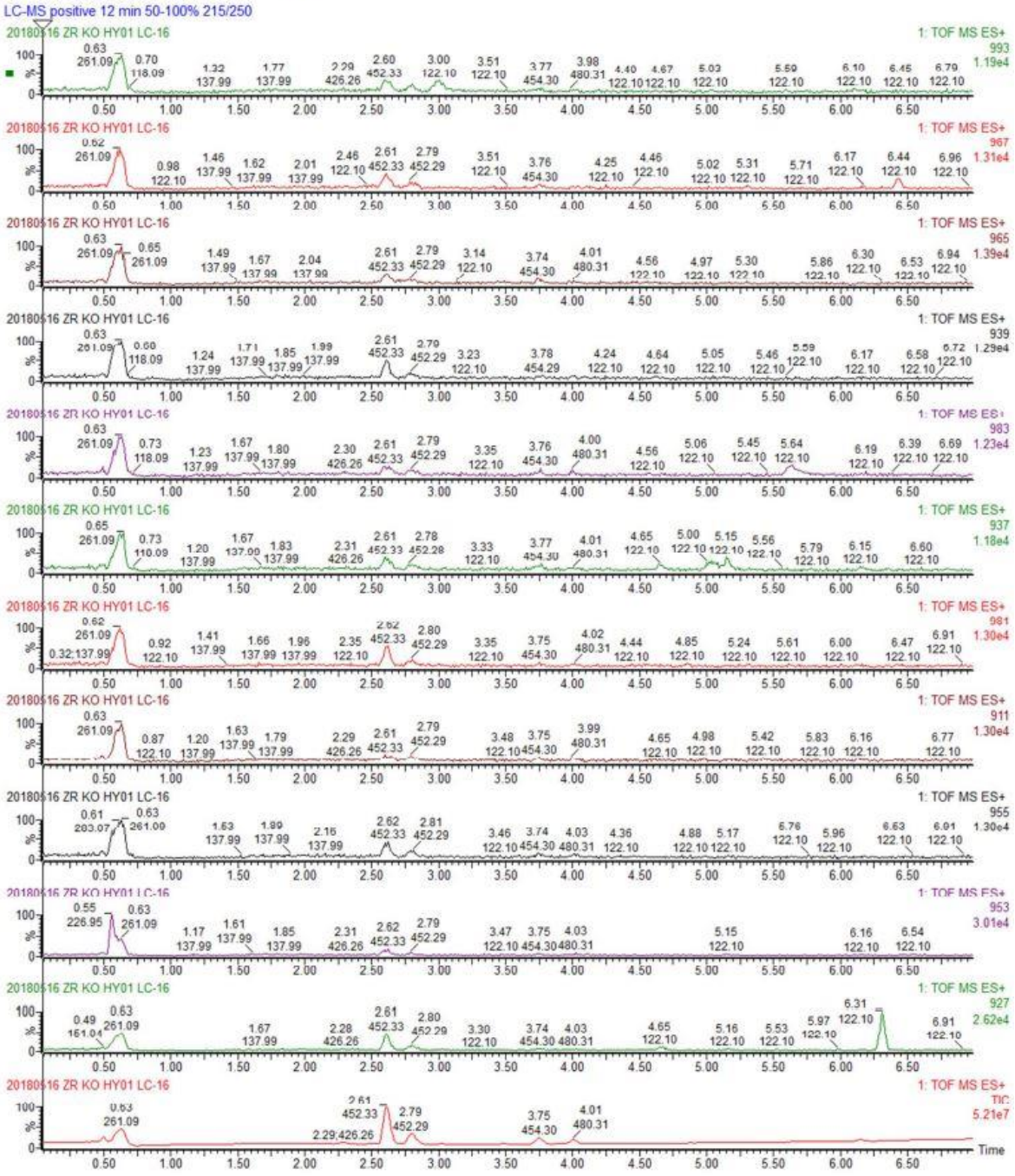

Figure 4.3. continued.

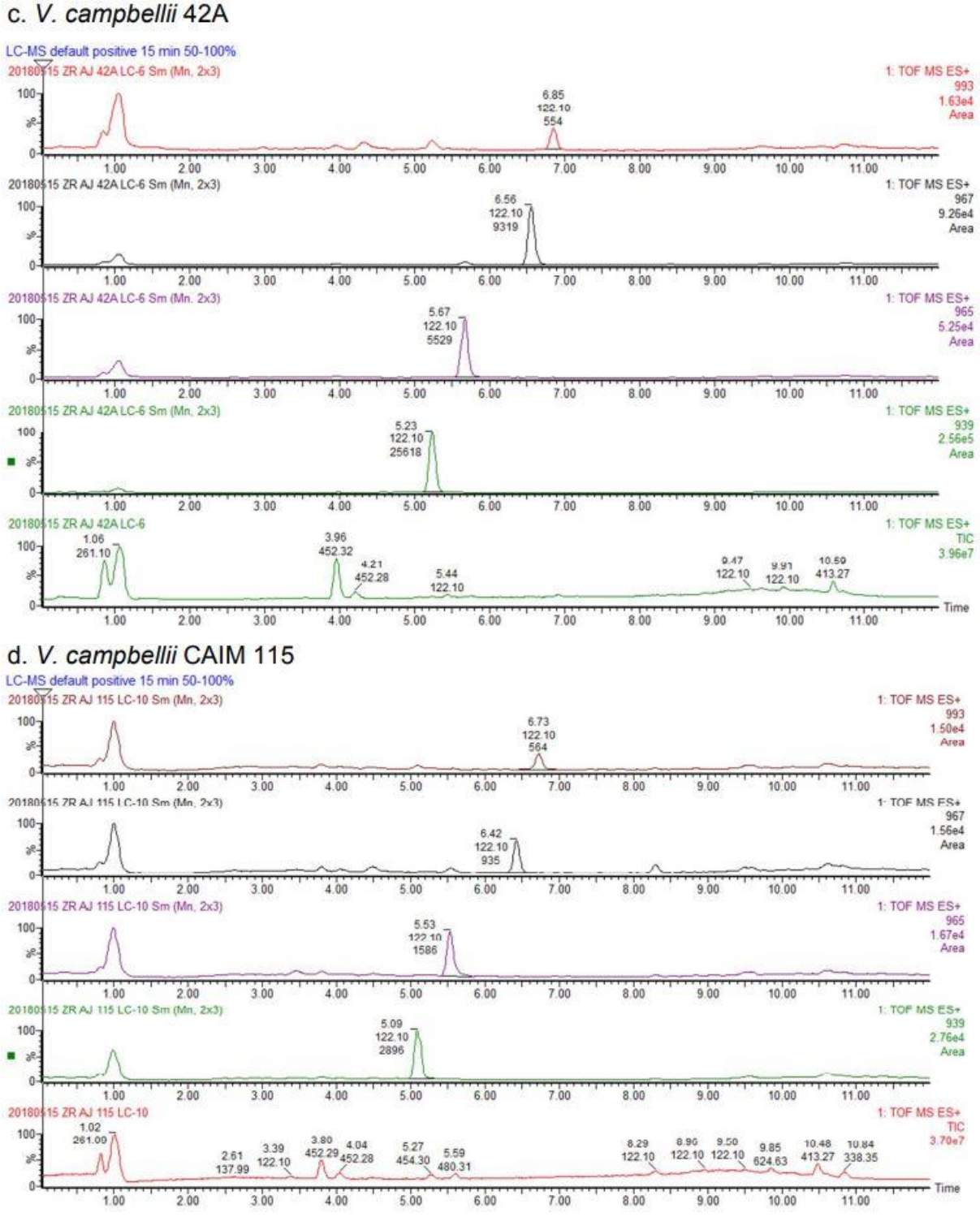

Figure 4.3. continued.

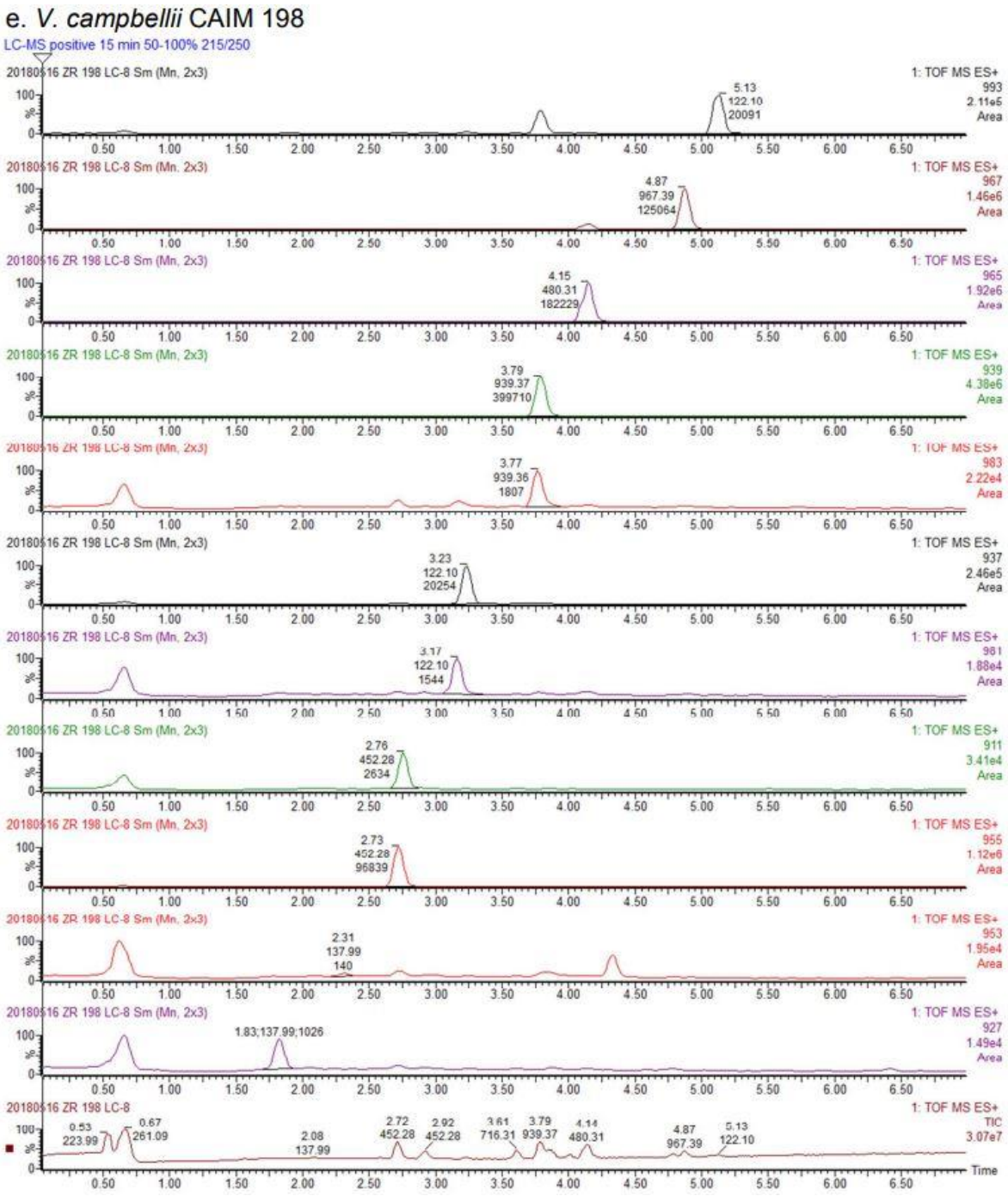

Figure 4.3. continued.

f. *V. campbellii* CAIM 519

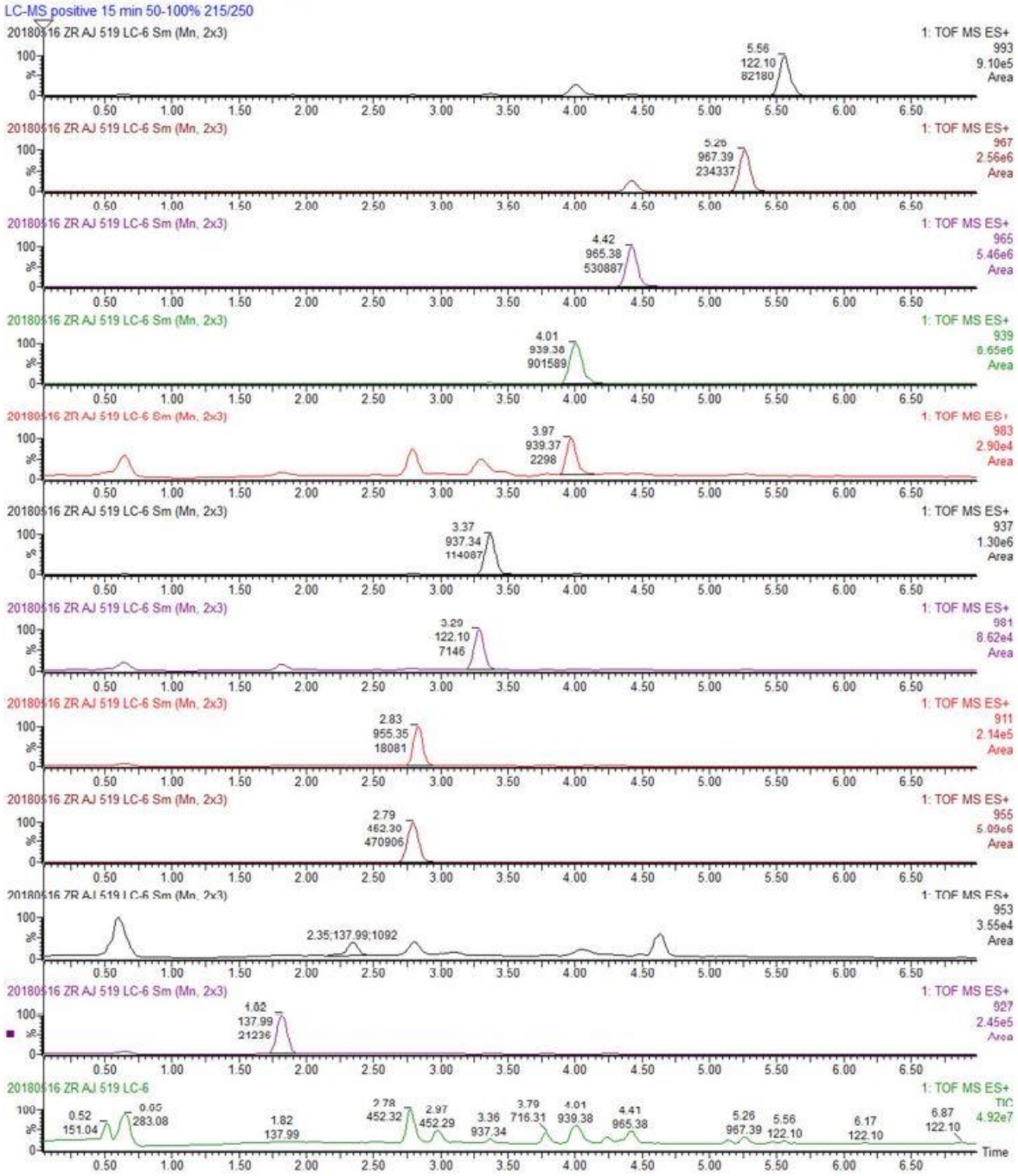

Figure 4.3. continued.

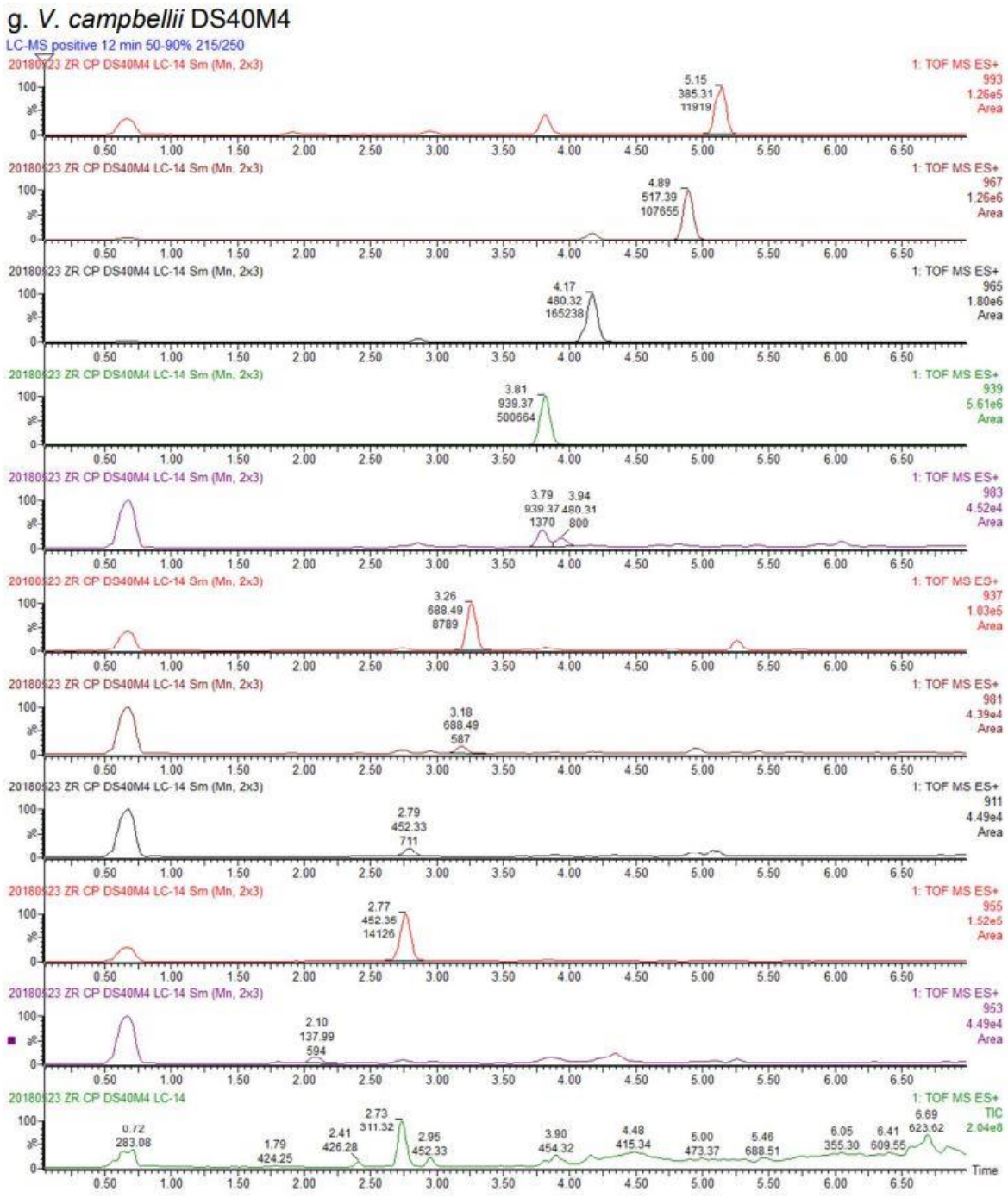

Figure 4.3. continued.

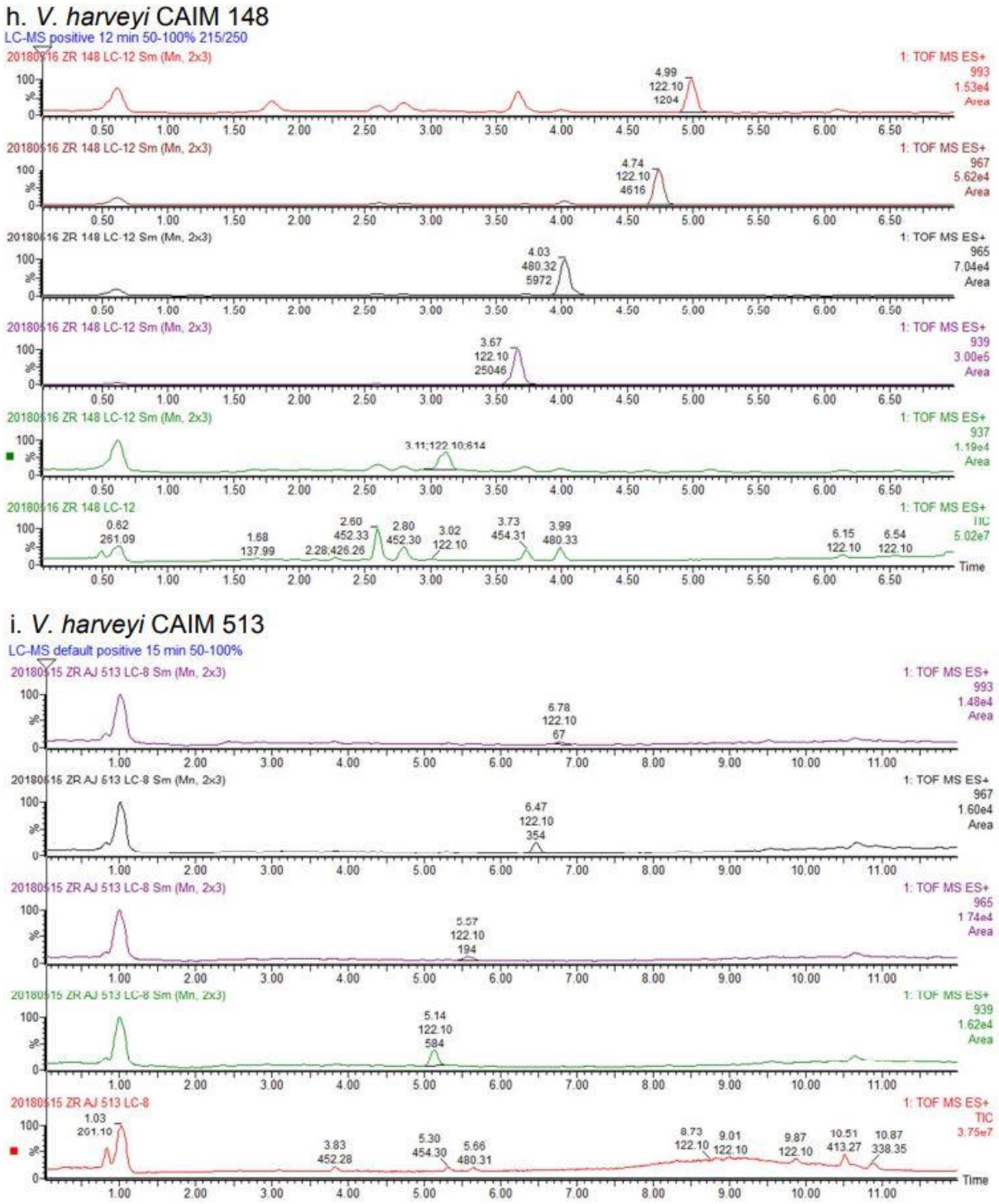

Figure 4.3. continued.

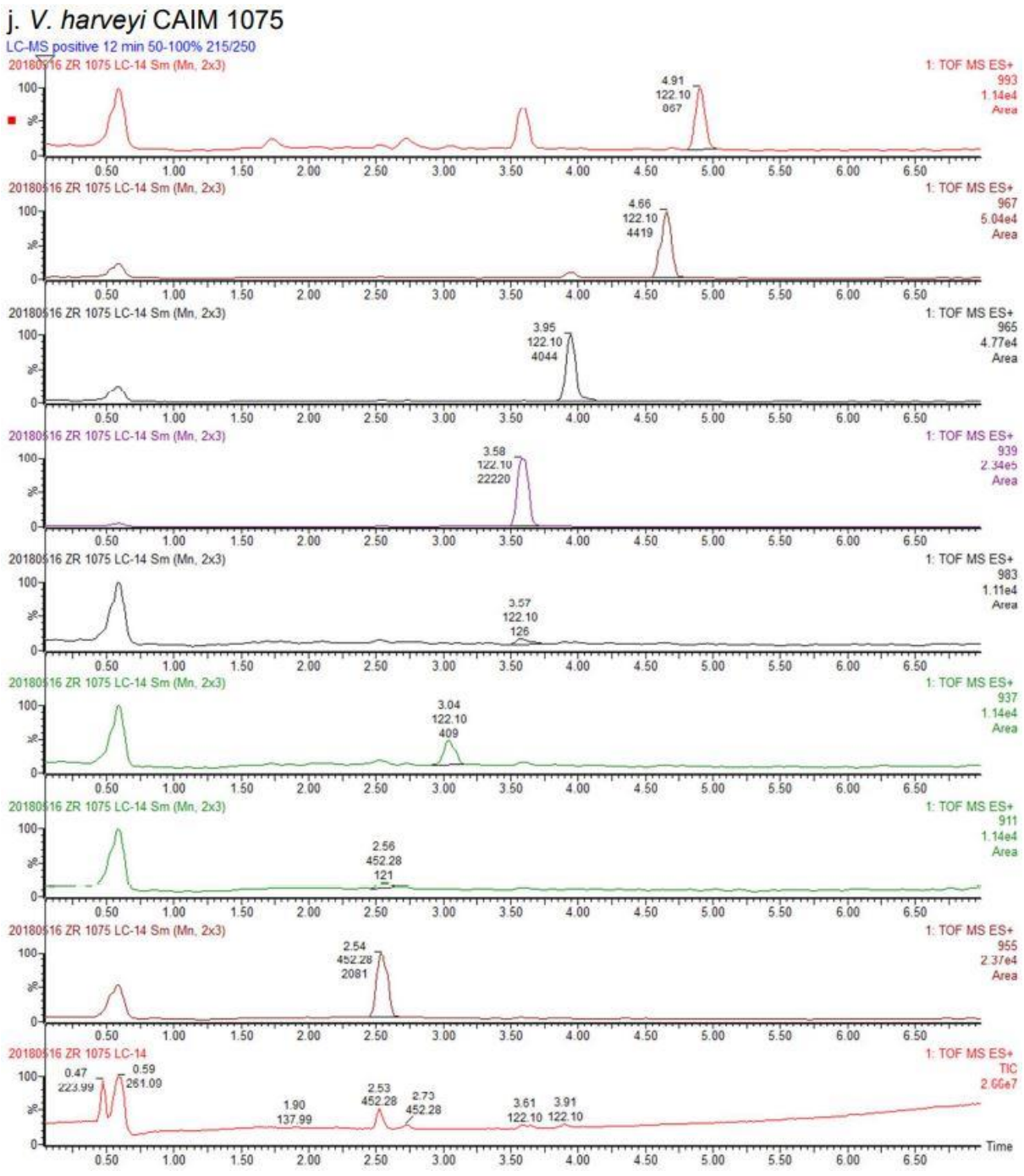

Figure 4.3. continued.

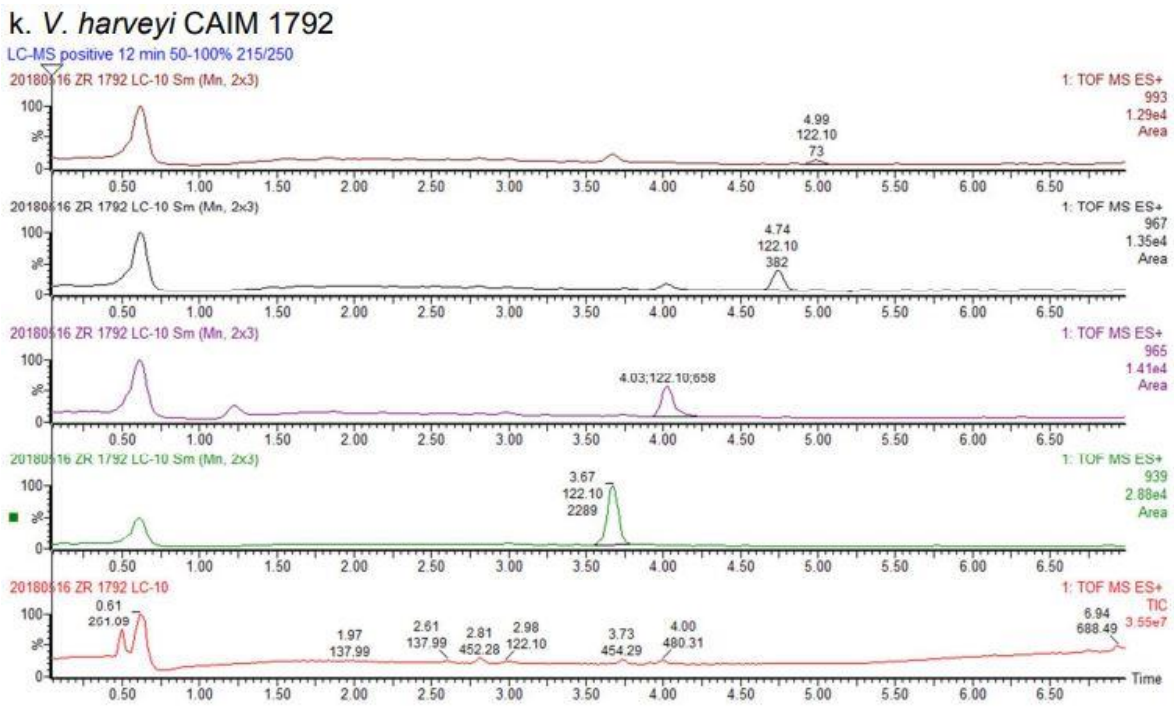

Figure 4.3. continued.

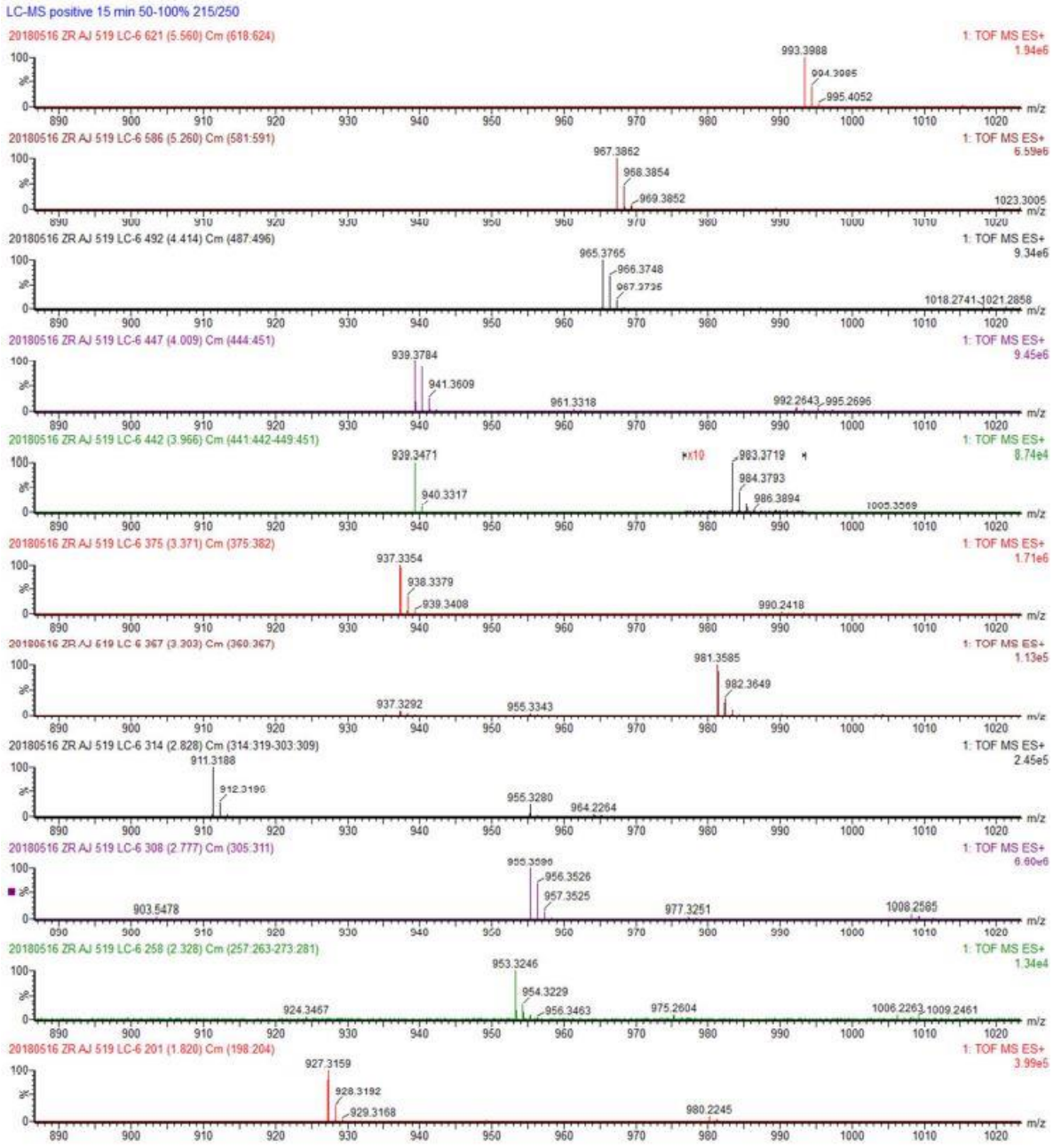

Figure 4.4. Molecular ions for each of the amphi-enterobactins found in *Vibrio* species. Masses were collected in positive ion mode ESI-MS on a waters Xevo G2-XS QTof coupled to a Waters Acquity H-Class UPLC system. Traces are shown in order of elution time (bottom to top).

4.4.2. Newly Identified Amphi-Enterobactins - C10:0, C14:0 OH, C14:0 and C16:0 FA

Four amphi-enterobactin species (with fatty acid tails, C10:0, C14:0 OH, C14:0 and C16:1) were newly identified, in addition to the other seven amphi-enterobactin siderophores that were previously found in *V. campbellii* BAA-1116.[3] The following strains produced all four of the new amphi-enterobactin species: *V. campbellii* CAIM 198, CAIM 519, DS40M4, and *V. harveyi* CAIM 1075 (Table 4.6 and Figure 4.5). The remaining strains only produced two of the new species: C14:0 and C16:1. A suite of ten amphi-enterobactin siderophores were also detected from *V. campbellii* DS40M4 which has been previously reported to produce anguibactin, as well as mono, di- and trivanchrobactin.[32]

Table 4.6. Distribution of new amphi-enterobactin species produced by the following *V. harveyi* and *V. campbellii* strains used in this study.

Strain	Fatty acid tail: Species	10:0 *m/z* 911	14:0 OH *m/z* 983	14:0 *m/z* 967	16:1 *m/z* 993
HY01	*V. campbellii*	–	–	+	+
42A	*V. campbellii*	–	–	+	+
CAIM 115	*V. campbellii*	–	–	+	+
CAIM 198	*V. campbellii*	+	+	+	+
CAIM 519	*V. campbellii*	+	+	+	+
DS40M4	*V. campbellii*	+	+	+	+
CAIM 148	*V. harveyi*	–	–	+	+
CAIM 513	*V. harveyi*	–	–	+	*
CAIM 1075	*V. harveyi*	+	+	+	+
CAIM 1792	*V. harveyi*	–	–	+	+

+, production of new amphi-enterobactin; -, absence

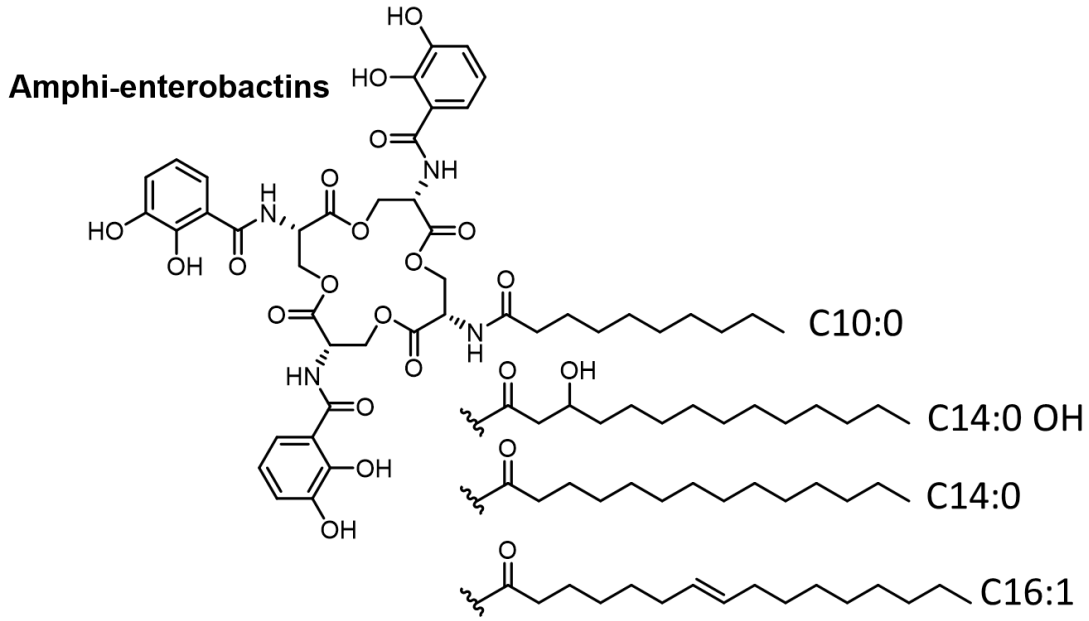

Figure 4.5. Structure of amphi-enterobactin with the newly reported fatty acid tails. At this time, the identity of the specific fatty acids (i.e., the sites of hydroxylation or site of desaturation) were not determined.

4.4.3. Qualitative Analysis of Siderophore Production in Knockout Strains

Newly discovered putative enzyme families are further studied *in vivo*, in *V. campbellii* HY01 knockout mutants. Our collaborators, Dr. Hiroaki Naka and Dr. Margo Haygood constructed the deletion mutant strains in *Vibrio campbellii* HY01 (Figure 4.2 and Table 4.2). Wild-type *Vibrio campbellii* HY01 and the seven deletion mutant strains were grown in AB medium.

4.4.3.1. Effect of Mutation on Siderophore Production Observed Phenotypically

The chrome azurol sulphonate (CAS) agar plate assay was used to screen for siderophore production. Colonies of the wild-type (WT) strain and the mutant strains

(WTΔ*est1*, Δ*angRΔest1*, WT*Δest2*, and Δ*angRΔest2*) were grown overnight on the CAS agar plate formed yellow halos (Figure 4.6). Genes encoding Esterase 1 (*aebH*) and Esterase 2 (*aebI*) are embedded in the amphi-enterobactin biosynthesis cluster (Figure 4.2). Due to the homology of the unknown proteins to an erythromycin esterase, these two are hypothesized to function as esterases, cleaving the macrolactone and in turn releasing the ferric iron.

Single and double mutants of the esterase genes, *aebH* and *aebI* were constructed using a suicide plasmid with deletion fragments. *Vibrio campbellii* HY01 produces both anguibactin and amphi-enterobactin.[33] [31] There have been cases where one siderophore frequently affects the other one due to competition between two siderophores. Therefore, a double mutant was constructed from an anguibactin production minus strain, *V. campbellii* HY01ΔangR that added the deletion of the esterase genes (Δ*angRΔest1*, and Δ*angRΔest2*). The phenotype of the mutant strains along with the wildtype were analyzed on CAS agar plates. The WT, WTΔ*est1*, and WT*Δest2* showed very little halo formation, with the halo appearing to be approximately the same size. The halo around Δ*angRΔest1* appears to be the smallest, while the halo around the Δ*angRΔest2* colony is larger than the WT and the other mutant strains. Larger halo formation suggests siderophore uptake is not occurring as efficiently, which can have an effect on growth rate.

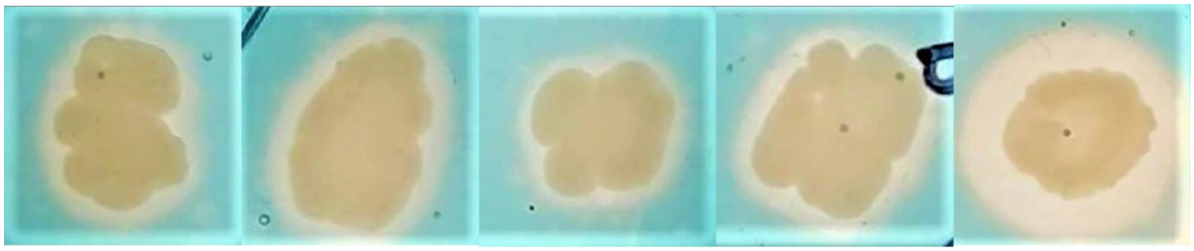

Figure 4.6. Phenotypes of anguibactin and esterase mutants. Colonies left to right of wild type (WT), WTΔest1, ΔangRΔest1, WTΔest2, and ΔangRΔest2 on CAS agar after one day of inoculation on plate.

4.4.3.2. Effect of Mutation on Growth Rate

To investigate the effect of the mutations on growth rate of *V. campbellii* HY01, the growth of each knockout mutant strain along with the wildtype was monitored under low-iron conditions. It is hypothesized that removing the esterase responsible for hydrolyzing amphi-enterobactin and releasing ferric iron would decrease the growth rate of the strain in comparison to the wildtype *V. campbellii* HY01. The WTΔ*est1* and WTΔ*est2* did not show a diminished growth rate, while Δ*angR*Δ*est1* and Δ*angR*Δ*est2* showed a slight decrease in comparison to the wildtype (Figure 3.7). The diminished growth rate in Δ*angR*Δ*est1* and Δ*angR*Δ*est2* is expected since the biosynthesis of anguibactin, the other siderophore produced by *V. campbellii* HY01, has been mutated. Due to the sequence homology of AebH and AebI, these two proteins may be redundant, which may explain why the growth rate remains the same for the WTΔ*est1* and WTΔ*est2*. Overall, the growth curves of *V. campbellii* HY01 and the mutant strains grew to similar optical density over the same amount of time, suggesting that the knockout of the putative esterase genes do not have a direct effect on the growth of the bacterial strain.

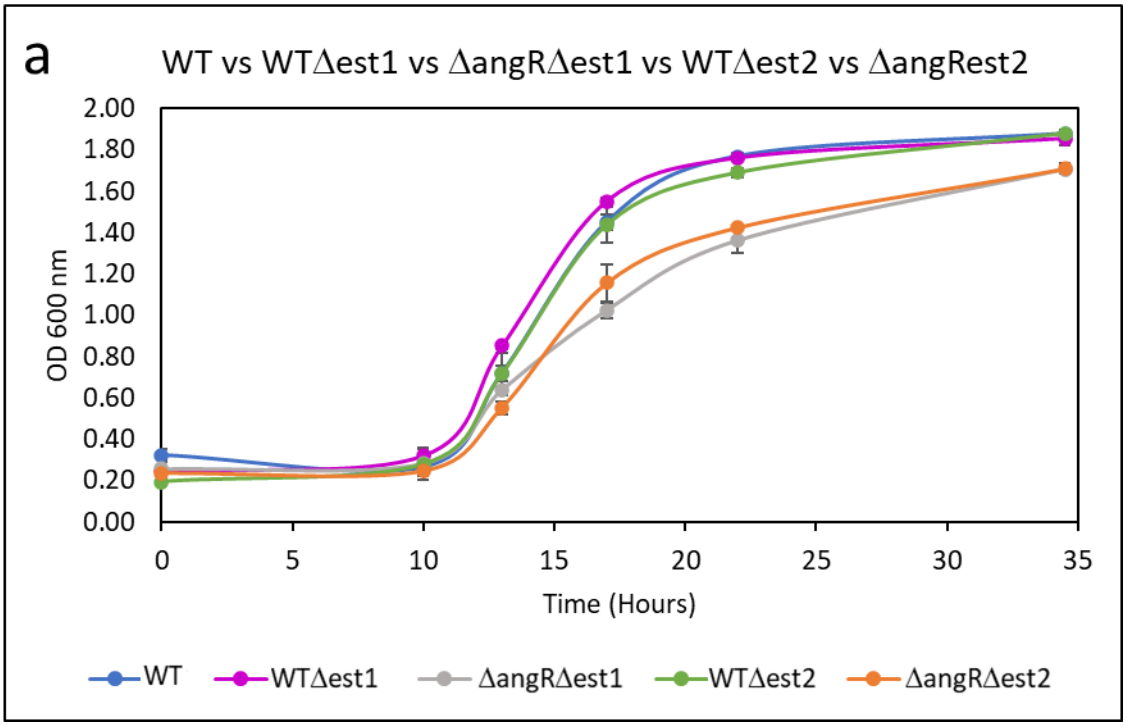

Figure 4.7. a-c: Growth curve analysis of putative esterase mutants. **a.** Growth of WT (blue), WTΔest1 (purple), ΔangRΔest1 (gray), WTΔest2 (green), and ΔangRΔest2 (orange) knockout mutants in iron-depleted medium. **b.** Growth comparison of WT (blue), WTΔest1 (purple), and WTΔest2 (gray). **c.** Growth comparison of WT (blue), ΔangRΔest1 (green), and ΔangRΔest2 (orange).

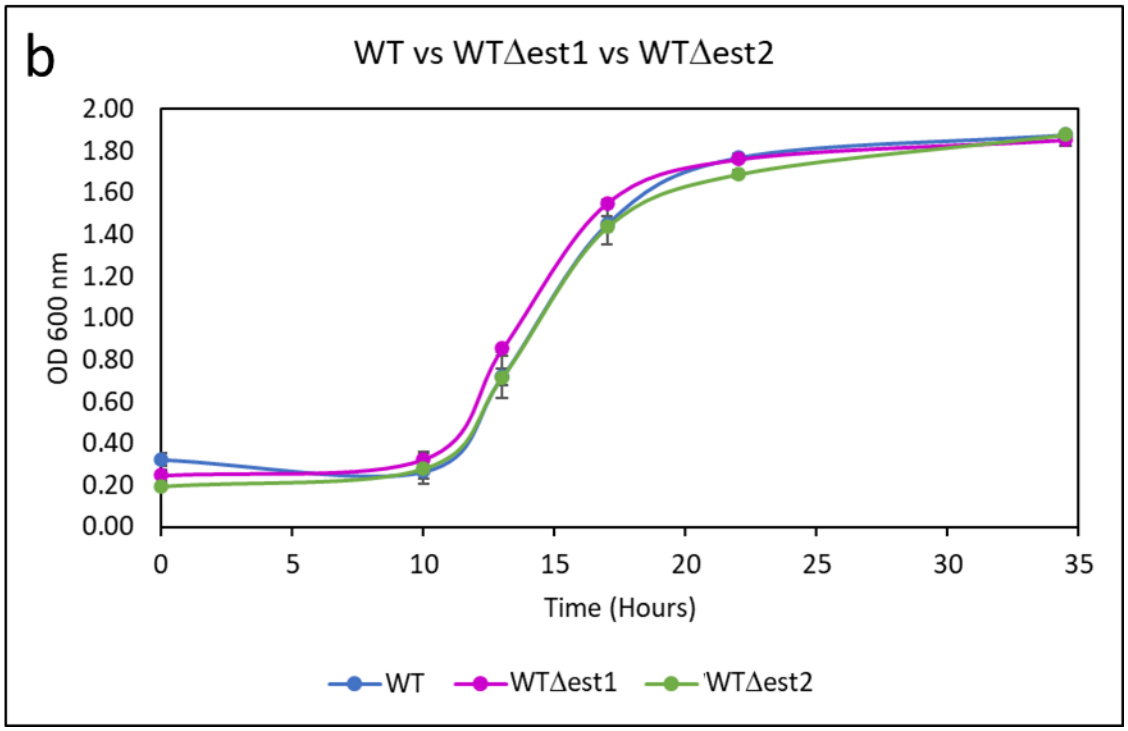

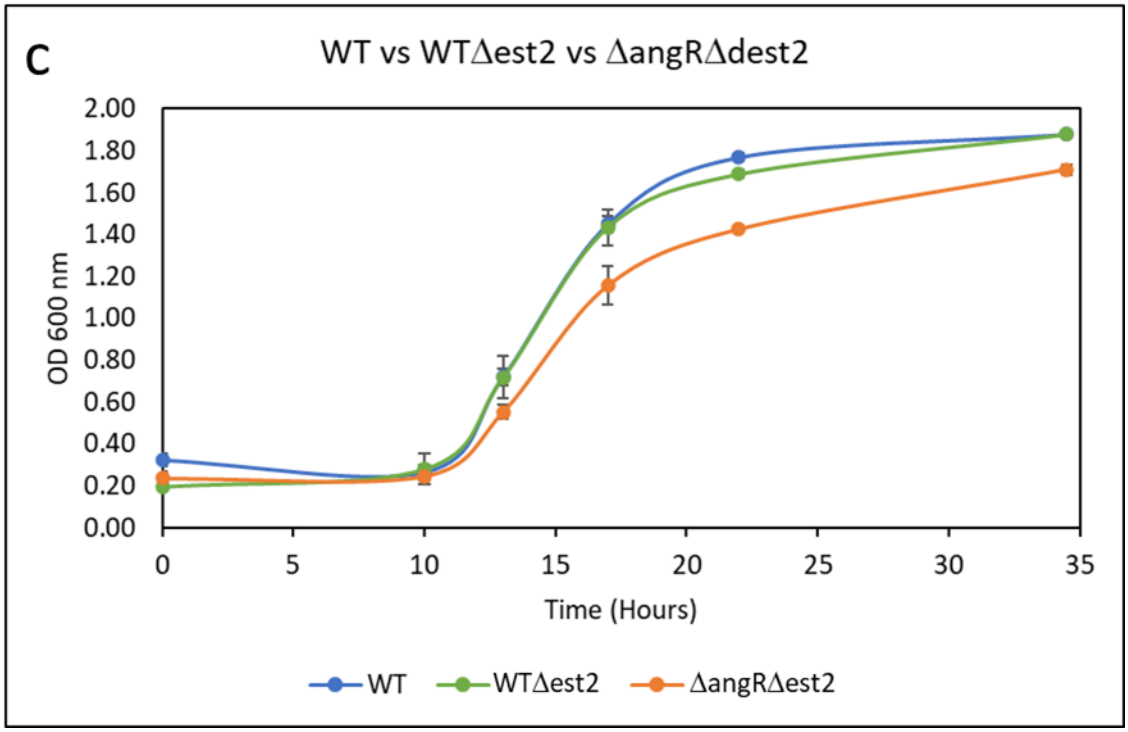

Figure 4.7. continued.

4.4.3.3. Detection of Siderophores in Mutant Strains

We next examined the production of amphi-enterobactin breakdown products in *V. campbellii* HY01 WT and mutant strains by UPLC-MS. Ultimately, we want to identify the function of the unknown genes embedded in the amphi-enterobactin biosynthesis gene cluster. If these genes encode esterases, then knocking out these genes would eliminate the presence of the amphi-enterobactin breakdown products.

While it has been established that *Vibrio campbellii* HY01 WT produces a suite of amphi-enterobactins, with fatty acids ranging from C_{12} to C_{16}, and either saturated or monohydroxylated[31], fragments of these amphi-enterobactins are also present in the culture supernatant (Figure 4.8). Supernatant extracts of *V. campbellii* HY01 WT and mutant strains were analyzed through positive ion mode ESI-MS on a Waters Xebo G2-XS QTof coupled to a Waters Acquity H-Class UPLC system.

The 2-Ser-1-DHB-FA$^{C10:0-OH}$ (*m/z* 499.2 $[M+H]^+$) elutes at 4.42 minutes while the 2-Ser-1-DHB-FA$^{C12:0-OH}$ (*m/z* 527.2 $[M+H]^+$) elutes around 5.24 minutes. Three of the four mutant strains, WTΔ*est1*, WTΔ*est2*, Δ*angR*Δ*est2*, and the wildtype show the presence of the 2-Ser-1-DHB-FA$^{C10:0-OH}$, protonated mass of *m/z* 499 $[M+H]^+$, and 2-Ser-1-DHB-FA$^{C12:0-OH}$, protonated mass of *m/z* 527 $[M+H]^+$ (Figure 4.8, Table 4.7). The mutant strain Δ*angR*Δ*est1* did not show the presence of the amphi-enterobactin hydrolysis products.

Table 4.7. Distribution of amphi-enterobactin hydrolysis products observed in the *V. campbellii* HY01 mutant strains.

Fatty acid tail: Mutant Strain	10:0 OH *m/z* 499	12:0 OH *m/z* 527
WT HY01	+	+
WTΔ*est1*	+	+
WTΔ*est2*	+	+
Δ*angR*Δ*est1*	–	–
Δ*angR*Δ*est2*	+	+

+, presence of amphi-enterobactin hydrolysis products;
-, absence

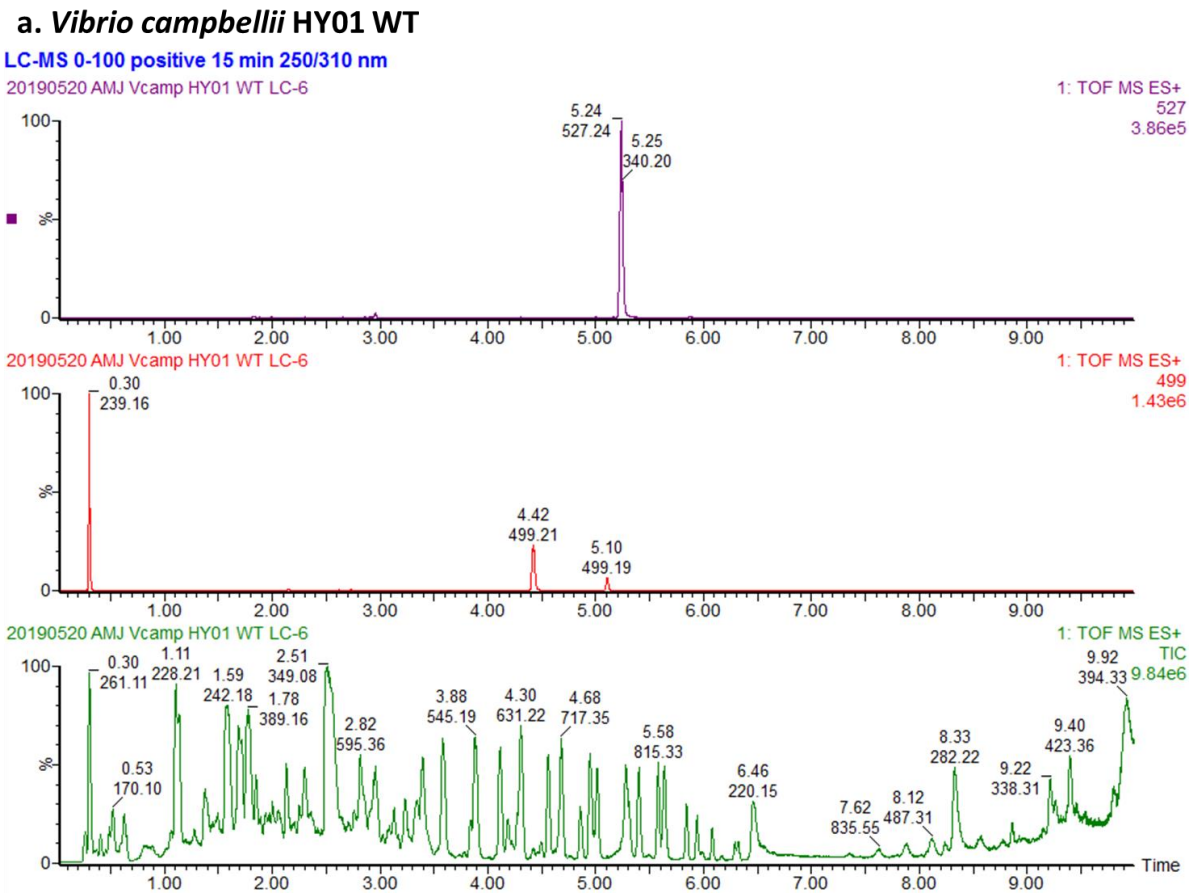

Figure 4.8. a-d: UPLC/ESI-MS analysis of *Vibrio* species. Ethanolic cell pellet extracts were analyzed through positive ion mode ESI-MS on a Waters Xevo G2-XS QTof coupled to a Waters Acquity H-Class UPLC system. A Waters BEH C18 column was used with an acetonitrile/water (both with 0.1% w/v formic acid) gradient shown at the top of each stacked trace. For each strain, the bottom trace is an ESI-MS total ion count (TIC) over time. TIC peaks are labeled with the elution time (top) and base peak (bottom). Chromatograms for masses of interest were generated with MassLynx 4.1, shown stacked above the TIC. The mass of interest is shown to the right of each trace.

b. *Vibrio campbellii* HY01 WTΔest1

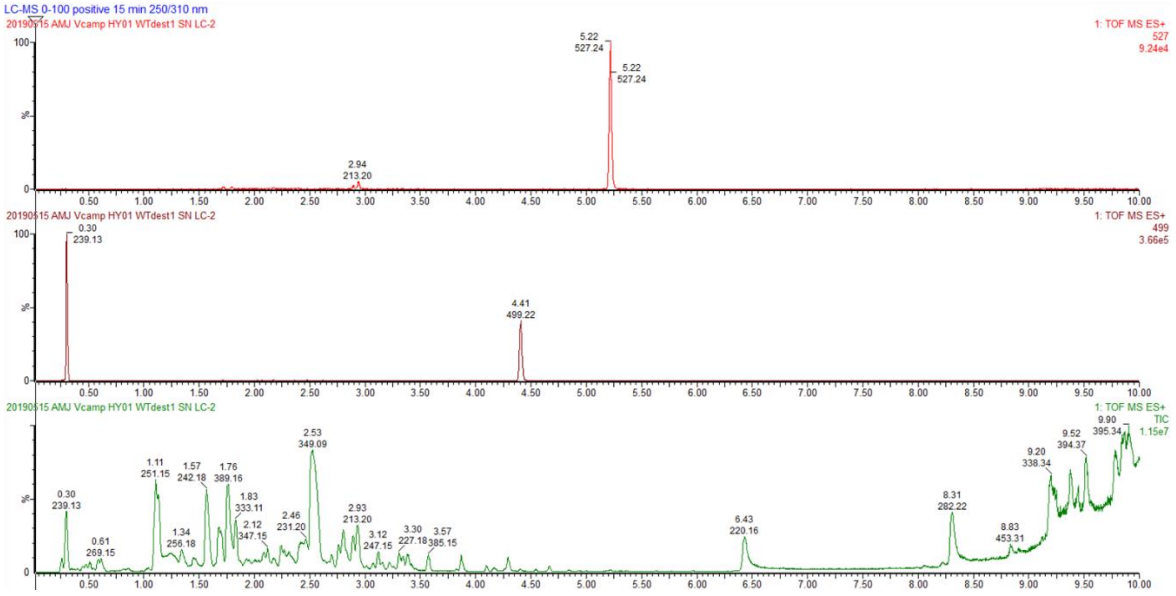

c. *Vibrio campbellii* HY01 WTΔest2

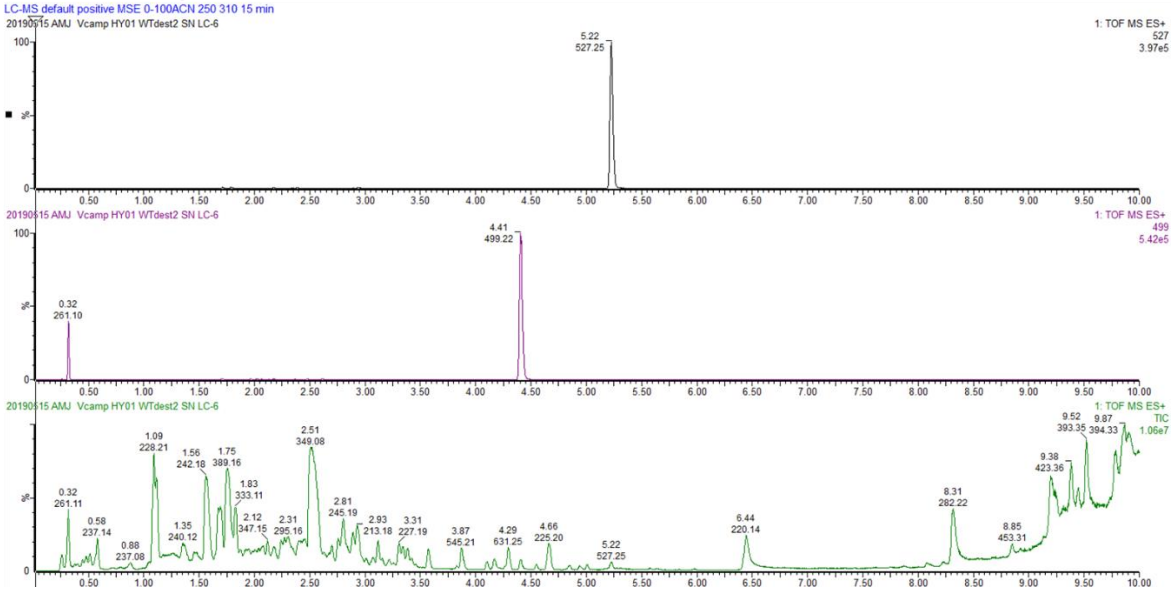

Figure 4.8. Continued.

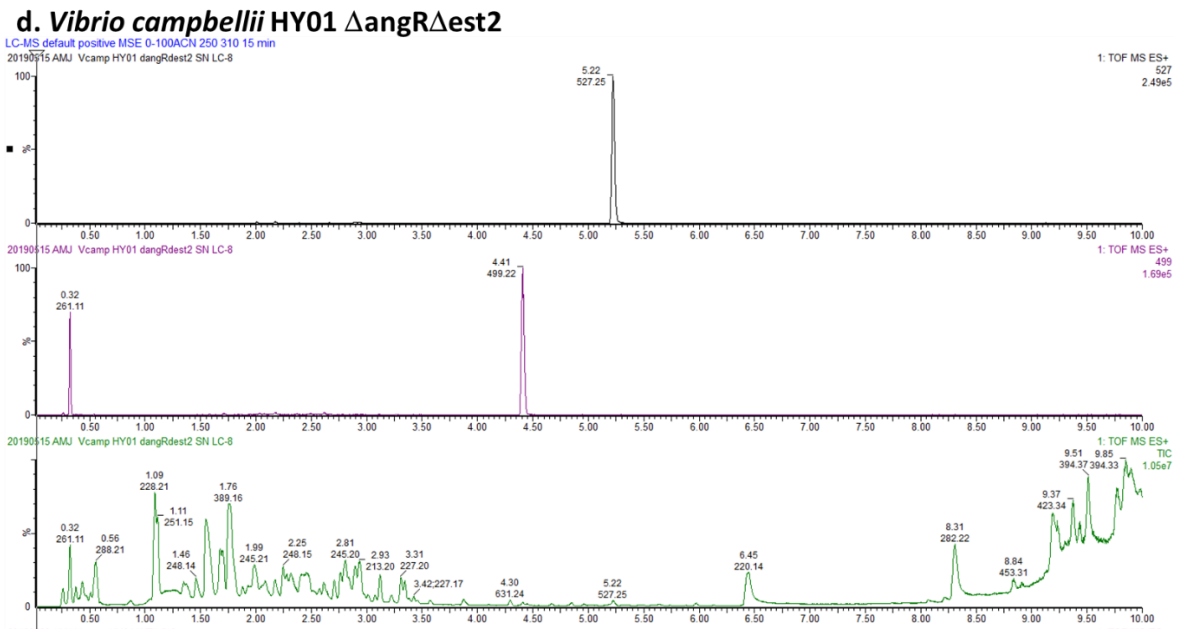

Figure 4.8. Continued.

4.4.3.4. Effect of Mutant and Complement Strains on Phenotypic Siderophore Production

The chrome azurol sulphonate (CAS) agar plate assay was used to screen for siderophore production. Colonies of the wild-type (WT) strain HY01 grown overnight on the CAS agar plate formed yellow halos. To determine if knocking out the esterase has an effect on iron uptake, mutant and complement strains: WT+emp, Δ*est1*+emp, Δ*est1*+*est1*, Δ*est2*+emp, Δ*est2*+*est2*, Δ*est1*Δ*est2*+emp, Δ*est1*Δ*est2*+*est1*, and Δ*est1*Δ*est2*+*est2* were grown on CAS agar plates. The size of the halo formation was compared to the WT colony (Figure 4.9). There is very little halo formation in any of the mutant or complement strains. These results are inconclusive about the effect the mutation has on siderophore production.

Liquid cultures of the mutant and complement strains were grown with chloramphenicol and IPTG and the production of amphi-enterobactin was observed. The wildtype complement (WT+emp) did not show production of amphi-enterobactin, suggesting the vector might be affecting amphi-enterobactin growth. The mutant and complement strains also did not show amphi-enterobactin production. Further studies are necessary to confirm if the *est1* and *est2* genes are necessary for hydrolysis of amphi-enterobactin, or to identify the function of these genes as they are embedded in the biosynthetic gene cluster for amphi-enterobactin.

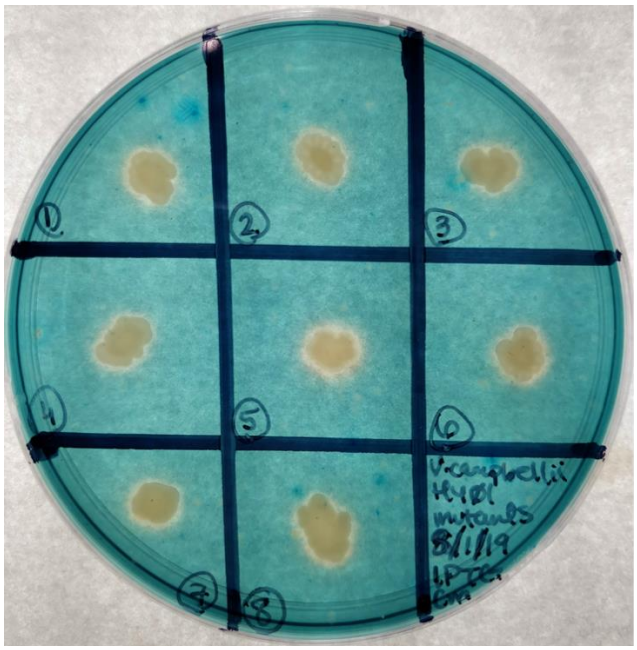

1. WT + emp
2. Δest1 + emp
3. Δest1+ est1
4. Δest2 + emp
5. Δest2 + est2
6. Δest1Δest2 +emp
7. Δest1Δest2 + est1
8. Δest1Δest2 + est2

Figure 4.9. Phenotypes of esterase mutants and complement strains with a conjugated vector. Colonies of mutants and complement strains grown on CAS agar plates for one day. Colonies are numbered left to right, top to bottom (1-8). 1. WT+emp; 2. Δest1+emp; 3. Δest1+est1; 4. Δest2+emp; 5. Δest1+est2; 6. Δest1Δest2+emp; 7. Δest1Δest2+est1; 8. Δest1Δest2+est2

4.4.4. Periplasmic Binding Proteins that Interact with Fe(III)-Enterobactin

The following sections used a BLAST search to identify and compare key proteins involved in Fe(III)-enterobactin uptake. The goal is to identify the trends among a wide range of bacterial strains that utilize enterobactin as a xenosiderophore.

Interaction with a periplasmic binding protein (PBP) is a key component in the iron uptake mechanism of Gram-negative bacteria. In *E. coli*, the periplasmic binding protein, FepB, binds to Fe(III)-enterobactin.[34] The PBP involved in transport of enterobactin in *Vibrio cholerae*, VctB, differs in comparison to the PBPs of *E. coli* and *V. anguillarum*, in the sense that VctB recognizes only the linearized enterobactin complexes, whereas FepB recognizes cyclic enterobactin.[35] The same is suspected in *V. parahaemolyticus* since the iron transport system shows homology to *V. cholerae*.[36]

For *Campylobacter jejuni*, it was originally proposed that once the Fe(III)-bound cyclic enterobactin was transported into the periplasm, this complex was recognized by the PBP CeuE, and ultimately transported into the cytoplasm. [37] [38] [39] However, further research has demonstrated that *C. jejuni* utilizes enterobactin hydrolysis products for the uptake of iron. [37] [40] [41] [42] The OMR's of *C. jejuni* are able to recognize cyclic enterobactin and transport the complex into the periplasm. The sole trilactone esterase is located in the periplasm and hydrolyzes the Fe(III)-enterobactin complex.[40] Further analysis of this *Campylobacter* Fe(III) acquisition model has shown that the PBP CeuE has preference for the enterobactin hydrolysis product, $[Fe(bisDHBS)]^{2-}$ with higher affinity than $[Fe(Ent)]^{3-}$.[42]

Low denticity siderophores can be used as a competitive advantage for the bacteria that are able to use them. Further investigations of CeuE with other periplasmic binding proteins like YclQ from *Bacillus subtilis* and VctP from *Vibrio cholerae* has shown similar traits.[41] It was identified that two residues of CeuE, His227 and Tyr 288, interact with the tetradentate siderophore $[Fe(bisDHBS)]^{2-}$, and that these two residues are conserved among the three periplasmic binding proteins, CeuE, YclQ, and VctP.[41] When CeuE interacts with a tetradentate siderophore, the two coordination sites of the octahedral Fe(III) center that are left open become occupied by the nitrogen atom of the nearby His227 and oxygen from Tyr288.[41] Overall, these two residues are conserved among the periplasmic binding proteins that only recognize linearized enterobactin.

The goal now is to identify if these residues are conserved among other periplasmic binding proteins. A Needleman-Wunsch Global Alignment was completed to identify the percent identity of each PBP to one another (Table 4.8). The three PBPs previously mentioned have a precent identity ranging from 26% for CeuE with VctP and 39% for CeuE with YclQ. Of the

strains that use enterobactin as an xenosiderophore, the highest percent identity is between *V. parahaemolyticus* and *V. cholerae* with a 59% identity. Again, the OMR of *Vibrio cholerae* does not recognize cyclic enterobactin but instead its linear products.

Table 4.8. Global alignment of ferric-siderophore interacting periplasmic binding proteins.

PBP Needleman-Wunsch Global Align			Percent Identity								
Strain/PBP		**Ref. Seq.**	*E. coli*	*S. enterica*	*B. subtilis*	*V. anguillarum*	*V. parahaemolyticus*	*V. cholerae*	*C. jejuni*	BAA-1116	CAIM 519
E. coli	FepB	WP_001234311.1	100	79	22	17	20	22	20	20	20
S. enterica	FepB	WP_080226359.1	79	100	21	18	21	22	21	23	23
B. subtilis	YclQ	WP_003246619.1	22	21	100	16	34	33	39	35	35
V. anguillarum	FvtB	WP_013856874.1	17	18	16	100	17	17	17	17	19
V. parahaemolyticus	VctP	WP_025767869.1	20	21	34	17	100	59	32	81	80
V. cholerae	VctP	WP_000842240.1	22	22	33	17	59	100	26	55	54
C. jejuni	CeuE	YP_002344743.1	20	21	39	17	32	26	100	32	32
V. campbellii ATCC BAA 1116		WP_012129633.1	20	23	35	17	81	55	32	100	98
V. campbellii CAIM 519		WP_005530604.1	20	23	35	19	80	54	32	98	100

Sequence alignment of the selected periplasmic binding proteins identified that *Vibrio parahaemolyticus* and two strains of *Vibrio campbellii*, ATCC BAA-1116 and CAIM 519, contain the same conserved residues as in *C. jejuni*, CeuE, *B. subtilis* YclQ, and *V. cholerae* VctP (Figure 4.10). Since these two residues, His227 and Tyr288, are conserved in *V. parahaemolyticus*, it suggests that the uptake mechanism for the xenosiderophore enterobactin is most similar to *V. cholerae*, where the OMR does not recognize cyclic enterobactin but rather the linearized products. There also may be a possible stronger preference for the tetradentate siderophore $[Fe(bisDHBS)]^{2-}$) as was seen in *C. jejuni*. The two *V. campbellii* strains, ATCC BAA-1116 and CAIM 519 produce amphi-enterobactins, a siderophore similar to enterobactin.[3, 31] The uptake mechanism for amphi-enterobactin has not been thoroughly studied, but this result of the conserved residues may provide insight that there is a preference for the hydrolysis of the siderophore to occur in the periplasm and these hydrolysis products are then transported into the cytoplasm via the ABC-transporter.

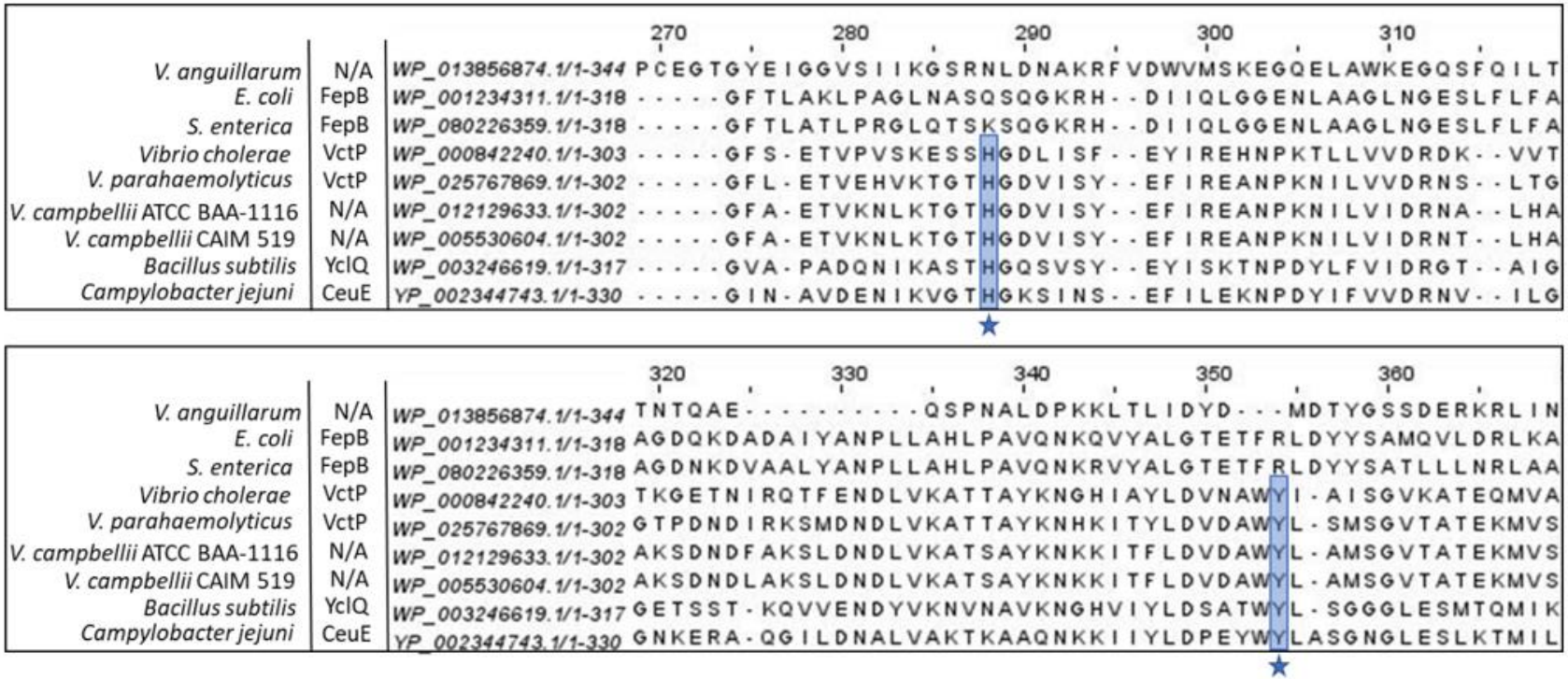

Figure 4.10. Sequence alignment of selected periplasmic siderophore binding proteins. Residues boxed/starred in blue indicate the conserved residues that have been previously identified as the residues interacting with the Fe(III)-center of the iron-siderophore complex in CeuE. Following on from the sequence alignment from Raines et. al; 2013. [41] On top of CeuE (*Campylobacter jejuni*), YclQ (*Bacillus subtilis*), VctP (*Vibrio cholerae*), and FetB (*Neisseria meningitidis*), we see conserved residues in *V. parahaemolyticus* and the two *V. campbellii* strains with the PBPs yet to be identified.

4.4.5. Esterases that Interact with Enterobactin

Mechanisms of iron release from siderophores falls under three possible pathways: a chemical modification, typically a hydrolysis of a macrolactone backbone, proton-assisted dissociation of the complex, and/or a reductase mediated reduction Fe(III) to Fe(II).[17]

Fes is the most well-known esterase that hydrolyzes serine-ester-containing catecholate siderophores. Within this class of esterases, IroD and IroE in *Salmonella enterica* hydrolyze salmochelin and BesA in *Bacillus subtilis* hydrolyzes bacillibactin.[8 9 43 44] Of the strains mentioned that take up enterobactin as an xenosiderophore, only three esterases have been identified: PfeE for *P. aeruginosa*,[45] VabH *for V. anguillarum*,[46 47] and Cee for *C. jejuni.*[40]

A Needleman-Wunsch Global Alignment was completed on the esterases discussed to provide an average percent identity of the proteins. Pairwise global protein identities were calculated by the Needleman-Wunsch algorithm (NCBI BLAST).[28]

There are four esterases with highest similarities to one another: Fes, IroD, VabH, and "unknown" from *V. parahaemolyticus* (Table 4.9). The unknown protein in *V. parahaemolyticus* does not have an assigned function but through a BLAST search was identified as a potential esterase. All four of these esterases are localized in the cytoplasm, but not all of them are solely enterobactin specific esterases. IroD also hydrolyzes salmochelin, while VabH also hydrolyzes vibriobactin. Interestingly, the "unknown" putative esterase found in *V. parahaemolyticus* has the highest percent identity (74%) to Fes and suggests that this esterase may be able to hydrolyze cyclized enterobactin. The next highest percent identity to Fes is VabH, an esterase in *V. anguillarum* with the ability to hydrolyze both the native siderophore, vanchrobactin, and the xenosiderophore enterobactin. IroD, the last esterase of

the four, has a 26% identity to Fes. The two periplasmic esterases, IroE and PfeE have 30% similarity to one another.

Lastly, BesA, has the highest similarity to the periplasmic proteins IroE (25%) and PfeE (27%). BesA is the esterase from *Bacillus subtilus*, a Gram-positive bacterium and has the ability to hydrolyze its native siderophore bacillibactin and xenosiderophore enterobactin.

Overall, despite these proteins coming from different bacterial species, all have the ability to hydrolyze Fe(III)-enterobactin along with hydrolyzing their native siderophores. The function of the unknown esterase in *V. parahaemolyticus* has not been identified and require further studies to determine if this putative esterase has the ability to hydrolyze the iron bound cyclic enterobactin. The four strains *P. aeruginosa*, *V. anguillarum*, *V. parahaemolyticus*, *and V. cholerae* do not contain the biosynthetic gene cluster for enterobactin but do express proteins involved in recognizing Fe(III)-enterobactin and promoting iron release from the complex through hydrolysis.

Table 4.9. Global alignment of selected siderophore esterase sequences.

	Needleman-Wunsch Global Align			Percent Identity							
Strain	Enterobactin Esterase name	Ref. Seq.	Location	Fes	IroD	IroE	BesA	PfeE	VabH	Unknown	Cee
E. coli	Fes	WP_000125846.1	cytoplasmic	100	26	17	17	18	34	74	14
S. enterica	IroD	NP_461702.1	cytoplasmic	26	100	15	19	20	25	28	15
S. enterica	IroE	NP_461703.1	**periplasmic**	17	15	100	25	30	16	17	24
B. subtilis	BesA	WP_003220638.1	cytoplasmic	17	19	25	100	27	18	17	26
P. aeruginosa	PfeE	WP_194488307.1	**periplasmic**	18	20	30	27	100	17	16	21
V. anguillarum	VabH	WP_019281793.1	cytoplasmic	34	25	16	18	17	100	34	15
V. parahaemolyticus	unknown	KKF71262.1	cytoplasmic	74	28	17	17	16	34	100	13
C. jejuni	Cee	YP_002344764.1	**periplasmic**	14	15	24	26	21	15	13	100
V. cholerae	N/A			Linear Ent							

4.4.6. Reductases that Interact with Fe(III)-Enterobactin

Successive events following the hydrolysis of the ferric trilactone scaffolds, specifically the process of iron release is not yet fully understood. Focusing on the ferric enterobactin complex, after hydrolysis of the complex, the formation constant of the hydrolysis product still favors complex formation over iron dissociation, which emphasizes the need for a reductase.[17 48] Once the ferric siderophore is hydrolyzed, the stability constant is lowered, and the reduction potential of Fe(III) falls into a range similar to that of ferric hydroxamate siderophores that are known to involve a ferric reductase for iron release, thus suggesting a reductase mediated Fe(III) reduction and iron release. Unfortunately, very little is known about ferric-siderophore dissociation involving reductases and only a couple siderophore pathways have been investigated. For the hydrolyzed Fe(III)-enterobactin complex, a NADPH-dependent reductase, YqjH, has been identified. The reductase YqjH directly follows hydrolysis and is able to catalyze iron release from enterobactin and several other iron chelators.[49]

YqjH belongs to the ferredoxin reductase-like family but differs from a ferredoxin reductase (FNR) in that YqjH favors the flow of electrons from NADPH to ferric substrates, whereas a FNR transfers an electron from reduced ferredoxin to $NADP^+$.[49] This characteristic shows that the goal of YqjH is iron assimilation rather than NADPH generation.[49] Substrate binding studies have also shown that YqjH has high binding affinity to the ferric substrate and that single alanine substitution of K55 and R130 identified that this lysine and arginine residues have a strong impact on catalytic efficiency, in particular for the hydrolyzed ferric triscatecholate substrates.[49] Further deletion studies of both Fes and YqjH have revealed that YqjH does not act in parallel, but rather downstream of Fes.[49] This result further confirmed the need for either an

esterase to hydrolyze ferric enterobactin or the presence of the already hydrolyzed ferric triscatecholate species to acquire iron from the ferric substrate.

Iron-siderophore dissociation can occur in either the periplasm or cytoplasm. For *E. coli,* dissociation occurs in the cytoplasm where the esterase is located, while the esterase in *Pseudomonas aeruginosa* is located in the periplasm. Even though PfeE (esterase) contributes to the dissociation of iron from the siderophore in *P. aeruginosa*, the entire dissociation process has not been elucidated. The Fe(III)-enterobactin complex still requires a reductase to complete the dissociation, but unfortunately a reductase for enterobactin in *P. aeruginosa* has not yet been identified.

Another known reductase ViuB, found in *V. cholerae,* is known to reduce the Fe(III)-vibriobactin complex.[35 50] It is also identified as a siderophore-interacting protein (SIP) and belongs to the SIP oxidoreductase family along with YqjH. Vibriobactin is a triscatecholate siderophore with a nonhydrolyzable backbone therefore an esterase is not necessary to promote iron release. These two known reductases already differ, where YqjH is efficient in reducing the hydrolyzed enterobactin, while ViuB favors the intact ferric triscatecholate complex.

There have not been many siderophore reductases characterized, but after a quick sequence similarity search in the strains identified to take up enterobactin, we see that strains *C. jejuni, S. enterica,* and *V. parahaemolyticus* show high sequence similarity (51 to 80%) to YqjH (Table 5.4). Interestingly, in this sequence similarity search, no putative reductases were found for *Bacillus subtilis* and *Vibrio anguillarum*. A sequence-level analysis (Figure 5.5) of the putative reductases revealed that the two amino acids, K55 and R130 that have a strong impact on catalytic efficiency, are conserved among the aforementioned strains. *Vibrio campbellii* ATCC BAA-1116, an amphi-enterobactin producing siderophore, despite it have a low sequence similarity (21%) (Figure 5.5)

has K55 conserved, but not R130. These putative reductases most possibly fall into the same ferredoxin reductase-like family as YqjH.

Table 4.10. Sequence similarity search of putative reductases similar to YqjH, the enterobactin reductase.

PBP Needleman-Wunsch Global Align Strain/PBP		Ref. Seq.	*E. coli* YqjH	*V. cholerae* ViuB
E. coli	YqjH	NP_417541.1	100	27
V. cholerae	ViuB	WP_000064348.1	27	100
V. parahaemolyticus		KKF68733.1	80	25
C. jejuni		VTQ52188.1	51	23
S. enterica		GAS70983.1	75	25
S. enterica		ECI4400604.1	100	27
V. campbellii ATCC BAA-1116		ARV75241.1	21	31
B. subtilis				
V. anguillarum				

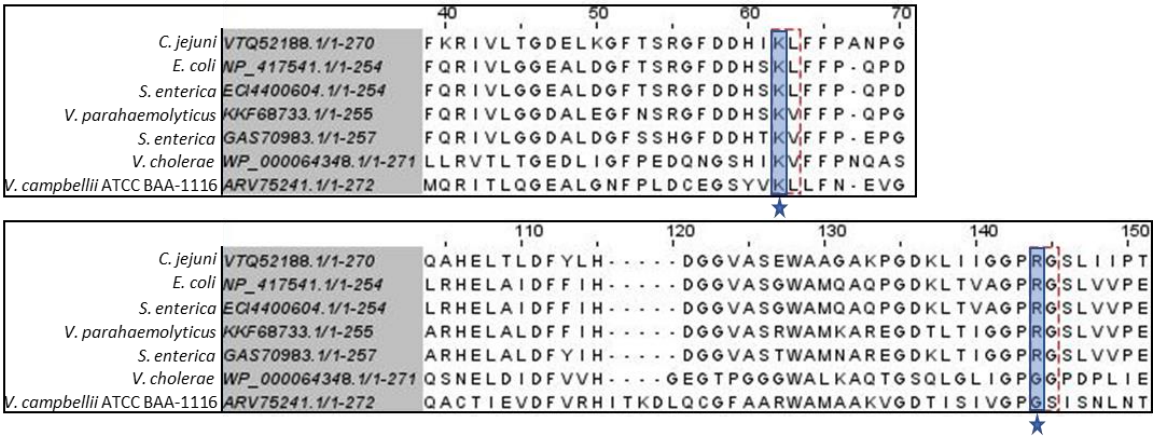

Figure 4.11. Sequence alignment of putative reductases along with YqjH (*E. coli*) and ViuB (*V. cholerae*). Residues boxed/starred in blue indicate the conserved residues among the sequences that have been previously identified as the two residues in YqjH that have a strong impact on catalytic efficiency. The sequence for ViuB and the putative reductase in V. campbellii ATCC BAA-1116 do not have the arginine residue conserved.

4.5. Discussion

Amphi-enterobactin production was tested via ESI-MS analysis of extracts from various *V. campbellii* and *V. harveyi* strains. All of these strains showed production of a suite of amphi-enterobactins with various fatty acid appendages. The amount of amphi-enterobactin however, varied among the *V. campbellii* and *V. harveyi* strains. In the course of this investigation, four new amphi-enterobactin species, with fatty acid tails, C10:0, C14:0 OH, C14:0 and C16:1, were identified, two of which were reported by McRose et al.[6] These results indicate the versatility of the amphi-enterobactin biosynthetic gene cluster among the marine bacterial strains, *V. campbellii* and *V. harveyi.*

The Fes esterase found in enterobactin-producing species catalyzes the hydrolysis of Fe(III)-enterobactin to promote iron release from the catechol ligands.[9] The amphi-enterobactin hydrolysis products that have been characterized are likely coming from an enzymatic hydrolysis. However, to this date, a homolog of Fes has not been identified in *V. campbellii* and *V. harveyi* strains that produce amphi-enterobactin. Instead, two putative esterases embedded in the amphi-enterobactin BGC, have shown homology to an erythromycin esterase. Knockout mutants of these two putative esterases were constructed and tested for the presence of amphi-enterobactin hydrolysis products. The hydrolysis products, *m/z* 499 and *m/z* 527, were identified in three of the four mutant strains, WTΔ*est1*, WTΔ*est2*, and Δ*angR*Δ*est2*. In the mutant strain Δ*angR*Δ*est1*, hydrolysis products were not observed. The experiments of the mutant and complement strains were inconclusive and require further investigations. The control strain of *V. campbellii* HY01 with the plasmid did not produce amphi-enterobactin, therefore either the growth conditions may be affecting siderophore production or the inserted plasmid. Future studies may focus on these mutant and complement strains and identifying the presence of the hydrolysis fragments.

In respect to the genome analysis of the iron acquisition mechanism of Fe(III)-enterobactin among varying bacterial strains, it was summarized that microorganisms have had to adapt to their receptor and transport proteins to adjust to the evolution of diverse siderophores and compete with other microorganisms.[15]

The iron uptake pathway in *E. coli*, especially for enterobactin has been the model mechanism in the field and is thought that the molecular mechanism would apply to enterobactin as a xenosiderophore in other Gram-negative bacteria. However, further findings have shown that even the same siderophore may experience a different uptake pathway in other bacterial strains. In some cases, like in *P. aeruginosa* and *V. anguillarum*, cyclic Fe(III)-enterobactin is recognized and the two strains contain an esterase, either in the periplasm or the cytoplasm that helps hydrolyze the complex. The other three strains, *V. cholerae, V. parahaemolyticus,* and *C. jejuni* have a stronger preference for the hydrolysis products of enterobactin. In particular, *V. cholerae* and *V. parahaemolyticus* lack the outer membrane receptors and esterase for cyclic enterobactin and instead recognize the linear dimer/trimers. *C. jejuni* is able to recognize cyclic enterobactin, but once the complex is in the periplasm, an esterase must hydrolyze the siderophore so that it can be transported into cytoplasm and iron is released. Through bioinformatic analysis, key residues previously identified as interacting with the tetradentate siderophore in *C. jejuni* is conserved among other strains that utilize enterobactin hydrolysis products as xenosiderophores.

4.6. References

1. Lin, B.; Wang, Z.; Malanoski, A. P.; O'Grady, E. A.; Wimpee, C. F.; Vuddhakul, V.; Alves, N., Jr.; Thompson, F. L.; Gomez-Gil, B.; Vora, G. J., Comparative genomic analyses identify the *Vibrio harveyi* genome sequenced strains BAA-1116 and HY01 as *Vibrio campbellii*. *Environ Microbiol Rep* **2010,** *2* (1), 81-89.
2. Urbanczyk, H.; Ogura, Y.; Hayashi, T., Taxonomic revision of *Harveyi* clade bacteria (family *Vibrionaceae*) based on analysis of whole genome sequences. *International Journal of Systematic and Evolutionary Microbiology* **2013,** *63* (Pt_7), 2742-2751.
3. Zane, H. K.; Naka, H.; Rosconi, F.; Sandy, M.; Haygood, M. G.; Butler, A., Biosynthesis of Amphi-enterobactin Siderophores by *Vibrio harveyi* BAA-1116: Identification of a Bifunctional Nonribosomal Peptide Synthetase Condensation Domain. *Journal of the American Chemical Society* **2014,** *136* (15), 5615-5618.
4. Naka, H.; Actis, L. A.; Crosa, J. H., The anguibactin biosynthesis and transport genes are encoded in the chromosome of *Vibrio harveyi*: a possible evolutionary origin for the pJM1 plasmid–encoded system of Vibrio anguillarum? *MicrobiologyOpen* **2013,** *2* (1), 182-194.
5. Thode, S. K.; Rojek, E.; Kozlowski, M.; Ahmad, R.; Haugen, P., Distribution of siderophore gene systems on a *Vibrionaceae* phylogeny: Database searches, phylogenetic analyses and evolutionary perspectives. *PLoS One* **2018,** *13* (2), e0191860.
6. McRose, D. L.; Baars, O.; Seyedsayamdost, M. R.; Morel, F. M. M., Quorum sensing and iron regulate a two-for-one siderophore gene cluster in *Vibrio harveyi*. *Proceedings of the National Academy of Sciences* **2018,** *115* (29), 7581.
7. Jelowicki, A. M.; Butler, A., On the origin of amphi-enterobactin fragments produced by *Vibrio campbellii* species. *JBIC Journal of Biological Inorganic Chemistry* **2022**.
8. Brickman, T. J.; McIntosh, M. A., Overexpression and purification of ferric enterobactin esterase from *Escherichia coli*. Demonstration of enzymatic hydrolysis of enterobactin and its iron complex. *Journal of Biological Chemistry* **1992,** *267* (17), 12350-12355.
9. Lin, H.; Fischbach, M. A.; Liu, D. R.; Walsh, C. T., In Vitro Characterization of Salmochelin and Enterobactin Trilactone Hydrolases IroD, IroE, and Fes. *Journal of the American Chemical Society* **2005,** *127* (31), 11075-11084.
10. Hantke, K.; Nicholson, G.; Rabsch, W.; Winkelmann, G., Salmochelins, siderophores of *Salmonella enterica* and uropathogenic *Escherichia coli* strains, are recognized by the outer membrane receptor IroN. *Proc Natl Acad Sci U S A* **2003,** *100* (7), 3677-82.
11. Miethke, M.; Klotz, O.; Linne, U.; May, J. J.; Beckering, C. L.; Marahiel, M. A., Ferri-bacillibactin uptake and hydrolysis in *Bacillus subtilis*. *Molecular Microbiology* **2006,** *61* (6), 1413-1427.
12. Nikaido, H., Molecular Basis of Bacterial Outer Membrane Permeability Revisited. *Microbiology and Molecular Biology Reviews* **2003,** *67* (4), 593-656.
13. Bradbeer, C., The proton motive force drives the outer membrane transport of cobalamin in *Escherichia coli*. *Journal of Bacteriology* **1993,** *175* (10), 3146-3150.
14. Krewulak, K. D.; Vogel, H. J., TonB or not TonB: is that the question? *Biochemistry and Cell Biology* **2011,** *89* (2), 87-97.
15. Krewulak, K. D.; Vogel, H. J., Structural biology of bacterial iron uptake. *Biochimica et Biophysica Acta (BBA) - Biomembranes* **2008,** *1778* (9), 1781-1804.

16. D'Onofrio, A.; Crawford, J. M.; Stewart, E. J.; Witt, K.; Gavrish, E.; Epstein, S.; Clardy, J.; Lewis, K., Siderophores from neighboring organisms promote the growth of uncultured bacteria. *Chem Biol* **2010,** *17* (3), 254-64.
17. Harrington, J. M.; Crumbliss, A. L., The redox hypothesis in siderophore-mediated iron uptake. *BioMetals* **2009,** *22* (4), 679-689.
18. Raymond, K. N.; Dertz, E. A.; Kim, S. S., Enterobactin: An archetype for microbial iron transport. *Proceedings of the National Academy of Sciences* **2003,** *100* (7), 3584-3588.
19. Cooper, S. R.; McArdle, J. V.; Raymond, K. N., Siderophore electrochemistry: relation to intracellular iron release mechanism. *Proceedings of the National Academy of Sciences* **1978,** *75* (8), 3551.
20. Rattanama, P.; Srinitiwarawong, K.; Thompson, J. R.; Pomwised, R.; Supamattaya, K.; Vuddhakul, V., Shrimp pathogenicity, hemolysis, and the presence of hemolysin and TTSS genes in *Vibrio harveyi* isolated from Thailand. *Dis Aquat Organ* **2009,** *86* (2), 113-22.
21. Lin, B.; Wang, Z.; Malanoski, A. P.; O'Grady, E. A.; Wimpee, C. F.; Vuddhakul, V.; Alves Jr, N.; Thompson, F. L.; Gomez-Gil, B.; Vora, G. J., Comparative genomic analyses identify the *Vibrio harveyi* genome sequenced strains BAA-1116 and HY01 as *Vibrio campbellii*. *Environmental Microbiology Reports* **2010,** *2* (1), 81-89.
22. Karsch-Mizrachi, I.; Nakamura, Y.; Cochrane, G.; The International Nucleotide Sequence Database Collaboration. *Nucleic Acids Research* **2011,** *40* (D1), D33-D37.
23. Dias, G. M.; Thompson, C. C.; Fishman, B.; Naka, H.; Haygood, M. G.; Crosa, J. H.; Thompson, F. L., Genome Sequence of the Marine Bacterium *Vibrio campbellii* DS40M4, Isolated from Open Ocean Water. *Journal of Bacteriology* **2012,** *194* (4), 904-904.
24. Johnson, F. H.; Shunk, I. V., An Interesting New Species of Luminous Bacteria. *Journal of Bacteriology* **1936,** *31* (6), 585-593.
25. Soto-Rodriguez, S. A.; Gomez-Gil, B.; Lozano, R.; del Rio-Rodríguez, R.; Diéguez, A. L.; Romalde, J. L., Virulence of *Vibrio harveyi* responsible for the "Bright-red" Syndrome in the Pacific white shrimp Litopenaeus vannamei. *J Invertebr Pathol* **2012,** *109* (3), 307-317.
26. Morales, V. M.; Bäckman, A.; Bagdasarian, M., A series of wide-host-range low-copy-number vectors that allow direct screening for recombinants. *Gene* **1991,** *97* (1), 39-47.
27. Haft, D. H.; DiCuccio, M.; Badretdin, A.; Brover, V.; Chetvernin, V.; O'Neill, K.; Li, W.; Chitsaz, F.; Derbyshire, M. K.; Gonzales, N. R.; Gwadz, M.; Lu, F.; Marchler, G. H.; Song, J. S.; Thanki, N.; Yamashita, R. A.; Zheng, C.; Thibaud-Nissen, F.; Geer, L. Y.; Marchler-Bauer, A.; Pruitt, K. D.,: An update on prokaryotic genome annotation and curation. *Nucleic Acids Res* **2018,** *46* (D1), D851-d860.
28. Johnson, M.; Zaretskaya, I.; Raytselis, Y.; Merezhuk, Y.; McGinnis, S.; Madden, T. L., NCBI BLAST: a better web interface. *Nucleic Acids Res* **2008,** *36* (Web Server issue), W5-9.
29. Edgar, R. C., MUSCLE: multiple sequence alignment with high accuracy and high throughput. *Nucleic Acids Research* **2004,** *32* (5), 1792-1797.
30. Madeira, F.; Park, Y. M.; Lee, J.; Buso, N.; Gur, T.; Madhusoodanan, N.; Basutkar, P.; Tivey, A. R. N.; Potter, S. C.; Finn, R. D.; Lopez, R., The EMBL-EBI search and sequence analysis tools APIs in 2019. *Nucleic acids research* **2019,** *47* (W1), W636-W641.
31. Naka, H.; Reitz, Z. L.; Jelowicki, A. L.; Butler, A.; Haygood, M. G., Amphi-enterobactin commonly produced among *Vibrio campbellii* and *Vibrio harveyi* strains can be taken up by a novel outer membrane protein FapA that also can transport canonical Fe(III)-enterobactin. *JBIC Journal of Biological Inorganic Chemistry* **2018,** *23* (7), 1009-1022.

32. Sandy, M.; Han, A.; Blunt, J.; Munro, M.; Haygood, M.; Butler, A., Vanchrobactin and anguibactin siderophores produced by *Vibrio* sp. DS40M4. *Journal of natural products* **2010,** *73* (6), 1038-1043.
33. Naka, H.; Liu, M.; Crosa, J. H., Two ABC transporter systems participate in siderophore transport in the marine pathogen *Vibrio anguillarum* 775 (pJM1). *FEMS Microbiol Lett* **2013,** *341* (2), 79-86.
34. Stephens, D. L.; Choe, M. D.; Earhart, C. F., *Escherichia coli* periplasmic protein FepB binds ferrienterobactin. *Microbiology* **1995,** *141* (7), 1647-1654.
35. Wyckoff, E. E.; Allred, B. E.; Raymond, K. N.; Payne, S. M., Catechol Siderophore Transport by *Vibrio cholerae*. *Journal of bacteriology* **2015,** *197* (17), 2840-2849.
36. Tanabe, T.; Funahashi, T.; Shiuchi, K.; Okajima, N.; Nakao, H.; Miyamoto, K.; Tsujibo, H.; Yamamoto, S., Characterization of *Vibrio parahaemolyticus* genes encoding the systems for utilization of enterobactin as a xenosiderophore. *Microbiology* **2012,** *158* (8), 2039-2049.
37. Naikare, H.; Butcher, J.; Flint, A.; Xu, J.; Raymond, K. N.; Stintzi, A., *Campylobacter jejuni* ferric–enterobactin receptor CfrA is TonB3 dependent and mediates iron acquisition from structurally different catechol siderophores†. *Metallomics* **2013,** *5* (8), 988-996.
38. Xu, F.; Zeng, X.; Haigh, R. D.; Ketley, J. M.; Lin, J., Identification and characterization of a new ferric enterobactin receptor, CfrB, in *Campylobacter*. *Journal of bacteriology* **2010,** *192* (17), 4425-4435.
39. Stahl, M.; Butcher, J.; Stintzi, A., Nutrient Acquisition and Metabolism by *Campylobacter jejuni*. *Front Cell Infect Microbiol* **2012,** *2* (5).
40. Zeng, X.; Mo, Y.; Xu, F.; Lin, J., Identification and characterization of a periplasmic trilactone esterase, Cee, revealed unique features of ferric enterobactin acquisition in *Campylobacter*. *Molecular Microbiology* **2013,** *87* (3), 594-608.
41. Raines, D. J.; Moroz, O. V.; Wilson, K. S.; Duhme-Klair, A.-K., Interactions of a Periplasmic Binding Protein with a Tetradentate Siderophore Mimic. *Angewandte Chemie International Edition* **2013,** *52* (17), 4595-4598.
42. Raines, D. J.; Moroz, O. V.; Blagova, E. V.; Turkenburg, J. P.; Wilson, K. S.; Duhme-Klair, A.-K., Bacteria in an intense competition for iron: Key component of the *Campylobacter jejuni* iron uptake system scavenges enterobactin hydrolysis product. *Proceedings of the National Academy of Sciences* **2016,** *113* (21), 5850.
43. Zhu, M.; Valdebenito, M.; Winkelmann, G.; Hantke, K., Functions of the siderophore esterases IroD and IroE in iron-salmochelin utilization. *Microbiology* **2005,** *151* (7), 2363-2372.
44. Abergel, R. J.; Zawadzka, A. M.; Hoette, T. M.; Raymond, K. N., Enzymatic Hydrolysis of Trilactone Siderophores: Where Chiral Recognition Occurs in Enterobactin and Bacillibactin Iron Transport. *Journal of the American Chemical Society* **2009,** *131* (35), 12682-12692.
45. Perraud, Q.; Moynié, L.; Gasser, V.; Munier, M.; Godet, J.; Hoegy, F.; Mély, Y.; Mislin, G. L. A.; Naismith, J. H.; Schalk, I. J., A Key Role for the Periplasmic PfeE Esterase in Iron Acquisition via the Siderophore Enterobactin in *Pseudomonas aeruginosa*. *ACS Chemical Biology* **2018,** *13* (9), 2603-2614.
46. Balado, M.; Osorio, C. R.; Lemos, M. L., A gene cluster involved in the biosynthesis of vanchrobactin, a chromosome-encoded siderophore produced by *Vibrio anguillarum*. *Microbiology* **2006,** *152* (12), 3517-3528.

47. Naka, H.; Crosa, J. H., Identification and characterization of a novel outer membrane protein receptor FetA for ferric enterobactin transport in *Vibrio anguillarum* 775 (pJM1). *BioMetals* **2012,** *25* (1), 125-133.
48. Schröder, I.; Johnson, E.; de Vries, S., Microbial ferric iron reductases. *FEMS Microbiology Reviews* **2003,** *27* (2-3), 427-447.
49. Miethke, M.; Hou, J.; Marahiel, M. A., The Siderophore-Interacting Protein YqjH Acts as a Ferric Reductase in Different Iron Assimilation Pathways of *Escherichia coli*. *Biochemistry* **2011,** *50* (50), 10951-10964.
50. Butterton, J. R.; Calderwood, S. B., Identification, cloning, and sequencing of a gene required for ferric vibriobactin utilization by *Vibrio cholerae*. *Journal of bacteriology* **1994,** *176* (18), 5631-5638.